Characterising Host Factors Required for CRISPR Cas Adaptation in *Escherichia coli*

Harry Edwards, MRes, B.Sc (Hons)

School of Life Sciences

University of Nottingham



Thesis submitted for the Degree of

Doctor of Philosophy

December 2022

Abstract

The evolution of diverse prokaryotic immune systems has been driven by the constant threat of invasion by foreign genetic elements. Many prokaryotes contain the CRISPR-Cas system, which provides adaptive immunity through the acquisition of unique spacer sequences into the CRISPR array. These sequences guide the effector complexes to destroy the complementary invading genetic elements.

The function of the Cas proteins is well understood, due to their proximity to the CRISPR array. Other host factors have been discovered to play a role in spacer acquisition, such as IHF and DnaQ. However, aspects of spacer capture and integration by the Cas1 and Cas2 proteins remain elusive. This work aimed to determine and presents evidence for a broader collection of host factors required for CRISPR Cas adaptation in *E. coli*.

I demonstrate that the catalytic activity of the Cas1-Cas2 complex triggers activation of the SOS response and induces filamentation by *sulA* expression. This is due to non-specific activity across the genome, not just at the CRISPR array. Use of the *lexA3* allele and overexpression of *recX*, which prevent induction of the SOS response, decreases the rate of spacer acquisition. Furthermore, induction of the SOS response, via growth in sub-inhibitory antibiotic concentrations, increases the rate of adaptation.

I also provide evidence for an equilibrium between the FtsH-HflKC and FtsH-LapB complexes governing the level of adaptation. The deletion of *hflC* or *hflK* and overexpression of *lapB* decreases the rate of spacer acquisition, whilst overexpression of *hflKC* or *ftsH* increases the rate of adaptation. Furthermore, mutation of negative regulators of *lapB* reduces the rate of spacer acquisition. This suggests that HflKC and LapB compete to form complexes with FtsH, with the formation of FtsH-HflKC complexes promoting adaptation.

Taken together, these results reveal the link between cell division and spacer acquisition.

Contents

1 Introduction **1**

1.1 Preventing Phage Adsorption . . . 2
1.1.1 Blocking Phage Receptors . . . 2
1.1.2 Production of an Extracellular Matrix . . . 4
1.1.3 Competitive Inhibitors . . . 4
1.2 Restriction Modification Systems . . . 5
1.3 Abortive Infection . . . 6
1.3.1 Toxin-Antitoxin Systems . . . 6
1.3.2 CBASS . . . 7
1.3.3 STAND NTPases . . . 8
1.4 Argonaute . . . 9
1.5 CRISPR Cas . . . 10
1.5.1 Interference . . . 13
1.5.2 Adaptation . . . 14
1.6 Cas1-Cas2 . . . 16
1.7 Location of Integration . . . 18
1.8 Choice of Substrate for Spacers . . . 20
1.9 Classification of CRISPR Cas Systems . . . 23
1.9.1 Class I, Type I CRISPR Systems . . . 24
1.9.2 Class I, Type III CRISPR Systems . . . 24
1.9.3 Class I, Type IV CRISPR Systems . . . 25
1.9.4 Class II, Type II CRISPR Systems . . . 26
1.9.5 Class II, Type V CRISPR Systems . . . 27
1.9.6 Class II, Type VI CRISPR Systems . . . 27
1.10 Regulation of Cas gene Expression . . . 28
1.10.1 H-NS and LeuO . . . 29
1.10.2 CRP-cAMP . . . 30
1.10.3 BaeSR . . . 32
1.10.4 Iron Transport System . . . 32

1.10.5 Quorum sensing . . . 33
1.10.6 Calcium-Responsive Kinase . . . 34
1.11 Scope of the Thesis . . . 34

2 Materials and Methods **36**
2.1 Reagents . . . 37
2.2 Strains Used and Created . . . 37
2.3 Plasmids and Oligonucleotides . . . 43
2.3.1 Plasmid List . . . 43
2.3.2 Oligonucleotide List . . . 46
2.4 Solution Composition . . . 52
2.4.1 Media . . . 52
2.4.2 Antibiotics . . . 52
2.5 Cloning and DNA Manipulation . . . 53
2.5.1 Polymerase Chain Reaction . . . 53
2.5.2 Digests . . . 54
2.5.3 Phosphorylation . . . 54
2.5.4 Dephosphorylation . . . 54
2.5.5 Ligation . . . 54
2.5.6 Gibson Assembly . . . 54
2.5.7 Plasmid Purification . . . 55
2.5.8 Phenol Chloroform Extraction . . . 55
2.5.9 Ethanol Precipitation . . . 55
2.6 Gel Electrophoresis . . . 56
2.6.1 Agarose Gel Electrophoresis . . . 56
2.6.2 Agarose Gel Extraction Protocol . . . 56
2.6.3 Running Buffers . . . 56
2.7 Competent Cells . . . 56
2.7.1 Making Chemically Competent Cells . . . 56
2.7.2 Competent Cell Transformation Protocol . . . 57
2.7.3 Making Electrocompetent Cells . . . 57
2.7.4 Electrocompetent Cell Transformation Protocol . . . 58
2.8 Conjugation . . . 58
2.9 Genetic Manipulation by P1 Transduction . . . 59
2.9.1 Generation of P1 bacteriophage lysates . . . 59
2.9.2 Genetic Manipulation by P1 Transduction . . . 59
2.9.3 FLP-*frt* Recombination . . . 60
2.10 Bacterial Assays . . . 61
2.10.1 Papillation Assay . . . 61

2.10.2 Spacer Integration Assay (SPIN) 62
2.10.3 Detection of Spacer Acquisition by Fluorescence 62
2.10.4 Separation of filamenting cells by Filtration 63
2.10.5 Cell Sorting 63
2.10.6 Determination of Growth Rate 64
2.11 Marionette eYFP Fluorescence Titration 64
2.12 Microscopy 65
2.13 Measurement of SOS Response Induction by GFP Fluorescence . . 65

3 Optimisation of the Papillation Assay for Spacer Acquisition 67
3.1 Introduction 68
3.2 Determination of the choice of Cas1-Cas2 Expression Vector 73
3.3 Optimisation of Salt Concentration 74
3.4 Liquid Culture Assays 75
3.5 Testing the compatibility of the Marionette vector collection with the spacer acquisition reporter system 77
3.6 Precise Genetic Deletions 81
3.7 Complementation of gene deletions restores the papillation phenotype 83
3.8 Chapter Summary 85

4 Cas1-Cas2 Induces Filamentation by Activation of the SOS Response and SulA Expression 86
4.1 Introduction 87
4.2 Cas1-Cas2 expression induces filamentation 88
4.3 Spacer acquisition is not more abundant in filamentous cells 90
4.4 Cas1-Cas2 induces the SOS response 92
4.5 Chapter Summary 95

5 Induction of the SOS Response Aids in Spacer Acquisition 96
5.1 Introduction 97
5.2 The un-cleavable *lexA3* allele prevents induction of the SOS response and decreases the level of papillation 99
5.3 Inhibition of *recA* decreases the rate of spacer acquisition 102
5.4 Deletion of *recA* increases the rate of adaptation 103
5.5 *SulA* overexpression increases the level of papillation 107
5.6 Overexpression of *ymfM* increases the level of papillation 108
5.7 Deletion of *sulA* and *ymfM* does not alter the level of papillation . . . 110
5.8 Growth in the presence of sub-inhibitory concentrations of antibiotics increases the level of papillation 112
5.9 Mitomycin C and nalidixic acid induce the SOS response 115

5.10 Antibiotics Induce Spacer Acquisition Events 117
5.11 Chapter Summary 119

6 Degradation of FtsZ by HflKC/FtsH Supports CRISPR Cas Adaptation 120
6.1 Introduction 121
6.2 Deletion of genes from the *hflC* and *miaA* operon 122
6.3 Deletion of *miaA* inhibits papillation but not spacer acquisition 123
6.4 Deletion of *hflK* or *hflC* reduces the rate of spacer acquisition 124
6.5 Complementation of *hflK* and *hflC* restores spacer acquisition 126
6.6 Overexpression of the *hflKC* complex increases the rate of spacer acquisition 126
6.7 Overexpression of *ftsH* increases the rate of adaptation 129
6.8 Overexpression of *ftsZ* decreases the rate of adaptation 131
6.9 Chapter Summary 133

7 Deletion of LapB/FtsH Inhibitors Decreases the Rate of Spacer Acquisition 134
7.1 Introduction 135
7.2 Truncation of *lapC* reduces the rate of spacer acquisition 136
7.3 Deletion of *waaG* and *waaQ* decreases the rate of spacer acquisition 137
7.4 Deletion of *rfaH* decreases the rate of spacer acquisition 138
7.5 Overexpression of *lapB* decreases the rate of papillation 140
7.6 Chapter Summary 142

8 Discussion and Future Work 143
8.1 Coupling the SOS Response and CRISPR Adaptation 144
8.2 Effect of Sub-inhibitory concentrations of Antibiotics 148
8.3 HflKC and LapB: Equilibrium of FtsH Specificity Factors 149
8.4 FtsZ: the keystone of spacer acquisition 152
8.5 Future Work of SOS and Adaptive Immunity 154
8.6 Future Work of Membrane Stress and Adaptive Immunity 158

Figures

1.1 Strategies to prevent receptor recognition by bacteriophages 3
1.2 Action of a Restriction Modification System 5
1.3 Action of a Toxin-Antitoxin System 7
1.4 Action of antiviral STAND 9
1.5 General Structure of a CRISPR locus 11
1.6 Summary of CRISPR Cas Immunity 12
1.7 Mechanism of Cas3 cleavage 14
1.8 Crystal Structure of the *E. coli* Type I-E Cas1-Cas2 Complex 17
1.9 Mechanism of Spacer Integration into the CRISPR Array 18
1.10 IHF binds DNA to induce DNA bending 19
1.11 The nuclease activity of RecBCD explains the preference for spacer acquisition from foreign genetic elements during naïve adaptation . . 22
1.12 Classification of CRISPR systems 23
1.13 Mechanisms of CRISPR regulation 31

3.1 PCR amplification of the CRISPR locus to show spacer acquisition . 68
3.2 Papillation assay reporter scheme 70
3.3 Location of the Reporter CRISPR Array 72
3.4 Optimisation of papillation assay expression vector 74
3.5 Salt concentration alters the rate of papillation 75
3.6 Optimisation of Cas1-Cas2 expression vector choice for use in JB028 liquid culture assays 76
3.7 Use of Marionette inducer molecules or plasmids does not alter the rate of papillation 78
3.8 The Marionette vanillic acid promoter is titratable in the adaptation reporter 80
3.9 P1 transduction strategy gene transfer in *E. coli* 82
3.10 Papillation is restored in JB028 Δ*IHF*α when IHFα is complemented back on an inducible plasmid 84

4.1 The catalytic activity of Cas1-Cas2 induces filamentation 89
4.2 Spacer acquisition is not more abundant in filamentous cells 91
4.3 Cas1-Cas2 expression induces the SOS response 93

5.1 LexA-mediated regulation of the SOS response 98
5.2 The *lexA3* allele prevents induction of the SOS response 100
5.3 The *lexA3* allele reduces the rate of spacer acquisition 101
5.4 Overexpression of *recX* reduces the level of papillation 102
5.5 Chemical inhibition of RecA decreases the level of papillation 103
5.6 Deletion of *recA* increases the level of papillation 104
5.7 Deletion of *recA* increases the rate of spacer acquisition 105
5.8 Deletion of *recA* prevents induction of the SOS response 106
5.9 Overexpression of *sulA* in the *lexA3* background increases the level of papillation to wild type 108
5.10 Overexpression of *ymfM* increases the level of papillation 109
5.11 Deletion of *sulA* and *ymfM* does not alter the level of papillation . . . 111
5.12 Growth in sub-inhibitory concentrations of antibiotics increases the level of papillation in JB028 113
5.13 Growth in sub-inhibitory concentrations of antibiotics decreases the level of papillation in JB028 *lexA3* 114
5.14 Growth in sub-inhibitory concentrations of nalidixic acid and mitomycin C induces the SOS response 116
5.15 Antibiotics induce spacer acquisition 118

6.1 Tn5 insertion into *hflC* and *miaA* reduces the rate of papillation . . . 121
6.2 Deletion of *miaA*, *hflC* and *hflK* reduces the rate of papillation. 122
6.3 Deletion of *miaA* reduces the rate of papillation but spacers are acquired in SPIN assays 124
6.4 Deletion of *hflK* or *hlfC* inhibits adaptation 125
6.5 Complementation of *hflK* and *hflC* restores the adaptation defect phenotype 127
6.6 Overexpression of *hflKC* causes papillae to arise earlier and a higher rate of papillation 128
6.7 Overexpression of *FtsH* increases the rate of papillation 130
6.8 Overexpression of *ftsZ* decreases the rate of spacer acquisition . . . 132

7.1 Tn5 insertion into *lapC*, *rfaH*, *waaG* and *waaQ* reduces the rate of papillation 135
7.2 Truncation of *lapC* reduces the rate of adaptation 136
7.3 Deletion of *waaG* and *waaQ* decreases the rate of spacer acquisition 138

7.4 Deletion of *rfaH* reduces the rate of spacer acquisition 139
7.5 Overexpression of *lapB* reduces the rate of papillation 141

8.1 Model linking induction of the SOS response to spacer acquisition . . 145
8.2 The equilibrium of FtsH specificity factors determines the choice of substrate 150
8.3 Linking the SOS Response, HflKC-FtsH and LapB-FtsH 152
8.4 Gene Crossover Assay for Cas1-Cas2 as a DNA roadblock 156
8.5 Cell-to-cell transformation as a substrate for spacers 157
8.6 Principle of an *E. coli* two-hybrid system based on functional complementation of GFP fragments to study FtsH/HflKC and FtsH/LapB Interactions 158
S1 Control Images of BL21-AI 166
S2 Overexpression of Cas1-Cas2 from either a T7 or pBAD plasmid induces filamentation 167
S3 ClpX overexpression from a T7 promoter does not induce filamentation 168
S4 Overexpression of dCas1-Cas2 does not induce filamentation 168
S5 Overexpression of Cas1 or Cas1 does not induce filamentation . . . 169
S6 Cas1-Cas2 overexpression induces filamentation in BL21-AI *IHF*α . 170
S7 Passing cells through a 1.2 μm filter separates filamentous from rod-shaped cells 170
S8 Verification of YFP Spacer Acquisition Reporter Strain 171
S9 YFP- cells grow faster than YFP+ cells 172
S10 Deletion of *yjaB* does not alter the rate of papillation or induction of the SOS Response 173
S11 Verification of *yjaB* deletion from *lexA3* to remove the *Tn9* marker . . 174
S12 Verification of spacer acquisition in MLS989 $\triangle$*recA* 175
S13 Overexpression of *sulA* increases the rate of papillation in JB028 . . 176
S14 Overexpression of *sulA* increases the rate of papillation in JB028 *lexA3* 177
S15 Deletion of *sulA* by P1 transduction from the Keio collection abolishes papillation but complementation does not restore adaptation . . 178
S16 Papillation assays performed in the presence of sub-inhibitory concentrations of antibiotics in the $\triangle$*recA* background decreases the rate of papillation 179
S17 Overexpression of *hflK* does not increase the rate of papillation . . . 180
S18 Overexpression of *hflC* does not increase the rate of papillation . . . 181
S19 All genetic deletion strains grown on M9 minimal media agar 182
S20 Deletion of *kilR* does not alter the rate of papillation 183
S21 Deletion of *clpX* or *clpP* does not alter the rate of papillation 183

S22 Electroporation of spacer DNA and Cas1-Cas2 complex results in spacer acquisition in the CRISPR array 184

Tables

2.1 List of Strains 42
2.2 List of Plasmids 46
2.3 List of Oligonucleotides 51
2.4 List of Media 52
2.5 Concentrations of Antibiotics 53
2.6 Range of Sub-Inhibitory Concentration of Antibiotics used 53
2.7 List of Running Buffers 56

S1 Licence numbers for the reproduction of published figures in this work.161
S2 Raw Fluorescence Intensity and P Values 164
S3 Raw Cell Sorting Data 165

List of Abbreviations

a.a.	Amino acid(s)
Abi	Abortive Infection
AbR	Antibiotic Resistance
Ago	Argonaute
Amp	Ampicillin
AmpR	Ampicillin resistance
Ara	Arabinose
Avs	antiviral STAND
BME	β-mercaptoethanol
Bp	Base pair(s)
Cas	CRISPR Associated
CBASS	Cyclic-Oligonucleotide-Based Anti-Phage Signalling Systems
Cef	Cefalexin
chi	Crossover hot-spot instigator
CHIR-090	N-aroyl-L-threonine hydroxamic acid
Cm	Chloramphenicol
CmR	Chloramphenicol resistance
CRISPR	Clustered and Regularly Interspaced short Palindromic Repeats
crRNA	CRISPR RNA
CUMA	Cuminic Acid
DNA	Deoxyribonucleic acid
DOG	2-deoxy-D-Galactose
dsDNA	Double-stranded DNA
DTT	Dithiothreitol
EDTA	Ethylenediaminetetraacetic acid
frt	flippase recognition target

FLP	Flippase Recombinase
g	Gram
	Gravitational Force
GFP	Green Fluorescent Protein
IHF	Integration Host Factor
IPTG	Isopropyl β-D-1-thiogalactopyranoside
Kan	Kanamycin
KanR	Kanamycin resistance
kb	Kilobase
kDa	Kilodalton
L	Litre
LAS	Leader Anchoring Sequence
LB	Lysogeny Broth
LPS	Lipopolysaccharides
M	Molar
MDR	Multi Drug Resistant
MMC	Mitomycin C
mRNA	Messenger RNA
NA	Nalidixic Acid
NEB	New England Biolabs
O.D.	Optical Density
ORF	Open Reading Frame
Ori	Origin of replication
OriT	Origin of Transfer
PAGE	Polyacrylamide Gel Electrophoresis
PAM	Protospacer Adjacent Motif
PBS	Phosphate Buffered Saline
PCR	Polymerase chain reaction
PIWI	P-element-induced wimpy testis

PLL	N-α-palmitoyl-L-lysyl-L-lysine ethyl ester dihydrochloride
pre-crRNA	Precursor-CRISPR RNA
RBS	Ribosome Binding Site
RM	Restriction Modification
RNA	Ribonucleic acid
RNAP	RNA polymerase
RPM	Revolutions per minute
RT	Room Temperature
Sal	Salicylic Acid
SC	Supercoiled
SDS	Sodium dodecyl sulfate
ssDNA	Single-stranded DNA
Spect	Spectinomycin
SpectR	Spectinomycin Resistance
STAND	Signal Transduction ATPases with Numerous Domains
TBE	Tris-Borate-EDTA
TE	Transposon End
Tet	Tetracycline
TetR	Tetracycline Resistance
TIS	Transposon Insertion Sequencing
Van	Vanillic Acid
WT	Wild type
X-Gal	5-bromo-4-chloro-3-indolyl-β-D- galactopyranoside
YFP	Yellow Fluorescent Protein

Chapter 1

Introduction

Prokaryotes are under constant threat from bacteriophage infection and invasion by mobile genetic elements introduced by natural transformation and conjugation. This exposes them to a diverse range of genetic material that can be beneficial, for example, antibiotic resistance genes and virulence factors. However, this also makes prokaryotes vulnerable to parasitic elements that can reduce the fitness of the population. To combat the negative threat of invasion, prokaryotes have evolved innate defences such as the barrier function of the cell wall, abortive infection and restriction modification systems. In addition, many prokaryotes have an adaptive immune system called CRISPR-Cas [1, 2]. These defence systems often cluster together to create defence islands in the genome [3]. Mechanisms of defence consist of up to 10% of prokaryotic genomes [4].

1.1 Preventing Phage Adsorption

Bacteriophages initiate infection by binding to specific cell-surface receptors. These include proteins, lipopolysaccharides (LPS) and pili. Only after adsorption can the phage genome be introduced into the cytoplasm. Therefore, bacteria have evolved multiple mechanisms to avoid or reduce phage adsorption. These can be divided into three categories: blocking phage receptors, production of an extracellular matrix and use of competitive inhibitors (Figure 1.1) [5].

1.1.1 Blocking Phage Receptors

One mechanism to prevent phage adsorption is to mask the receptor. For example, TraT is a lipoprotein encoded on F plasmid that binds to OmpA to prevent phage binding in *E. coli* [6]. This method is also employed by phage T5 to prevent superinfection [7]. Expression of a phage-encode lipoprotein irreversibly binds to FhuA, the T5 receptor.

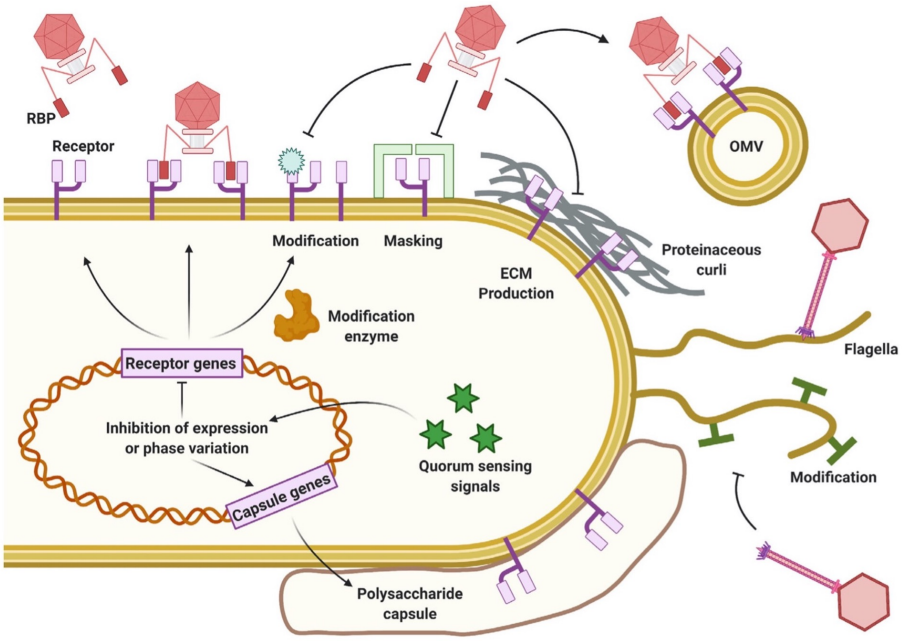


Figure 1.1. Strategies to prevent receptor recognition by bacteriophages
Taken and adapted from (Isaev et al., 2020).

Another mechanism that prevents phage adsorption is the appearance of point mutations in the cell-surface receptor. These affect the ability of bacteriophages to interact with their receptor. For example, point mutations in *E. coli* LamB give rise to resistance against phage lambda [8]. Similarly, in *Vibrio cholerae*, mutations in the OmpU protein provide resistance to vibriophage ICP2 [9]. In *Sulfolobus*, mutations in the genes encoding surface receptors provide resistance to SIRV2 infection [10]. However, point mutations may interfere with receptor function and phage can quickly acquire suppressor mutations.

Chemical modification is another way to mask receptors. For example, glycosylation of type IV pilus in *Pseudomonas aeruginosa* and of O12-antigen in *Salmonella enterica serovar Typhimurium* is used to block phage adsorption [11, 12]. Modification can be transient to generate phase variation and a heterogeneous phenotype within a bacterial population [13]. In these cases, chemical modification provides defence without compromising receptor function.

Another defence mechanism is to down-regulate the expression of the phage receptor. Quorum sensing molecules have been shown to downregulate the ex-

pression of phage-receptor-encoding genes. *N*-acyl-L-homoserine lactone (AHL) synthesis decreases bacteriophage lambda receptors in *E. coli* [14]. OmpK levels in *Vibrio anguillarum* are also regulated by quorum-sensing molecules, which is the receptor of phage KVP40 [15]. This strategy reduces the concentration of receptors when the risk of bacteriophage adsorption is highest.

1.1.2 Production of an Extracellular Matrix

Bacterial communities that form biofilms tend to be more resistant to antibiotics and viral infection [16]. Cells within the biofilm are protected by their inaccessibility. Furthermore, cells exposed on the surface are often metabolically inactive and fail to support efficient phage replication [17]. This is exemplified by curli, the amyloid fibre network in E. coli [18]. Phages fail to penetrate the biofilm because they are sequestered by binding to the fibres.

Individual cells without biofilms can express a polysaccharide capsule, which prevents the phage from interacting with its receptors [19]. For example, the overproduction of the polysaccharide colanic acid in the *E. coli* capsule is a generic defence mechanism that reduces sensitivity to a wide range of phages [20]. This is also seen in *Pseudomonas fluorescens*, where the secretion of the exopolysaccharide alginate protects against invasion by phages [21].

1.1.3 Competitive Inhibitors

Excretion of molecules into the extracellular matrix can act as decoys to prevent phage adsorption to the cell surface [22, 23]. For example, fluorescently labelled KVP40 phage has been shown to get trapped in the extracellular matrix produced by *V. anguillarum* [22]. Receptors can also be used as phage decoys. Extracellular vesicles produced by *E. coli* and *vibrio* contain surface receptors. These can be bound by phages, which causes a reduction in the environmental titer and prevents productive phage infections [24, 25].

1.2 Restriction Modification Systems

Restriction modification systems play an important role in defence against foreign genetic elements. They are found in about two-thirds of prokaryotic genomes [26]. Many species contain multiple restriction modification systems, such as *Neisseria gonorrhoeae* which contain up to 16 different systems. These restriction systems destroy foreign DNA sources after it has been injected into the host.

Restriction modification systems are generally composed of two enzymatic activities to recognise foreign DNA and destroy it [27]. A restriction endonuclease recognises a 4 - 8 bp sequence and cleaves foreign DNA. Protection of the host genome is achieved by modification. A methyltransferase transfers a methyl group to the same specific DNA sequence in the host genome [28]. Modification inhibits the cleavage of host DNA due to steric hindrance (Figure 1.2).

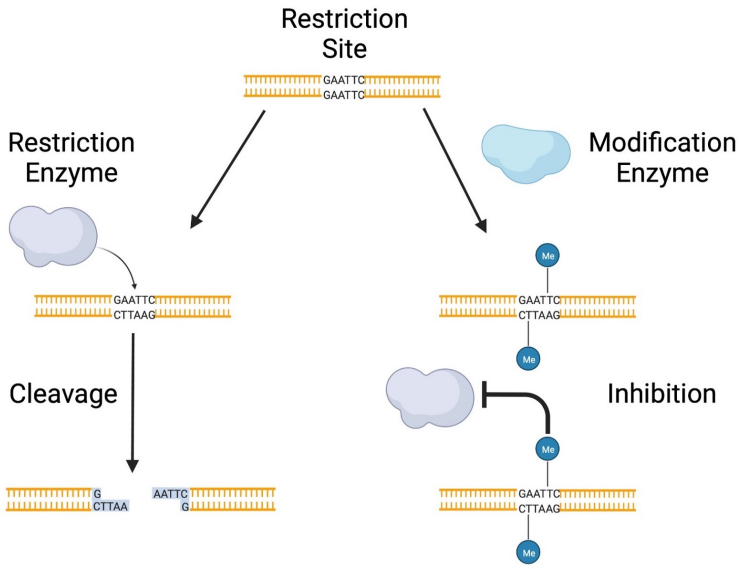


Figure 1.2. Action of a Restriction Modification System

Modification of the host genome provides defence from host restriction enzymes by steric hindrance. Unmodified foreign DNA is degraded by host restriction enzymes.

Due to the ability to distinguish between self and non-self DNA, restriction modification systems are considered primitive immune systems [29, 30]. These can provide a 10-10^8 fold protection against phage invasion [31]. Consequently, phages have evolved mechanisms to avoid degradation, such as by methylation and glycosylation of DNA [32].

1.3 Abortive Infection

Abortive infection (abi) is a strategy where the bacterial cell commits suicide when bacteriophage infection is detected. This prevents the completion of the phage life cycle. Abi is a last line of defence that is only activated at the mid or late stage of the phage life cycle if other defences have failed [33, 34].

Lambda lysogens *E. coli* contain the RexAB (Rex) abortive infection system. Activation of the Rex phenotype results in depolarization of the cytoplasmic membrane, stops cellular macromolecular synthesis, reduces cellular respiration and induces death in the majority of cells [35]. The RexA protein detects a protein-DNA complex produced as an intermediate of phage replication [36]. Two molecules of RexA then activate RexB, an inner membrane ion channel [37]. Activation of RexB causes depolarisation of the cytoplasmic membrane potential, which depletes cellular ATP and results in cell death.

1.3.1 Toxin-Antitoxin Systems

Toxin-antitoxin systems are abundant in prokaryotic genomes, with *E. coli* K12 having 33 [38]. The toxin and antitoxin are usually co-transcribed. The toxin targets an essential cellular process, which results in dormancy or death. This is neutralised by the presence of a cognate antitoxin under normal growth conditions (Figure 1.3). There are five classes of TA systems based on the mechanism of the antitoxin to inhibit the activity of the toxin molecule [39]. These can be used to maintain plasmids in the absence of selection pressure [40].

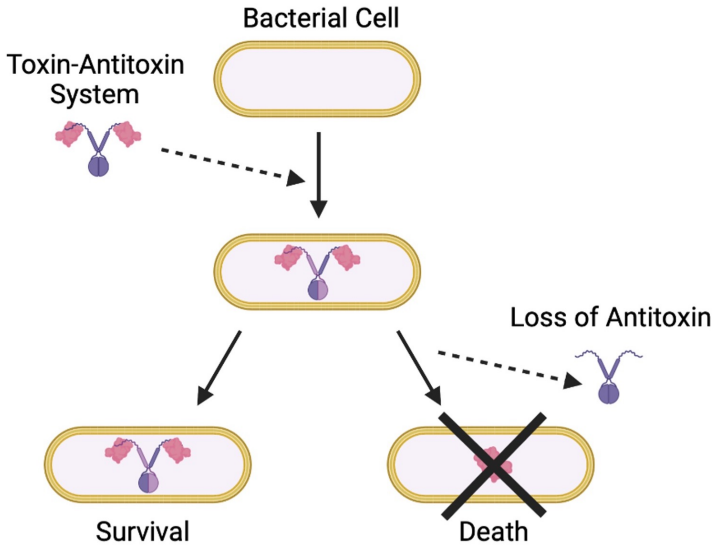


Figure 1.3. Action of a Toxin-Antitoxin System

A Toxin-Antitoxin system enters a bacterial cell and establishes itself in the lineage. The toxin is constitutively expressed and neutralized by the antitoxin. Loss of antitoxin expression triggers cell death.

Abortive infection can also be achieved through toxin-antitoxin (TA) systems. The MazEF TA system was the first to be discovered located on the prokaryotic chromosome [41]. MazF is a sequence-specific endoribonuclease that acts on ssRNAs [42]. Following activation, MazF blocks protein synthesis by cleavage of cellular mRNAs. This is counteracted by the labile antitoxin MazE [41]. The MazE antitoxin is suppressed following T4 bacteriophage infection of *E. coli*.

1.3.2 CBASS

More recently, Abi systems named Cyclic-oligonucleotide-based anti-phage signalling systems (CBASS) have been discovered [43]. These detect phage infection by an unknown mechanism. CBASS uses a cyclic oligonucleotide signalling to elicit an anti-phage response. The production of the cyclic oligonucleotide cGAMP in *V. cholerae* activates a phospholipase that degrades the inner bacterial membrane [44]. This results in the production of cGAMP, which then induces phospholipase activity and causes cell death.

1.3.3 STAND NTPases

The signal transduction ATPases with numerous domains (STAND) are large, multi-domain proteins found in all three kingdoms of life [45]. They are well characterised in eukaryotes, where they play a key role in immunity, cell signalling and programmed cell death [46, 47]. STAND NTPases have a conserved tripartite domain structure: a central NTPase domain, a C-terminal sensor and an N-terminal effector [48].

Four families of prokaryotic STAND NTPases have recently been demonstrated to provide innate immunity against bacteriophages [49]. These protect bacteria from tailed phages and are termed antiviral STAND (Avs). Avs are pattern-recognition receptors against two phage proteins: the large terminase subunit and the portal. These are two of three signature proteins of the Duplodnaviria virus realm [50]. The terminase is the motor protein that packages the phage genome into the capsid at high density and pressure [51]. It also cleaves DNA concatemers into genome-size units, so each of the progeny receives one copy. The portal protein nucleates virion assembly, provides the attachment site for the phage tail and serves as the channel for genome entry into and exit from the capsid [52]. These proteins have a highly conserved structure due to being under strong selective constraints. Avs proteins recognize the conserved structural features of their cognate targets [49]. This facilitates the ability to recognise terminase and portal proteins from both tailed phages and archaeal viruses.

Upon detection of the hallmark viral proteins, the Avs tetramerizes with the C-terminal sensor domain bound to a single target protein [49]. This activates the N-terminal effector domains as the active dimeric configuration is formed. DNA endonucleases have specific dsDNA activity but do not degrade ssDNA or RNA. Endonuclease activity abrogates infection by the induction of cell death to prevent phage propagation (Figure 1.4).

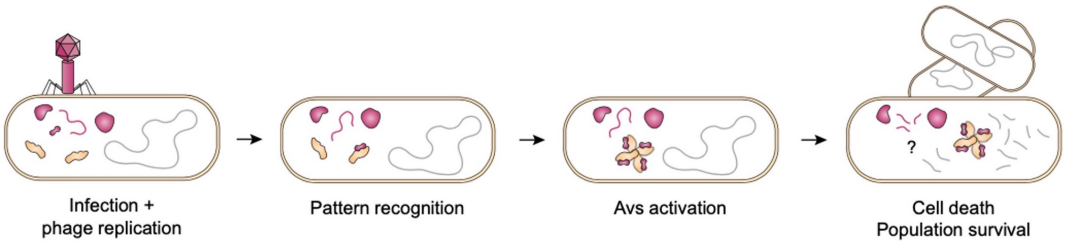


Figure 1.4. Action of antiviral STAND

Bacteriophage infection results in the injection of its genome into the host cell for replication. Target binding triggers the formation of Avs tetramers, which activates an N-terminal effector to trigger cell death. This disrupts the viral life cycle to ensure the survival of the host population. Taken and adapted from (Gao et al., 2022).

Many prokaryote genomes encode multiple different STAND NTPases [48]. Several are predicted to have a defence function due to their enrichment in genome regions adjacent to known defence systems in defence islands [53]. These have been suggested to be triggered by other pathogen-related patterns that remain to be determined [49].

1.4 Argonaute

Argonaute proteins are a family of guide-dependent nucleases present in all domains of life [54]. They are best understood in eukaryotes, where they act as a piece of the RNA interference system [55, 56]. These systems have a wide range of functions, including the formation of heterochromatin and the regulation of gene expression [57–59]. Eukaryotic argonautes bind to 20 - 30 nt 5'-phosphorylated RNAs made by the Dicer endoribonuclease [60]. When bound to its target, the argonaute protein either sequesters or cleaves the target with its PIWI endonuclease domain [56].

Argonautes were discovered within prokaryotic defence islands and are more diverse than those in eukaryotes [54]. These can target ssDNA, dsDNA or RNA [61]. pAgos use short 18-21 nt ssDNA guides to target endonuclease activity to protect the bacteria from the foreign genetic elements [62–64]. They have been shown to provide defence against both plasmid propagation and bacteriophage infection

[63, 65, 66].

Guide-free Ago attacks dsDNA to generate nicks on each DNA strand to generate fragments of various lengths [67]. Guide molecules are then selected from the pool of DNA fragments. Guide-loaded Ago then attacks complementary DNA with high efficiency and specificity to degrade the foreign genetic element.

Prokaryotic argonautes can contain inactivated PIWI domains, implying that Argoautes without endonuclease function can play a role in directing the activity of alternative effector proteins [54]. The pAgo from the *Sulfolobus islandicus* is genetically linked to the Aga1 and Aga2 proteins [68]. All three genes are required for immunity. pAgo has guide-directed target nucleic acid activity. Aga1 aids pAgo in guide and target binding. pAgo and Aga1 form a complex in the cytoplasm. Aga2 is a transmembrane protein that binds phospholipids in the membrane to result in membrane depolarization and cell death. When Ago–Aga1 complex interacts with Aga2, a ternary complex is formed to activate the abortive infection response.

1.5 CRISPR Cas

In addition to the innate defences described above, many prokaryotes have an adaptive immune system called CRISPR-Cas [1, 2]. CRISPR-Cas systems are found in the genomes of ~90 % of archaea and ~50 % of bacteria [69]. The advantage of possessing these systems is that they can make a heritable change to the host genome to provide a memory of past infections.

Small DNA fragments, known as protospacers, are captured from invading genetic elements. These are integrated into the CRISPR array, where they serve as a memory to guard against future encounters with the same element. The CRISPR array is composed of a series of fixed-length repeats and spacers [70–72]. Spacers are usually about 30 bp in length and repeat sequences that flank the spacers and are usually about 25 - 50 base pairs in length [73].

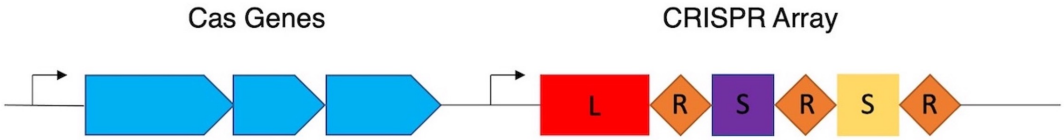


Figure 1.5. General Structure of a CRISPR locus

The CRISPR array contains consists of a leader sequence (Red) followed by regularly interspaced repeat (orange) and spacer (purple and yellow) sequences. CRISPR arrays usually co-localise with a set of CRISPR associated genes (cas) genes (blue). These genes facilitate every step of the CRISPR immune response. Promoters are represented as an arrow in the direction of transcription.

Adjacent to the array are genes encoding the Cas proteins that maintain the array and provide immunity [73] (Figure 1.5). These are separated into four different modules depending on their function: Adaptation, Expression, Interference, and Signal transduction/Ancillary [74]. The adaptation module captures and integrates new spacers into the CRISPR array. This module includes the Cas1-Cas2 proteins, which are the only genes conserved in all CRISPR systems. In addition, the adaptation module in some systems includes the Cas4 nuclease. The expression module processes pre-crRNA into mature crRNA. This can be encoded by a *Cas* gene or a host RNAse. The interference module encodes all of the genes needed to allow the crRNA to bind to its complementary DNA sequence in the invading genetic element and degrade it. Some CRISPR systems also contain a signal transduction/ancillary gene module.

To increase preference for acquisition against foreign DNA, type I and II systems use a 2-5nt protospacer adjacent motif (PAM) to identify suitable protospacers for integration [75]. This is not present in the array due to the presence of repeats, which prevents self-targeting and allows the differentiation between self and invader DNA [76]. The PAM is necessary to choose protospacers in adaptation and for target selection during interference [75, 77]. The PAM sequence directs spacer orientation in arrays [75].

The CRISPR array is transcribed and processed into CRISPR RNAs (crRNAs) in the process of expression. Each crRNA is derived from a spacer-repeat segment

[78]. The interference machinery is guided to target DNA by mature crRNA [79]. The biogenesis and maturation of crRNAs can be split into three steps [80]. A precursor CRISPR RNA transcript (pre-crRNA) is produced by transcription through the CRISPR array from a promoter found in the leader sequence. Primary cleavage follows in a sequence-specific manner inside the repeat sequence. In some CRISPR systems, a second cleavage step follows to produce mature crRNA.

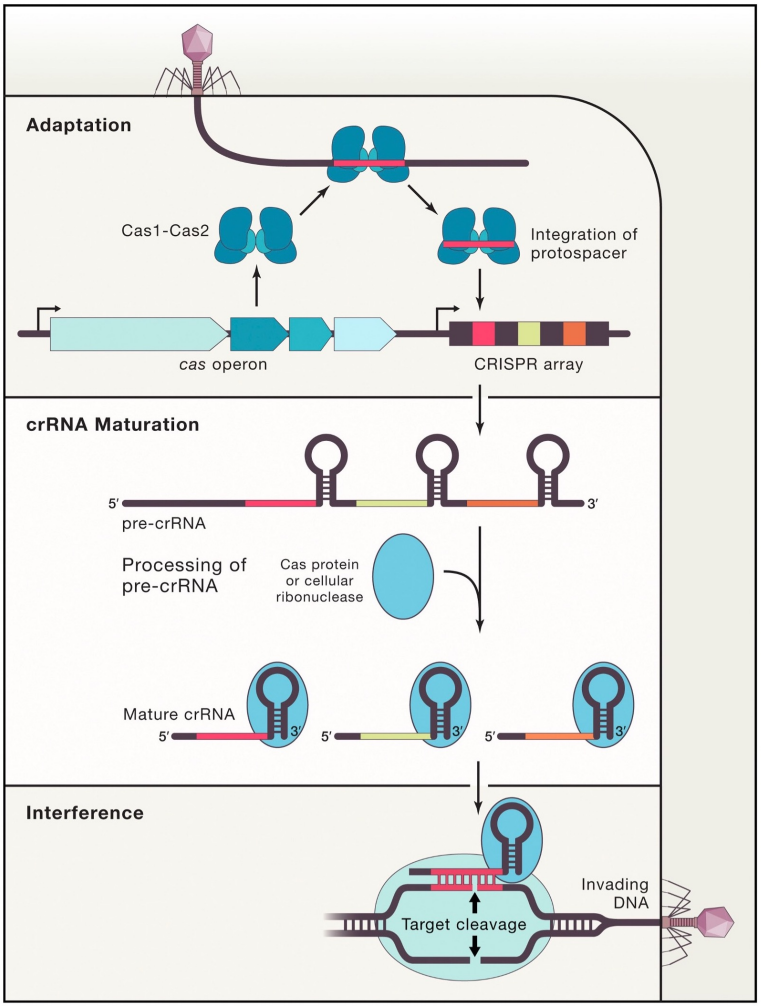


Figure 1.6. Summary of CRISPR Cas Immunity

During adaptation, the Cas1-Cas2 complex selects a part of the foreign genetic element and integrates it into the CRISPR array. In the next stage (crRNA maturation), the CRISPR array is transcribed into a long pre-crRNA that is further processed by Cas proteins or, in some cases, by cellular RNases. In the interference stage, the mature crRNAs guide Cas nucleases to the cognate foreign DNA. The Cas proteins cleave the foreign nucleic acid upon binding the crRNA to the target sequence. In class 1 systems, the interference machinery is a multi-Cas-protein complex, whereas class 2 systems utilize a single Cas protein for target cleavage. Taken and adapted from (Hille et al., 2018).

1.5.1 Interference

During Interference, crRNAs associate with Cas proteins to recognize foreign genetic elements [81]. This is achieved by base-pairing interactions between the crRNA and its complementary sequence in the invading nucleic acid. Complementarity to either the coding or the non-coding strand of the foreign DNA supports immunity. The invading genetic element is then cleaved by the effector complex to result in its destruction.

The simplest effector is the Cas9 protein. It has two nuclease domains that cleave alternate DNA strands to generate double-strand breaks. A RuvC-like nuclease cleaves the crRNA non-complementary DNA strand and a HNH nuclease cleaves the complementary strand [82, 83].

The interference enzyme in *E. coli*, Cascade, is a multisubunit complex with a seahorse architecture [84, 85]. Complex formation starts when the crRNA becomes tightly bound to Cas6 after maturation [86]. This ribonuclear complex acts as a platform for the other Cascade subunits to assemble upon [86, 87]. The 5' handle of the crRNA is bound by Cas5 and Cas7 polymerises along the backbone. Two Cas11 subunits form salt bridges with Cas7 to stabilise the complex. Finally, Cas8 binds to Cas5 at the bottom of the complex [81, 84, 88].

Surveillance of target sites for degradation is hypothesised to proceed by a 'PAM first' model [84, 86]. Cascade binds dsDNA to search for a 3 bp PAM motif needed for cleavage [87]. Following the detection of a PAM sequence, the dsDNA is unwound to allow the crRNA to bind to its complementary sequence in the target DNA. This supports efficient target screening, as the DNA that needs to be unwound by Cascade is reduced [89]. This also stops Cascade from binding spacers in the array, to prevent accidental cleavage or transcription inhibition. Interactions between Cas8 and the PAM sequence cause DNA bending, which initiates unwinding [88, 90]. This allows R-loop formation between the dsDNA target and the

crRNA. Upon full R-loop formation, Cas11 locks the R-loop in place [91, 92].

Conformational changes in Cascade during R-loop formation act as a signal to recruit the Cas3 helicase/nuclease to the target DNA [92–94]. The interaction between Cas3 and DNA is Cascade dependent [95]. When Cas3 binds to target DNA, degradation is initiated by nicking the non-target strand [96]. The nicked DNA can then be unwound by Cas3 [95]. Cas3 remains bound to Cascade and translocates along the non-target DNA strand [97]. The non-target DNA strand is fed through the Cas3 helicase domain and undergoes intermittent cleavage as the target DNA strand is extruded in a loop [89]. Further Cas3 enzymes can be recruited to the ssDNA gap to degrade the target DNA further (Figure 1.7).

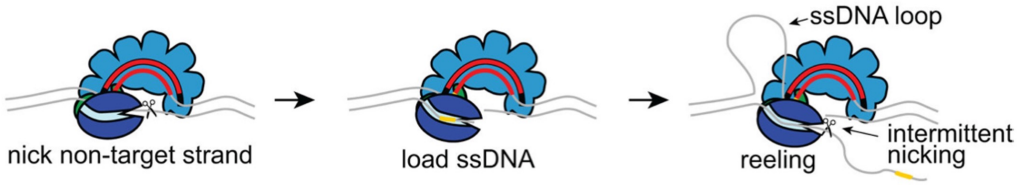


Figure 1.7. Mechanism of Cas3 cleavage

Following its recruitment to the Cascade-target DNA R-loop, Cas3 nicks the non-target strand. The nicked strand is then loaded into the Cas3 helicase domain, which stabilizes the interaction between Cas3 and Cascade. The Cas3 helicase domain then reels the non-target strand, whilst the target strand is extruded and forms a ssDNA loop. Taken and adapted from (Xue & Sashital, 2019).

1.5.2 Adaptation

Adaptation is the process where a spacer-repeat unit is added to the CRISPR array to provide a genetically encoded record of previous interactions with foreign genetic elements [98]. 80-90% of identifiable spacers match DNA sequences found in viral genomes [99]. Spacers are added at the leader end of the array [1]. The leader-proximal repeat is used as the template for duplication, with a single repeat being sufficient for spacer acquisition [100, 101]. In the type II-A system of *Streptococcus pyogenes*, expression of the crRNA of the first spacer in the array is twice as

abundant as the fifth [102]. This allows the CRISPR Cas system to defend the cell from the most recent invading foreign genetic element, which poses the greatest threat. Only the final step of integration is fully understood. The earlier steps by which prespacers are generated and processed are less well known.

The Cas1-Cas2 complex catalyzes adaptation with the assistance of other host factors [100, 103, 104]. When a spacer is inserted into the CRISPR locus from a foreign DNA element that it has not been previously encountered, it is termed naïve adaptation. Naïve adaptation is rare, measured at only 1 in 10^7 infected cells in the type II-A system of *Streptococcus pyogenes* [102].

Point mutations in the protospacer or PAM are known as escape mutants since they protect nucleic acids from destruction [105–107]. This leads to primed adaptation, where new spacers are acquired from the vicinity of crRNA targets of pre-existing spacers in the array. Primed adaptation is a positive feedback loop, which is >500 times more efficient in type I-F systems and >1000 times more efficient in type I-E systems than naïve adaptation [108–110]. New spacers can be either up or downstream of the escape target, over 100 kb from the protospacer [110, 111]. Primed adaptation is robust and can tolerate 13 mutations in the PAM and protospacer in the type I-E system [107].

Primed adaptation is a system that has evolved to overcome the cost associated with the loss of efficiency of interference [112]. Rapid degradation observed in interference does not support priming [113, 114]. Mutations in either the protospacer or the PAM reduce effector complex affinity [106]. This still supports R-loop formation, Cas3 recruitment and degradation, but at a reduced rate [112, 114]. The reduced cleavage rates mean that DNA substrates persist for longer durations, increasing the time for the Cas1-Cas2 complex to catalyse adaptation.

Around 90% of spacers acquired in primed adaptation are complementary to the priming protospacer strand, with the majority of primed spacers having an AAG PAM in the type I-E system [105, 107, 108, 115]. In primed adaptation, spacers with the consensus PAM sequence in the protospacer are strongly selected against, unlike in naïve adaptation [116].

The CRISPR adaptation module is believed to have evolved from a type of transposon, casposons [117, 118]. Some casposons also encode Cas4, another nuclease involved in the adaptation process of many CRISPR Cas systems [119]. The mechanism of adaptation mirrors the biochemistry of the DD[D/E] family of transposons, where the enzyme uses the 3'-OH of the donor DNA to make a staggered cut and joins the donor to the target DNA at the 5' phosphate [120].

Directly upstream of the CRISPR array is an AT-rich Leader sequence which typically spans 100-300 bp [73]. It encodes promoters for transcription of the CRISPR array [73, 103, 121]. There are also elements in the Leader sequence to guide the integration of new spacers [100]. These are recognised by Cas proteins and cellular host factors [122, 123]. Truncation of the Leader sequence to remove these elements significantly decreases the rate of spacer integration [122].

1.6 Cas1-Cas2

Cas1 and Cas2 are conserved across all CRISPR systems, except the type IV [74]. In the type I-E system of *E. coli*, overexpression of both these proteins results in naïve adaptation *in vivo* [124]. Other systems require accessory factors for adaptation, such as Cas9 and Csn2 in the type II-A system of *S. thermophilus*, Cas2/3 and Csy complex in the type I-F system of *P. aeruginosa* and Cas4 and Csa1 in the *S. islandicus* I-A system [103, 104, 125, 126].

Cas1 and Cas2 form a heterohexameric complex ($Cas1_2$-$Cas2)_2$ (Figure 1.8) [127, 128]. Cas1 functions as the integrase that catalyses spacer integration [129]. The nuclease activity of Cas1 is needed for spacer acquisition, as nuclease-deficient

mutants do not facilitate adaptation *in vivo* [130]. Cas2 stabilises prespacer binding and controls its length [127]. Cas2 active site mutants undergo adaptation, but deletion of the C-terminal region of Cas2, which interacts with Cas1, prevents spacer acquisition as the complex is unable to form [129].

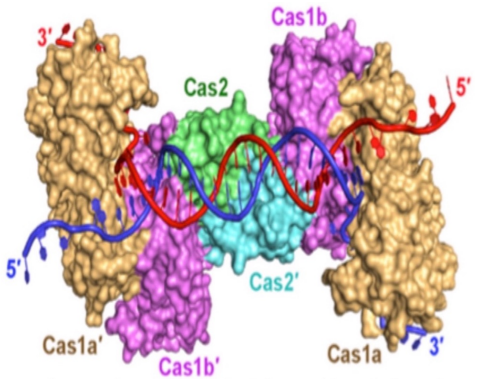


Figure 1.8. Crystal Structure of the *E. coli* Type I-E Cas1-Cas2 Complex

Protospacer DNA is shown in red and dark blue. Cas1 is shown in brown and purple. Cas2 is shown in green and light blue. The protospacer DNA is stabilised by Cas2 and its length is selected at 23 bp. The 3' overhangs are threaded through the C-terminal domain of Cas1a. Taken and Adapted from (Wang et al., 2015).

The preferred integration substrate in the type I-E system is a 23 bp duplex with 5 nt overhangs on the 3' end of each strand [127, 131]. The binding of the protospacer enhances the affinity of the Cas1-Cas2 complex to the CRISPR array [132]. Full-site integration needs two transesterification reactions, with the 3'-OH of each end of the protospacer attacking the 5' border of the repeat in a nucleophilic reaction catalysed by the Cas1-Cas2 complex [120, 121, 127, 131, 133]. Half-site recognition arises sequentially, as the two active sites are unable to access the DNA simultaneously [134]. There is a structural rearrangement in Cas1-Cas2 when it is bound by the protospacer that enables the search for integration sites [127, 135]. A Cas1 dimer rotates clockwise and the other anticlockwise to generate a flat surface in the complex that binds the dsDNA. The 3' strands of the protospacer are threaded through the C-terminal domain of Cas1a [127]. When a PAM-complementary protospacer is bound, this is stabilised by the tail of Cas1b. This covers the catalytic pocket of Cas1a, meaning the initial integration event is of

the non-PAM strand at the leader-repeat border [131, 133]. The PAM-derived ss-DNA end is then integrated at the spacer-repeat border. This mechanism helps to ensure the correct orientation of spacer integration. The Cas1-Cas2 complex then disengages from the CRISPR array by an unknown mechanism. The gaps following integration are filled by host DNA repair enzymes [136] (Figure 1.9).

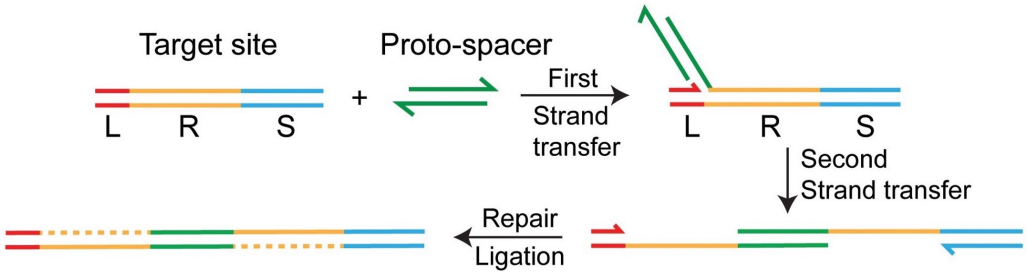


Figure 1.9. Mechanism of Spacer Integration into the CRISPR Array

Illustration of protospacer (green) integration into a minimal CRISPR locus comprised of the leader (L, red), repeat (R, yellow), and spacer (S, blue). The protospacer is integrated at the leader-repeat border. The reaction follows the cut-and-paste DNA transposition mechanism with a duplication of the repeat sequence. The 3'-hydroxyls that perform nucleophilic attacks at the L-R junction (top strand) and the R-S junction (bottom strand) are indicated by the split arrowheads.
Taken and Adapted from (Ma et al., 2021).

1.7 Location of Integration

Spacer acquisition arises at the leader-repeat border [100]. In the type I-E system, Integration Host Factor (IHF) is essential for adaptation *in vivo*, as it guides the Cas1-Cas2 complex to the leader-repeat of the array [123]. There is a binding site for IHF in the leader sequence of the CRISPR array [137, 138]. This is present in the 60bp segment of the CRISPR I leader in BL21 *E. coli* [100]. The CRISPR II array in BL21 has no A-T rich leader sequence, so it does not acquire spacers *in vivo*. Placing the CRISPR I leader with the IHF binding site upstream of the CRISPR II array allows adaptation in the presence of IHF [123].

IHF is a heterodimeric protein made up of IHFα and IHFβ subunits which share ~30% sequence identity [139]. IHF binds tightly to the minor groove of DNA regions

with the 13-bp consensus sequence and A/T-rich elements upstream [140, 141]. The α subunit recognises the consensus sequence and the backbone of each subunit acts as a clamp to bind across the minor groove [139, 142]. The distortion in the DNA is stabilised by multiple hydrogen bonds with the body of IHF.

IHF binding the leader sequence causes DNA to bend 120°, resulting in a reversal of the direction and a distortion in the DNA (Figure 1.10) [137, 138]. Cas1-Cas2 makes protein contacts with IHF and sequence-specific interactions up- and downstream to catalyse the first step of the reaction [137]. This targets the Cas1-Cas2 complex to this locus, helping to catalyse the nucleophilic attack of the integration reaction at the leader-repeat border and ensure the polarised addition of spacers into the array [137, 138]. IHF also promotes integration with specificity at the leader-repeat boundary in the type I-F system [128].

In vitro, IHF is required for integration into linear DNA [123]. Supercoiled DNA undergoes integration *in vitro* in the absence of IHF, adjacent to every repeat in the CRISPR array [120]. The addition of IHF helps to control the site of integration, resulting in ~80% integration at the first repeat in the supercoiled plasmid substrate [123].

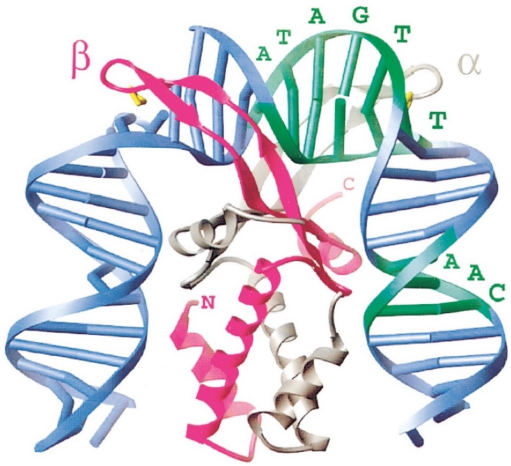


Figure 1.10. IHF binds DNA to induce DNA bending

The DNA is shown in blue and green. IHFα is shown in grey and IHFβ is shown in pink. Taken and adapted from (Rice et al., 1996).

IHF is only found in Gram-negative bacteria [143]. In type II systems, no additional host factors are required to support spacer integration by the adaptation machinery [144]. The Cas1-Cas2 complex from the type II-A system in *Streptococcus pyogenes* catalyses integration *in vitro* with a profile that resembles the type I-E system of *E. coli* in the presence of IHF [144]. A leader-anchoring site (LAS) is present in type II systems which guides the site of integration [102]. This is located adjacent to the first repeat of the array and includes $\leq$ 6 nucleotides of the repeat [101, 102]. Mutation of the first two nucleotides of the array does not support spacer acquisition [101]. The addition of an additional LAS in the middle of the array results in adaptation downstream of both sequences [101]. Deletion of the LAS results in non-polarized ectopic integration downstream of a spacer with a pseudo-LAS sequence [102]. The type II-A Cas1-Cas2 complex of *E. faecium* makes frequent contact with every repeat in the array, but only dwells long enough at the leader repeat to support productive integration [135].

An α-helix from Cas1 binds to the DNA in a sequence-specific manner in the Leader sequence [134, 144]. This positions the spacer in the correct orientation so that additional host factors are not required. The initial integration event in the first step of the reaction can happen at either end of the repeat, but extra contacts with the Leader sequence favour faster integration at the leader-proximal end [144].

1.8 Choice of Substrate for Spacers

Cas1-Cas2 from the Type I-E system has a preference for plasmid-derived spacers, although chromosomal DNA is present in ~25-50X excess [100]. Overexpression of Cas1-Cas2 from a plasmid results in 22% of spacers being chromosome-derived, but leaky expression reduces this to just 2% [145]. This shows a 100 - 1000 X preference for plasmid DNA, but also that a lower expression level of Cas1-Cas2 increases specificity for foreign genetic elements. However, this may be an under-representation, due to the negative effects that may result from the acquisition of

spacers from the chromosome [146]. Any self-derived acquisition events that result in cell death will not be revealed and consequently will increase the apparent preference for plasmid-derived spacers.

The preference for acquiring spacers from foreign genetic elements might be explained by a model where Cas1-Cas2 has a preference for stalled replication forks as a template [145]. During replication of the bacterial chromosome, two replication forks travel in opposite directions from the oriC to the Ter. Plasmids replicate unidirectionally so will only have one replication fork. However, as the majority of replication forks will be present on multi-copy plasmids, the majority of stalled replicated forks will be present on multi-copy plasmids, meaning that the probability of acquiring chromosomal-derived spacers is significantly lower compared to plasmids.

The RecBCD complex is proposed to play a role in the generation of prespacers for naïve adaptation in Gram-negative organisms [136, 145]. When there is a dsDNA break, RecBCD binds to the exposed end to unwind and degrade the DNA until a Chi site is reached, where activity is stopped [147]. Chi sites arise on average every ~5kb in the *E. coli* chromosome. Deep-sequence analysis of acquired spacers shows protospacer hotspots are located between stalled replication forks and Chi sites, suggesting that the fragments produced by RecBCD degradation are used as a template by Cas1-Cas2 for adaptation (Figure 1.11) [145]. In the absence of either RecB, RecC or RecD, spacers are still acquired, but at a lower rate and with ~ten times greater preference for chromosome-derived DNA [145]. This shows there must be other pathways to produce prespacers.

Restriction nucleases can also provide a substrate to generate protospacer DNA [148]. This generates free DNA ends in the phage genome, which can act as substrates for protospacers [31, 149]. Infection with a combination of modified and unmodified phage increases CRISPR-resistant survivors proportional to the amount of restriction-sensitive phage [150]. Restriction nucleases protect against phage

infection before methylation (Section 1.2) [148]. This activity stimulates spacer acquisition as soon as 30 minutes after infection. Spacers are acquired from both sides of the cleaved DNA, which can be further processed by the host's DNA repair enzymes, for example, RecBCD in *E. coli*. This generates a hotspot between the restriction site and the first Chi site.

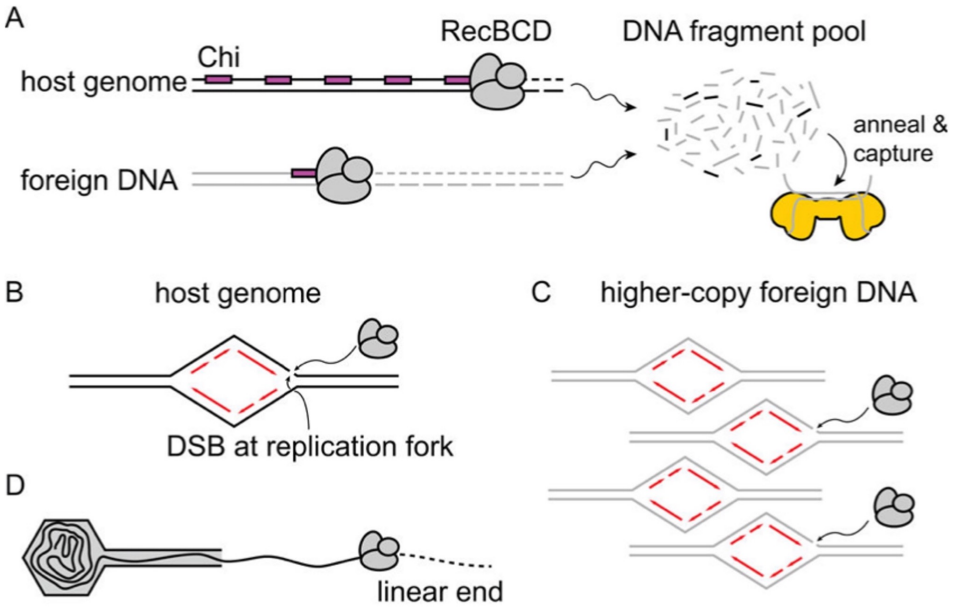


Figure 1.11. The nuclease activity of RecBCD explains the preference for spacer acquisition from foreign genetic elements during naïve adaptation

(A) Chi sites (magenta) lower the frequency of RecBCD cleavage. Chi sites are more frequent on the host chromosomes than on foreign DNA. This leads to a higher frequency of spacer substrates for the Cas1-Cas2 complex (yellow) originating from foreign DNA.
(B) DNA replication can produce stalled replication forks, which are common sites for double-strand breaks (DSBs) which are RecBCD targets.
(C) Foreign DNA replicates more frequently, which leads to more DSBs and more RecBCD recruitment.
(D) Phage DNA is injected as a linear species. RecBCD can only degrade linear DNA, so this injected DNA is targeted.
Taken and Adapted from (Xue & Sashital, 2019).

1.9 Classification of CRISPR Cas Systems

CRISPR systems are classified according to their *Cas* genes, which mainly reflect the mechanism of interference [151]. Each of the six different types uses functionally distinct effector complexes to degrade foreign nucleic acids. CRISPR systems can target either DNA, RNA or both. Class I systems have a multi-subunit effector, such as Cascade in *E. coli*, while Class II systems have a monomeric effector, such as Cas9 in *S. pyogenes*. The classes are then divided into types and subtypes based on their effector complexes and ancillary genes linked to the Cas-CRISPR loci [74] (Figure 1.12).

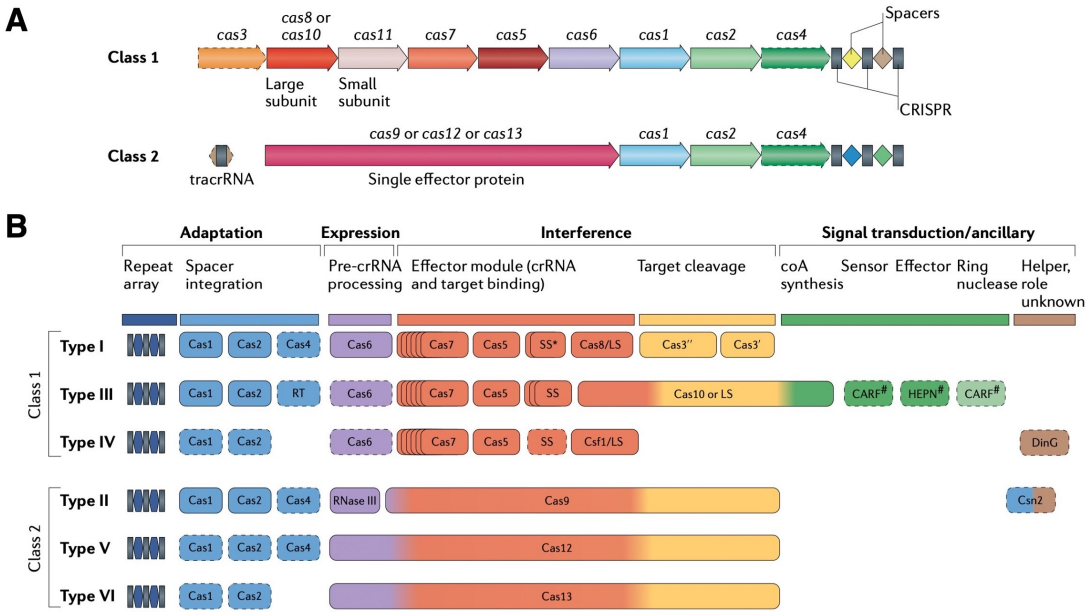


Figure 1.12. Classification of CRISPR systems

(A) CRISPR systems are classified into two classes depending on the architecture of their interference machinery. Class 1 systems have a multi-subunit interference complex. The interference machinery of Class 2 systems is comprised of a single enzyme.
(B) There are six types of CRISPR systems, each composed of a unique complement of *Cas* genes. *Cas* genes are labelled with the current nomenclature, and dotted lines indicate where *Cas* genes of a given system are not always present. Taken and adapted from (Makarova et al., 2020).

1.9.1 Class I, Type I CRISPR Systems

The type I CRISPR Cas system is the most abundant in nature [74]. These are made up of nine subtypes, I-A - I-F with I-F a combination of three more subtypes (1,2,3). Type I systems contain the Cas3 HD nuclease/helicase.

The multi-protein effector complex of type I systems is named Cascade (Cas complex for antiviral defense). The type I-E Cascade consists of five Cas proteins (Cas5, Cas6, Cas7, Cas8 and Cas11) at different stochiometry. Cas6 processes pre-crRNA into mature crRNA. Cas6 then binds the 3' hairpin of the crRNA with Cas5 holding the 5' handle. Cas7 provides the backbone of Cascade along the length of the crRNA. Cas11 stabilises the R-loop formed between the crRNA and the target DNA strand. Cas8 recognises the PAM sequence and recruits Cas3 [152]. When activated, Cas3 processively cleaves the target foreign DNA.

Type I systems are diverse. Two type I-F systems have a Cas2-3 protein fusion [69]. This shows the importance of Cas3 in the production of new spacers for integration [69, 128]. Type I-B and I-F systems have been discovered inside Tn7-like transposons [153]. Cas3 is absent in these systems, so they are presumed to be interference deficient. They have been shown to perform alternate roles, such as in the RNA-guided transposition of mobile genetic elements [154, 155].

1.9.2 Class I, Type III CRISPR Systems

Interference in type III systems is dependent upon the transcription of the target DNA [156–158]. The effector complex binds to mRNA and tethers itself to the transcription bubble. When bound, the Cas10 HD nuclease domain is activated and cleaves nearby foreign DNA [156, 159].

Type III systems do not use the PAM-based mechanism to differentiate between foreign and host DNA [160]. Extended base pairing between the 5' handle of the crRNA and the CRISPR repeats protects from autoimmunity [76]. This switches off

interference, presumably by inhibiting nuclease recruitment. DNA cleavage, however, requires the presence of a short sequence adjacent to the target sequence in the activating target RNA, i.e. an RNA PAM [158].

There are six subtypes of Type III CRISPR systems, which contain two families of effector complexes: Csm and Cmr. The structures of typical Type III effector complexes are similar to that of Cascade [81, 161]. Cas10, the type III large subunit, binds to the complex in a position analogous to Cas8 in Cascade. The backbone of the effector complex consists of the Cas5 and Cas7 family proteins. However, there are distinct differences in their function and composition. Type III systems rely on the crRNA processing activity of neighbouring CRISPR loci. Only one of the subtypes contains a Cas6 protein and this does not interact with the main effector complex [161]. The Csm and Cmr complexes are capable of both DNA and RNA degradation so they do not require the recruitment of additional nucleases, like Cas3 with Cascade [162–164].

Type III systems utilise unique signalling systems [165, 166]. RNA binding activates the Palm polymerase domain of Cas10 in subtype IIIA/B/C systems to produce cyclic oligonucleotide second messengers. These activate the nonspecific RNases, Csm6 and Csx1.

1.9.3 Class I, Type IV CRISPR Systems

Type IV systems include CRISPR arrays but typically lack the *Cas1* and *Cas2* genes and an associated nuclease for target cleavage [69]. This implies that type IV systems do not provide adaptive immunity by the same mechanism as other CRISPR systems. There is a positive correlation between the presence of type IV-A and type I-E systems in the same host, which suggests that the adaptation machinery from other systems may be utilised to perform spacer acquisition [167, 168]. They could have been recruited for alternative functions or adaptive immunity not involving target cleavage [169].

There are three subtypes of type IV CRISPR Systems [74]. These are primarily located on plasmids [151]. Many spacers present in type IV CRISPR arrays are complementary to DNA sequences found in other plasmids, with conjugation apparatus components being particularly common targets [168, 170]. Consequently, they appear to play a role in plasmid competition [167].

1.9.4 Class II, Type II CRISPR Systems

Cas9 is the effector protein of Type II systems. It recognises and binds to the pre-crRNA before RNase III is recruited to produce a mature crRNA [171]. Cas9 has two nuclease domains that cleave alternate DNA strands. A RuvC-like nuclease cleaves the crRNA non-complementary DNA strand and a HNH nuclease cleaves the complementary strand [82, 83].

The type II loci also encode a trans-acting CRISPR RNA (tracrRNA) [172]. These are characterized by complementarity to the repeat region of crRNA precursor transcripts [171]. The tracrRNA directs the maturation of crRNAs by the activities of RNAse III endonuclease. This is needed as the repeat sequences are only weekly palindromic, so they do not form the stem-loop structures that support Cas6-like cleavage of pre-crRNA within the repeats of type I systems [172, 173].

Adaptation in type II systems requires the use of two additional proteins to Cas1-Cas2, Csn2 and Cas9 [103, 104]. Csn2 interacts with both Cas1 and Cas9 to link the adaptation and interference machinery [174, 175]. During naïve adaptation, Cas9 recognises the PAM sequence in type II systems [104]. The nuclease domains of Cas9 are not required for spacer acquisition, but the substrate of spacers changes [103, 104].

1.9.5 Class II, Type V CRISPR Systems

Cas12 is the effector protein of type V systems. It employs a different interference mechanism from that of Cas9. A single RuvC domain cleaves both strands of the target DNA [176, 177]. Cas12 can then indiscriminately chop up ssDNA when activated by a target DNA molecule complementary to its spacer sequence [178].

Cas12 also contains RNAse activity to process precursor crRNAs into mature crRNAs [177, 179]. It cleaves in the repeat region with a sequence- and structure-dependent mechanism [177]. Both the RNAse and DNAse activities of Cas12 are highly specific, only cutting RNA or DNA respectively.

1.9.6 Class II, Type VI CRISPR Systems

Type VI CRISPR systems exclusively target RNA. Their effector arm, Cas13, has two higher eukaryotes and prokaryotes nucleotide-binding (HEPN) ribonuclease domains [180]. Cas13 contains a nonspecific RNase activity which is activated after the crRNA binds its target [181]. The crRNA needs to bind to two regions in the target RNA to initiate cleavage [182]. Once activated, Cas13 degrades all nearby RNA regardless of the sequence [181]. Therefore, the defence strategy of type VI systems seems to link adaptive immunity with programmed cell death or induction of dormancy.

Cas13 can process crRNA using a distinct ribonuclease domain away from the HEPN domains [183]. It cleaves in the repeat region in both a structure- and sequence-dependent manner [182, 184]. Pre-crRNA processing proceeds via a metal-independent mechanism, whereas target cleavage requires a divalent cation [182, 184].

1.10 Regulation of Cas gene Expression

When challenged by foreign genetic elements, CRISPR-Cas systems provide an effective defence mechanism that can be passed on to future generations. When unchallenged, the CRISPR-Cas immune response is likely a burden to the host, primarily due to the threat of a cytotoxic autoimmune response [185]. There is a balancing act between the benefits that these systems provide and the possible negatives. Constitutive defence systems, such as cell surface modifications, are always active, so they pose a constant deleterious fitness effect, regardless of whether they are needed [5, 186]. Inducible defence systems, such as CRISPR Cas, only impose a fitness cost when active [186]. This allows the fitness cost to be ameliorated when the systems are not expressed but provides immunity when infection risk is greatest. A combination of CRISPR-Cas and restriction modification systems provide multiple orders of magnitude increases in defence against phage infection [187].

Analysis of the spacers present in CRISPR arrays of 330 species of bacteria and archaea revealed that only 0.4% are self-targeting [146]. Interestingly, the CRISPR repeats on either side of the self-targeting spacer are twice as likely to contain mutations, presumably to counteract the negative self-targeting effects [146]. The presence of interference-deficient dCas9 increases self-targeting acquisition events to 96% in *S. thermophilus* [103]. This implies that self-targeting spacer acquisition is more prevalent, but selected against due to interference. Regulation of expression reduces the likelihood of acquiring chromosome-derived spacers and the risks of autoimmunity. The self-targeting spacers present probably play a role in other functions of CRISPR Cas systems separate from immunity, such as transcriptional regulation and mRNA cleavage [185]. This is reviewed in detail by Wimmer & Biesel, 2020 [185].

Expression of CRISPR Cas systems imposes a metabolic cost to the host [186, 188]. The effector protein Cas9 is expressed constitutively in *S. thermophilus*,

which results in a fitness cost, shown by a shorter lag growth phase in a Δ*cas9* mutant [188, 189]. However, there is not a difference in maximum growth rate. Overexpression of *Csa3a*, which activates the CRISPR Cas system in *Sulfolobus islandicus*, results in a reduced growth rate compared to the parental wild-type and knock-out strains [190]. Expression of *Cas1* in *Mycobacterium tuberculosis* reduces tolerance to environmental and antibiotic stresses [191]. Consequently, tight regulation of expression is required to ameliorate the associated fitness costs in the absence of infection risk. Constitutive defences are selected for when infection risk is high, as the fitness effects of CRISPR Cas systems are too great [186].

Additionally, 80% of genomes with CRISPR-Cas systems contain spacers that target integrative conjugative elements (ICEs) [192]. ICEs play a role in adaptation to new environments as a source of horizontal gene transfer. This is shown by a significant negative correlation between the presence of novel antibiotic resistance and CRISPR-Cas loci discovered in *Enterococcus faecalis* [193].

Consequently, the regulation of CRISPR Cas systems is necessary for the survival of prokaryotic populations. Below, I detail the best-studied transcriptional regulators of CRISPR-Cas gene expression (Figure 1.13):

1.10.1 H-NS and LeuO

HNS is a global transcriptional silencer, which plays a key role in the organisation of the chromosome in bacteria [194–196]. Approximately 5% of genes in *E. coli* are under its regulation [197]. H-NS preferentially binds to DNA sequences that are AT-rich, such as the CRISPR leader sequence [73, 198]. When H-NS binds to target sites, the DNA is condensed to form looped structures of DNA-protein-DNA bridges [199, 200]. Condensation of DNA sequesters promoters from host RNA polymerases to inhibit gene expression [201]. An AT-rich region upstream of *Cas3* in *E. coli* was determined to be a H-NS binding site [202]. Consequently, H-NS represses the expression of both the *Cas* genes and their cognate crRNAs. A

similar repression mechanism has been identified in *Salmonella enterica Serovar Typhi* [203].

H-NS-mediated repression of the CRISPR locus is antagonised by LeuO in both *E. coli* and *Salmonella enterica Serovar Typhi* [203, 204]. LeuO is a member of the LysR family of transcription regulators that regulates 140 genes in *E. coli* [205, 206]. LeuO binds to the intragenic DNA region upstream of *Cas8* to induce *Cas* gene expression [204]. LeuO does not alleviate H-NS repression when H-NS is already bound. Instead, LeuO binds and prevents the cooperative polymerisation of H-NS.

1.10.2 CRP-cAMP

The catabolite repressor protein (CRP) is a transcription factor that binds DNA regulatory elements in the presence of its allosteric regulator, cAMP, to regulate the transcription of several genes [207]. The cAMP signalling molecule is synthesised by adenylate cyclase in response to low glucose concentrations. CRP binds to the *Cas8* promoter in *E. coli* to repress the Cas operon in the absence of glucose [208]. The recognition sites of LeuO and CRP overlap. Consequently, CRP competes to prevent LeuO-mediated expression of the *Cas* genes when cellular glucose concentration is low.

CRP is an activator of the *Cas* gene expression in *T. therophilus*, but not the crRNA of the I-E and III-A systems [209, 210]. Similar findings were presented in *P. atrosepticum* [211]. CRP-cAMP binds to the *Cas1* promoter to induce the expression of *Cas1* and a *Cas2-3* fusion protein of the type I-F system.

Differential regulation of Cas gene expression by CRP appears paradoxical. This may result from the different growth requirements of the host [211]. Further investigation is needed to resolve this.

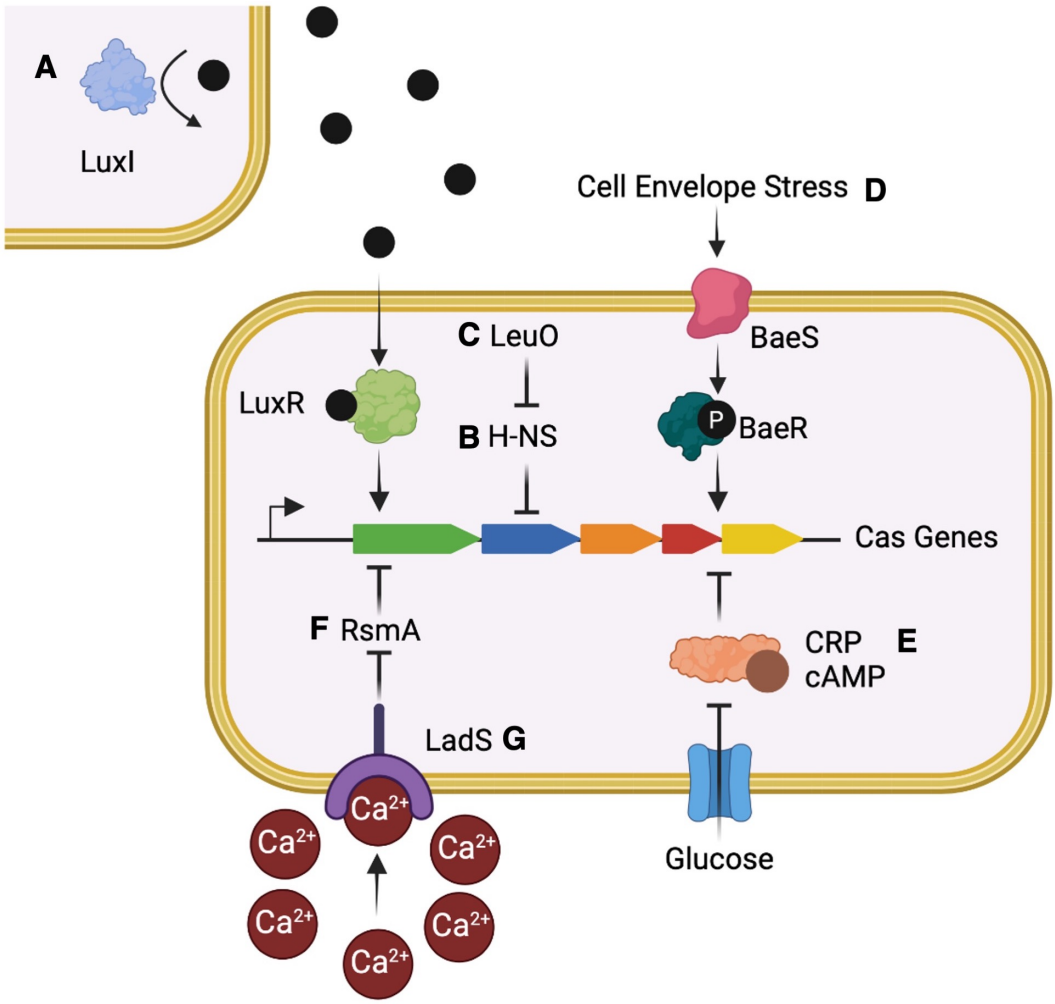


Figure 1.13. Mechanisms of CRISPR regulation

(A) The *Cas* genes are induced at high cell density due to LuxI/LuxR quorum sensing. LuxI (blue) synthesises the AHL (black) signalling molecule. High concentrations of AHL activate the LuxR (light green) transcription regulator. Activated LuxR induces *Cas* gene expression. (B) H-NS polymerization represses the *Cas* genes. (C) LeuO can inhibit H-NS repression. LeuO binds upstream of *Cas8* to prevent H-NS polymerisation. (D) Cell envelope stress activates the BaeS histidine kinase (pink). BaeS phosphorylates BaeR (dark green), which binds upstream of *Cas8* to upregulate *Cas* gene expression. (E) CRP (orange) is activated by cAMP (brown) and binds upstream of *Cas8* to inhibit *Cas* gene expression. The presence of glucose inhibits cAMP synthesis. (F) RsmA binds to cas mRNAs to decrease their expression. (G) In the presence of calcium, the activity of RsmA is antagonised by the calcium-responsive kinase LadS (purple).
The bent black arrow represents the Cas promoter, pointing in the direction of transcription. Straight black arrows indicate expression induction. Lines with bars indicate repression of expression.

1.10.3 BaeSR

BaeSR is a two-component regulatory system activated under cell envelope stress [212, 213]. BaeS is a membrane histidine kinase that phosphorylates BaeR. When phosphorylated, BaeR acts as a transcriptional activator to induce target gene expression. Detection of membrane stress upregulates *Cas* gene expression by binding upstream of *Cas8* [214, 215]. Phage infection has been shown to induce membrane stress in *Lactococcus lactis* [216]. Therefore, the *Cas* genes are likely to be expressed by the activity of BaeSR after phage injection due to the induction of the cell envelope stress response.

1.10.4 Iron Transport System

The CRISPR Cas system in *Pseudomonas PA14* is under the control of an iron-dependent regulatory mechanism [217]. The extracytoplasmic sigma factor PvdS forms a complex with the Core RNA polymerase to bind to one of two binding sites in the *Cas1* promoter to induce cas operon expression [217, 218]. In a $\triangle$*pvdS* mutant, primed adaptation is ~60% of wild type in the CRISPR II array in iron-depleted conditions [217]. However, in the presence of iron, there is no difference.

In the presence of iron, Fur represses the expression of *pvdS* by blocking access to the promoter [219]. This prevents activation of the *pvdS* target genes. *Fur* mutation upregulates *Cas* gene expression in both iron-depleted and normal conditions [217]. Therefore, $\triangle$*fur* derepresses *pvdS* to allow *Cas* gene expression.

TonB-dependent transporters are expressed in iron-limiting conditions to aid in iron uptake [220]. Bacteriophage target these to inject their nucleic acids during infection [5]. Coupling expression of the CRISPR Cas system and iron uptake mechanisms is an adaptive response to provide adaptive immunity from phage invasion when risk is high. The upregulation of CRISPR Cas systems is a pre-emptive measure to deal with bacteriophage infection.

1.10.5 Quorum sensing

The risk of infection for a bacterium is proportional to the density of the culture. In a sparsely populated community, the risk of phage infection is low. Consequently, the metabolic burden of expressing inducible defence systems outweighs the protection benefits. Therefore, defence systems are expressed in relation to the density of the culture [14].

Quorum sensing (QS) is a bacterial signalling system that changes gene expression following changes in population density. A signalling chemical, called an autoinducer, is excreted by the bacteria. As the population density increases, the concentration of autoinducer increases. Once the autoinducer crosses a threshold concentration, gene expression patterns change. The primary QS system of gram-negative bacteria is LuxI/LuxR [221].

The expression of CRISPR Cas systems in *Serratia* are regulated by QS pathways [222]. *Serratia* contains the LuxIR homologues SmaI and SmaR [223]. SmaI synthesises the autoinducer N- butanoyl-L-homoserine lactone (C4-HSL) molecule [224]. The expression of the *Cas* genes are significantly increased in the type I-E, I-F, and III-A CRISPR systems of *Serratia* upon reaching the threshold concentration of C4-HSL [222]. SmaR is a repressor of *Cas* gene expression, but when it forms a complex with C4-HSL, it is unable to bind to DNA [222].

QS systems also regulate *Cas* gene expression in *P. aeruginosa PA14*. LasI synthesises the autoinducer 3-oxo-C12-homoserine lactone (3OC12-HSL), which activates LasR to induce target gene expression. RhlI produces the autoinducer C4-homoserine lactone (C4-HSL), which activates gene expression by RhlR. The deletion of both *lasI* and *rhlI* results in a significant decrease in *Cas3* expression [225]. This provides good evidence that both QS systems regulate the expression of *Cas* genes at high cell density.

1.10.6 Calcium-Responsive Kinase

The CRISPR Cas systems in *Serratia*, *Pectobacterium* and *Pseudomonas* are regulated by the Rsm post-transcriptional regulatory pathway [226, 227]. Rsm controls multiple cellular functions, such as virulence, motility and biofilm formation [228]. RsmA is the central protein of this pathway, which binds to the 5' untranslated and early coding regions of mRNAs to alter transcription elongation, translation or RNA stability.

RsmA binds to cas mRNAs to decrease their expression [226, 227]. This down-regulates both adaptation and interference. The expression of the crRNAs is not affected. Deletion of the *rsmA* gene in *Erwinia amylovora* upregulates the expression of the *Cas* genes of the type I-E system [229].

LadS is a calcium-responsive kinase that inhibits the activity of RsmA [230, 231]. Deletion of *ladS* decreases *Cas* gene expression and immunity against phage where the CRISPR array contains a complementary protospacer [227]. In the presence of calcium, LadS inhibits RsmA-mediated repression of the *Cas* genes to upregulate the activity of the CRISPR Cas system [227].

1.11 Scope of the Thesis

The work performed in this thesis aimed to discover any remaining host factors in the *E.coli* genome that are required for CRISPR Cas adaptation. The pathways involved were probed to see the effect that deletion or overexpression of genes had on spacer acquisition. An overview of the work is detailed below:

Chapter 3 describes the optimisation of papillation assays performed in an *E.coli* reporter strain to detect spacer acquisition. Assay conditions and choice of expression vectors were studied. This optimises the conditions that were used for the work performed later in this thesis.

Chapter 4 studies the effect of Cas1-Cas2 expression on *E. coli* cell morphology. I show that the catalytic activity of the Cas1-Cas2 complex induces filamentation by the activation of the SOS response and *sulA* expression.

Chapter 5 details the link between spacer acquisition and the SOS response. I show that the *lexA3* mutation decreases the rate of adaptation and the overexpression of *sulA* and *ymfM* causes spacer acquisition to taken place earlier. Growth in the presence of sub-inhibitory concentrations of antibiotics also increases the rate of papillation.

Chapter 6 describes the link between the HflKC complex and FtsH in CRISPR adaptation. Deletion of the *hflK* and *hflc* genes decreases the rate of spacer acquisition. Overexpression of both HflC and HflK simultaneously or FtsH caused papillation to arise earlier.

Chapter 7 outlines the effect that negative regulators of LapB have on the rate of spacer acquisition. Truncation of *lapC* and the deletion of *waaG* and *waaQ* reduces the rate of papillation. Overexpression of *lapB* also decreases the rate of adaptation.

Finally, the data presented here is linked to show how the studied pathways play a role in facilitating spacer acquisition. The work outlined above is discussed in the context of previously published work. I discuss how these chapters link through the inhibition of FtsZ polymerisation. I discuss the work as part of a large network of a global stress response as a defence mechanism against invasion by foreign genetic elements. Additionally, the future implications of the data presented in this thesis are discussed.

Chapter 2

Materials and Methods

2.1 Reagents

All enzymes and PCR materials were purchased from New England Biolabs (NEB). All primers and oligos were purchased from Sigma Aldrich. DNA purification kits: QIAprep Spin Miniprep Kit, QIAGEN Plamsid Maxi Kit, QIAquick PCR purification kit and QIAquick gel extraction kit were all supplied by Qiagen^{TM}. All plasmids constructed were digest verified and then Sanger sequenced by Source Bioscience.

2.2 Strains Used and Created

Strain	Relevant Genotype	Source and Description
NEB5α	fhuA2 a(argF-lacZ)U169 phoA glnV44 a80a(lacZ)M15 gyrA96 recA1 relA1 endA1 thi-1 hsdR17	NEB. Cloning strain.
RC5079	endA1 hsdR17 (rk-mk-) supE44 thi-1 recA1 gyrA (Nalr) relA1 Δ(lacIZYA-argF) U169deoR (φ80dlacd(lacZ)M15) λpir	DH5α λpir. Used for plasmid extraction of R6K origin of replication plasmids
BL21-AI	B F– ompT gal dcm lon hsdSB(rB–mB–) [malB+]$_{K\text{-}12}$(λS) araB::T7RNAP-tetA	Invitrogen. B strain for SPIN assays
BL21-AI Δ*IHF*α	BL21-AI *IHF*α :: KanRFRT	This Study. BL21-AI with *IHF*α deleted via P1 transduction from the Keio collection and replaced with KanR FRT.

Strain	Relevant Genotype	Source and Description
DE407	lexA3(Ind-) malB::Tn9 sulA211 thi-1 Δ(lac-gpt)5 ilv(Ts) mtl-1 rpsL31	Gift from Roger Woodhouse. lexA3 (Ind-) mutant linked to malB::Tn9 marker. [232]
DH10β	F– mcrA Δ(mrr-hsdRMS-mcrBC) φ80lacZΔM15 ΔlacX74 recA1 endA1 araD139 Δ(ara-leu)7697 galU galK λ– rpsL(StrR) nupG	Thermofisher. Cloning strain.
DH10β Marionette	DH10β Marionette Cassette	Marionette Cloning Strain. Used for eYFP fluorescence control assays [233].
E811	lacI^q PN25-tetR SpR deoR supE44 Δ(lacZYA-argFV169) Phi80 lacZΔM15 hsdR17(rK-mK+) recA1 endA1 gyrA96 thi-1 relA1 P2 lysogen	Cloning strain for replication of pE-flp [234]
SM10 (λpir)	thi thr leu tonA lacY supE recA::RP4-2-Tc::Mu Km::λpir	Conjugative donor strain.
MG1655	K-12 F– λ– ilvG– rfb-50 rph-1	Wild Type $E.\ coli$ K Strain.
EAW13	MG1655 ΔsulA::KanR	Gift from Roger Woodhouse. MG1655 with *sulA* replaced by Kanamycin restsance marker by lambda red recombindation [235].

Strain	Relevant Genotype	Source and Description
MLS989	MG1655 araB::T7pol tetA, ΔaraA, ΔCas3- CRISPR-I, ΔCRISPR-II, GalK::J23101 CRISPR-II link SYFP2 opt	Type II (A) YFP CRISPR reporter [236].
MLS989 ΔrecA	MLS989 ΔrecA::FRT	This study. MLS989 with recA deleted via P1 transduction from the Keio collection. KanR removed by FLP-frt recombination
MLS990	MG1655 araB::T7pol tetA, ΔaraA, ΔCas3- CRISPR-I, ΔCRISPR-II, GalK::J23101 CRISPR-II +1nt link SYFP2 opt	Type II (A) YFP CRISPR reporter positive control [236].
JB028	MG1655 ΔlacZ ΔCRII locus araBAD::T7 RNAP tetA argE:: J23100 Type II (A) Reporter	Dr. Jack Braithwaite. Type II (A) CRISPR reporter strain. [237]
JB028 ΔcysH	JB028 ΔCysH::KanR FRT	This study. JB028 with cysH deleted via P1 transduction from the Keio collection.
JB028 ΔhflC	JB028 ΔhflC::FRT	This study. JB028 with hflC deleted via P1 transduction from the Keio collection. KanR removed by FLP-frt recombination.

Strain	Relevant Genotype	Source and Description
JB028 ΔhflK	JB028 ΔhflK::FRT	This study. JB028 with hflK deleted via P1 transduction from the Keio collection. KanR removed by FLP-frt recombination.
JB028 ΔIHFα	JB028 ΔIHFα::FRT	This study. JB028 with IHFα deleted via P1 transduction from the Keio collection. KanR removed by FLP-frt recombination
JB028 ΔlacY	JB028 ΔlacY :: KanR FRT	This study. JB028 with lacY deleted via P1 transduction from the Keio collection.
JB028 Truncated lapC	JB028 lapC :: Tn5	Produced by Dr. Jack Braithwaite during a random mutagenesis screen.
JB028 lexA3	JB028 lexA3(Ind-) malB::Tn9	This study. JB028 with the lexA3 (Ind-) malB::Tn9 inserted by P1 transduction.
JB028 lexA3 ΔyjaB	JB028 lexA3(Ind-) ΔyjaB::FRT	This study. Tn9 marker removed from JB028 lexA3 by deleted of yjaB by P1 transduction from the Keio collection. KanR removed by FLP-frt recombination.

Strain	Relevant Genotype	Source and Description
JB028 ΔrecA	JB028 ΔrecA::FRT	This study. JB028 with recA deleted via P1 transduction from the Keio collection. KanR removed by FLP-frt recombination.
JB028 ΔrfaH	JB028 ΔrfaH::FRT	This study. JB028 with rfaH deleted via P1 transduction from the Keio collection. KanR removed by FLP-frt recombination
JB028 ΔsulA	JB028 ΔsulA::FRT	This study. JB028 with sulA deleted via P1 transduction from the Keio collection. KanR removed by FLP-frt recombination
JB028 ΔsulA:: KanR	JB028 ΔsulA::KanR	This study. JB028 with sulA deleted via P1 transduction from EAW13.
JB028 ΔwaaG	JB028 ΔwaaG::FRT	This study. JB028 with waaG deleted via P1 transduction from the Keio collection. KanR removed by FLP-frt recombination.
JB028 ΔwaaQ	JB028 ΔwaaQ::FRT	This study. JB028 with waaQ deleted via P1 transduction from the Keio collection. KanR removed by FLP-frt recombination.

Strain	Relevant Genotype	Source and Description
JB028 ΔyjaB	JB028 ΔyjaB::FRT	This study. JB028 with yjaB deleted via P1 transduction from the Keio collection. KanR removed by FLP-frt recombination
JB028 ΔymfM	JB028 ΔymfM::FRT	This study. JB028 with ymfM deleted via P1 transduction from the Keio collection. KanR removed by FLP-frt recombination
JB028 ΔymfM ΔsulA:: KanR	JB028 ΔymfM::FRT ΔsulA::KanR	This study. JB028 with ymfM deleted via P1 transduction from the Keio collection. SulA replaced with KanR via P1 transduction from EAW13.

Table 2.1. List of Strains

2.3 Plasmids and Oligonucleotides

2.3.1 Plasmid List

Name	Description
pCP20	For FLP-frt mediated recombination. Yeast FLP recombinase expression vector with the pL lambda promoter. Temperature-sensitive replication origin. AmpR and CmR. [238].
pCP20 OriT	pCP20 with RP4 origin of transfer to allow conjugation from SM10 donor strain. AmpR and CmR.
pE-flp	For FLP-frt mediated recombination. Yeast FLP recombinase expression vector under the control of the strong constitutive pE promoter from phage P2. Temperature-sensitive replication origin. AmpR. [234]
pRC1620	pBAD with Cas1-Cas2 inserted into NcoI site. pCas1-Cas2 arabinose inducible expression vector. AmpR.
pRC1644	Type-II (A) Spacer acquisition positive control (additional spacer and repeat). KanR.
pRC1653	pBAD with Cas1 inserted into NcoI site. pCas1 arabinose inducible expression vector. AmpR.
pRC1655	pBAD with Cas2 inserted into NcoI site. pCas2 arabinose inducible expression vector. KanR.
pRC1656	pBAD with Cas1-Cas2 inserted into NcoI site. pCas1-Cas2 arabinose inducible expression vector. KanR.

Name	Description
pRC1657	pBAD with Cas1-Cas2 inserted into NcoI site. pCas1-Cas2 arabinose inducible expression vector. CmR.
pRC1658	pBAD Cas1-Cas2 with D221A inactivating point mutation in Cas1. KanR.
pRC2703	RecA arabinose inducible expression vector. Temperature-sensitive replication origin. AmpR.
pRC2713	pET21aClpX purchased from addgene. Contains a ClpX expresssion vector under the control of a T7 promoter and lac operator. AmpR. Purchased from addgene.
pRC2715	pT7Cas1-Cas2. Contains Cas1-Cas2 expression vector under the control of a T7 promoter and lac operator. pCDFDUET derived. SpectR. A gift from Virgis Šikšnys.
pRC2747	pMARIONETTE$_{Ara}$ with Cas1-Cas2 inserted. pMARI$_{Ara}$Cas1-Cas2 arabinose inducible expression vector. KanR.
pRC2748	pMARIONETTE$_{CUMA}$ with Cas1-Cas2 inserted. pMARI$_{CUMA}$Cas1-Cas2 Cuminic acid inducible expression vector. KanR.
pRC2749	pMARIONETTE$_{Van}$ with Cas1-Cas2 inserted. pMARI$_{Van}$Cas1-Cas2 Vanillic acid inducible expression vector. KanR.
pRC2750	pMARIONETTE$_{Sal}$ with Cas1-Cas2 inserted. pMARI$_{Sal}$Cas1-Cas2 Salicylic acid inducible expression vector. KanR.
pRC2764	pMARIONETTE$_{CUMA}$ with eYFP. Cuminic acid inducible vector. KanR.

Name	Description
pRC2766	pMARIONETTE$_{Van}$ with eYFP. Vanillic acid inducible vector. KanR.
pRC2773	pMARIONETTE$_{Sal}$ with eYFP. Salicylic acid inducible vector. KanR.
pRC2777	pMARIONETTE$_{Van}$ with FtsZ inserted. pMARI$_{Van}$FtsZ vanillic acid inducible expression vector. KanR.
pRC2781	pMARIONETTE$_{Van}$ with SulA inserted. pMARI$_{Van}$SulA vanillic acid inducible expression vector. KanR.
pRC2789	pMARIONETTE$_{Van}$ with FtsH inserted. pMARI$_{Van}$FtsH vanillic acid inducible expression vector. KanR.
pRC2790	SOS reporter plamid. A gfp under the contol of the sulA promoter. p15a origin of replication. CmR. Purchased from addgene [239].
pRC2792	pMARIONETTE$_{Van}$ with hflK inserted. pMARI$_{Van}$hflK vanillic acid inducible expression vector. KanR.
pRC2793	pMARIONETTE$_{Van}$ with hflC inserted. pMARI$_{Van}$hflC vanillic acid inducible expression vector. KanR.
pRC2794	pMARIONETTE$_{Van}$ with hflK and hflC inserted. pMARI$_{Van}$hflC-K vanillic acid inducible expression vector. KanR.
pRC3004	pMARIONETTE$_{Van}$ with IHFα inserted. pMARI$_{Van}$IHFα vanillic acid inducible expression vector. KanR.
pRC3005	pMARIONETTE$_{Van}$ with rfaH inserted. pMARI$_{Van}$rfaH vanillic acid inducible expression vector. KanR.
pRC3012	pMARIONETTE$_{Van}$ with LapB inserted. pMARI$_{Van}$LapB vanillic acid inducible expression vector. KanR.
pRC3017	pMARIONETTE$_{Van}$ with recX inserted. pMARI$_{Van}$recX vanillic acid inducible expression vector. KanR.

Name	Description
pRC3018	$pMARI_{Van}$recX vanillic acid inducible expression vector with pSC101 Ori. SpectR.
pRC3021	$pMARIONETTE_{Van}$ with *ymfM* inserted. $pMARI_{Van}$ymfM vanillic acid inducible expression vector. KanR.

Table 2.2. List of Plasmids

2.3.2 Oligonucleotide List

Name	Sequence	Description
BL21 Locus F	ATTTTGCGTTTCGTTCAGGT	Anneal either side of the CRISPR locus in BL21-AI.
BL21 Locus R	TGGATGTGTTGTTTGTGT	
Cas1-Cas2 for Mar F	TTAATACTAGAGAAAGAGGGGA AATACTAGATGGCCTGG CTTCCCCTTAATC	Anneal to *Cas1-Cas2* in MG1655. For Gibson assembly to insert into marionette plasmid backbone.
Cas1-Cas2 for Mar R	GCCTCTTTTCTGGAATTTGG TACCGAGTTACCGCT CAAACAGGTAAAAAAGACACC	
ClpXP F	GCAGCATAACGCGCTAAATTCG	Anneal either side of *clpXP* in MG1655. Used to test for deletion of *clpXP*.
ClpXP R	GATAAACCACCACATCGCGCAG	
FtsH for Marionette F	TTAATACTAGAGAAAGAG GGGAAATACTAGATGGCG AAAAACCTAATACTCTG	Anneal to *ftsH* in MG1655. For Gibson assembly to insert into

Name	Sequence	Description
FtsH for Marionette R	GCCTCTTTTCTGGAATTTGG TACCGAGTTTTACTT GTCGCCTAACTGC	marionette plasmid backbone.
FtsZ for Marionette F	TTAATACTAGAGAAAGAGGGGA AATACTAGATGTTTGAAC CAATGGAACTTACC	Anneal to *ftsZ* in MG1655. For Gibson assembly to insert into marionette plasmid backbone.
FtsZ for Marionette R	GCCTCTTTTCTGGAATTTGGTA CCGAGTTATTAATCAGC TTGCTTACGCAGG	
HflC for Marionette F	TTAATACTAGAGAAAGAGGG GAAATACTAGATGCG TAAGTCAGTTATCGCG	Anneal to *hflC* in MG1655. For Gibson assembly to insert into marionette plasmid backbone.
HflC for Marionette R	GCCTCTTTTCTGGAATTTGG TACCGAGTTATTAACG CGTTGCGGAAGTC	
HflK for Marionette F	TTAATACTAGAGAAAGAGGG GAATACTAGATG GCGTGGAATCAGCC	Anneal to *hflK* in MG1655. For Gibson assembly to insert into marionette plasmid backbone.
HflK for Marionette R	GCCTCTTTTCTGGAATTTGG TACCGAGTTATTATT CCCCCTGACGCTG	
HflKC F	TTGATCGATTACCT GATCTAACGGCG	Anneal either side of *hflKC* in MG1655. Used to test for deletion of *hflK* and *hflC*.
HflKC R	GCCCTAAACCTTCCAGTACCAAAAC	
IHFα F	ACGGTGACTCTTCGACAG	Anneal either side of *IHFα* in MG1655.

Name	Sequence	Description
IHFα R	CCGTCGCCAAATGTGTAG	Used to test for deletion of *IHFα*.
IHFα for Marionette F	TTAATACTAGAGAAA GAGGGGAAATACTAGA TGGCGCTTACAAAAGCTG	Anneal to *IHFα* in MG1655. For Gibson assembly to insert into marionette plasmid backbone.
IHFα for Marionette R	GCCTCTTTTCTGGAATTTGG TACCGAGTTATTACTC GTCTTTGGGCGAAG	
LapB for Marionette F	TTAATACTAGAGAAAG AGGGGAAATACTAGATGC TGGAGTTGTTGTTTCTG	Anneal to *LapB* in MG1655. For Gibson assembly to insert into marionette plasmid backbone.
LapB for Marionette R	GCCTCTTTTCTGGAATTT GGTACCGAGTTATTACAGG CCATCAAGACCG	
LexA F	GATCGAGGGAAGGATTTCAGA AATGAAAGCGTTAACGGCC	Anneal either side of *lexA* in MG1655. Used to test for deletion of *lexA*.
LexA R	GGTCGACTCTAGAGGATCCGT TACAGCCAGTCGCCGTTG	
LexA Sequence	AATGAAAGCGTTAACGGCC	Anneal to products of the PCR using LexA F and R primers for sequence determination of point mutations.
Marionette F	CTCGGTACCAAATTCCAG	Anneal to marionette collection to amplify the backbone for use in Gibson assembly.
Marionette R	CTAGTATTTCCCCTCTTTCTC	

Name	Sequence	Description
MiaA F	CACGAAATCTGATGAGCGAACATGC	Anneal either side of *lexA* in MG1655.
MiaA R	GCGTTCAGGAACGG ATCTTGTAAAGA	Used to test for deletion of *miaA*.
Sp Aq F	GGCTAGCAGGAGGAATTCACC	Anneal either side of the Type-II reporter locus in JB028. To detect spacer acquisition events.
Sp Aq R	CGCATCGTAACCGTGCATCTG	
SulA F	GATCCGCTTATAGGAGAGGC	Anneal either side of *sulA* in MG1655. Used to test for deletion of *sulA*.
SulA R	GGCGATGTAAAGTCTACAACG	
SulA for Marionette F	TTAATACTAGAGAAAGAGGG GAAATACTAGATGTAC ACTTCAGGCTATGC	Anneal to *sulA* in MG1655. For Gibson assembly to insert into marionette plasmid backbone.
SulA for Marionette R	GCCTCTTTTCTGGAATTTGGT ACCGAGTTATTAATGATACA AATTAGAGTGAATTTTTAGCCC	
RecA F	CAGATGCGACCCTTGTGTATC	Anneal either side of *recA* in MG1655. Used to test for deletion of *recA*.
RecA R	CGGTATTACCCGGCATGAC	
RecA for Marionette F	TTAATACTAGAGAAA GAGGGGAAATACTAGAT GGCTATCGACGAAAACAAAC	Anneal to *recA* in MG1655. For Gibson assembly to insert into

Name	Sequence	Description
RecA for Marionette R	GCCTCTTTTCTGGAATTTG GTACCGAGTTATTAAAAAT CTTCGTTAGTTTCTGCTACG	marionette plasmid backbone.
RecX for Marionette F	TTAATACTAGAGAAA GAGGGGAAATACTAGATG ACAGAATCAACATCCCG	Anneal to *recA* in MG1655. For Gibson assembly to insert into marionette plasmid backbone.
RecX for Marionette R	GCCTCTTTTCTGGAATTTG GTACCGAGTTATCAG TCGGCAAAATTTCGC	
RfaH F	GTAGCCTCTTAATCTGCGCC	Anneal either side of *rfaH* in MG1655. Used to test for deletion of *rfaH*.
RfaH R	GCGCATGGAATTTATATCGGC	
WaaG/Q F	CGACCCGGCATGAACTTG	Anneal to *waaG/Q* in MG1655. Used to test for deletion of *waaG/Q*.
WaaG/Q R	CACGACTGTGTATATACCCGAAC	
YFP Reporter F	GCTAGCTACTAGAGAAAGAGG	Anneal either side of the Type-II reporter locus in MLS989 for the detection of spacer acquisition events.
YFP Reporter R	AATTCAACTAAGATCGGTACTAC	
YjaB F	CAGCTGAATATCGACCTGC	Anneal either side of *yjaB* in MG1655.
YjaB R	GGAGACGCTGCCTTCAG	Used to test for deletion of *yjaB*.
Ymfm F	CGTTCAGCAATCGAAGACGG	Anneal either side of *ymfB* in MG1655.

Name	Sequence	Description
Ymfm R	GTGATATTCATCCACCACGGC	Used to test for deletion of *ymfM*.
YmfM Mar F	TTAATACTAGAGAAAGAGG GGAAATACTAGATGAACA GTTTAACAACACACTACCG	Anneal to *ymfM* in MG1655. For Gibson assembly to insert into marionette plasmid backbone.
YmfM Mar R	GCCTCTTTTCTGGAATTTG GTACCGAGTTACTATTTC CCTGAATTTACGACGAAACTG	

Table 2.3. List of Oligonucleotides

2.4 Solution Composition

2.4.1 Media

Media	Composition
LB Broth	10 g/L Yeast Extract, 5 g/L NaCl, 5 g/L Tryptone, 2 mL/L 1 M NaOH. (Agar added to 15 g/L for plates)
SOC	20 g/L Tryptone, 5 g/L Yeast Extract, 0.5 g/L NaCl, 2.5 mM KCl, 10 mM $MgCl_2$, 10 mM $MgSO_4$, 20 mM glucose
Minimal Media	1 X M9 salts, 0.1% carbon source, 2 mM $MgSO_4$, 0.1 mM $CaCl_2$. (Agar added to 15 g/L for plates). Where a reporter system has been inserted into the ArgE locus, 0.1 g/L L-arginine was also added to the media
10 X M9 Salts	60 g/L Na_2HPO_4, 30 g/L KH_2PO_4, 5 g/L NaCl, 10 g/L NH_4Cl
Terrific Broth	24 g/L Yeast Extract, 20 g/L Tryptone, 4 mL/L glycerol, 0.017 M KH_2PO_4, 0.072 M K_2HPO_4

Table 2.4. List of Media

2.4.2 Antibiotics

Antibiotics were used at the following concentrations:

Antibiotic	**Working concentration for Single copy resistance (μg/mL)**	**Working concentration for multi-copy resistance (μg/mL)**
Ampicillin	50	100
Chloramphenicol	5	35
Kanamycin	30	50
Spectinomycin	50	100

Tetracycline	12.5	25

Table 2.5. Concentrations of Antibiotics

Sub-inhibitory concentrations of antibiotics were used across the following range of concentrations:

Antibiotic	Concentration Range (μg/mL)
Ampicillin	0-8.0
Cefalexin	0-8.0
Mitomycin C	0-1.0
Nalidixic Acid	0-8.0

Table 2.6. Range of Sub-Inhibitory Concentration of Antibiotics used

2.5 Cloning and DNA Manipulation

2.5.1 Polymerase Chain Reaction

Reactions performed with Q5^{TM} DNA polymerase contained 1X Q5 reaction buffer, 200 nM of each primer, 500 μM dNTPs, 10 ng of template DNA and 1 unit of enzyme per 50 μL. Standard reaction conditions were: initial denaturation at 98 °C for 30 seconds, denaturation at 98 °C for 15 seconds, annealing at the temperature calculated by the NEB website for 15 seconds, extension for 30 seconds per kb at 72 °C, for 35 cycles followed by a final extension at 72 °C for 2 minutes. Products were visualised by gel electrophoresis.

Reactions performed with Taq DNA polymerase contained 1X Standard Taq buffer, 200 μM dNTPs, 200 nM of each primer, 1 μL culture as template and 1.25 unit of enzyme per 50 μL. Standard reaction conditions were: initial denaturation at 98 °C for 5 minutes, denaturation at 95 °C for 30 seconds, annealing at the temperature calculated by the NEB website for 30 seconds, extension for 1 minute per kb at

68 °C, for 30 cycles followed by a final extension at 68 °C for 5 minutes. Products were visualised by gel electrophoresis.

2.5.2 Digests

Restriction digests were performed according to manufacturers instructions.

2.5.3 Phosphorylation

T4 Polynucleotide Kinase (T4 PNK) was used to perform phosphorylation reactions according to manufacturers instructions.

2.5.4 Dephosphorylation

Calf Intestinal Phosphatase (CIP) was used for dephosphorylation reactions according to manufacturers instructions.

2.5.5 Ligation

T4 DNA Ligase was used for ligation reactions. 200 units of enzyme was used in 1X T4 DNA Ligase buffer or Cutsmart buffer with 1 mM ATP added. The insert fragment was used at a 3:1 molar ratio to the vector. Linearised vector was used at ~50 ng. The reaction was made up to 20 μL with dH_20. Reactions were incubated at 16°C overnight. 2 μL of the mixture was added to 100 μL of chemically competent NEB5α for transformation (Section 2.7.2).

2.5.6 Gibson Assembly

Gibson assembly was used as a method to clone fragments of DNA. Pieces of DNA to be joined contained 30bp homology sections. These were added to the 5' end of the PCR primer. Amplified products were gel extracted and purified. A homemade gibson assembly mix was made to give a final concentration of 100 mM Tris HCl pH 7.5, 10 mM MgCl2, 10 mM DTT, 1 mM NAD+, 1 mM of each

dNTP, 5 % w/v PEG 8000, 0.005 U/μL of T5 Exonuclease, 0.03 U/μL Phusion Polymerase and 5.3 U/μL Taq DNA ligase. 0.02-0.5 $_p$moles of DNA was added to the reaction. dH_20 was added to make the reaction volume 20 μL. Placed at 50 °C for 2 hours. The reaction was cooled and 2 μL of the mixture was added to 100 μL of electrocompetent DH10β cells for transformation (Section 2.7.4).

2.5.7 Plasmid Purification

Plasmids were purified by Qiagen miniprep or maxiprep kits following the instructions. Terrific Broth was used in place of LB broth for p15A origin of replication plasmids to increase the DNA yield.

2.5.8 Phenol Chloroform Extraction

An equal volume of the sample and phenol:chloroform:isoamyl alcohol (25:24:1) were added and vortexed vigorously. This was centrifuged at 16,000g for 5 minutes. The aqueous phase was removed and ethanol precipitated.

2.5.9 Ethanol Precipitation

To a sample, 20 μg glycogen, 0.5 X volume 7.5M NH_4OAc and 3 X volume 100% ethanol was added. Samples were placed at -80 °C for at least 1 hour to precipitate DNA. This was centrifuged at 16,000g for 30 minutes at 4 °C. The supernatant was discarded and the DNA was washed with 150 μL 70 % ethanol. The sample was centrifuged at 16,000g for 2 minutes at 4 °C. This was repeated. The remaining ethanol was pipetted off. The DNA pellet was resuspended in an appropriate volume of TE buffer.

2.6 Gel Electrophoresis

2.6.1 Agarose Gel Electrophoresis

Agarose gel electrophoresis was performed with a BioRad gel electrophoresis system. Gels were 0.8-2.0% agarose buffered with Tris-Borate-EDTA (TBE). The agarose concentration was dependent on the molecular weight of the DNA fragments of interest. Standard cloning gels were electrophoresed at 5-8 V/cm in the presence of 1 μg/mL Ethidium Bromide. Analytical gels were electrophoresed overnight at 1.5 V/cm. These were post-stained for 30 minutes in 0.5X TBE containing 1 μg/mL Ethidium Bromide. To determine the size of DNA samples, 1 kb and 100 bp NEB ladders were used. Gels were imaged under UV light.

2.6.2 Agarose Gel Extraction Protocol

Gel extraction was performed according to the manufacturer's instructions.

2.6.3 Running Buffers

Running Buffer	Composition
10X TBE	1 M Trizma Base, 1 M Boric Acid, 0.02 M EDTA pH 8.0

Table 2.7. List of Running Buffers

2.7 Competent Cells

2.7.1 Making Chemically Competent Cells

To make chemically competent cells, the frozen glycerol of the cell strain was streaked out onto LB agar plates and grown overnight at 37 °C. From a single colony, a 5 mL LB broth culture was inoculated and grown overnight at 37 °C rotating. A 1:100 dilution was performed in fresh LB broth and grown at 37 °C shaking ~165 rpm until OD_{600} ~0.5. The cells were cooled shaking in an ice slurry for 20

minutes. The cells were centrifuged at 6000g at 4 °C for 10 minutes. The supernatant was discarded and cells were resuspended in 1/3 volume TFB1 (30 mM potassium acetate, 50 mM $MgCl_2$, 100 mM KCl, 10 mM $CaCl_2$, 15% glycerol). The cells were placed on ice for 1 hour. The cells were centrifuged again, supernatant discarded and resuspended in 1/12 volume TFB2 (10 mM MOPS pH 7.0, 75 mM NaCl, KCl, 15% glycerol). 200 μL aliquots were flash frozen on dry ice and stored at -80 °C for later use.

2.7.2 Competent Cell Transformation Protocol

Competent cells were thawed on ice. 2 ng of plasmid was added to 100 μL of competent cells and left on ice for 30 minutes. Cells were heat shocked at 42 °C for 1 minute and then placed back on ice for 5 minutes. 900 μL of LB broth was added and cells were outgrown at 37 °C for 1 hour rotating. A dilution was performed to produce single colonies and spread evenly across an LB agar plate supplemented with antibiotic. Plates were incubated overnight.

2.7.3 Making Electrocompetent Cells

To make electrocompetent competent cells, the frozen glycerol of the cell strain was streaked out onto LB agar plates and grown overnight at 37 °C. From a single colony, a 5 mL LB broth culture was inoculated and grown overnight at 37 °C rotating. A 1:100 dilution was performed into fresh 300 mL LB broth and grown at 37 °C shaking ~165 rpm until OD_{600} ~0.5. The cells were cooled shaking in an ice slurry for at least 20 minutes. The cells were centrifuged at 6000g at 4 °C for 10 minutes. The supernatant was discarded and the cells were resuspended in 100 mL ice cold dH_2O. The cells were centrifuged at 6000g at 4 °C for 10 minutes. The supernatant was discarded and the cells were resuspended in 100 mL ice cold 10% glycerol. This was repeated. Cells were then resuspended in 5 mL ice cold 10% glycerol. This was centrifuged at 16000g for 1 minute. The supernatant was discarded and resuspended in 1 mL ice cold 10% glycerol. 50 μL aliquots were flash frozen on

dry ice and stored at -80 °C for later use.

2.7.4 Electrocompetent Cell Transformation Protocol

Competent cells were thawed on ice. 1ng of plasmid was added to 50 μL of competent cells. Cells were electroporated at 1.80 kV, 200 Ω, and 25 μF in a 1 mM cuvette. This was added to 950 μL SOC and outgrown at 37 °C for 1 hour. A dilution was performed to produce single colonies and spread evenly across an LB agar plate supplemented with antibiotic. Plates were incubated overnight.

2.8 Conjugation

The conjugative plasmid of interest was transformed into chemically competent SM10 (Section 2.7.2). 5 mL overnight cultures were produced of donor SM10 and recipient strains in selective antibiotics. Cultures were grown at 37 °C unless a temperature sensitive plasmid was used where growth was at 30 °C. Overnight cultures were pelleted by centrifugation at 6000g for 1 minute. The supernatant was discarded and the cells were resuspended in 1 mL LB broth. This was repeated twice. 100 μL of cells were added to sterile filter paper on an LB agar plate. This was placed at either 37 °C unless a temperature sensitive plasmid was used so this was placed at 30 °C. The conjugation was left for 4 hours. The filter paper was removed and added to a 50 mL falcon tube containing 1 mL LB broth. This was thoroughly vortexed for 30 seconds. This mixture was looped onto LB agar supplemented with antibiotics to select for successful transconjugants in the recipient strain. Plates were incubated overnight at the temperature for plasmid maintenance.

2.9 Genetic Manipulation by P1 Transduction

2.9.1 Generation of P1 bacteriophage lysates

Gene knockouts were produced by P1 transduction. The Keio collection was used to make phage lysate that can transduce the kanamycin resistance gene across to select for deletions [240]. An overnight culture was diluted 1:40 in LB broth supplemented with 5 mM $CaCl_2$ and grown until OD_{600} ~0.8. 100 μL was added to 42 ^{o}C 0.6 % agar along with a phage gradient. This was poured onto P1 plates (LB agar supplemented with 0.13 % glucose and 5 mM $CaCl_2$). The plates were placed upright in the 37 ^{o}C incubator overnight.

To make the *recA* P1 lysate, pRC2703 was transformed into the Keio *recA* mutant strain and plated onto LB agar plates supplemented with ampicillin. These were incubated at 30 ^{o}C overnight. From single colonies, a 5 mL overnight culture was grown in LB broth supplemented with ampicillin at 30 ^{o}C. The overnight culture was diluted 1:40 in LB broth supplemented with 5 mM $CaCl_2$, ampicillin and 0.2 % L-arabinose to induce *recA* expression and grown at 30 ^{o}C until OD_{600} ~0.8. The method described above was then followed.

The two plates with best lysis were scraped into a 50 mL falcon tube with 1 mL MC buffer [100 mM $MgSO_4.7H_2O$ and 5 mM $CaCl_2$] and 500 μL chloroform. This was vortexed thoroughly and centrifuged at 7000 g for 10 minutes. The supernatant was poured into a 15 mL falcon tube along with 500 μL chloroform and stored at 4 ^{o}C prior to use.

2.9.2 Genetic Manipulation by P1 Transduction

A 5 mL overnight culture of recipient strain was centrifuged at 6000 rpm for 5 minutes. The supernatant was discarded and the cells were resuspended in 1 mL MC Buffer. 100 μL of cells was added to a gradient of phage and placed in the 37 ^{o}C water bath for 30 minutes. Following infection, 300 μL of 1M sodium citrate was

added and placed on ice. This was added to 4 mL 42 °C 0.6 % agar and poured on LB agar plated supplemented with single copy antibiotic and 5 mM sodium citrate. These were placed upright in the 37 °C incubator overnight. Single colonies were subcultured on LB agar plates supplemented with 5 mM sodium citrate and placed in the 37 °C incubator overnight three times. The gene deletion was verified by colony PCR or Sanger sequencing.

2.9.3 FLP-*frt* Recombination

The removal of Kan-FRT was achieved by use of the FLP recombinase encoded pCP20 (Cherepanov and Wackernagel, 1995) [238]. pCP20 contains the temperature sensitive pSC101 ori and the FLP recombinase under the control of the temperature inducible lambda promoter. pCP20 was transformed into competent cells and plated onto LB agar plates supplemented with ampiciilin (Section 2.7.2 and 2.7.4). These were incubated at 30 °C overnight. From single colonies, a 5 mL overnight culture was grown in LB broth in the absence of antibiotics at 42 °C. This was looped onto an LB agar plate and incubated at 37 °C. Single colonies were then subcultured on LB agar plates supplemented with ampicillin, kanamycin and LB agar only and grown at 37 °C. Successful deletions grew on LB agar only. The gene deletion was verified by colony PCR.

Where pCP20OriT was used, a 5 mL overnight culture of cells containing a successful insertion by P1 transduction was produced in LB broth at 37 °C. A 5 mL overnight culture of SM10 (λpir) pCP20OriT was produced in LB broth supplemented with ampicillin at 30 °C. Cells were pelleted by centrifugation. The supernatant was discarded. The donor SM10 (λpir) pCP20OriT cells were resuspended in 1 mL LB broth and recipient JB028 KanR-FRT containing cells were resuspended in 5 mL LB broth. 100 μL of each cell strain was added to filter paper on an LB agar plate. This was placed at 30 °C for 4 hours. The filter paper was resuspended in 1mL LB broth by thorough vortexing. This mixture was looped onto LB agar supplemented with ampicillin and placed at 30 °C overnight. From

single colonies, a 5 mL overnight culture was grown in LB broth in the absence of antibiotics at 42 °C. This was looped onto an LB agar plate and incubated at 37 °C overnight. Single colonies were then subcultured on LB agar plates supplemented with ampicillin, kanamycin and LB agar only and grown at 37 °C. Successful deletions grew on LB agar only. The gene deletion was verified by colony PCR.

Where pE-flp was used, the plasmid was transformed into electrocompetent cells and plated on LB agar supplemented with 50 μg/mL ampicillin and incubated at 30 °C (Section 2.7.4). Overnight cultures of successful transformants were produced in LB broth spinning at 37 °C. This was looped onto LB agar plates in the absence of antibiotics at 37 °C. Single colonies were then subcultured on LB agar plates supplemented with ampicillin, kanamycin and LB agar only and grown at 37 °C. Successful deletions grew on LB agar only. The gene deletion was verified by colony PCR.

All transductants were grown on minimal media to ensure no metabolic genes had been accidentally disrupted. A 5 mL overnight was grown in LB broth. 1 mL of this culture was pelleted by centrifugation at 13000 rpm for 1 minute. The supernatant was discarded and the pellet was resuspended in 1 mL sterile PBS. This was repeated twice more. 5 μL was looped onto minimal media plates with glucose as the carbon source. These were incubated at 37 °C 72 hours. Growth of colonies show that there has been no disruption to any metabolic genes (Figure S19).

2.10 Bacterial Assays

2.10.1 Papillation Assay

Plasmids were transformed into a competent reporter strain (Sections 2.7.2 and 2.7.4). This was plated onto LB agar supplemented with relevant antibiotics, 0.1% lactose, 40 μg/mL X-gal and arabinose. Arabinose concentration used depended on the choice of expression vector. For pBAD Cas1-Cas2, expression was induced by 0.002 % L-arabinose. For pMARI$_{Ara}$ Cas1-Cas2, expression was induced by

0.02 % L-arabinose. Colonies were present at 25-50 per plate. All plates were incubated at 37 °C for 5 days. Representative colonies were imaged by light microscope.

2.10.2 Spacer Integration Assay (SPIN)

The Cas1-Cas2 expression vector was transformed into cells (Sections 2.7.2 and 2.7.4). These were diluted to give single colonies when plated on LB agar supplemented with the relevant antibiotic. From a single colony, 5 mL overnight cultures were produced in LB broth supplemented with antibiotic and glucose. A 1:1000 dilution was performed into LB broth supplemented with antibiotic and inducer. pBAD Cas1-Cas2 expression was induced by 0.2% arabinose. pT7 Cas1-Cas2 expression was induced by 0.2 % L-arabinose and 0.1 mM IPTG. These were grown at 37 °C for 24 hours spinning. This dilution was repeated in fresh media. 1 mL of culture was pelleted by centrifugation and stored in the freezer before analysis.

PCR was used to check for an expanded CRISPR array. 1 μL of overnight cultures was used as the template for PCR amplification in a 25 μL Taq polymerase PCR. The primers used are listed in Table 2.3. The PCR reactions were analysed on a 1.8 % agarose gel pre-stained with Ethidium Bromide.

2.10.3 Detection of Spacer Acquisition by Fluorescence

A modified method based on Amlinger et al., was used 2017 [236]. pBAD Cas1-Cas2 was transformed into MLS989 and mutants. From a single colony, 5 mL overnight cultures were produced in LB broth supplemented with kanamycin. A 1:1000 dilution was performed into LB broth supplemented with kanamycin and 0 or 0.2% arabinose and grown 37 °C for 24 hours spinning. Cultures were diluted to ~200 colonies per plate and plated onto LB agar supplemented with kanamycin. These were incubated at 37 °C overnight. MLS990 was used as a YFP+ control [236]. Fluorescence was measured using the Cy3 setting on the Amersham ty-

phoon. The intensity was analysed using FIJI (Fiji Is Just ImageJ) [241]. YFP+ cells were verified for spacer acquisition by PCR using YFP reporter F and R primers, table 2.3. Colonies were resuspended in 100 μL LB broth and 1 μL was used as template. The PCR reactions were analysed on a 1.8 % agarose gel pre-stained with Ethidium Bromide.

2.10.4 Separation of filamenting cells by Filtration

A SPIN assay was performed with BL21-AI and MLS989 as described in 2.10.2. pT7 Cas1-Cas2 expression was induced for 6 or 24 hours. Cultures were passed through a Sartorius Minisart 1.2 μm Syringe Filter. The filter was washed with three times the filtered culture volume in fresh LB broth. The bacteria trapped in the filter were eluted in the same volume as the filtered sample. The OD_{600} of the filtered and unfiltered were normalised to be the same. Cultures were analysed by PCR as described in 2.10.2.

2.10.5 Cell Sorting

A modified method based on Amlinger et al., 2017 [236] was used. pT7 Cas1-Cas2 was induced and filamentous cells were separated as described in 2.10.4. Cells were diluted 1:100 in LB broth supplemented with spectinomycin and 25 mM glucose and grown for 5 hours to allow YFP maturation and resolve filamentation. Cells were diluted to ~10^6 per mL. Cells were sent for cell sorting using the Beckman Coulter CytoFLEX S Flow Cytometer. The gaiting conditions were determined to allow distinction between YFP+/- cells using cultures of MLS989 as a negative control and MLS990 as a positive control. Samples were run at 60 μL/min until 20000 cells had been sorted. Data was analysed using the CytExpert program.

For analysis of spacer acquisition in a colony environment, pRC2747 was transformed into MLS989 and $\triangle$*recA*. Cells were plated onto LB agar supplemented

with kanamycin and 0.02% L-arabinose at a density of ~50 colonies per plate. This was repeated in triplicate. Plates were incubated at 37 ºC for 5 days. The colonies were resuspended in 1 mL LB broth. The OD_{600} was measured and the cultures were diluted to ~10^6 cells per mL. Cell sorting was performed as described above.

For separation of filaments and rod cell assays, conditions were compared by ANOVA. For *recA* assays, conditions were compared by two-way t-test. The raw values and P values are listed in Table S3.

2.10.6 Determination of Growth Rate

Cells were streaked onto LB agar plates and incubated at 37 ºC overnight. Three colonies were picked and grown in LB broth at 37 ºC overnight spinning. The OD_{600} was measured and the cultures were diluted to an OD_{600} of 1. These were diluted 1:1000. 200 μL was added to a well in a 96-well plate. This was grown overnight in a Biotek Epoch 2 microplate spectrophotometer at 37 ºC shaking. The OD_{600} was measured every 15 minutes for 12 hours.

2.11 Marionette eYFP Fluorescence Titration

Cells were either streaked or transformed (Section 2.7.4) and plated onto LB agar plates supplemented with kanamycin. Three colonies were picked and grown in LB broth supplemented with kanamycin overnight spinning at 37 ºC. A 1:1000 dilution was performed into fresh media with a gradient of inducer for each replicate. This was placed spinning at 37 ºC overnight. The OD_{600} was measured and normalised to 2.0. 175 μL was added to a 96-well plate and a halving dilution was performed. LB broth only control wells were also included. Fluorescence was measured using the Cy3 setting on the Amersham typhoon. The intensity was analysed using FIJI (Fiji Is Just ImageJ) [241]. Intensity of LB only wells was subtracted from intensity of wells containing cells. This data was plotted using PRISM Graphpad. Conditions

were statistically compared using a two-way t-test. All intensity values and P values are listed in table S2.

2.12 Microscopy

Plasmids were transformed into BL21-AI (Section 2.7.2). Overnight cultures were produced in LB broth supplemented with antibiotics in the presence or absence of inducer molecules rotating at 37 ºC. The OD_{600} was measured and normalised to 0.5. 10 μL of culture was placed onto a microscope slide. A coverslide was placed on the culture without addition of bubbles and the cells were sealed by passing over a Bunsen Burner. Ten representative images were taken randomly for each condition with a Zeiss Axiovert S100 Inverted Phase contrast microscope using x63 magnification lens and ph2 contrast ring. Images taken using the Axiocam MRm camera. Representative images are presented in the appendix.

2.13 Measurement of SOS Response Induction by GFP Fluorescence

pRC2790 was transformed into cells (Sections 2.7.2 and 2.7.4). Overnight cultures were produced in LB broth supplemented with antibiotic and grown spinning at 37 ºC in triplicate. A 1:1000 dilution was performed into fresh media with a range of treatment for each replicate. These were placed spinning at 37 ºC overnight. The OD_{600} was measured and normalised to 2.0. 175 μL was added to a 96-well plate and a halving dilution was performed. LB broth only control wells were also included. GFP fluorescence was measured using the Cy2 setting on the Amersham typhoon. The intensity was analysed using FIJI (Fiji Is Just ImageJ) [267]. LB fluorescence intensity was subtracted from the intensity of cells. The data was plotted using PRISM Graphpad. Conditions were statistically compared using a two-way t-test. All intensity and P values are listed in table S2.

To verify induction of the SOS response by sub-inhibitory concentrations of antibi-

otics in papillation assays, an alternative method was used. pRC2790 was transformed into JB028 (Section 2.7.4). An overnight culture was produced in LB broth and chloramphenicol. This was diluted to give ~500 colonies and plated onto LB agar supplemented with sub-inhibitory concentrations of antibiotics. These were placed at 37 ^{o}C overnight. Colonies were resuspended in 1 mL LB broth. The OD_{600} was measured and normalised to 2.0. This was repeated in triplicate. Fluorescence detection and analysis was performed as described previously.

Chapter 3

Optimisation of the Papillation Assay for Spacer Acquisition

3.1 Introduction

There are several methods to detect the acquisition of spacers into a CRISPR array [242]. The most common approach, known as the Spacer Integration (SPIN) assay, is to amplify the CRISPR locus by PCR and visualise the products by gel electrophoresis [100]. Where spacer acquisition has taken place, there will be a larger molecular weight species that corresponds to the addition of a spacer-repeat unit to the CRISPR array (Figure 3.1). For example, in *E. coli*, the array will increase by 61 bp due to the addition of a 33 bp spacer and the duplication of the 28 bp repeat.

The drawback of the SPIN assay is the lack of sensitivity. The smaller unexpanded arrays are amplified more efficiently. It is estimated that the expanded array needs to make up 5% of the population to become detected by PCR [242]. Spacer acquisition is rare [102], so this limited sensitivity poses a detection problem.

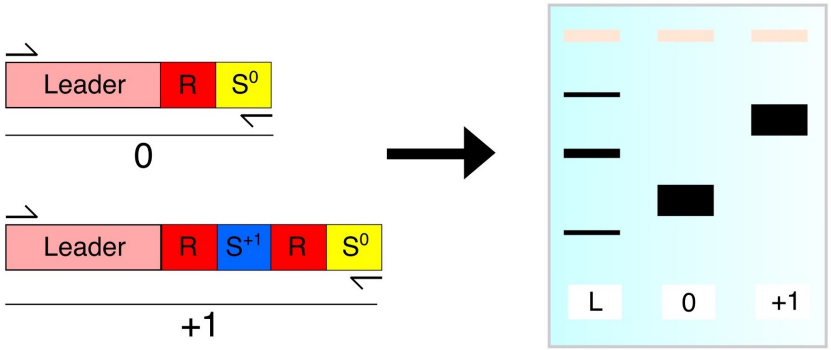


Figure 3.1. PCR amplification of the CRISPR locus to show spacer acquisition

The arrows indicate the location of spacer acquisition primers. Adding a spacer (S^{+1}) and duplicating the repeat (R) produces a larger molecular weight DNA product. S^{0} refers to the original spacer in the array. L refers to the molecular weight ladder.

An alternative to the SPIN assay is to clone a reporter gene upstream of a minimal CRISPR array made up of a single repeat or two repeats and a spacer. The reporter gene lacks a start codon and is translated as a fusion protein with a peptide encoded by the array. An unexpanded array will have a stop codon present in the Leader sequence to inhibit the expression of the reporter gene. The addition of a spacer-repeat unit results in a frameshift of the stop codon so that the reporter gene will be expressed. Previously, reporter genes have been a yellow fluorescent protein (YFP) and a chloramphenicol resistance gene [236, 243].

A novel papillation reporter strain was designed and constructed to study naïve CRISPR adaptation in *E. coli* [237]. This reporter strain, named JB028, contains an out-of-frame *lacZ* gene upstream of a constitutive promoter inserted into *argE* (Figure 3.2a). The reporter locus consists of an *E. coli* type A Leader sequence, two type A repeats and a spacer. The type A CRISPR locus in *E. coli* acquires spacers six times more efficiently than the type T CRISPR locus [236, 243]. Therefore, the native type-A locus was removed by lambda red recombination so that the majority of spacer acquisition events arise at the reporter locus. There is a STOP codon present in the Leader sequence that prevents the translation of *lacZ*. Spacers will be acquired from either the chromosome or the Cas1-Cas2 expression vector. The addition of a 61 bp spacer-repeat unit causes the STOP codon to be shifted out-of-frame and the *lacZ* gene to become in-frame. This provides the ability to metabolise lactose as a carbon source. When plated on LB agar supplemented with lactose and X-gal, spacer acquisition events are observed as small blue papillae on the surface of the white colony (Figure 3.2b&c). The isolation of papillae and performance of genomic PCR reactions across the reporter locus shows that this is due to a spacer acquisition event (Figure 3.2d).

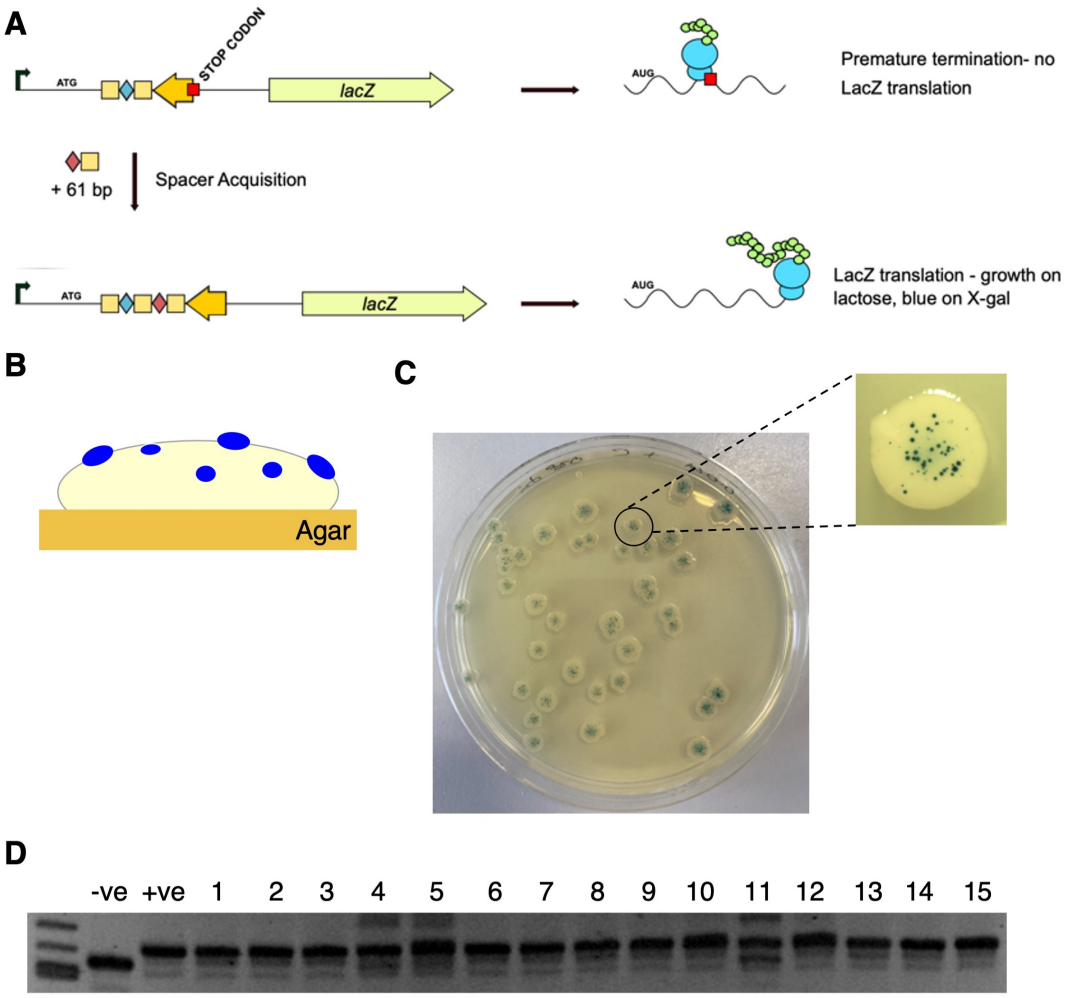


Figure 3.2. Papillation assay reporter scheme

(A) A minimal CRISPR array contains a Leader sequence (orange arrow), two type A repeats (yellow squares) and a single spacer (blue diamond). The Leader contains a stop codon (red square). The CRISPR array is inserted between a *lacZ* gene and a promoter with an RBS and a start codon. The *lacZ* is out-of-frame with the start codon to prevent translation. Acquisition of a spacer-repeat unit expands the CRISPR array by 61 bp. This induces a frameshift to place *lacZ* in-frame with the start codon and allows translation. Expression of *lacZ* results in a growth advantage and blue pigmentation. Taken with permission from (Braithwaite 2021).
(B) A cartoon representation of a papillating colony. The blue bumps represent papillae that have acquired a spacer so have a growth advantage due to the ability to metabolise lactose as a carbon source.
(C) An image of a papillation plate is shown. A single colony is highlighted.
(D) The PCR product generated by an unexpanded CRISPR array is 548 bp in length. An expanded array with an additional spacer-repeat unit 609 bp. PCR products from 15 papillae show bands at 609bp and therefore have a Lac^+ phenotype due to adaptation. Taken with permission from (Braithwaite 2021).

The number of papillae per colony is a semi-quantitative measure of spacer acquisition. This allows visual screening of conditions that alter the rate of adaptation. For example, to assess the contribution of factors such as growth conditions and mutations that change the rate of spacer acquisition.

Acquiring spacers that contain a stop codon will prevent *lacZ* expression, so papillae will not grow. Each 33 bp spacer adds 12 codons to the fusion protein. The first codon is made of the conserved TC from the end of the repeat and the first base in the spacer. The final codon will have a random base from the penultimate position in the spacer, a conserved C at the end of the spacer and a conserved G at the start of the repeat. These codons that start with TC and end in CG will not be STOP codons. As there are three stop codons, the other ten codons have a probability of 61/64 of not being a STOP codon. The size of acquired spacers also needs to be considered. 95% of spacers are 33 bp in length [243]. Spacers of a different length will not provide the frameshift required for *lacZ* expression. Consequently, only 59% of the acquisition events will result in papillation:

$$(61/64)^{10} \times 0.95 = 0.59$$

As spacers are acquired randomly, this is sufficient for a semi-quantitative measure of adaptation. More than one spacer acquisition event would shift the *lacZ* back out-of-frame and prevent expression. However, since the rate of spacer acquisition is so low, this is not a problem. Adaptation events that produce inviable cells will also not be visualised, as the papillae will be unable to grow (Figure 3.3). These factors need to be considered when calculating the absolute rate of adaptation.

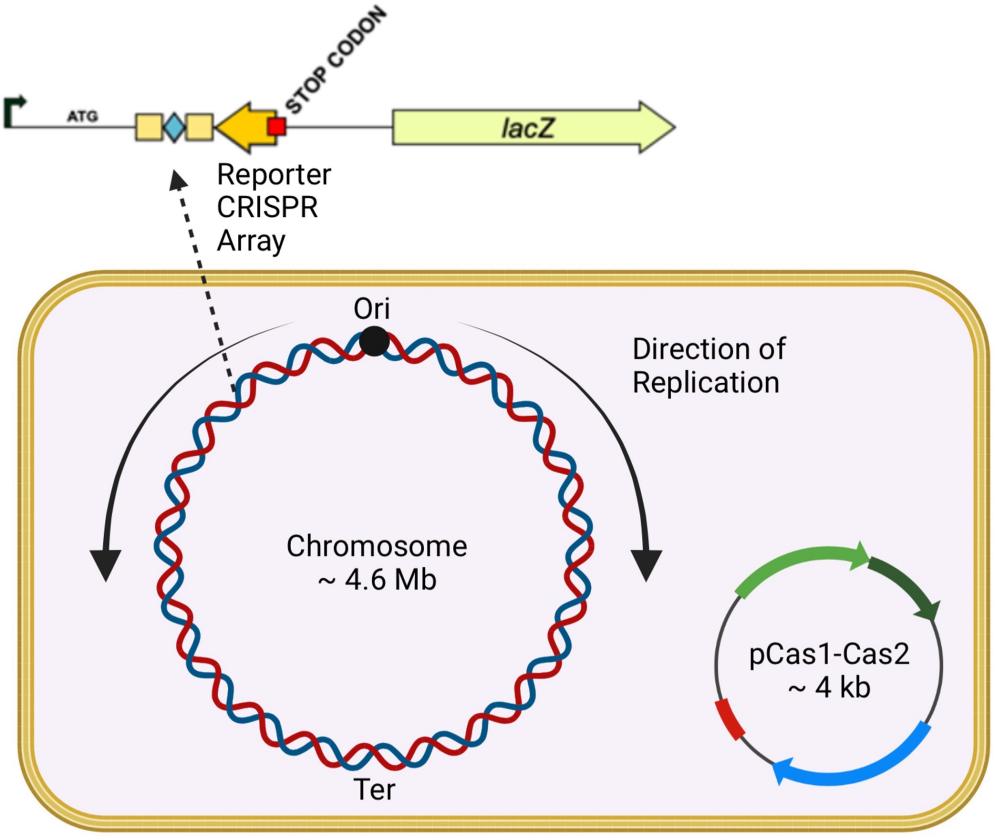


Figure 3.3. Location of the Reporter CRISPR Array

The reporter CRISPR array is inserted into the *argE* locus, located at 322°, close to the *ori*. Spacers are derived from either the chromosome or the Cas1-Cas2 expression vector. As the interference machinery is not expressed, self-targeting spacers are not lethal. The hotspots for spacers are the Cas1-Cas2 expression vector, at the *ter* and immediately upstream of the reporter CRISPR array, with regards to the replication fork [145]. Therefore, changing the location of the reporter CRISPR array would alter the location of a hotspot for chromosomal-derived spacers. In order for papillae to grow, the spacer-acquisition event must leave viable cells. Consequently, acquisition events that result in DNA damage that cannot be repaired by the cell, will not be visualised as the papillae will be unable grow through.

The black circle represents the chromosome origin of replication. The black arrows show the direction of chromosome replication. The black circle represents the Cas1-Cas2 expression vector, where the green arrows are Cas1-Cas2, the blue arrow is the antibiotic resistance gene and the red block is the plasmid origin of replication.

The reporter CRISPR array contains a Leader sequence (orange arrow), two type A repeats (yellow squares) and a single spacer (blue diamond). The Leader contains a stop codon (red square). The CRISPR array is inserted between a *lacZ* gene and a promoter with an RBS and a start codon. The *lacZ* is out-of-frame with the start codon to prevent translation. The reporter scheme is taken with permission from (Braithwaite 2021).

3.2 Determination of the choice of Cas1-Cas2 Expression Vector

The choice of Cas1-Cas2 expression vector needed to be optimised. Different inducible promoters with various strengths were tested in papillation assays. The use of a pBAD, pMARI$_{Ara}$ and pT7 expression vector was compared across a range of L-arabinose concentrations. The pBAD vector is leaky and not titratable, since 0.002 % L-arabinose has the highest rate of papillation (Figure 3.4). In contrast, the pMARI$_{Ara}$ expression vector is titratable. The T7 promoter resulted in the formation of white bumps with minimal papillae produced. The pMARI$_{Van}$ and pMARI$_{Sal}$ plasmids were also tested across a range of vanillic acid and salicylic acid concentrations. Neither of these expression vectors produced papillae.

Consequently, the pMARI$_{Ara}$ expression vector will be used for the majority of papillation assays. This contains an optimised arabinose inducible promoter that allows titratable Cas1-Cas2 expression [233]. As 0.02 % L-arabinose gives a moderate rate of papillation, this induction level will be used to detect conditions that lead to hypo and hyperactive papillation.

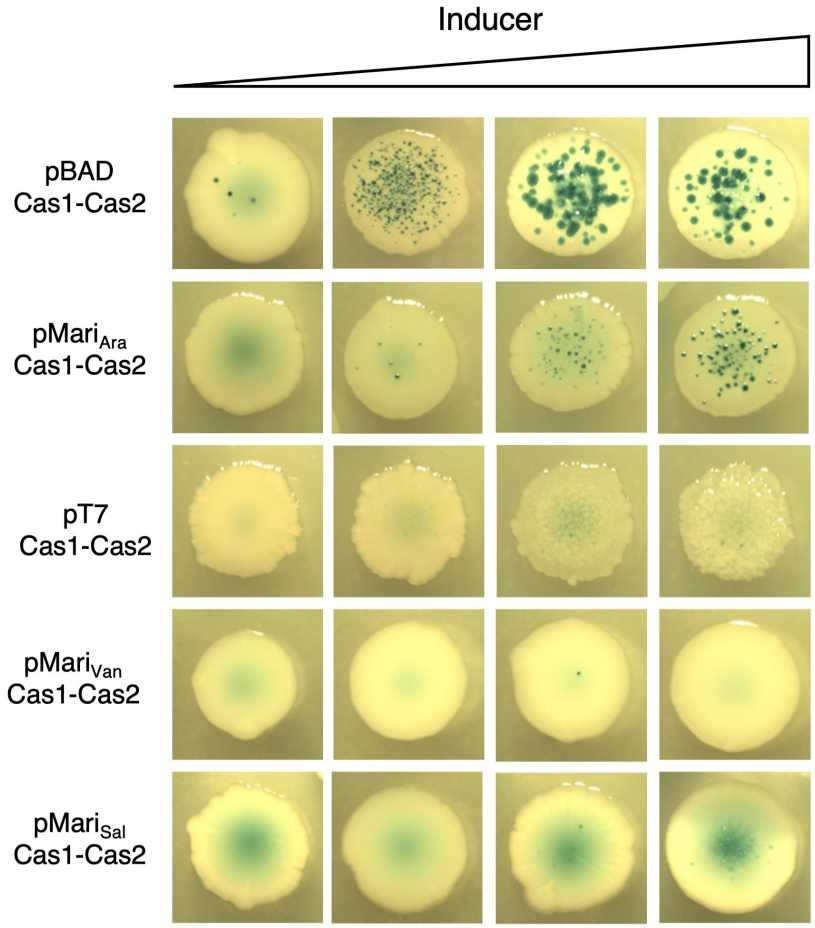


Figure 3.4. Optimisation of papillation assay expression vector

Papillation assays were performed in *E. coli* JB028 to determine the best Cas1-Cas2 expression vector. Arabinose was used at 0, 0.002%, 0.02% & 0.2% for pBAD, pMARI$_{Ara}$ & pT7. pT7 was also induced by 0.1 mM IPTG. 0, 1, 10 & 100 μM vanillic acid and salicylic acid were used for pMARI$_{Van}$ & pMARI$_{Sal}$, respectively. Representative day 5 colonies are shown.

3.3 Optimisation of Salt Concentration

Previous experiments in the lab have shown that the salt concentration in the medium alters the rate of papillation. To determine which salt concentration to use, papillation assays were performed across a range of 0 - 10 g/L NaCl (Figure 3.5). The use of low salt concentrations produced papillae that appeared flat and had a minimal growth advantage. At high salt concentrations, the number of papillae decreased. At 5 g/L, the papillae looked healthy and had an obvious growth advantage. Consequently, this will be used for future experiments.

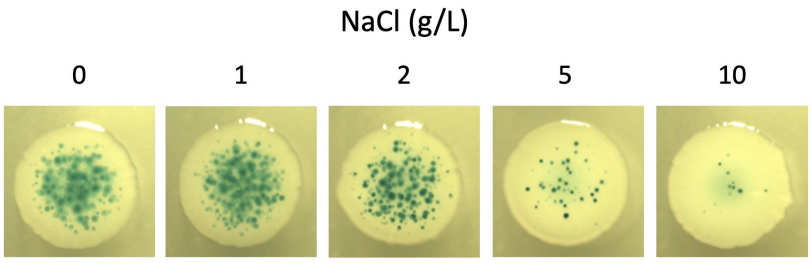


Figure 3.5. Salt concentration alters the rate of papillation

Papillation assays were performed in *E. coli* JB028. pMARI$_{Ara}$ Cas1-Cas2 expression was induced by 0.02 % L-arabinose. The NaCl concentration in the agar ranges from of 0 - 10 g/L. Representative day 5 colonies are shown.

3.4 Liquid Culture Assays

During transposon mutagenesis, it was discovered that not all hypopapillating mutants were spacer acquisition deficient [237]. For example, when *csyH* was deleted, the colony does not papillate (Figure 3.6a). This is due to the growth-inhibitory effects of a lack of cysteine. When all of the cysteine in the medium has been metabolised, the cells are unable to synthesise more, so they are unable to grow. Consequently, the medium is not carbon-limiting but instead cysteine-limiting. When *lacY* was deleted, no papillation arose. Lactose is not transported into the cell, so there is no growth advantage for those cells that have acquired a spacer and express *lacZ* (Figure 3.6a). Therefore, hypopapillating mutants will be verified using the pre-existing PCR based SPIN assay.

Liquid culture SPIN assays were performed in the reporter to determine the most suitable Cas1-Cas2 expression vector. Primers were designed to verify the insertion of a spacer into the reporter array (Table 2.3). The unexpanded array will produce a PCR product of 548 bp and the insertion of a spacer-repeat unit will give a 609 bp PCR product. There was no adaptation when the pT7 Cas1-Cas2 and pMARI$_{Ara}$ Cas1-Cas2 expression vectors were used (Figure 3.6b). The use of a pBAD Cas1-Cas2 expression vector results in visible spacer acquisition at higher arabinose concentrations. Consequently, the pBAD expression vector will be induced by 0.2 % L-arabinose for SPIN assays.

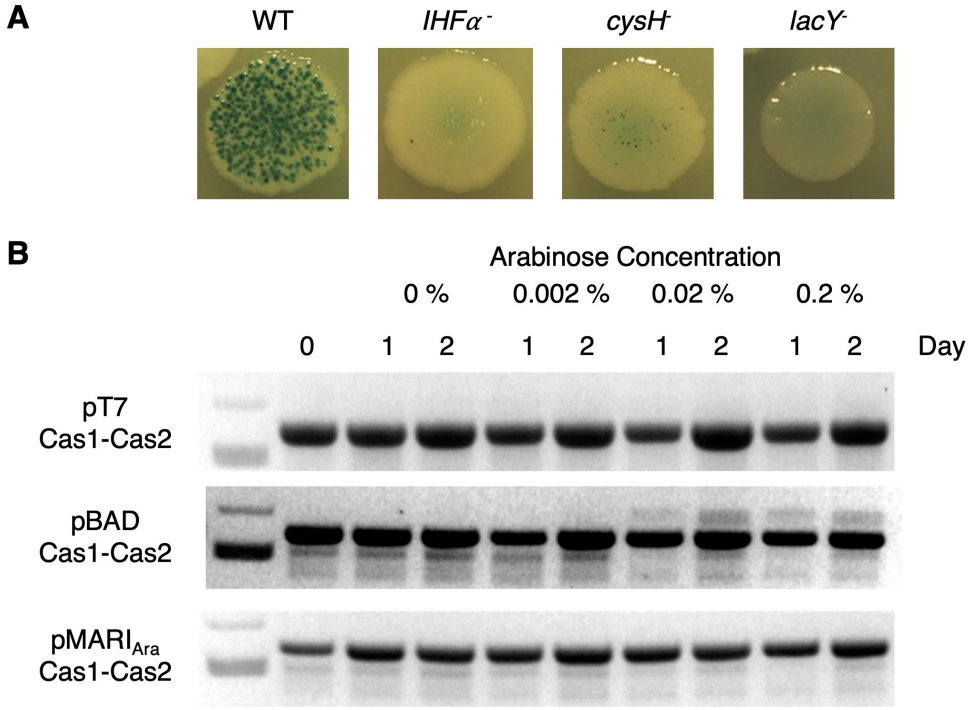


Figure 3.6. Optimisation of Cas1-Cas2 expression vector choice for use in JB028 liquid culture assays

(A) Metabolic Mutants do not papillate due to growth-inhibitory effects. Papillation assays performed in wild type JB028 *E. coli* and Tn5 insertion mutants. pBAD Cas1-Cas2 expression was induced by 0.002 % L-arabinose. IHF is included as a negative control. Day 5 colonies are shown. Images taken with permission from (Braithwaite, 2021).
(B) Liquid culture spacer acquisition assays were performed in *E. coli* JB028. Arabinose was used to induce Cas1-Cas2 expression at 0, 0.002 %, 0.02 % & 0.2 %. pT7 assays were also performed in the presence of 0.1 mM IPTG. Sub-cultures (1:1000 dilution) were initiated daily for two days. Spacer acquisition was determined by PCR. PCR Products were visualised by agarose gel electrophoresis.

3.5 Testing the compatibility of the Marionette vector collection with the spacer acquisition reporter system

The Marionette collection is a series of inducible expression vectors that can be used to overexpress genes in *E. coli* [233]. The promoters were evolved to tightly repress expression in the absence of and be highly titratable in the presence of the inducer molecule. There was no cross-talk between lactose, arabinose and the vanillic acid, salicylic acid or cuminic acid inducers. This should allow papillation assays to be performed in their presence and the rate of papillation will not be altered. The pBAD Cas1-Cas2 expression vector can be used in combination with the marionette plasmids due to the different origin of replications.

I first tested whether there was any cross-talk between the cuminic, salicylic and vanillic acid inducers on the rate of papillation in my reporter system. To do this, a range of 0 - 100 μM inducer was added to papillation plates. This range was used as the maximum promoter activity was achieved at 100 μM for all inducible plasmids [233]. None of the inducer molecules changed the rate of papillation (Figure 3.7a). I also determined the effect on papillation of expressing eYFP, which has no apparent connection to spacer acquisition. The gene was cloned into the cuminic, salicylic and vanillic acid expression vectors and transformed into the reporter along with pBAD Cas1-Cas2. Papillation assays were performed across a range of 0 - 100 μM for each inducer molecule. The rate of papillation was not altered when eYFP was expressed from the inducible expression vectors (Figure 3.7b).

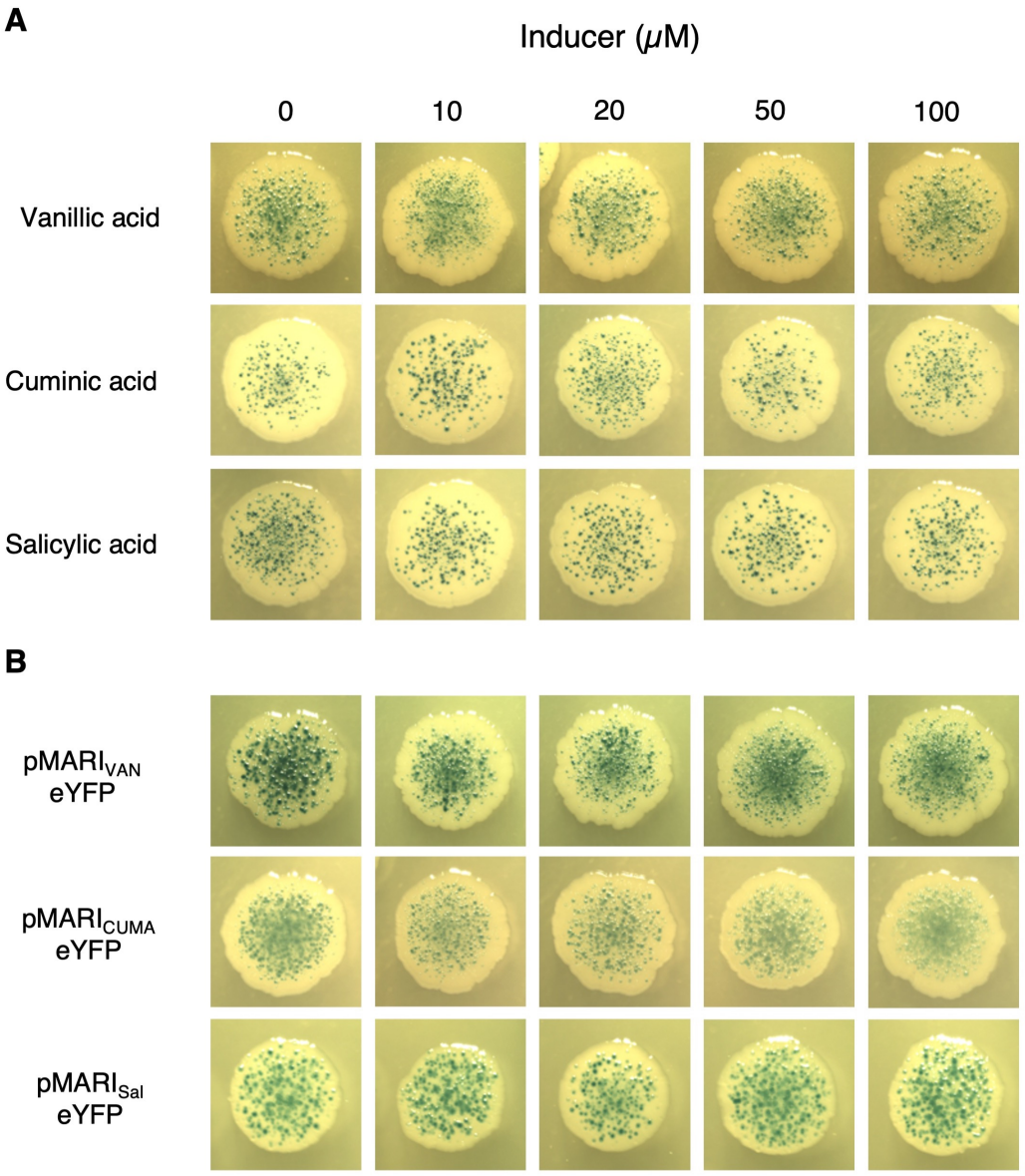


Figure 3.7. Use of Marionette inducer molecules or plasmids does not alter the rate of papillation

(A) Papillation assays were performed in *E. coli* JB028. pBAD Cas1-Cas2 expression was induced by 0.002% L-arabinose. The concentration of vanillic acid, cuminic acid and salicylic acid was titrated from 0 – 100 µM. Representative colonies from day 5 are shown.
(B) Papillation assays were performed in *E. coli* JB028 while overexpressing eYFP. pBAD Cas1-Cas2 expression was induced by 0.002% L-arabinose. eYFP expression was induced from $pMARI_{Van}$, $pMARI_{CUMA}$ and $pMARI_{Sal}$ plasmids across a range of 0 – 100 µM inducer. Representative day 5 colonies are shown.

The titratability of eYFP fluorescence was measured for each vector across a range of inducer concentrations in the Marionette cloning strain and the papillation reporter. Since the maximum promoter activity was achieved at 100 μM for all inducible plasmids, a range of 0 - 100 μM inducer was used [233]. All three expression vectors showed increased eYFP fluorescence in the Marionette cloning strain (Figure 3.8a-c). The vanillic acid plasmid was the most titratable, with a significant increase in eYFP fluorescence across every concentration tested. In the reporter strain, eYFP fluorescence increased with cuminic acid concentration. However, there is only a slight increase from 25 - 50 - 100 μM, with 50 - 100 μM not being significant (Figure 3.8d). The salicylic acid expression vector was not titratable, since fluorescence decreased when the inducer concentration increased above 25 μM (Figure 3.8e). As the concentration of vanillic acid increased, eYFP fluorescence increased to a significant level across all concentrations (Figure 3.8f). A control assay showed that growth in the presence of vanillic acid did not induce auto-fluorescence (Figure 3.8g). Furthermore, the presence of arabinose and Cas1-Cas2 expression did not alter the titratability of eYFP fluorescence (Figure 3.8h). Therefore, genes of interest will be overexpressed from the Marionette vanillic acid expression vector.

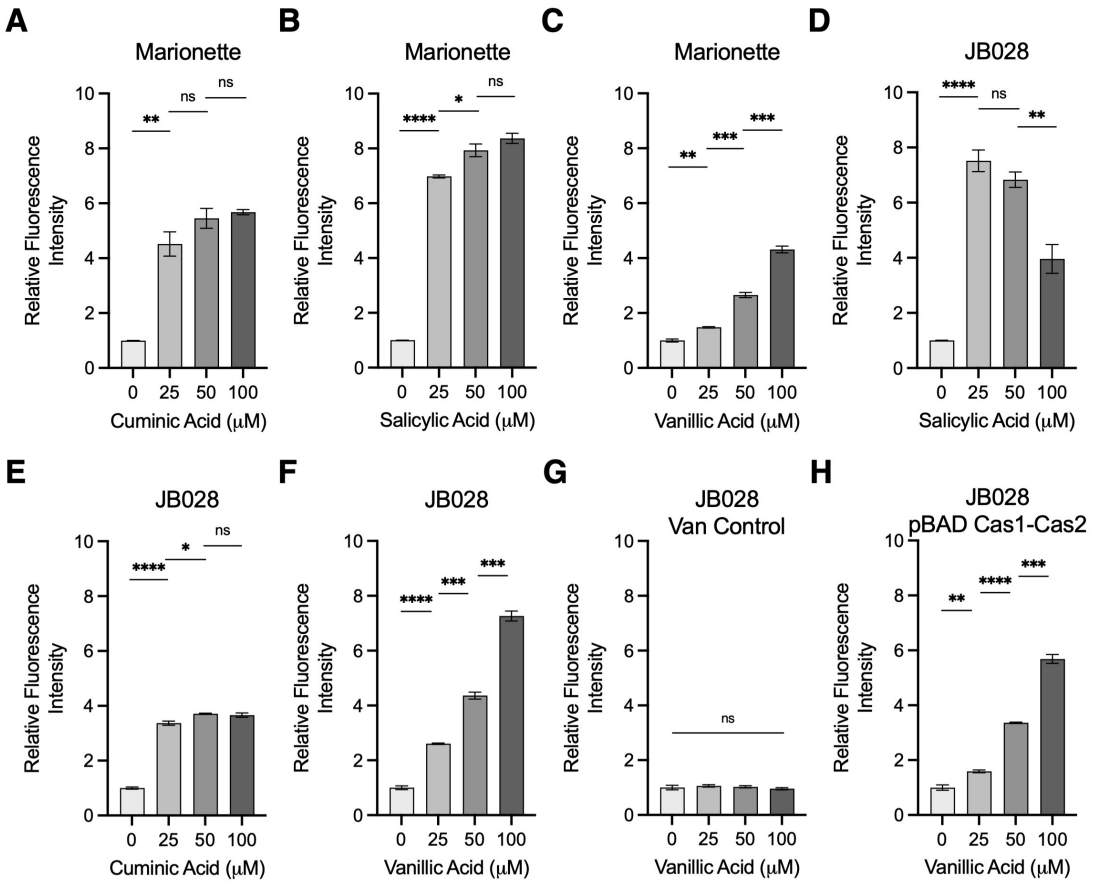


Figure 3.8. The Marionette vanillic acid promoter is titratable in the adaptation reporter

eYFP induced from the pMari$_{CUMA}$, pMari$_{Sal}$ and pMari$_{Van}$ in the Marionette DH10β (A-C) and JB028 (D-F) across a range of 0 - 100 μM inducer. (G) JB028 grown in the presence of vanillic acid without the vanillic acid eYFP expression vector. (H) pBAD Cas1-Cas2 expression was induced by 0.002% L-arabinose in JB028. pMari$_{Van}$eYFP expression was induced across a range of 0 - 100 μM vanillic acid. All experiments were repeated in triplicate. The mean is plotted and the error bars are SEM. YFP Intensity compared to the previous treatment by two-way t-test. P value: ns = not significant, * < 0.05, ** < 0.01, *** < 0.001, **** < 0.0001. Raw intensity and P values are listed in S2.

3.6 Precise Genetic Deletions

The Keio collection is a single-gene knockout deletion library of non-essential genes in *E. coli* K12 [240]. The genes are replaced by a kanamycin resistance gene flanked by FLP recombination sites. This gives non-polar deletions that do not disrupt the other genes in the operon. Removal of the resistance gene results in an in-frame deletion that encodes a 34 residue peptide.

P1 transduction can be used to move gene deletions from the Keio collection to the adaptation reporter strain. The donor strain is infected with P1 phage to make a lysate. This lysate is then used to infect the reporter strain and transfer the kanamycin marker to replace the gene of interest. As the integration event is due to homologous recombination, the selectable marker is inserted at the precise location in the genome. This insertion can be verified by PCR amplification across the target locus. The kanamycin resistance gene can then be removed by FLP recombination (Figure 3.9).

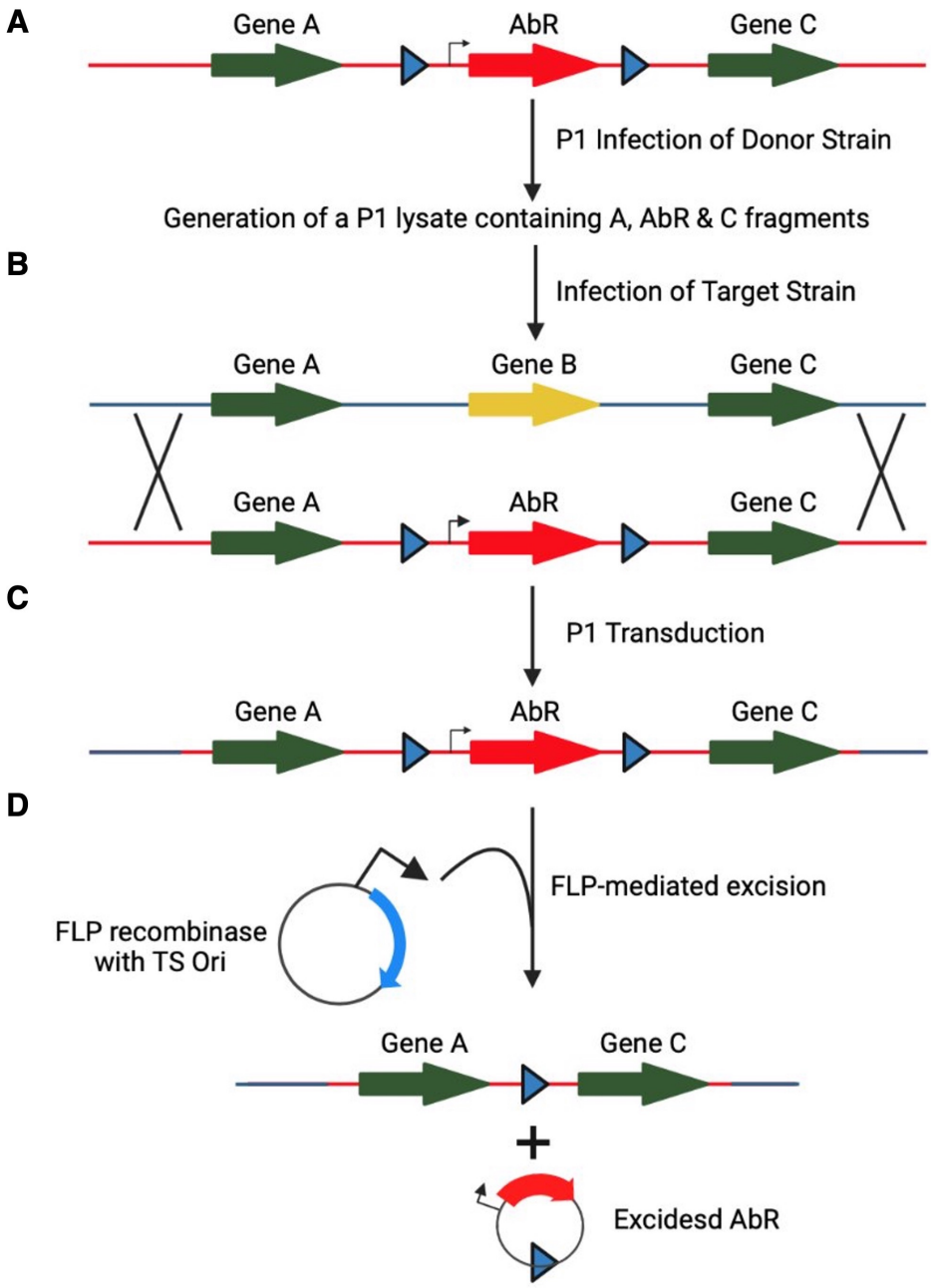


Figure 3.9. P1 transduction strategy gene transfer in *E. coli*

(A) A P1 lysate is prepared from a donor strain (red). The donor strain carries a mutation of interest with a neighbouring selectable marker (AbR, red arrow). The prepared lysate contains P1 phage particles carrying up to 100 kb fragments of the donor strain chromosome.
(B) A recipient strain (blue) is infected with the prepared P1 lysate to introduce 100 kb fragments of the donor strain chromosome. These fragments are integrated into the recipient chromosome at a low frequency through homologous recombination.
(C) Selection of the AbR marker reveals recipient colonies containing the mutation of interest.
(D) Recipients with the desired mutation are cured of the AbR marker by FLP recombination between frt sites (blue arrow).

3.7 Complementation of gene deletions restores the papillation phenotype

IHF is an essential host factor for spacer acquisition in the type I-E CRISPR system of *E. coli* [123]. *IHF*α was deleted from the reporter strain by P1 transduction from the Keio collection (Figure 3.10a). Papillation assays performed in the Δ*IHF*α background showed a reduced rate of adaptation compared to the wild type (Figure 3.10b).

To test if gene expression could restore the papillation phenotype, *IHF*α was cloned into the vanillic acid expression vector. This was transformed into the reporter along with pBAD Cas1-Cas2. Papillation assays were performed across a range of 0 - 50 μM vanillic acid. At low levels of *IHF*α overexpression, the rate of papillation increases (Figure 3.10c). At high levels of *IHF*α overexpression, the rate of papillation then decreases, but remains higher than the uninduced control.

To determine if papillation was due to bona fide spacer acquisition, six papillae were isolated and genomic PCR reactions were performed across the reporter locus. These were performed alongside a negative and positive control. The PCR product of all six papillae was the same size as the positive control (Figure 3.10d). These were approximately 61 bp larger than the product from the reporter, the size of a newly added spacer-repeat unit to the CRISPR array. Therefore, I concluded that spacer acquisition had occurred in the six papillae where IHFα was overexpressed from the marionette vanillic acid expression vector.

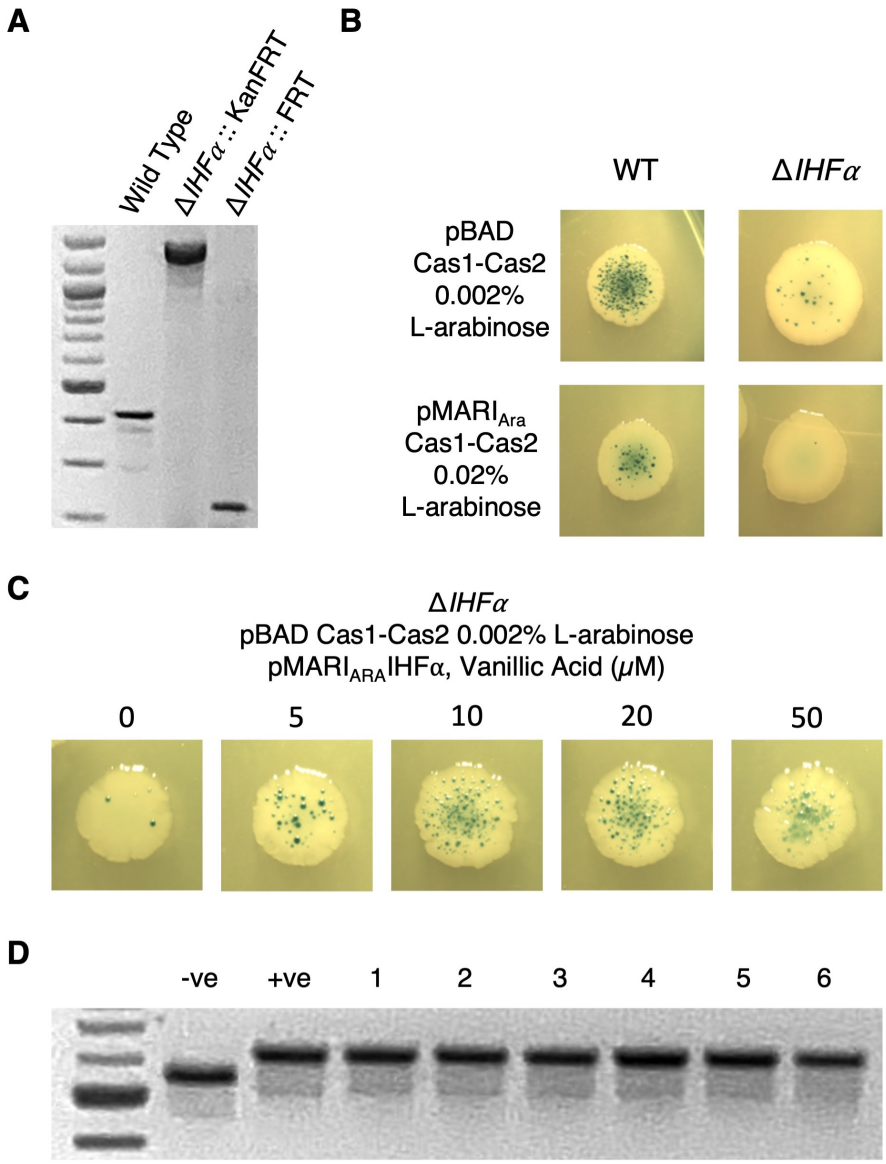


Figure 3.10. Papillation is restored in JB028 Δ*IHFα* when IHFα is complemented back on an inducible plasmid

(A) PCR Verification of Δ*IHFα* deletion from JB028.
(B) Papillation assays were performed in *E. coli* JB028 and Δ*IHFα*. pBAD Cas1-Cas2 expression was induced by 0.002% L-arabinose. pMARI$_{Ara}$ Cas1-Cas2 expression was induced by 0.02% L-arabinose. Representative of day 5 colonies are shown.
(C) Papillation assays were performed in JB028 Δ*IHFα* with *IHFα* complemented back. pMARI$_{Van}$IHFα expression was induced across 0 - 50 μM vanillic acid. pBAD Cas1-Cas2 expression was induced by 0.002% L-arabinose. Representative day 5 colonies are shown.
(D) PCR verification of six papillae from 20 μM induction in (C). The template for the wild type control is JB028. The positive control is pRC1644 which has an extra spacer added to the reporter CRISPR array.

3.8 Chapter Summary

- JB028 is a reporter strain to study spacer acquisition in *E. coli*.
- $pMARI_{Ara}$ Cas1-Cas2 produces a moderate rate of spacer acquisition that will allow hypo- and hyperpapillating mutants and conditions to be determined.
- Genes of interest can be overexpressed from the $pMARI_{Van}$ plasmid.
- P1 transduction is a strategy to precisely delete genes.
- The phenotype can be restored from a genetic deletion by complementation on the $pMARI_{Van}$ plasmid.

Chapter 4

Cas1-Cas2 Induces Filamentation by Activation of the SOS Response and SulA Expression

4.1 Introduction

The careful coordination of events during cell division is required to ensure that each daughter cell contains a complete copy of the genome [244]. Inhibition of cell division often produces filamentous cells, as cell growth and DNA replication continue in the absence of division. Filamentation is frequently induced in prokaryotes in response to environmental stimuli such as nutrient deprivation, exposure to antibiotics or to evade the immune system of a multicellular eukaryotic-host [245–248].

In *E. coli*, several different pathways are known to inhibit cell division. Both the MinCDE and Nucleoid Occlusion systems function to prevent cell division at locations away from the midcell to assist in DNA segregation to daughter cells [249, 250]. Downregulation of transcription of specific cell cycle genes can also induce filamentation [251]. Activation of the SOS response results in filamentation after DNA damage [252, 253]. This allows time for DNA repair to occur before cell division to prevent DNA damage from being passed onto daughter cells.

Cas1-Cas2 expression in *E. coli* has been reported to induce filamentation [254]. Separation of filament-enriched and rod-enriched cells seemed to show that the filamentous population had an increased rate of spacer acquisition. Filamentation arises first and is then followed by adaptation. My aim was first to reproduce these findings and then go on to determine the mechanism by which Cas1-Cas2 induces filamentation and why this increases the rate of spacer acquisition.

4.2 Cas1-Cas2 expression induces filamentation

To determine the effects of Cas1 and Cas2 expression on cell morphology, the corresponding genes were first cloned into the arabinose-inducible plasmid pBAD and the IPTG-inducible plasmid pT7. Expression of Cas1-Cas2 from either plasmid caused filamentation but the effect was more pronounced after expression from the stronger T7 promoter (Figure 4.1). As a control, I also tested the impact of arabinose and IPTG on morphology and the effects of expressing the Cas1 and Cas2 proteins separately. Since the cell morphology was unchanged, I can conclude that filamentation results from the activity of the Cas1-Cas2 complex.

To determine whether filamentation was caused by Cas1-Cas2 binding or by its catalytic activity, I introduced the D221A mutation. This mutant is often referred to as dead-Cas1 (dCas1) because it abolishes catalytic activity but not site-specific binding to the CRISPR Leader [100]. When dCas1-Cas2 was expressed from the arabinose promoter on pBAD, the cells did not filament (Figure 4.1d). This suggests that filamentation is caused by the nuclease activity of Cas1-Cas2 rather than DNA binding.

IHF is required for the integration of spacers into the CRISPR array, as it binds to and bends the Leader sequence to stabilise the binding of the Cas1-Cas2 complex [120]. To see whether filamentation is the result of Cas1-Cas2 activity at the CRISPR locus, a BL21-AI $\triangle$*IHF*α strain was made by P1 transduction from the Keio collection. Overexpression of Cas1-Cas2 from the arabinose promoter on pBAD induced filamentation in BL21-AI $\triangle$*IHF*α (Figure 4.1e). Filamentation, therefore, appears to arise from the nuclease activity of Cas1-Cas2 at non-specific sites across the genome.

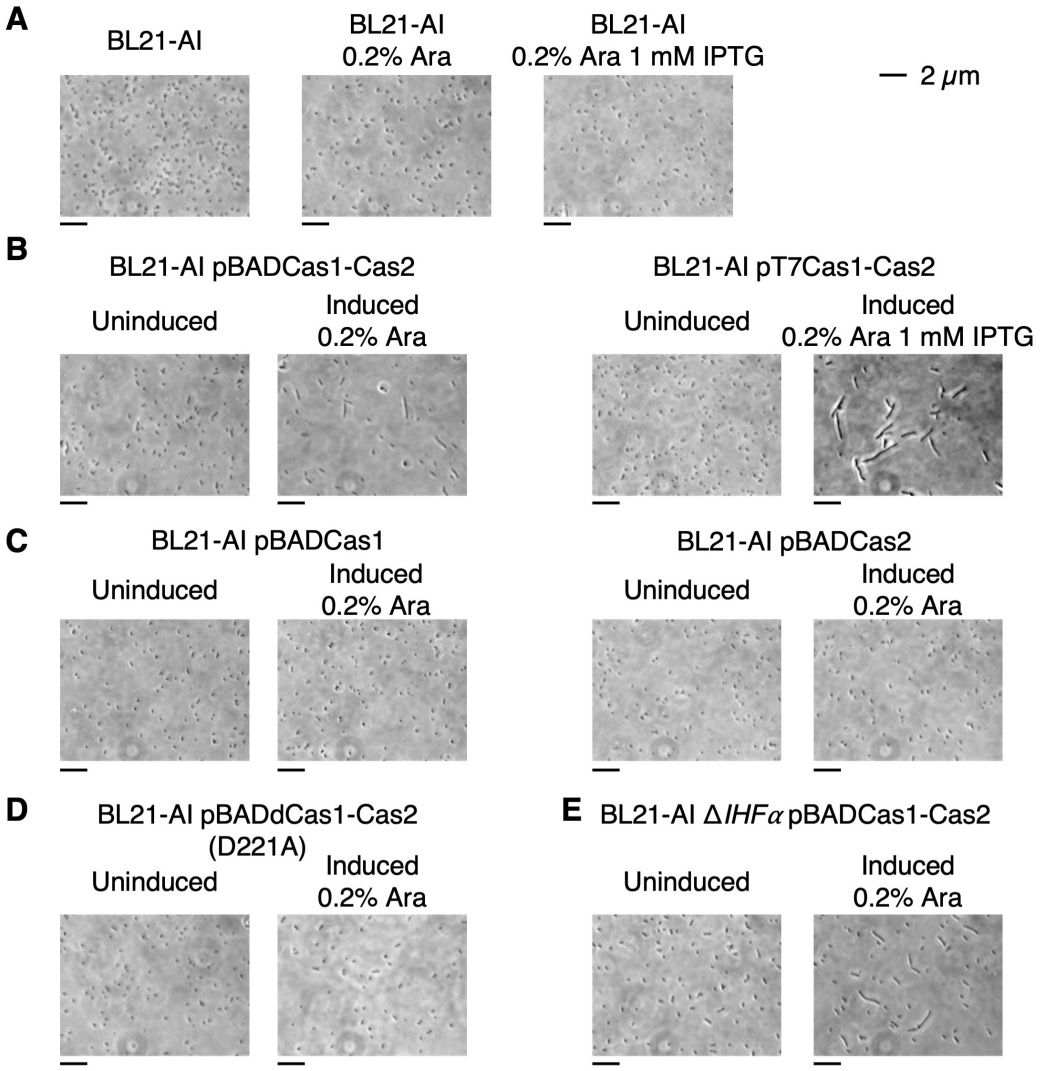


Figure 4.1. The catalytic activity of Cas1-Cas2 induces filamentation

(A) BL21-AI grown in LB broth, & 0.2% L-Arabinose and 0.2% L-Arabinose & 1 mM IPTG.
(B) pBADCas1-Cas2 & pT7Cas1-Cas2 overexpressed in BL21-AI.
(C) pBADCas1 & pBADCas2 overexpressed in BL21-AI.
(D) pBADdCas1-Cas2 overexpressed in BL21-AI.
(E) pBADCas1-Cas2 overexpressed in BL21-AI $\Delta IHF\alpha$.
pBAD plasmids induced by 0.2% L-Arabinose. pT7 plasmid induced by 0.2% L-Arabinose & 1 mM IPTG. Ten images were taken for each condition. The scale bar is 2 μm. These are presented in the appendix.

4.3 Spacer acquisition is not more abundant in filamentous cells

Wang et al., reported that spacer acquisition is more abundant in filament-enriched cells than in rod-enriched cells [254]. I wanted to determine the reproducibility of this data. Cas1-Cas2 was expressed from the IPTG-inducible plasmid pT7 for 6 or 24 hours in BL21-AI. A 1.2 μm filter was used to separate the filaments and rod cells (Figure 4.2a). PCR-based SPIN assays for adaptation showed that the filament-enriched cell population did not have an increased rate of spacer acquisition for either of the time points (Figure 4.2b). This directly contradicts the results of Wang et al. [254].

I wanted to quantify the rate of spacer acquisition in filaments and rod cells. I used the MLS989 YFP reporter strain [236], which contains a minimal CRISPR array with a stop codon in the Leader sequence and a downstream out-of-frame *yfp* gene (Figure S8a). The addition of a spacer-repeat unit into the reporter array will shift the stop codon out-of-frame and the *yfp* in-frame to induce fluorescence. Control assays showed that fluorescence detection allowed YFP- and YFP+ cells to be differentiated and this fluorescence arose because of spacer acquisition (Figure S8b&c).

Cells that either express or do not express YFP can be separated by flow cytometry and their numbers counted. Cas1-Cas2 expression was induced from the IPTG-inducible plasmid pT7 for 6 or 24 hours in the MLS989 YFP reporter strain. A 1.2 μm filter was used to separate the filaments and rod cells. The populations were diluted in LB broth supplemented with 25 mM glucose and outgrown to allow YFP maturation and resolve filamentation. There was no significant difference in the proportion of YFP+ cells between the filaments or rod cells (Figure 4.2c). Therefore, I concluded that spacer acquisition is not more abundant in filamentous cells. This directly contrasts with that published by Wang et al. [254].

YFP- cells grow faster than YFP+ cells (Figure S9). Therefore, the rate of spacer

acquisition will be higher than that calculated by flow cytometry. However, since I wanted to compare the rate of adaptation in filamentous and rod cells, this will not be an issue, as all conditions will be affected equally.

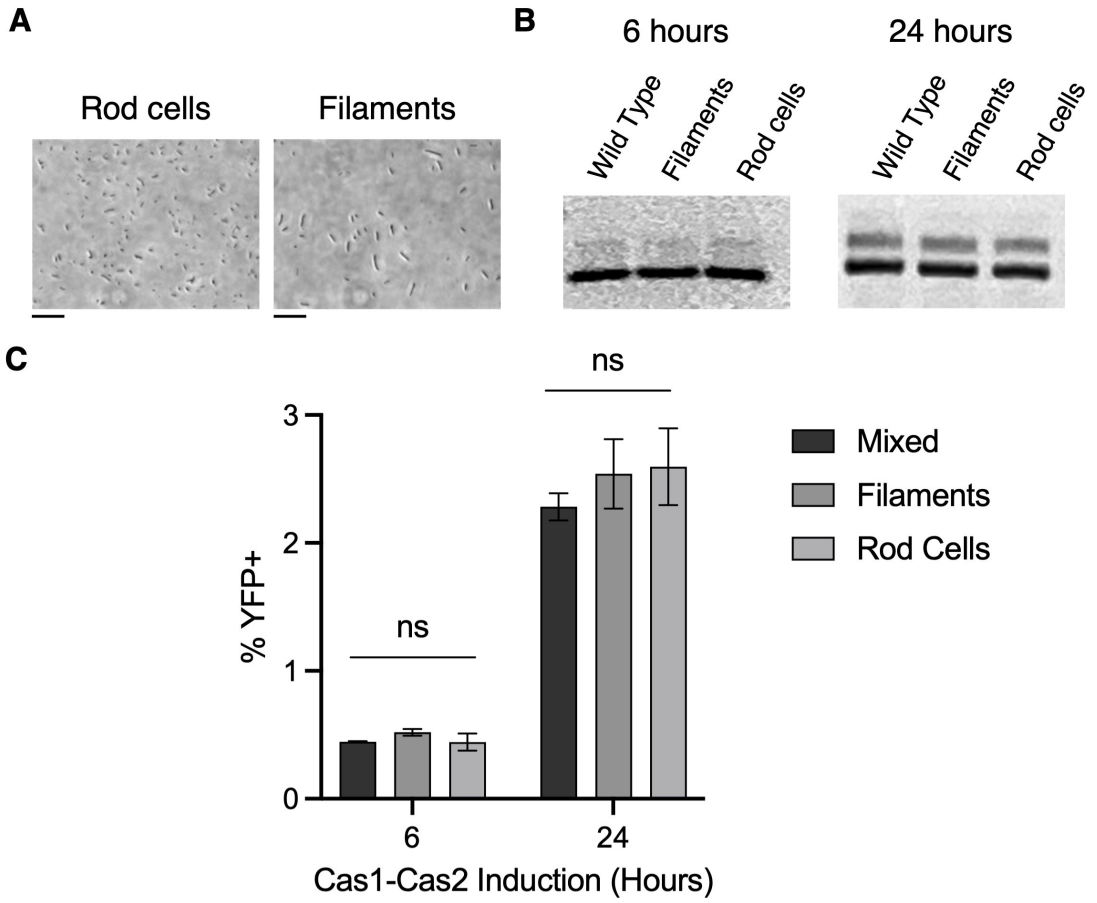


Figure 4.2. Spacer acquisition is not more abundant in filamentous cells

(A) Passing cells through a 1.2 μm filter separates rod cells and filaments. The scale bar is 2 μm.
(B) pT7 Cas1-Cas2 was overexpressed at 0.1 mM IPTG and 0.2 % L-arabinose in BL21-AI for 6 or 24 hours. The culture was passed through a 1.2 μm filter to separate filaments and rods. PCR-based SPIN assays for adaptation were performed on the different populations.
(C) pT7 Cas1-Cas2 was overexpressed at 0.1 mM IPTG and 0.2 % L-arabinose in the MLS989 YFP reporter strain for 6 or 24 hours. The culture was passed through a 1.2 μm filter to separate filaments and rods. The cells were outgrown in LB broth + 25 mM glucose for 5 hours to support YFP maturation and resolve filamentation. Flow cytometry was performed to test the proportion of YFP+ cells in each population. Repeated three times. The mean is plotted and the error bars are SEM. Populations compared by ANOVA. The raw data is presented in S3.

4.4 Cas1-Cas2 induces the SOS response

The induction of the SOS response after DNA damage results in filamentation by inhibition of FtsZ polymerisation, owing to the activity of SulA [252, 253]. In *E. coli*, DNA damage is signalled via the cleavage of the LexA repressor, which allows the expression of genes of the SOS regulon, including the cell cycle inhibitor *sulA*. Since the catalytic activity of Cas1-Cas2 induces filamentation (Figure 4.1), I wondered whether the expression of Cas1-Cas2 induces the SOS response.

A reporter plasmid that contains a *gfp* gene under the control of the *sulA* promoter was used to detect the induction of the SOS response [239]. The reporter plasmid will express *gfp* at the same time as the expression of the chromosomal *sulA*. Cells that are GFP+ have induced the SOS response (Figure 4.3a). The higher the level of induction, the higher the level of GFP expression.

Nalidixic acid is a DNA gyrase inhibitor that induces the SOS response by the introduction of dsDNA breaks [255, 256]. To test the SOS reporter plasmid, BL21-AI was grown in LB broth supplemented with subinhibitory concentrations of nalidixic acid. GFP fluorescence increased with the concentration of nalidixic acid. Growth at all concentrations of nalidixic acid resulted in a significant increase in *gfp* expression compared to nalidixic acid free controls (Figure 4.3b).

Since a pBAD vector will be used for Cas1-Cas2 expression, the effect of arabinose on the induction of the SOS response was also studied. Cells were grown overnight in LB broth supplemented with either 0, 0.05, 0.1, or 0.2 % arabinose. Increasing the concentration of arabinose did not alter *gfp* expression (Figure 4.3c). Therefore, as expected, arabinose does not induce the SOS response.

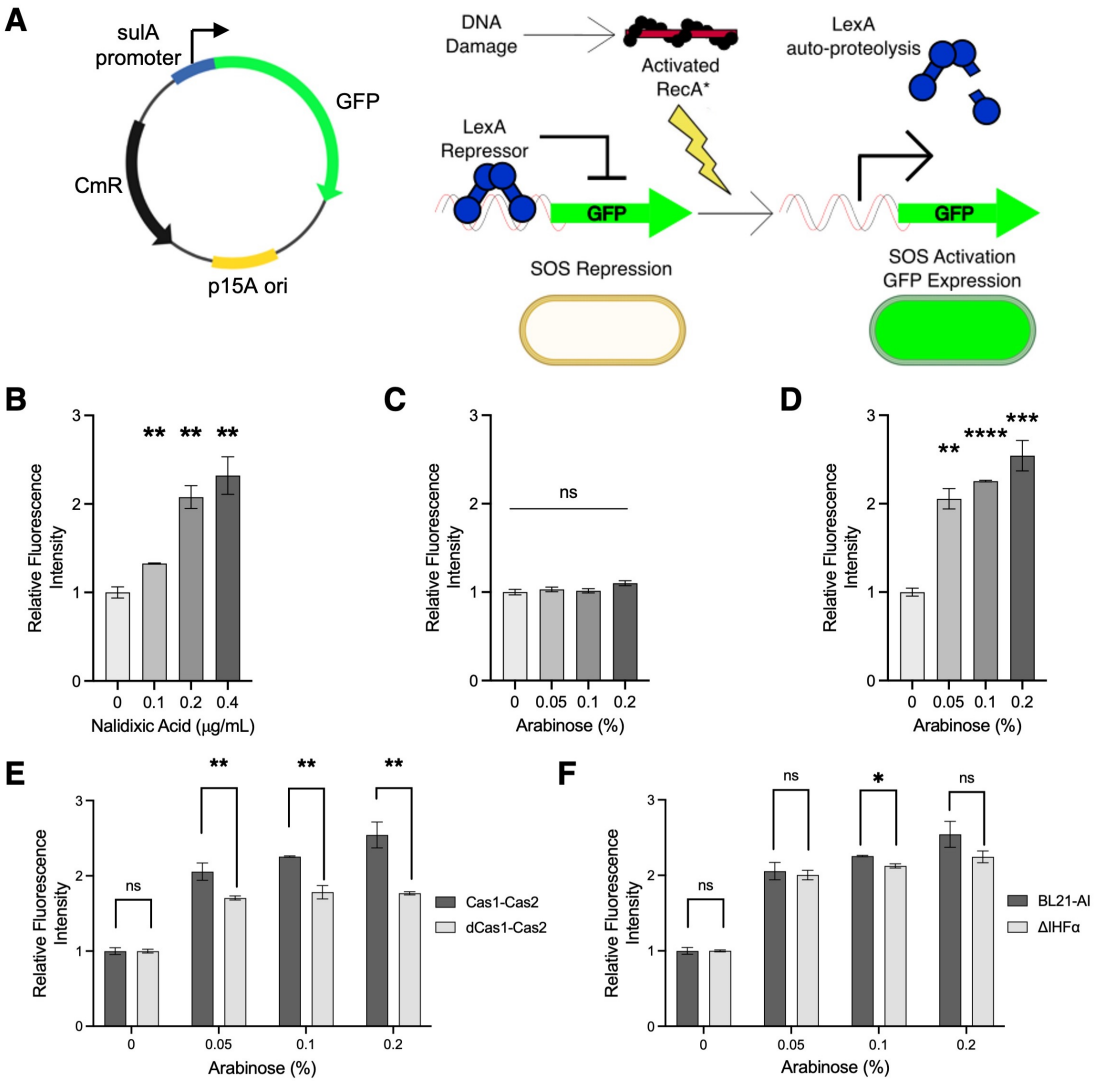


Figure 4.3. Cas1-Cas2 expression induces the SOS response

(A) Schematic of the SOS reporter plasmid (pRC2790). DNA damage results in the formation of RecA filaments which triggers LexA autoproteolysis and activation of the SOS response. The SOS reporter plasmid contains a *gfp* gene downstream of the *sulA* promoter, a gene of the SOS regulon. Induction of the SOS response is observed by GFP fluorescence.
(B) BL21-AI grown across a range of 0 – 0.4 µg/mL nalidixic acid.
(C) BL21-AI grown across a range of 0 - 0.2 % arabinose.
(D) pBADCas1-Cas2 induced by 0 – 0.2 % arabinose in BL21-AI.
(E) pBADdCas1-Cas2 induced by 0 – 0.2 % arabinose in BL21-AI.
(F) pBADCas1-Cas2 induced by 0 – 0.2 % arabinose in BL21-AI $\Delta IHF\alpha$.
GFP intensity measured by expression from the SOS reporter plasmid. All assays were repeated in triplicate. The mean is plotted and the error bars are SEM. For (B), (C) & (D), raw intensity values compared to no treatment control by two-way t-test. For (E) & (F), raw intensity values were compared to the same level of arabinose concentration in (D) by a two-way t-test. P value: ns = non-significant, * < 0.05, ** < 0.01, *** < 0.001, **** < 0.0001. The raw intensity and P values are listed in S2.

To determine if Cas1-Cas2 induces the SOS response, it was overexpressed in BL21-AI from the pBAD expression vector in LB broth supplemented with 0, 0.05, 0.1 or 0.2 % arabinose. GFP fluorescence increased with the concentration of arabinose. Growth at all concentrations of arabinose resulted in a significant increase in *gfp* expression compared to the arabinose free controls (Figure 4.3d). Therefore, Cas1-Cas2 expression induces the SOS response, and filamentation is due to the activity of SulA.

To determine why dCas1-Cas2 does not induce filamentation, it was overexpressed from the pBAD expression vector in BL21-AI grown in LB broth supplemented with 0, 0.05, 0.1 or 0.2 % arabinose. In the absence of arabinose, the induction of the SOS response is not significantly different compared to Cas1-Cas2 (Figure 4.3d). However, at all arabinose concentrations, GFP fluorescence was significantly higher for Cas1-Cas2 compared to dCas1-Cas2. There was no increase in GFP fluorescence from 0.05 to 0.2 % arabinose with dCas1-Cas2. As the expression of dCas1-Cas2 does not induce filamentation, this level of *sulA* expression must be insufficient to inhibit the polymerisation of FtsZ.

Since BL21-AI Δ*IHF*α undergoes Cas1-Cas2-induced filamentation, I investigated whether Cas1-Cas2 induces the SOS response in this strain. Cas1-Cas2 was overexpressed at 0, 0.05, 0.1 or 0.2 % arabinose from the pBAD expression vector. There were no statistically significant difference in GFP fluorescence between BL21-AI Δ*IHF*α and BL21-AI at 0, 0.05 & 0.2 % arabinose (Figure 4.3d). At 0.1 % arabinose, induction of the SOS response was higher in BL21-AI. The expression of Cas1-Cas2 in BL21-AI Δ*IHF*α increases the induction of the SOS response to a statistically significant level compared to dCas1-Cas2 at all arabinose concentrations. This shows that Cas1-Cas2 induced filamentation is due to *sulA* expression in BL21-AI Δ*IHF*α.

4.5 Chapter Summary

- The catalytic activity of the Cas1-Cas2 complex induces filamentation.
- The deletion of *IHF*α results in Cas1-Cas2 induced filamentation.
- Spacer acquisition is not more abundant in filamentous cells.
- The expression of Cas1-Cas2 induces the SOS response and expression of *sulA*.

Chapter 5

Induction of the SOS Response Aids in Spacer Acquisition

5.1 Introduction

The SOS response is an inducible DNA damage repair pathway that coordinates the reaction of global regulatory systems to allow bacteria to adapt to and survive environmental stresses [257]. Unrepaired DNA damage poses a severe challenge to a cell as it may result in deleterious mutations or cell death. Bacterial cells can detect DNA damage and block cell division to allow time for DNA repair [252, 258].

The LexA protein is the master regulator of the SOS response in *E. coli* [259, 260]. It functions as a dimer, where each monomer binds to half of the LexA box, an imperfect inverted DNA repeat [261, 262]. LexA represses transcription by blocking access of RNA polymerase to the promoters of the genes of the SOS regulon [259, 260]. Most LexA-regulated genes have one LexA box, but there can be two or three that overlap to provide additional regulation, which presumably reduces the leaky expression of repressed genes [263].

Activated RecA triggers autoproteolysis of DNA-free LexA [264, 265]. DNA damage activates RecA, which results in the formation of RecA filaments on ssDNA [266]. The LexA binding and cleavage site is only formed in RecA filaments [267]. A decrease in LexA levels causes the derepression of genes in the SOS regulon and the consequent induction of the SOS response (Figure 5.1).

Expression of *sulA*, as part of the SOS response, inhibits cell division and causes filamentation in *E. coli* [252, 253]. It competitively interacts with free FtsZ subunits to prevent polymerisation and the formation of higher-order structures [268–271]. SulA, therefore, prevents premature segregation of damaged DNA to daughter cells during cell division to provide time for repair by DNA polymerases II, IV, V and other repair proteins [252, 258].

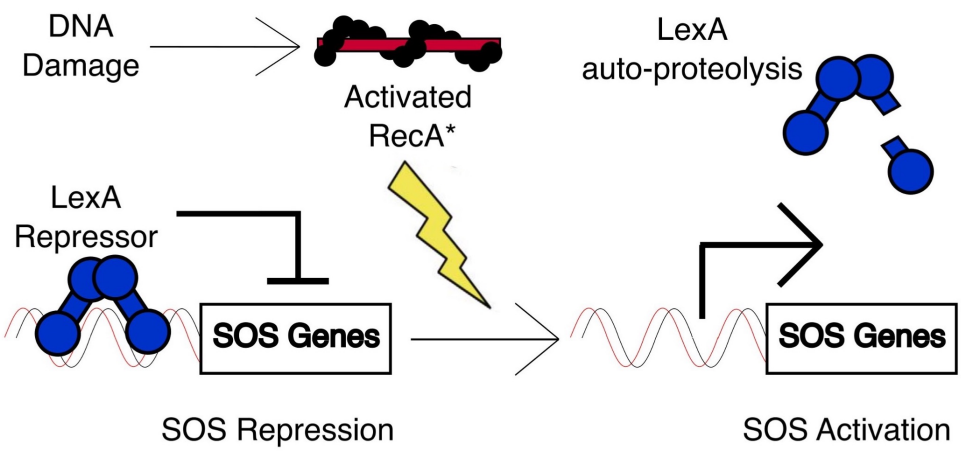


Figure 5.1. LexA-mediated regulation of the SOS response

Under non-stressful conditions, LexA dimers repress the SOS response by binding within the promoters of the SOS regulon genes. RecA binds to ssDNA produced by DNA damage, forming RecA* filaments that trigger LexA autoproteolysis. LexA proteolysis relieves repression to induce the expression of the genes of the SOS regulon.

The level of induction of the SOS response is proportional to the strength of the stimulus, with the expression of the particular gene dependent upon the sequence of the cognate LexA binding site. The deviation of a LexA box away from the consensus is characterised by the heterology index (HI) [272]. The lower the HI value, the higher the affinity of the LexA repressor to the sequence and, consequently, the lower the concentration that is required to facilitate gene expression. Higher levels of DNA damage result in increased RecA-promoted LexA cleavage, which reduces the cellular concentration of LexA [257]. This allows the SOS response to be proportionate to the stimulus, where DNA repair can be achieved at low levels of DNA damage without blocking cell division.

In Chapter 4, I showed that the catalytic activity of the Cas1-Cas2 complex induces filamentation by activation of the SOS response and the consequent expression of *sulA*. I, therefore, wanted to determine whether the SOS response plays a role in spacer acquisition.

5.2 The un-cleavable *lexA3* allele prevents induction of the SOS response and decreases the level of papillation

LexA is the master regulator of the SOS response in *E. coli* [259, 260]. The *lexA3* allele has a G85D amino acid substitution in the cleavage site, which abolishes recA-dependent proteolysis without affecting its DNA binding activity [273]. The genes of the SOS regulon are, therefore, not induced following DNA damage.

The *lexA3* allele from *E. coli* DE407 was transduced into the papillation reporter strain using the Tn9 chloramphenicol resistance gene inserted into the nearby *malB* gene. The successful transduction of the *lexA3* allele was confirmed by PCR amplification and DNA sequencing (Figure 5.2a). I removed the *yjaB* gene from this new *lexA3* papillation-reporter strain by P1 transduction from the Keio collection (Figure S11a). This gene is located on the other side of the *malB* gene, with respect to the *lexA3*. This transduction served to remove the Tn9 chloramphenicol marker (Figure S11b). The *yjaB* gene was selected because it encodes a protein lysine acetyltransferase that would not be expected to play a role in CRISPR adaptation [274]. This was confirmed because the level of papillation was unchanged when this gene was deleted from the wild-type papillation reporter strain by P1 transduction from the Keio collection (Figure S10).

To determine whether the SOS response can be induced in the *lexA3* reporter strain, I transformed it with an SOS reporter plasmid encoding *gfp* under the control of the *sulA* promoter, which is strongly repressed by LexA [275]. When the cells were treated with nalidixic acid to damage the DNA [255, 256], GFP fluorescence increased in the reporter strain but not in the *lexA3* derivative (Figure 5.2b). Control assays showed that exposure to nalidixic acid induced the SOS response in the $\triangle$*yjaB* mutant (Figure S10). Therefore, the *lexA3* allele prevents nalidixic acid induced activation of the SOS response.

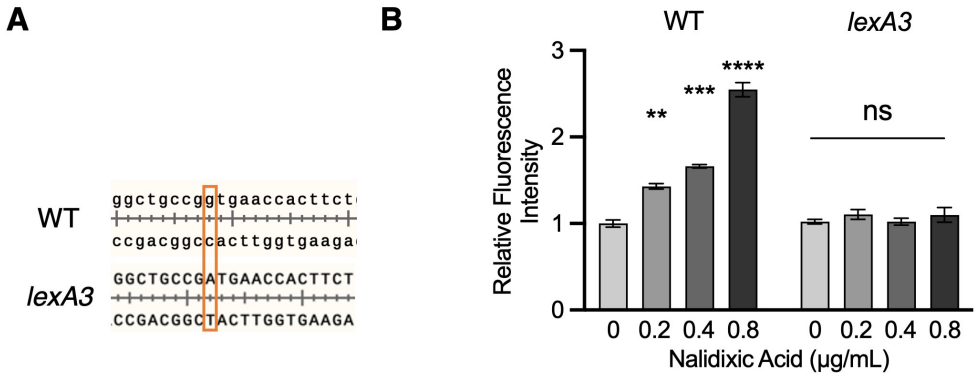


Figure 5.2. The *lexA3* allele prevents induction of the SOS response

(A) Transduction of the *lex3A* allele was confirmed by PCR amplification of the locus followed by Sanger sequencing.
(B) *E. coli* JB028 and JB028 *lexA3* Δ*yjaB* were grown in LB broth supplemented with 0 - 0.8 µg/mL Nalidixic Acid. The GFP SOS reporter plasmid (pRC2790) was used to measure the induction of the SOS response. Repeated in triplicate. The mean is plotted and the error bars are SEM. Intensity compared to the no treatment control by two-way t-test. P value: ns = non-significant, * < 0.05, ** < 0.01, *** < 0.001, **** < 0.0001. Raw intensity values and P values are listed in S2.

To assess the role of the SOS response in CRISPR adaptation, I tested the rate of spacer acquisition in the papillation reporter JB028 and its *lexA3* derivative (Figure 5.3a and b). The number of papillae per colony was significantly lower in the *lexA3* background compared to the wild type. A similar result was obtained in the SPIN assay, where the PCR product for the +1 expanded array was significantly reduced by *lexA3*. Therefore, the inability to induce the SOS response decreases the rate of CRISPR adaptation.

To determine whether the Cas1-Cas2 complex induces the SOS response *in vivo*, I transformed the papillation reporter strain with the GFP reporter and the pBAD Cas1-Cas2. Induction of Cas1-Cas2 expression with arabinose caused an increase in fluorescence in the wild type, indicating induction of the SOS response (Figure 5.3c). As expected, the SOS response was not induced following Cas1-Cas2 expression in the *lexA3* background (Figure 5.3c). As a control, I confirmed that the *yjaB* deletion, introduced to eliminate the chloramphenicol resistance gene, did not affect SOS induction in an otherwise wild type background (Figure S10).

Therefore, the *lexA3* mutation prevents Cas1-Cas2 induced activation of the SOS response.

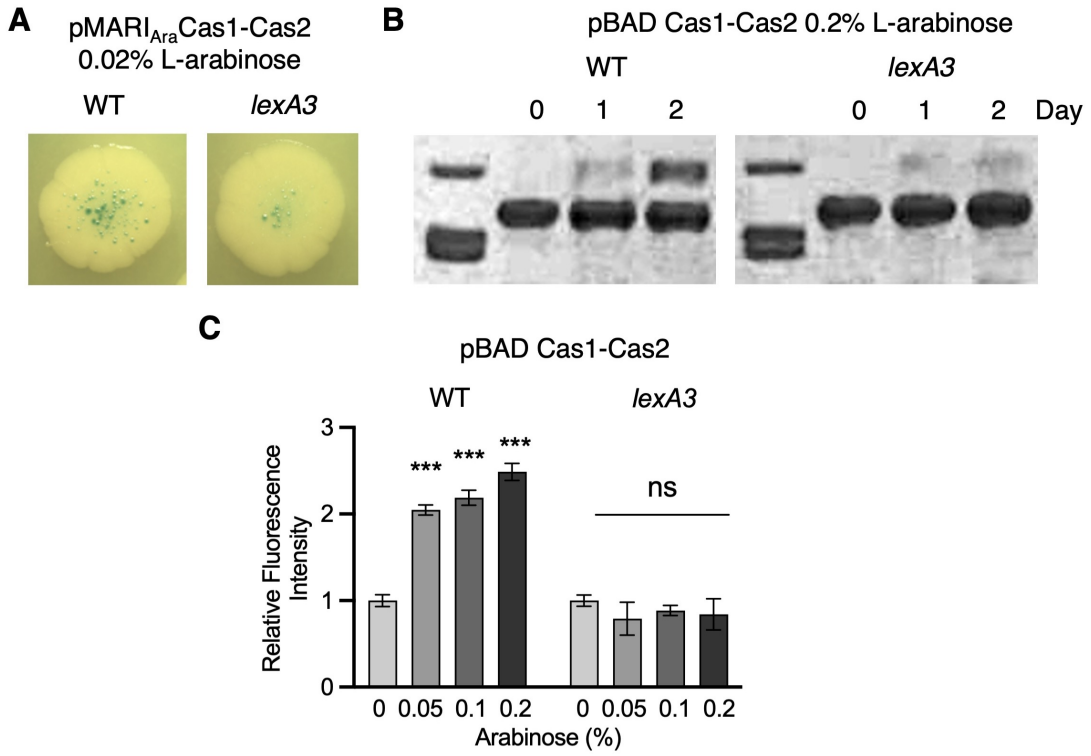


Figure 5.3. The *lexA3* allele reduces the rate of spacer acquisition

(A) Papillation assays were performed in *E. coli* JB028 and JB028 *lexA3*. pMARI$_{ARA}$ Cas1-Cas2 expression was induced by 0.02% L-arabinose. Representative day 5 colonies are shown.
(B) PCR-based SPIN assays were performed in *E. coli* JB028 and JB028 *lexA3*. pBAD Cas1-Cas2 expression was induced by 0.2 % L-arabinose. Sub-cultures (1:1000 dilution) were initiated daily for two days.
(C) Cas1-Cas2 was overexpressed from the pBAD expression vector in *E. coli* JB028 and JB028 *lexA3* across a range of 0 - 0.2% L-arabinose.
The GFP SOS reporter plasmid (pRC2790) was used to measure the induction of the SOS response. Repeated in triplicate. The mean is plotted and the error bars are SEM. Intensity compared to the no treatment control by two-way t-test. P value: ns = non-significant, * < 0.05, ** < 0.01, *** < 0.001, **** < 0.0001. Raw intensity values and P values are listed in S2.

5.3 Inhibition of *recA* decreases the rate of spacer acquisition

RecA is the trigger for LexA cleavage, to derepress the genes of the SOS regulon [264, 265]. RecX is an inhibitor of recA, whose overexpression decreases the level of SOS induction when cells are exposed to nalidixic acid [276–279]. To determine if the level of papillation is proportional to the level of induction of the SOS response, *recX* was cloned into the vanillic acid expression vector and transformed into the reporter strain along with pBAD Cas1-Cas2. Papillation assays were performed across a range of 0 - 50 μM vanillic acid. This revealed that overexpression of *recX* decreases the level of papillation (Figure 5.4).

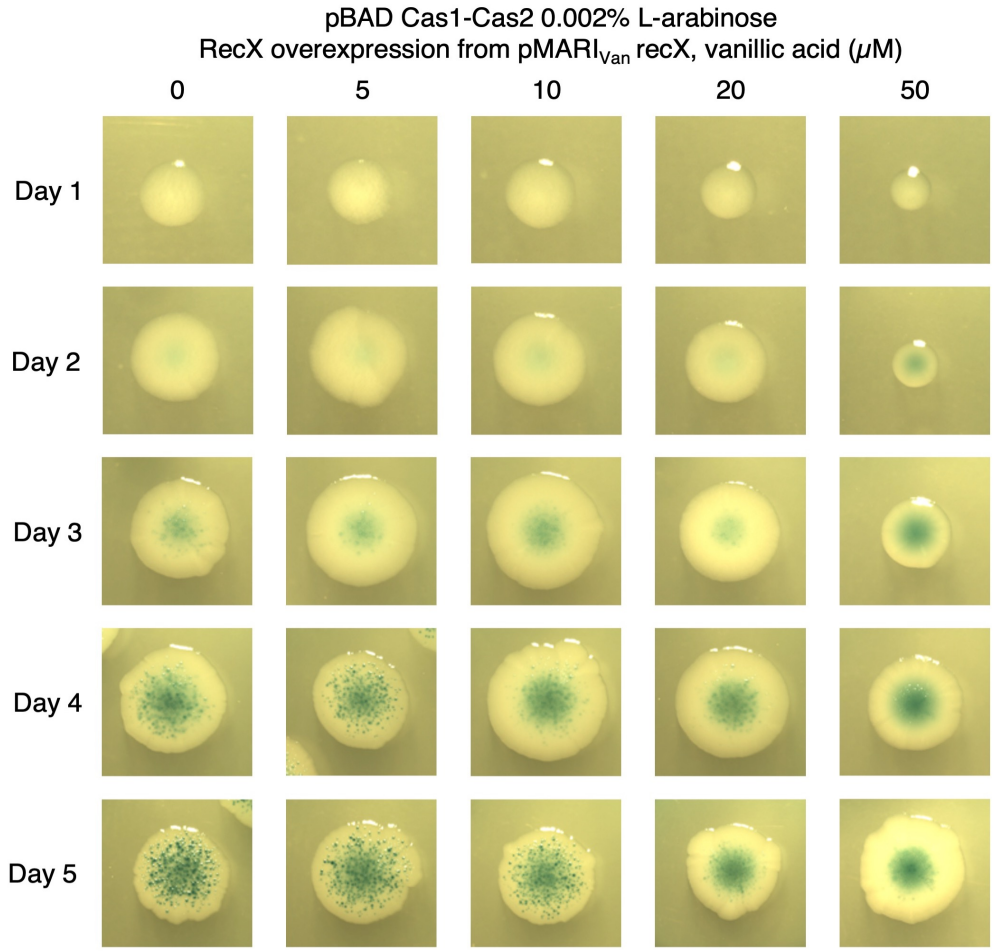


Figure 5.4. Overexpression of *recX* reduces the level of papillation

Papillation assays were performed while overexpressing *recX* in *E. coli* JB028. pBAD Cas1-Cas2 expression was induced by 0.002% L-arabinose. pMARI$_{Van}$recX expression was induced across 0 - 50 μM vanillic acid. Daily representative colonies are shown for all conditions.

Zinc reduces the expression of *recA* and the RecA-mediated cleavage of LexA by inhibiting its ATPase activity [280, 281]. To determine the effect of zinc on adaptation, papillation assays were performed across a range of 0 - 2 mM zinc chloride. Growth at 0.5 mM and above significantly decreased the level of papillation (Figure 5.5).

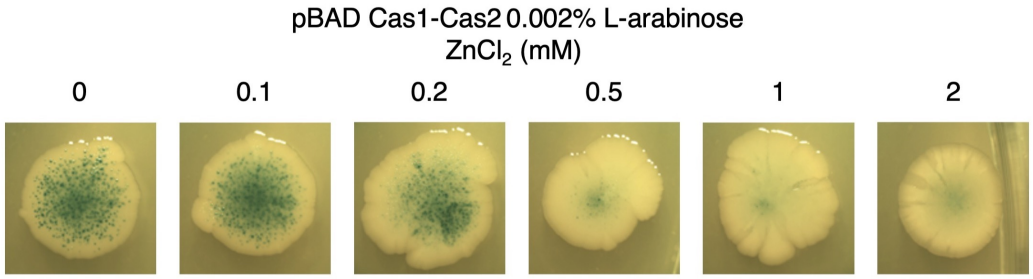


Figure 5.5. Chemical inhibition of RecA decreases the level of papillation

Papillation assays were performed in *E. coli* JB028 across a gradient of 0 - 2 mM $ZnCl_2$. pBAD Cas1-Cas2 expression was induced by 0.002% L-arabinose. Representative day 5 colonies are shown.

5.4 Deletion of *recA* increases the rate of adaptation

Zinc has multiple effects on the bacterium, such as the induction of the membrane stress response pathway and inhibition of iron-sulfur cluster biogenesis [282, 283]. Therefore, to more precisely determine the role of *recA* in spacer acquisition, the gene was deleted from the reporter strain by P1 transduction from the Keio collection (Figure 5.6a). Papillation assays performed in the Δ*recA* mutant showed an increased rate of adaptation compared to the wild type (Figure 5.6b). The kinetics of papillation are the same, but there are more papillae in the Δ*recA* background. PCR-based SPIN assays for adaptation were also performed. They confirmed an increased rate of spacer acquisition in Δ*recA* compared to the wild type (Figure 5.6c).

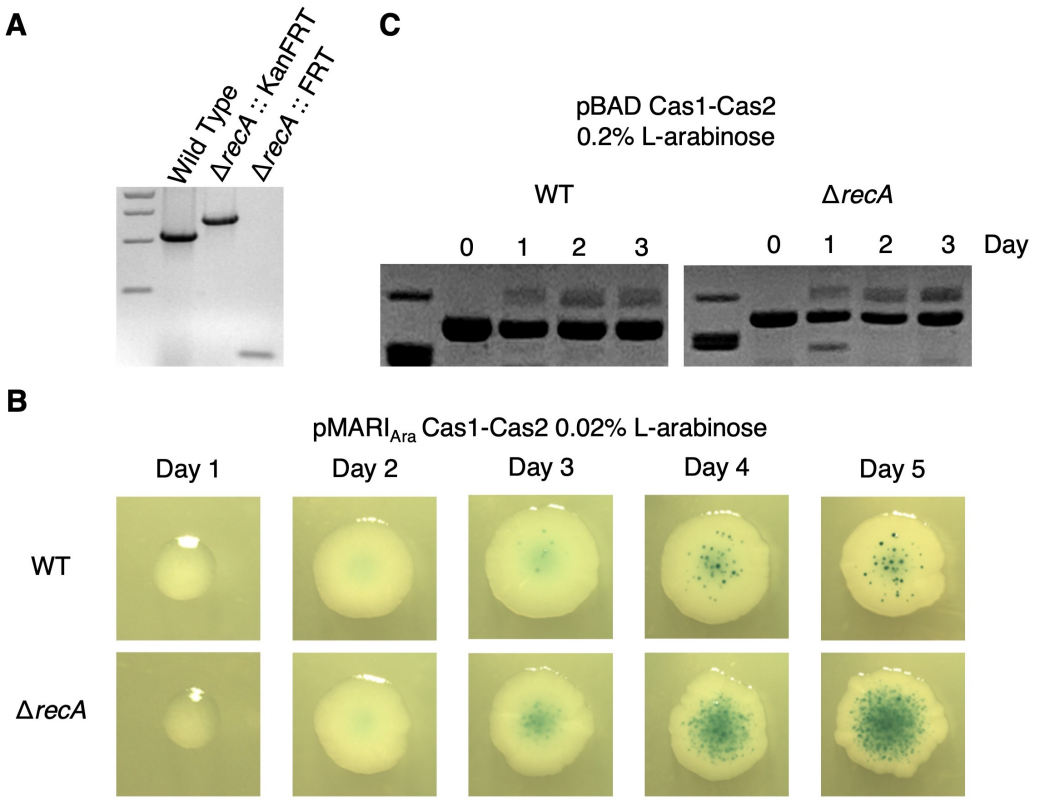


Figure 5.6. Deletion of *recA* increases the level of papillation

(A) PCR Verification of the deletion of *recA* from JB028.
(B) Papillation assays were performed in *E. coli* JB028 and Δ*recA*. pMARI$_{Ara}$ Cas1-Cas2 expression was induced by 0.02% L-arabinose. Representative day 1- 5 colonies are shown.
(C) PCR-based SPIN assays were performed in *E. coli* JB028 and Δ*recA*. pBAD Cas1-Cas2 expression was induced by 0.2% L-arabinose. Sub-cultures (1:1000 dilution) were initiated daily for three days.

The rate of spacer acquisition provided by the PCR-based SPIN and papillation assays are semi-quantitative. A more accurate measurement would be provided by using a cell sorter to count the number of LacZ+ cells after Cas1-Cas2 expression. In fact, such a system has already been described, using *yfp* in place of *lacZ* as the reporter gene [236]. This reporter strain, MLS989, contains a minimal CRISPR array with a stop codon in the Leader sequence and a downstream out-of-frame *yfp* gene (Figure S8a). The addition of a spacer-repeat unit into the reporter array will shift the stop codon out-of-frame and the *yfp* gene in-frame, so that the cells fluoresce. Control assays showed that YFP- & YFP+ cells could be distinguished and that the YFP fluorescence was due to spacer acquisition (Figure S8b&c).

The *recA* gene was removed from the MLS989 YFP reporter strain by P1 transduction from the Keio collection (Figure 5.7a). The cells were transformed with a Cas1-Cas2 expression vector and SPIN or papillation-like assays were performed. Flow cytometry was used to compare the rate of adaptation between the wild type and Δ*recA* backgrounds. The deletion of the *recA* gene significantly increased the rate of spacer acquisition in both plate and liquid media growth conditions (Figure 5.7b&c). Control assays showed that YFP fluorescence was a consequence of adaptation in the Δ*recA* background (Figure S12b&c). Therefore, the deletion of *recA* increases the rate of spacer acquisition in *E. coli*.

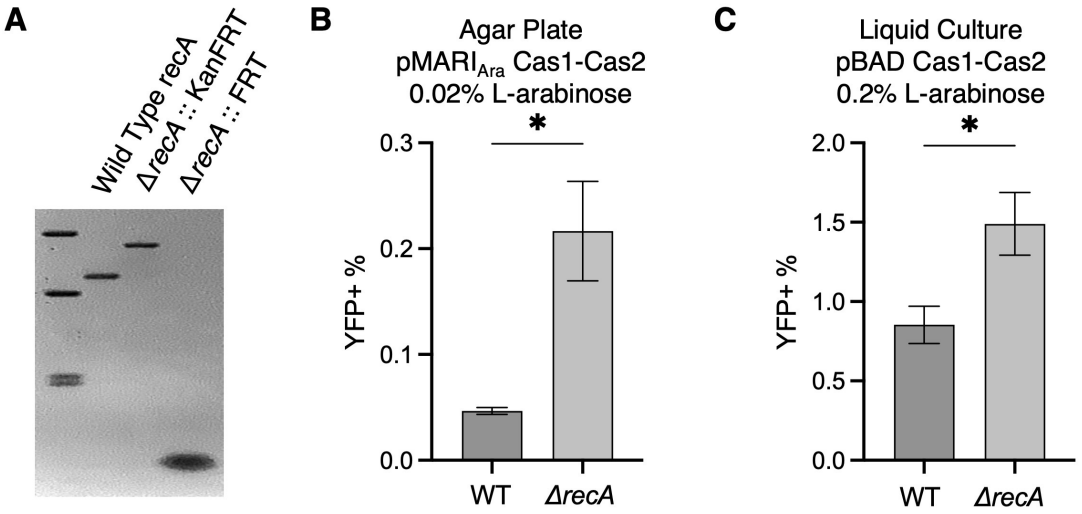


Figure 5.7. Deletion of *recA* increases the rate of spacer acquisition

(A) PCR Verification of the *recA* deletion from the MLS989 YFP reporter.
(B) *E. coli* MLS989 YFP reporter and Δ*recA* were transformed with pMARI$_{Ara}$ Cas1-Cas2. 50 colonies were plated onto LB agar supplemented with 0.02% L-arabinose to induce Cas1-Cas2 expression. These were incubated at 37°C for 5 days. The colonies were resuspended in 1mL LB broth. YFP-/+ cells were analysed by flow cytometry.
(C) Liquid culture assays were performed in the *E. coli* MLS989 YFP reporter and Δ*recA*. pBAD Cas1-Cas2 expression induced by 0.2% L-arabinose. Sub-cultures (1:1000 dilution) were initiated daily for two days. YFP-/+ cells were analysed by flow cytometry.
All assays were repeated in triplicate. The mean is plotted and the error bars are SEM. Conditions compared by two-way t-test. P value: * < 0.05. Raw intensity values and P values are listed in S2.

The increase in spacer acquisition in the $\triangle$*recA* background (Figures 5.6 and 5.7) is inconsistent with the lower rate of the *lexA3* allele (Figure 5.3). If the reduced rate of adaptation in the *lexA3* background is owing to the absence of an SOS response, we would expect the *recA* deletion to have the same effect. To exclude the impact of an unintended genetic change during the construction of the bacterial strains, I used the SOS reporter plasmid to test the result of the *recA* deletion on the ability to induce the SOS response. To do this, I transformed the SOS reporter plasmid into the papillation reporter strain and the $\triangle$*recA* derivative. The cells were grown in LB media supplemented with nalidixic acid and the fluorescence from the GFP-SOS reporter was measured. Nalidixic acid induced *gfp* expression in the wild type but not in the $\triangle$*recA* background (Figure 5.8a).

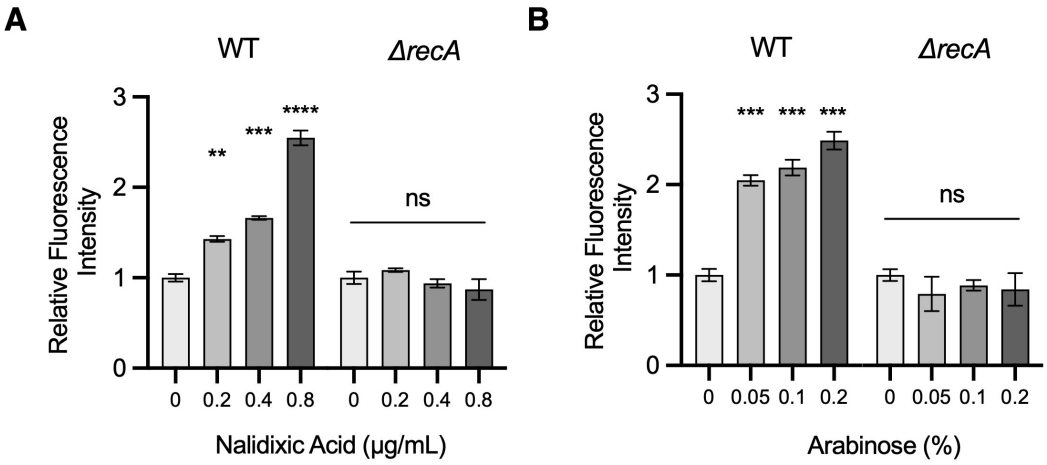


Figure 5.8. Deletion of *recA* prevents induction of the SOS response

(A) *E. coli* JB028 and JB028 $\triangle$*recA* were grown in LB broth supplemented with 0 - 0.8 μg/mL nalidixic acid.
(B) pBAD Cas1-Cas2 expression was induced by 0 - 0.2% L-arabinose in *E. coli* JB028 and JB028 $\triangle$*recA*.
The GFP SOS reporter plasmid (pRC2790) was used to measure the induction of the SOS response. Repeated in triplicate. The mean is plotted and the error bars are SEM. Intensity compared to no treatment control by two-way t-test. P value: ns = non-significant, * < 0.05, ** < 0.01, *** < 0.001, **** < 0.0001. Raw intensity values and P values are listed in S2.

I also tested the ability of Cas1-Cas2 expression to induce the SOS response in the $\triangle$*recA* background. The pBAD Cas1-Cas2 expression vector and the GFP-SOS reporter plasmid were transformed into the papillation reporter strain and $\triangle$*recA* mutant. These were grown in LB broth supplemented with 0 - 0.2 % L-arabinose to induce Cas1-Cas2 expression. The wild type showed a significant increase in *gfp* expression from the SOS reporter plasmid for all concentrations compared to the no treatment control (Figure 5.8b). For the $\triangle$*recA* mutant, there was no significant difference in GFP fluorescence at any arabinose concentration (Figure 5.8b). Therefore, these results suggest that deletion of the *recA* gene increases the rate of spacer acquisition by an alternative mechanism over and above the decrease caused by the loss of the SOS response.

5.5 *SulA* overexpression increases the level of papillation

SulA inhibits the polymerisation of FtsZ to induce filamentation as part of the SOS response in *E. coli* [252, 253]. Since Cas1-Cas2 expression causes filamentation by the induction of *sulA* expression (Figures 4.1 & 5.3c), I wanted to determine what happens when its expression is increased artificially in the absence of the other SOS responses. The *sulA* gene was cloned into the vanillic acid expression vector and transformed into the papillation reporter strain along with pBAD Cas1-Cas2. A range of 0 - 1 μm vanillic acid was used to induce *sulA* expression. By Day 5, the number of papillae across the titration are approximately equal (Figure 5.9). However, when *sulA* is overexpressed, the papillae arise earlier. This is clearest on Day 3 (Figure S13). This indicates that spacer acquisition is taking place earlier in the development of the colony.

The *lexA3* mutation prevents the induction of the SOS response (Figure 5.2). Since Cas1-Cas2 expression induces the SOS response and *sulA* expression (Figure 5.3c), I wanted to determine the effect of *sulA* overexpression in the *lexA3* background. The *sulA* vanillic acid expression vector and pBAD Cas1-Cas2 were transformed into the reporter strain with the *lexA3* allele. Papillation assays were per-

formed across a range of vanillic acid. The overexpression of *sulA* was less toxic than in the wild type, with growth achieved at 10 μM vanillic acid. Overexpression of *sulA* caused papillae to develop earlier and a higher number were present on day 5 (Figures 5.9 and S14). The number of papillae at the highest level of *sulA* induction in the *lexA3* background was approximately equal to that of the wild type. Therefore, the activity of *sulA* upregulates spacer acquisition.

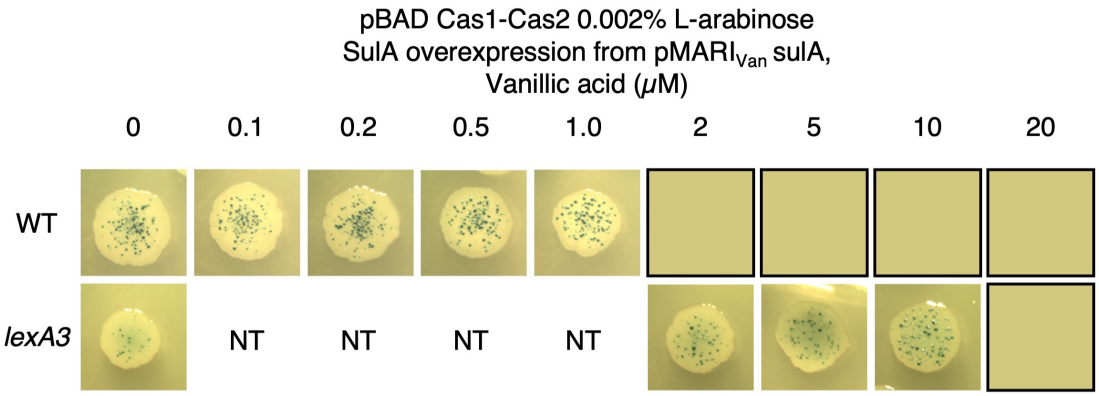


Figure 5.9. Overexpression of *sulA* in the *lexA3* background increases the level of papillation to wild type

Papillation assays were performed while overexpressing *sulA* in *E. coli* JB028 and JB028 *lexA3*. pBADCas1-Cas2 expression was induced by 0.002% L-arabinose. pMARI$_{Van}$sulA expression was induced by 0 – 20 μM vanillic acid. Representative day 5 colonies are shown. Green squares indicate conditions where colonies were not produced. NT refers to conditions not tested.

5.6 Overexpression of *ymfM* increases the level of papillation

YmfM prevents Z-ring formation at the first stage of assembly in *E. coli* [271, 284]. Its expression is repressed by YmfK rather than LexA, and is therefore expressed independently of *sulA* during the SOS response [284–286]. This is of interest, since the *lexA3* mutant has a decreased level of papillation, but it is not abolished.

The *ymfM* gene was cloned into the marionette vanillic acid expression vector and transformed into the papillation reporter strain along with pBAD Cas1-Cas2. Papillation assays were performed across a range of 0 - 20 μM vanillic acid to induce *ymfM* expression. By Day 5, the number of papillae across the titration are approximately the same. However, when *ymfM* is overexpressed, the papillae arise

earlier, which is most apparent on Day 3. This indicates that spacer acquisition is taking place earlier in the development of the colony.

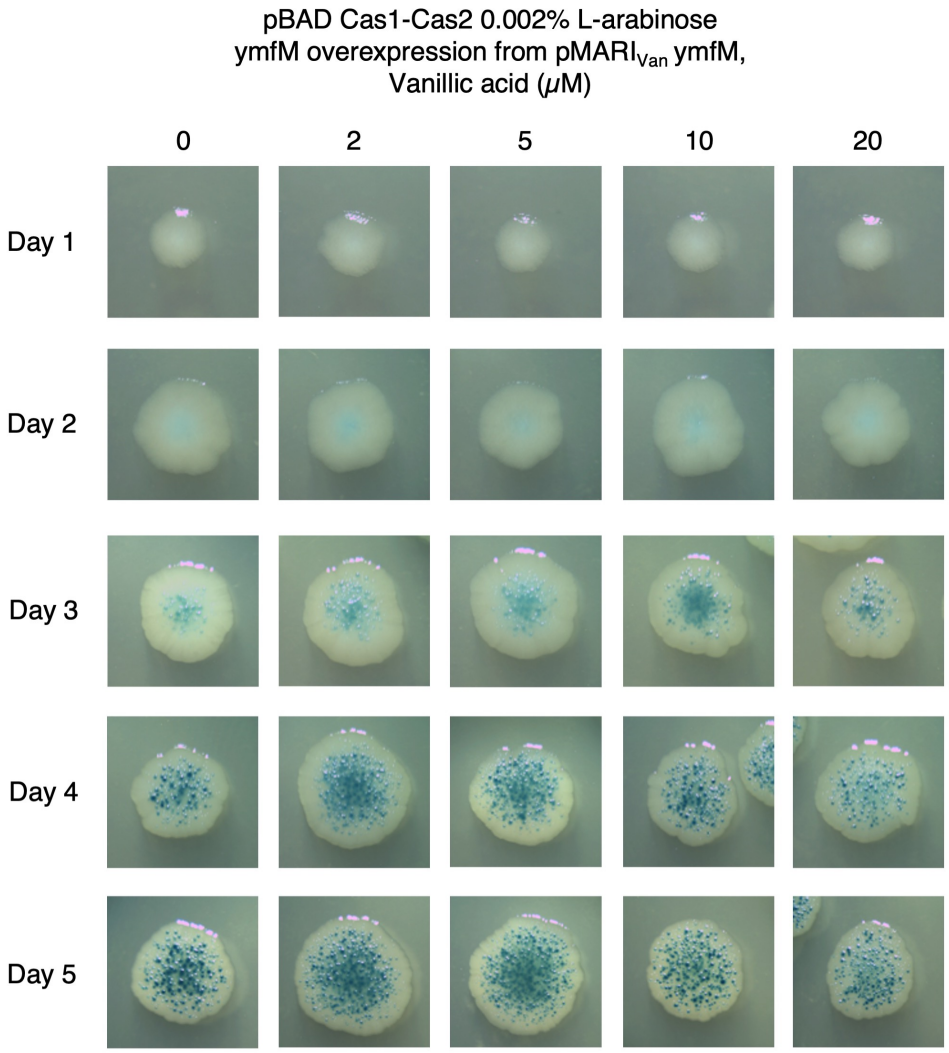


Figure 5.10. Overexpression of *ymfM* increases the level of papillation

Papillation assays were performed in *E. coli* JB028 while overexpressing *ymfM*. pBAD Cas1-Cas2 expression was induced by 0.002% L-arabinose. pMARI$_{Van}$ ymfM expression was induced across a range of 0 - 20 μM vanillic acid. Daily representative colonies are shown for all conditions.

5.7 Deletion of *sulA* and *ymfM* does not alter the level of papillation

As *sulA* overexpression causes papillae to develop earlier, I wanted to examine the effect of its deletion. The *sulA* gene was removed from the reporter strain by P1 transduction from the Keio collection. Papillation assays were performed in the Δ*sulA* mutant and no papillae were produced (Figure S15). This result is inconsistent with the effect of the *lexA3* background, as the level of papillation was decreased and not abolished (Figure 5.3). Furthermore, against expectation, overexpression of *sulA* from a plasmid did not restore papillation (Figure S15). To troubleshoot the result, I transduced the strain using a P1 lysate generated from the Keio *ycbZ* mutant to restore the native *sulA* gene. However, this did not restore papillation (Figure S15). These results suggest that the *sulA* mutant from the Keio collection has an unknown genetic change that interferes with CRISPR adaptation.

As an alternative to the Keio *sulA* mutant, I obtained an alternative deletion mutant in the form of *E. coli* EAW13 made by Roger Woodgate [235]. This is *E. coli* MG1655, with the *sulA* gene replaced by a *KanR* gene by lambda red recombination. When this *sulA* allele was transduced into the papillation reporter strain, there was no change in the level of papillation (Figure 5.11a&b).

Since *ymfM* overexpression also increases the level of papillation, I wanted to examine the effect of *ymfM* deletion. The *ymfM* gene was deleted from the reporter strain by P1 transduction from the Keio collection (Figure 5.11c). Papillation assays showed that the wild type and Δ*ymfM* had the same level of papillation (Figure 5.11c). Therefore, ymfM is not essential for adaptation.

I wanted to determine the effect of deletion of both *sulA* and *ymfM* genes. The P1 lysate from EAW13 was transduced into the Δ*ymfM* papillation reporter to remove the *sulA* gene (Figure 5.11e). Papillation assays performed in the Δ*ymfM*Δ*sulA*

background showed the same level of papillation as the wild type (Figure 5.11f). Therefore, *sulA* and *ymfM* are not essential for spacer acquisition.

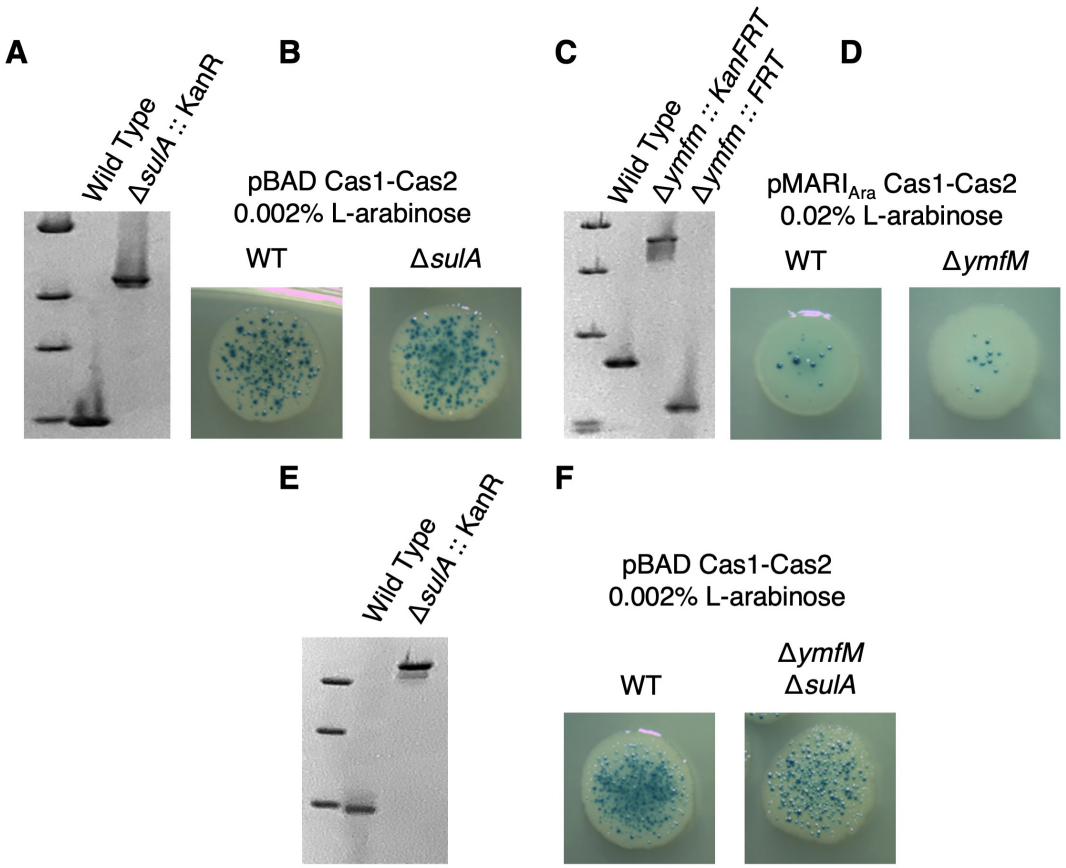


Figure 5.11. Deletion of *sulA* and *ymfM* does not alter the level of papillation

(A) PCR verification of the *sulA* deletion from JB028.
(B) Papillation assays were performed in *E. coli* JB028 and Δ*sulA*. pBAD Cas1-Cas2 expression was induced by 0.002% L-arabinose. Representative day 5 colonies are shown.
(C) PCR verification of the *ymfM* deletion from JB028.
(D) Papillation assays were performed in *E. coli* JB028 and Δ*ymfM*. pMARI$_{ARA}$ Cas1-Cas2 expression was induced by 0.02% L-arabinose. Representative day 5 colonies are shown.
(E) PCR verification of the *sulA* deletion from JB028 Δ*ymfM*.
(F) Papillation assays were performed in *E. coli* JB028 and Δ*ymfM*Δ*sulA*. pBAD Cas1-Cas2 expression was induced by 0.002% L-arabinose. Representative day 5 colonies are shown.

5.8 Growth in the presence of sub-inhibitory concentrations of antibiotics increases the level of papillation

As Cas1-Cas2 expression induces filamentation, I wanted to determine whether the chemical induction of filamentation also increases the rate of spacer acquisition. Exposure to some antibiotics has been shown to result in filamentation. This is achieved by the action of cell-wall targeting antibiotics, such as ampicillin and cefalexin, or by DNA-targeting antibiotics, such as mitomycin C and nalidixic acid [287–290]. Papillation assays were performed in the reporter strain in the presence of sub-inhibitory concentrations of these antibiotics. All four antibiotics increased the level of papillation (Figure 5.12).

Since the *lexA3* mutation prevents induction of the SOS response (Figure 5.3), papillation assays were also performed in the *lexA3* mutant in the presence of sub-inhibitory concentrations of antibiotics. When grown in the presence of ampicillin and cefalexin, there is a slight decrease in the level of papillation at high concentrations (Figure 5.13). This is in contrast to the wild type, which saw an increase. When grown in the presence of nalidixic acid and mitomycin C, the level of papillation was reduced at all concentrations. At high concentrations, white bumps also developed on the colonies. Growth at 8 µg/mL nalidixic acid and 1.0 µg/mL mitomycin C was not achieved in the *lexA3* background, unlike in the wild-type. Therefore, LexA and the SOS response are required for the stimulation of spacer acquisition in the presence of sub-inhibitory concentrations of antibiotics.

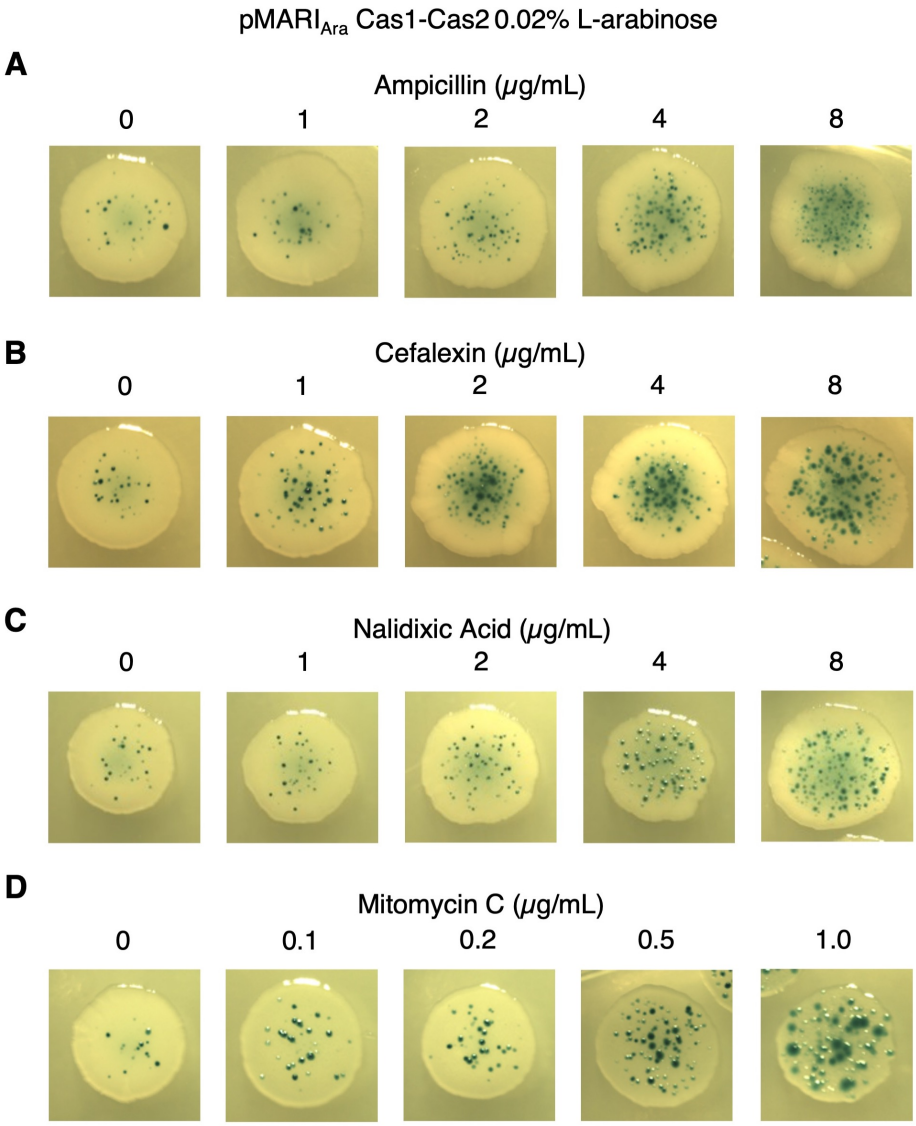


Figure 5.12. Growth in sub-inhibitory concentrations of antibiotics increases the level of papillation in JB028

Papillation assays were performed in *E. coli* JB028 in sub-inhibitory concentrations of antibiotics. Ampicillin (A), cefalexin (B) and nalidixic acid (C) were used across a gradient of 0 – 8 µg/mL. Mitomycin C (D) was used across a gradient of 0 – 1.0 µg/mL. pMARI$_{ARA}$ Cas1-Cas2 expression was induced by 0.02% L-arabinose. Representative day 5 colonies are shown.

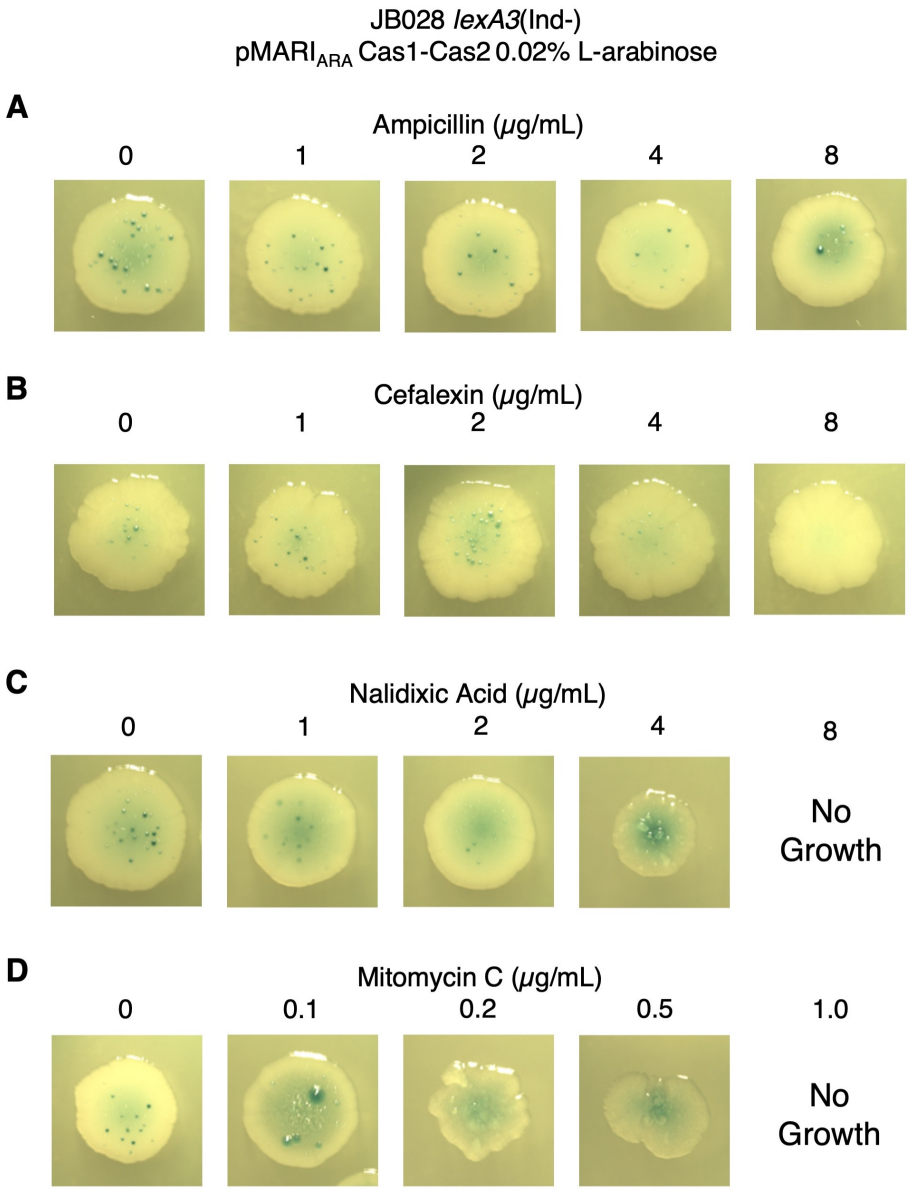


Figure 5.13. Growth in sub-inhibitory concentrations of antibiotics decreases the level of papillation in JB028 *lexA3*

Papillation assays were performed in *E. coli* JB028 *lexA3* in sub-inhibitory concentrations of antibiotics. Ampicillin (A), cefalexin (B) and nalidixic acid (C) were used across a gradient of 0 – 8 µg/mL. Mitomycin C (D) was used across a gradient of 0 – 1.0 µg/mL. pMARI$_{ARA}$ Cas1-Cas2 expression was induced by 0.02% L-arabinose. Representative day 5 colonies are shown.

5.9 Mitomycin C and nalidixic acid induce the SOS response

As nalidixic acid and mitomycin C decreased the level of papillation in the *lexA3* background (Figure 5.13), I wanted to determine if the concentration of antibiotics used induces the SOS response. The SOS reporter plasmid was transformed into the papillation reporter strain. This was grown on LB agar plates supplemented with the sub-inhibitory concentrations of antibiotics used in Figure 5.12. Exposure to ampicillin did not induce the SOS response (Figure 5.14a). Furthermore, cefalexin only induced *gfp* expression at a significant level at 8 μg/mL (Figure 5.14b). However, growth in the presence of nalidixic acid induced the SOS response to a significant level at 2 μg/mL and above (Figure 5.14c). Exposure to mitomycin C resulted in a significant induction of the SOS response at all concentrations (Figure 5.14d). Therefore, the increased level of papillation in cells treated with sub-inhibitory concentrations of nalidixic acid and mitomycin C is probably due to the induction of the SOS response, but the effects of ampicillin and cefalexin are due to an alternative mechanism.

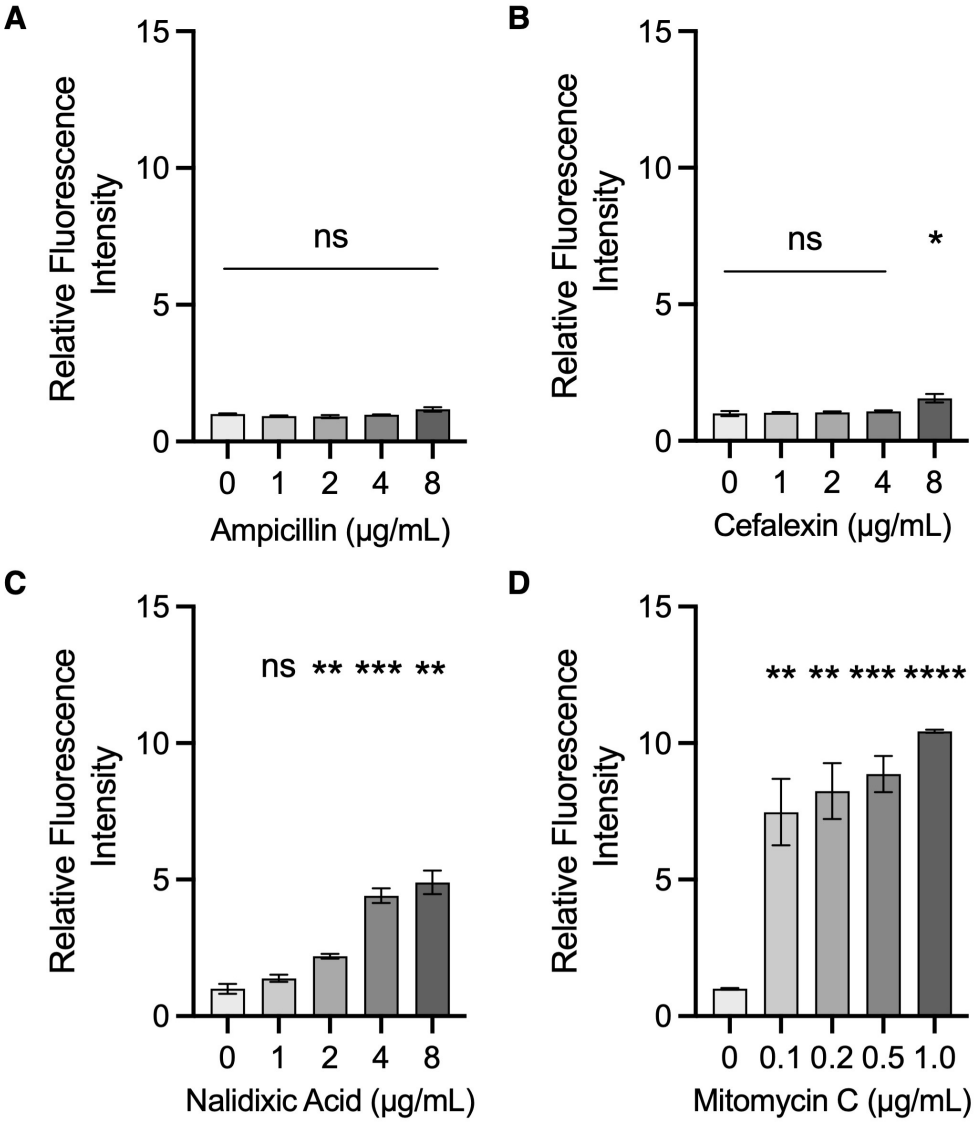


Figure 5.14. Growth in sub-inhibitory concentrations of nalidixic acid and mitomycin C induces the SOS response

E. coli JB028 was grown on LB agar supplemented with 0, 1, 2, 4, 8 μg/mL ampicillin (A), cefalexin (B) and nalidixic acid (C) or 0, 0.1, 0.2, 0.5, 1.0 μg/mL mitomycin C (D). The GFP SOS reporter plasmid (pRC2790) was used to measure the induction of the SOS response. All assays were repeated in triplicate. The mean is plotted and the error bars are SEM. The intensity is compared to the no antibiotic control by a two-way t-test. P value: ns = non-significant, * < 0.05, ** < 0.01, *** < 0.001, **** < 0.0001. Raw intensity values and P values are listed in S2.

5.10 Antibiotics Induce Spacer Acquisition Events

As part of the SOS response, three error-prone DNA polymerases are expressed in *E. coli* [291–293]. These allow the repair of DNA lesions that block DNA replication. All three SOS-inducible DNA polymerases play a role in mutagenesis, which can induce frameshift mutations [258]. Exposure to sub-inhibitory concentrations of beta-lactam antibiotics has been demonstrated to upregulate DNA polymerase IV independent of the SOS response [294, 295]. Frameshift mutations of *lacZ* have also been shown when cells reach stationary phase and lactose is the only carbon source, such as in the papillation assay [296]. If a +1 frameshift mutation arose between the promoter and the stop codon in the Leader of the reporter array, this would result in a frameshift to remove the stop codon and result in the expression of *lacZ*.

To show that the papillae produced from antibiotic exposure were due to bona fide spacer acquisition, 15 papillae from each treatment were isolated and subjected to genomic PCR reactions to determine the size of the CRISPR reporter locus. These were run alongside a negative and positive control. All PCR products were the same size as the positive control (Figure 5.15). Therefore, I concluded that exposure to antibiotics increases the rate of spacer acquisition.

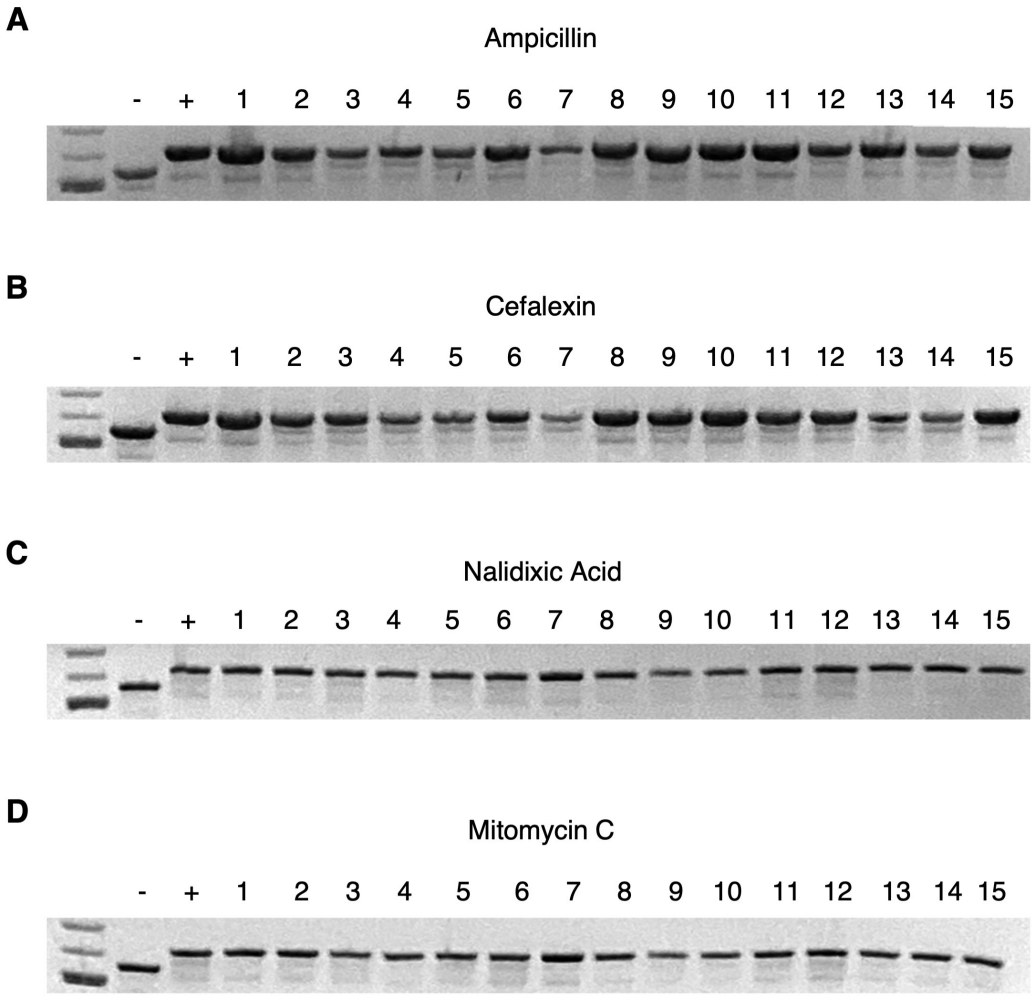


Figure 5.15. Antibiotics induce spacer acquisition

15 papillae were subcultured from papillation assays performed in the presence of 2 μg/mL ampicillin, cefalexin & nalidixic acid or 0.5 μg/mL mitomycin C (Figure 5.12). PCRs were performed across the reporter CRISPR locus using genomic DNA as template. The unexpanded CRISPR locus of JB028 was used as the template for the negative control. The template for the positive control was pRC1644, which contains an extra spacer-repeat unit to the reporter array. PCR products from papillae presented bands at expanded loci size and therefore had a Lac+ phenotype as a result of spacer acquisition.

5.11 Chapter Summary

- The use of a *lexA3* mutant decreases the rate of spacer acquisition.
- The overexpression of *recX* decreases the level of papillation.
- The deletion of *recA* increases the rate of adaptation.
- The overexpression of *sulA* and *ymfM* causes papillae to develop earlier.
- Growth in the presence of sub-inhibitory concentrations of antibiotics increases the rate of spacer acquisition.
- Sub-inhibitory concentrations of nalidixic acid and mitomycin C induce the SOS response, but ampicillin and cefalexin do not.

Chapter 6

Degradation of FtsZ by HflKC/FtsH Supports CRISPR Cas Adaptation

6.1 Introduction

The function of the *Cas* genes was quickly determined following their discovery as part of an adaptive prokaryotic immune system due to their proximity to the CRISPR array. Other host factors play a role in CRISPR adaptation, but their roles are less well understood. For example, IHF plays a mechanistic role in DNA bending at the CRISPR locus in the type I-E system to stabilise the interaction of the Cas1-Cas2 complex with the Leader [120]. The DnaQ exonuclease trims spacers before integration and aids in spacer orientation [297, 298].

To discover other host factors required for naïve CRISPR adaptation in *E. coli*, Dr. Jack Braithwaite performed a random Tn5 transposon mutagenesis screen to select for hypopapilating host mutants [237]. The screen recovered multiple transposon insertions into an operon encoding the *hflC* and *miaA* genes. Since the host mutants have extreme hypopapillation phenotypes (Figure 6.1), I decided to investigate them further.

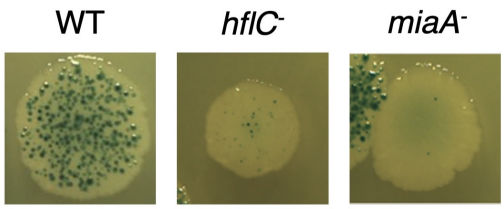


Figure 6.1. Tn5 insertion into *hflC* and *miaA* reduces the rate of papillation

Papillation assays were performed with the indicated Tn5 transposon insertion mutants. Compared to the wild type JB028 host, the mutants produced only a few very tiny papillae. Images of day 5 colonies are shown. Images taken with permission from (Braithwaite, 2021).

6.2 Deletion of genes from the *hflC* and *miaA* operon

The *hflC* and *miaA* genes are present in an operon of 12 genes (Figure 6.2a). The *yjeV* and *tsaE* gene are essential, and therefore, a genetic deletion is not present in the Keio collection. As *tsaE* has opposite polarity to *hflC* and *miaA*, the genes downstream of it were removed from the reporter strain by P1 transduction of the kanamycin resistance gene from the Keio collection. This gives non-polar deletions that do not disrupt the other genes in the operon. Papillation assays were performed in these mutant strains with the kanamycin resistance gene present. The deletion of *miaA*, *hflC* and *hflK* reduced the rate of papillation compared to the wild type, whereas the deletion of *hfq* increased the rate of papillation (Figure 6.2b). As hfq has been shown to regulate hundreds of mRNA transcripts, this mutant was not studied due to the pleiotropic effects that deletion will have on the bacterium [299, 300]. I, therefore, decided to focus on *miaA*, *hflK* and *hflC*.

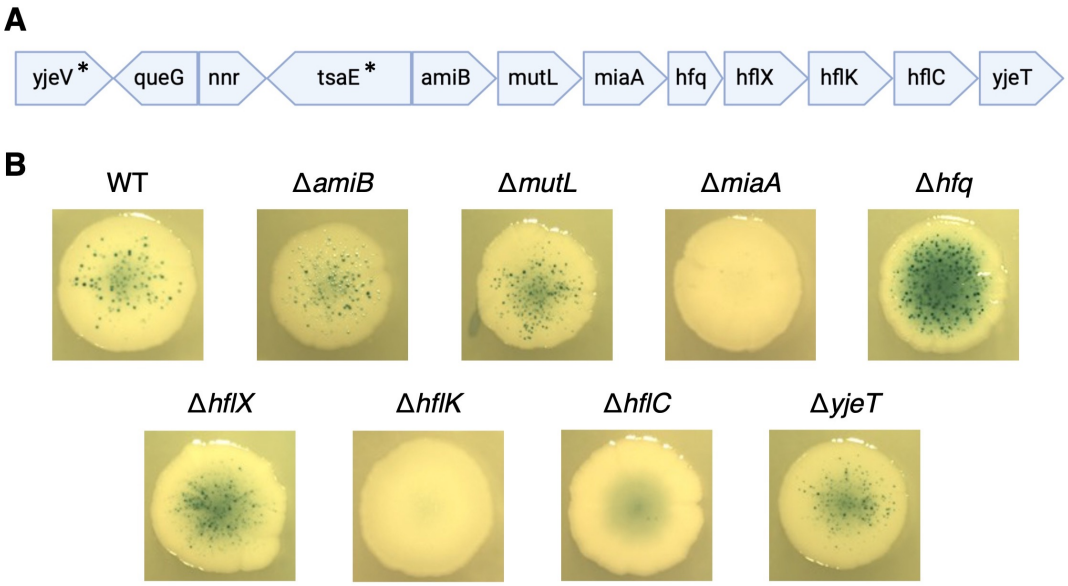


Figure 6.2. Deletion of *miaA*, *hflC* and *hflK* reduces the rate of papillation.

(A) The structure of the *miaA* and *hflC* operon. The orientation of the arrow shows relative gene polarity. * represents gene deletions not present in the Keio collection. (B) Papillation assays were performed in the wild type JB028 *E. coli* reporter strain and the indicated mutants created by P1 transduction from the Keio collection. pBAD Cas1-Cas2 expression was induced by 0.02 % L-arabinose. Representative day 5 colony images are shown.

6.3 Deletion of *miaA* inhibits papillation but not spacer acquisition

MiaA is a tRNA dimethylallyltransferase that catalyzes the first step of hypermodification of the A37 base of specific tRNAs, for example $tRNA^{Tyr}$ and $tRNA^{Phe}$ [301–303]. The *KanR-FRT* selection marker was removed from the $\triangle$*miaA* mutant reporter by *flp* recombination (Figure 6.3a). Papillation assays performed in the $\triangle$*miaA* background had a reduced rate of adaptation compared to the wild type (Figure 6.3b). This is the same as shown in Tn5 transposon mutagenesis (Figure 6.1).

To determine whether the deletion of the *miaA* gene inhibits papillation, PCR-based SPIN assays for adaptation were also performed. The $\triangle$*miaA* background acquired spacers at an equivalent rate to the wild type (Figure 6.3b). The deletion of the *miaA* gene must, therefore, prevent papillation but not spacer acquisition.

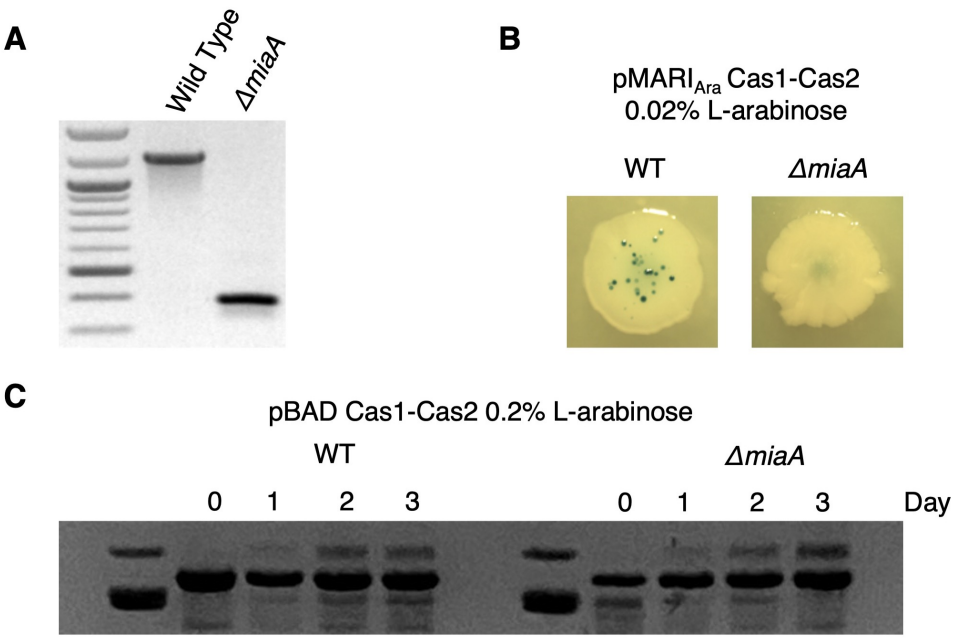


Figure 6.3. Deletion of *miaA* reduces the rate of papillation but spacers are acquired in SPIN assays

(A) PCR verification of the Δ*miaA* deletion from JB028.
(B) Papillation assays were performed in *E. coli* JB028 and Δ*miaA*. pMARI$_{Ara}$ Cas1-Cas2 expression was induced by 0.02% L-arabinose. Representative day 5 colonies are shown.
(C) PCR-based SPIN assays were performed in *E. coli* JB028 and Δ*miaA*. pBAD Cas1-Cas2 expression was induced by 0.2% L-arabinose. Sub-cultures (1:1000 dilution) were initiated daily for three days.

6.4 Deletion of *hflK* or *hflC* reduces the rate of spacer acquisition

The HflKC complex regulates the activity of the FtsH protease [304]. HflKC prevents FtsH-catalysed proteolysis of the cII protein of lambda bacteriophage, secY and sigma 32 [304–306]. When HflKC-FtsH recognises a proper substrate, HflK and HflC dissociate to allow the proteolytic activity of FtsH to degrade the target proteins [304]. Therefore, the HflKC complex has been suggested to be a FtsH specificity factor [305].

The *KanR-FRT* selection marker was removed from both the Δ*hflK* and Δ*hflC* mutants by *flp* recombination (Figure 6.4a). Papillation assays were performed and the deletion of both genes resulted in a decreased rate of papillation compared to the

wild type (Figure 6.4b). This is the same as that shown in Tn5 transposon mutagenesis (Figure 6.1). PCR-based SPIN assays were also performed. Both Δ*hflC* and Δ*hflK* mutants exhibited a decreased rate of spacer acquisition compared to the wild type (Figure 6.4c). However, the difference is smaller than that seen in the papillation assay. Therefore, the deletion of *hflK* or *hflC* reduces the rate of CRISPR adaptation.

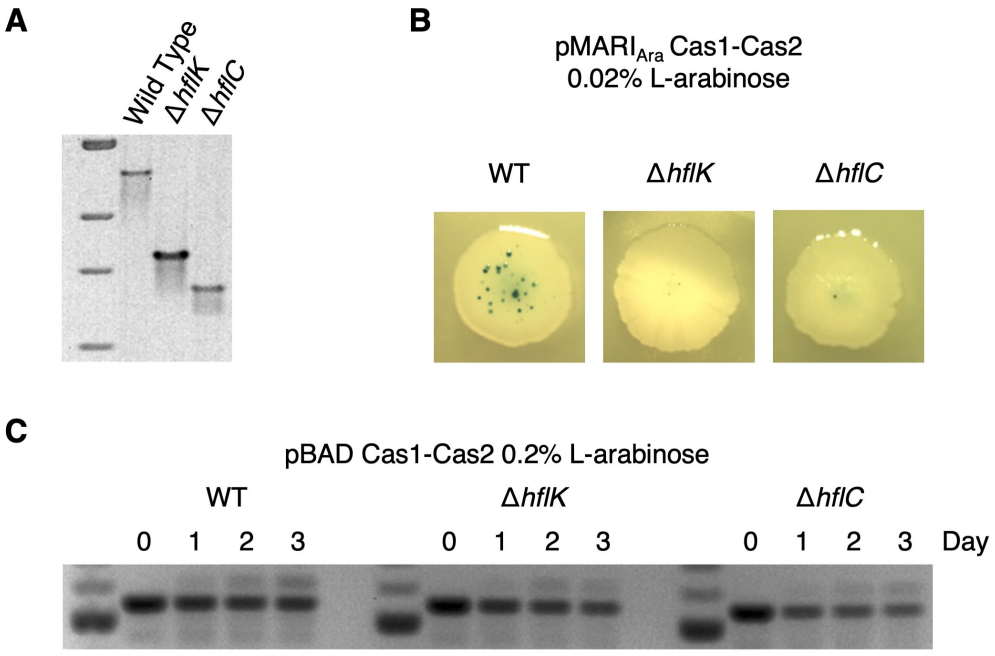


Figure 6.4. Deletion of *hflK* or *hlfC* inhibits adaptation

(A) PCR verification of the *hflK* and *hflC* deletion from JB028 by P1 transduction from the Keio collection.
(B) Papillation assays were performed in *E. coli* JB028, Δ*hflK* and Δ*hflC*. pMARI$_{Ara}$ Cas1-Cas2 expression was induced by 0.02% L-arabinose. Representative day 5 colonies are shown.
(C) SPIN assays were performed in *E. coli* JB028, Δ*hflK* and Δ*hflC*. pBAD Cas1-Cas2 expression was induced by 0.2% L-arabinose. Sub-cultures (1:1000 dilution) were initiated daily for three days.

6.5 Complementation of *hflK* and *hflC* restores spacer acquisition

The *hflK* and *hflC* genes were cloned into vanillic acid inducible expression vectors to test if they could complement the adaptation defect of the original mutants. These expression vectors were transformed into their respective deletion strains together with pBADCas1-Cas2. The *hflK* and *hflC* genes were induced across a range of 0 - 20 μM vanillic acid. Increasing the expression of *hflK* or *hflC* increased the rate of papillation (Figure 6.5a&b).

As complementation of *hflK* and *hflC* resulted in the formation of smaller papillae than usual, both genes were cloned into the vanillic acid expression vector. This was transformed into the deletion strains along with pBADCas1-Cas2. The expression of *hflKC* was induced across a range of 0 - 20 μM vanillic acid. Increasing the expression of *hflKC* increased the rate of papillation in both deletion strains. At 20 μM vanillic acid, the papillae had their usual large size not seen in the single complementation assays (Figure 6.5c&d).

6.6 Overexpression of the *hflKC* complex increases the rate of spacer acquisition

Since the deletion of the *hflK* and *hflC* genes reduces the rate of papillation, I wanted to determine the effect of overexpressing these genes. The *hflK* and *hflC* vanillic acid expression vectors were transformed into the reporter strain along with pBADCas1-Cas2. Overexpression of either gene did not alter the rate of papillation (Figures S17 and S18). Since uncomplexed subunits of hflK and hflC are unstable individually [307, 308], I decided to overexpress both genes from the vanillic acid expression vector. Induction of both *hflK* and *hlfC* simultaneously caused the papillae to arise earlier (Figure 6.6). This is most obvious on day 3.

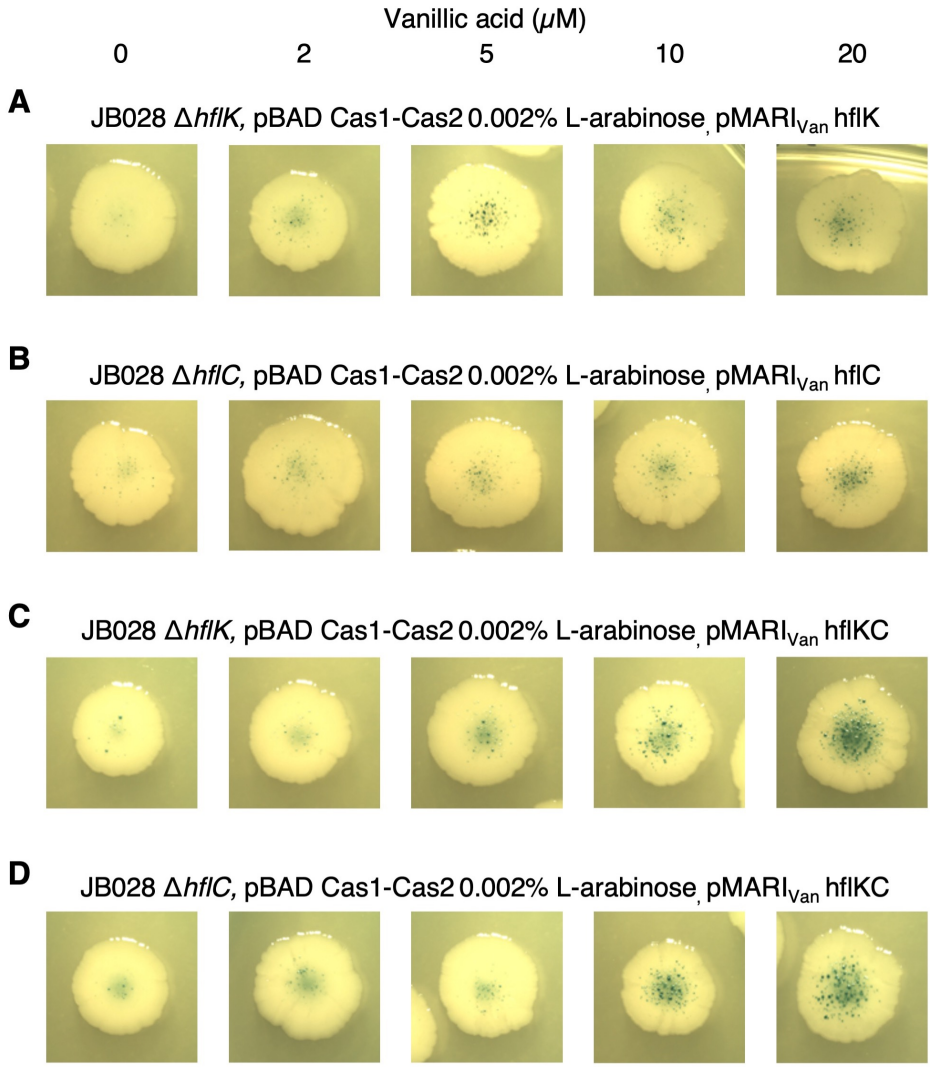


Figure 6.5. Complementation of *hflK* and *hflC* restores the adaptation defect phenotype

Papillation assays were performed complementing JB028 Δ*hflK* and JB028 Δ*hflC*. Either the deleted subunit (a&b) or both subunits (c&d) were overexpressed. $pMARI_{Van}$hflK is the hflK expression vector. $pMARI_{Van}$hflC is the hflC expression vector. $pMARI_{Van}$hflKC is the hflKC expression vector. Overexpression was induced across a gradient of 0 – 20 µM vanillic acid. pBAD Cas1-Cas2 expression was induced by 0.002% L-arabinose. Representative day 5 colonies are shown for each condition.

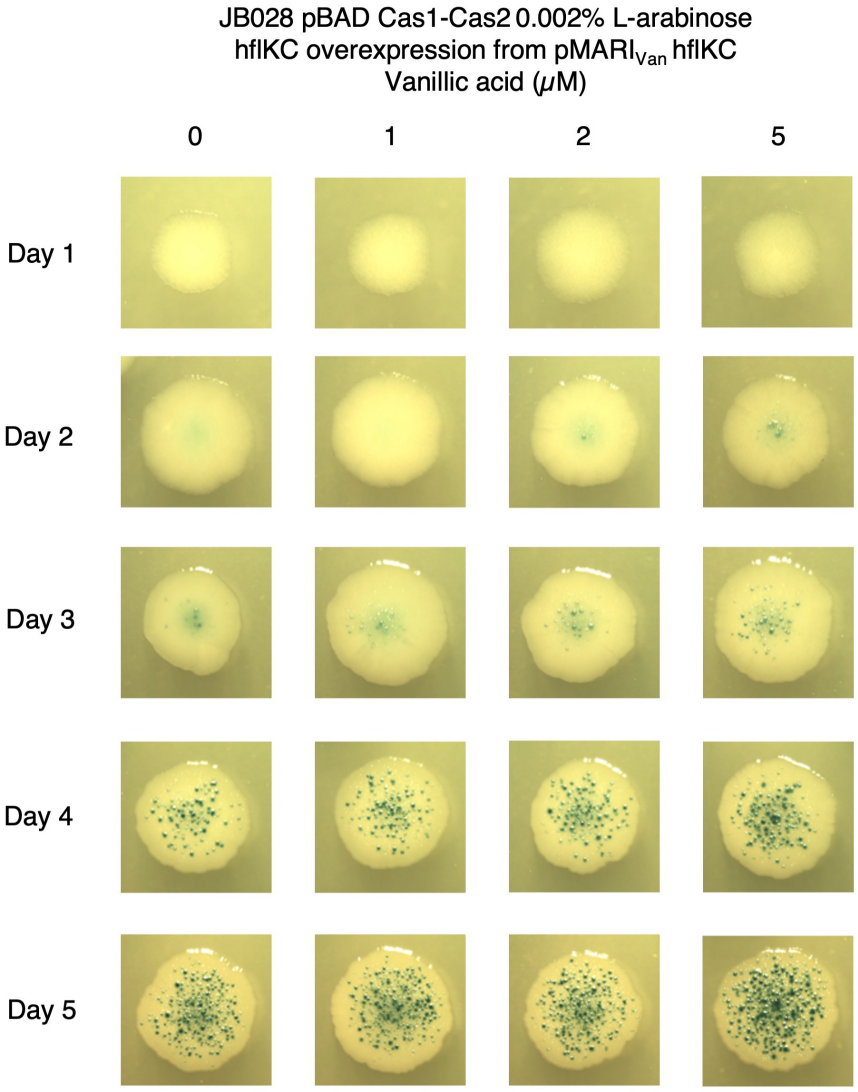


Figure 6.6. Overexpression of *hflKC* causes papillae to arise earlier and a higher rate of papillation

Papillation assays were performed while overexpressing *hflKC* in *E. coli* JB028. pBAD Cas1-Cas2 expression was induced by 0.002% L-arabinose. pMARI$_{Van}$hflKC expression was induced by 0 – 5 μM vanillic acid. Representative daily colonies are shown for each condition.

6.7 Overexpression of *ftsH* increases the rate of adaptation

Although it is possible that the HflKC complex directly affects the rate of CRISPR adaptation, it is more likely to act through one of its targets, such as the FtsH protease. FtsH is an ATP-dependent zinc metalloprotease located in the inner membrane of the *E. coli* cell envelope [309]. It degrades inner membrane and cytoplasmic proteins as part of a general stress response [310–312]. One of these substrates is the cell division protein FtsZ [313]. As Cas1-Cas2 expression induces filamentation due to the activity of SulA preventing the formation of FtsZ protofilaments (Chapter 4), I decided to study the role that FtsH plays in CRISPR Cas adaptation.

As *ftsH* is an essential gene in *E. coli* [309], I decided to clone it into the vanillic acid inducible expression vector to determine the effect of overexpression. This was transformed into the reporter strain along with pBAD Cas1-Cas2. Papillation assays were performed across a range of 0 - 5 μM vanillic acid to induce *ftsH* expression. Papillae appeared earlier when *ftsH* was overexpressed (Figure 6.7). The difference in the rate of papillation is most apparent on day 3. The same number was recorded on day 5, but they are larger at 5 μM vanillic acid induction, indicating that the spacer acquisition event arose earlier.

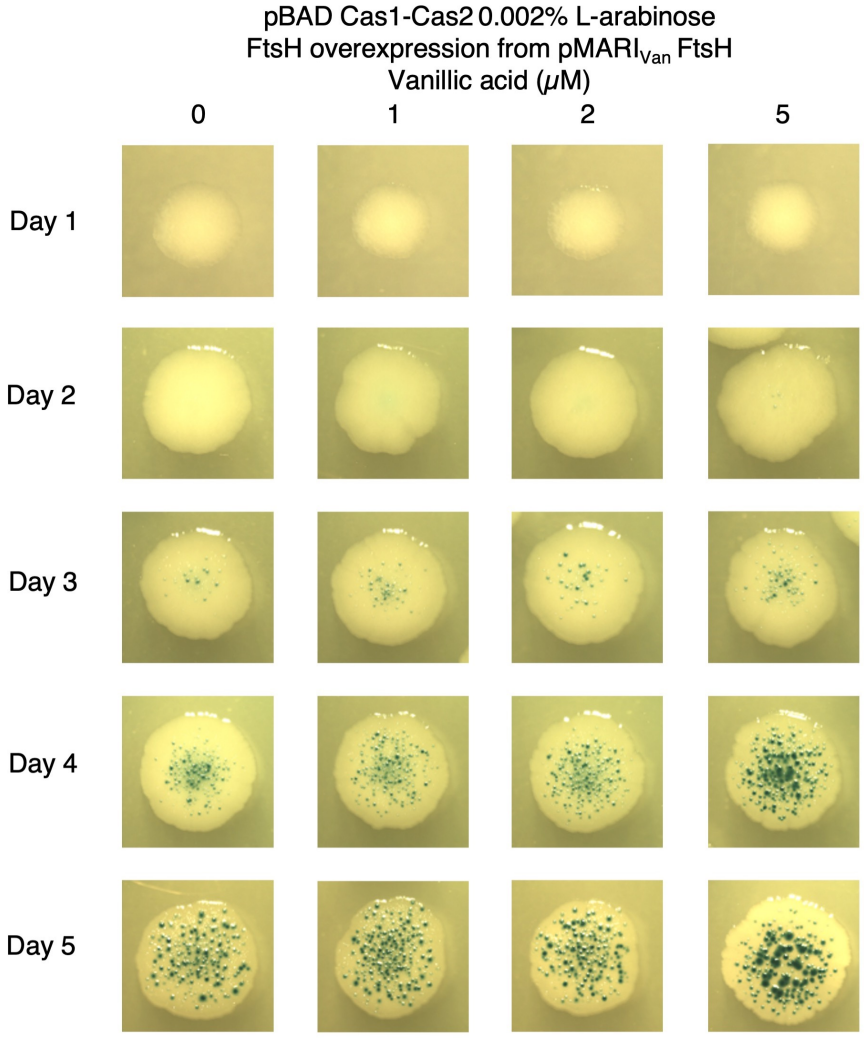


Figure 6.7. Overexpression of *FtsH* increases the rate of papillation

Papillation assays were performed while overexpressing *ftsH* in *E. coli* JB028. pBAD Cas1-Cas2 expression was induced by 0.002% L-arabinose. pMARI$_{Van}$ftsH expression was induced by 0 – 5 μM vanillic acid. Representative daily colonies are shown for each condition.

6.8 Overexpression of *ftsZ* decreases the rate of adaptation

As Cas1-Cas2 expression induces filamentation (Figure 4.1) and FtsH has been shown to degrade FtsZ *in vitro* [313], I wanted to determine the role that FtsZ plays in CRISPR adaptation. The *ftsZ* gene was cloned into the marionette vanillic acid expression vector and transformed into the reporter strain along with pBAD Cas1-Cas2. Overexpression of *ftsZ* was achieved across a range of 0 - 10 μM vanillic acid. Induction of *ftsZ* reduced the rate of papillation compared to the uninduced control (Figure 6.8a).

To determine whether the reduction in the rate of papillation was due to *ftsZ* overexpression negatively affecting the growth of papillae, PCR-based SPIN assays were also performed. Expression of the *ftsZ* gene was induced by 10 μM vanillic acid. PCR amplification of the CRISPR locus showed that overexpression of *ftsZ* reduced the spacer acquisition rate (Figure 6.8b).

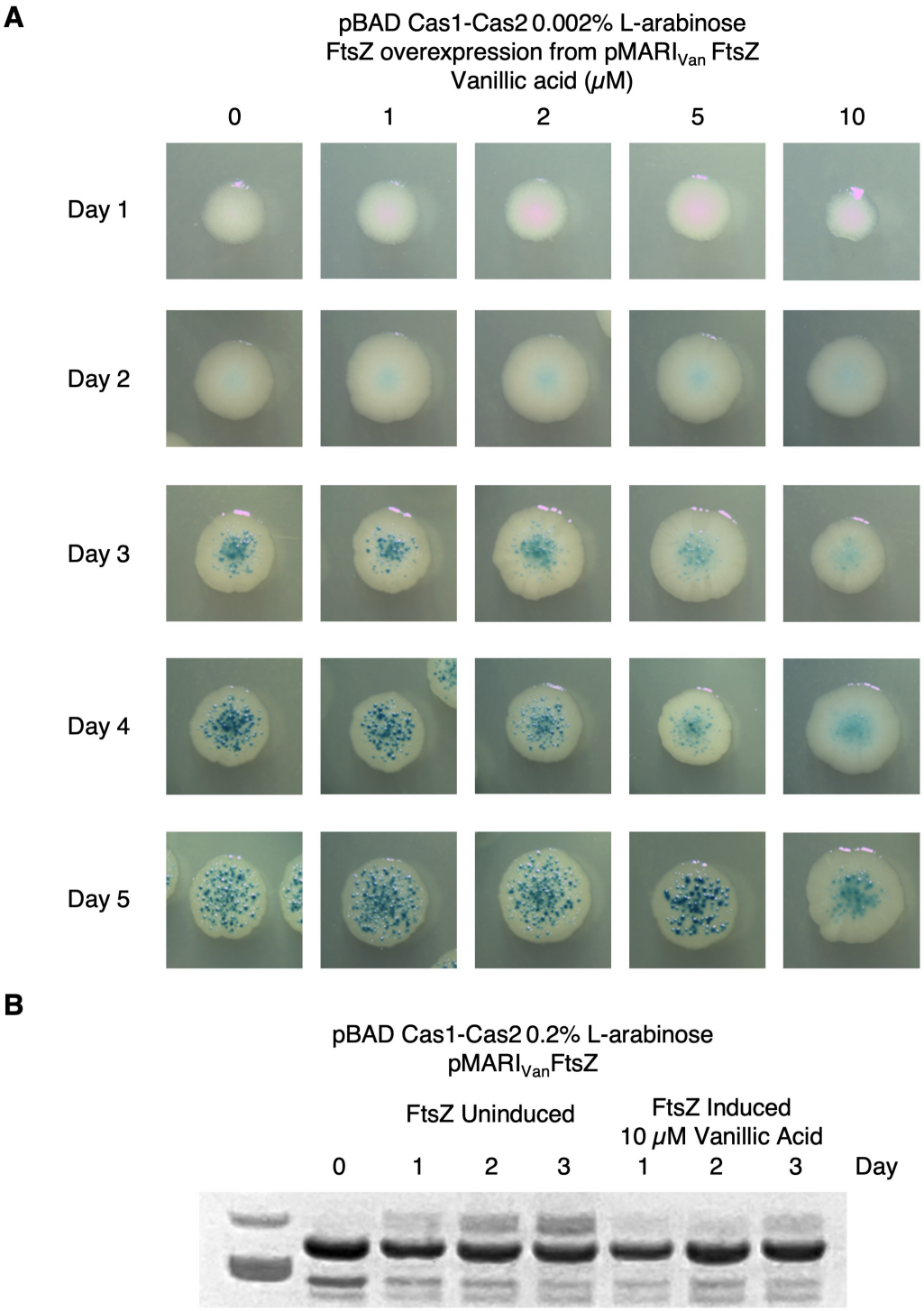


Figure 6.8. Overexpression of *ftsZ* decreases the rate of spacer acquisition

(A) Papillation assays were performed while overexpressing *ftsZ* in *E. coli* JB028. pBAD Cas1-Cas2 expression was induced at 0.002% L-arabinose. pMARI$_{Van}$ftsZ expression was induced by 0 – 10 μM vanillic acid. Representative daily colonies are shown for each condition.
(B) PCR-based SPIN assays were performed while overexpressing *ftsZ* in *E. coli* JB028. pBAD Cas1-Cas2 expression was induced by 0.2% L-arabinose. pMARI$_{Van}$ftsZ expression was induced by 0 or 10 μM Vanillic acid. Sub-cultures (1:1000 dilution) were initiated daily for three days.

6.9 Chapter Summary

- Deletion of *miaA* abolishes papillation but not spacer acquisition.
- Deletion of either *hflC* or *hflK* decreases the rate of adaptation.
- Overexpression of *hflC* or *hflK* does not affect the rate of spacer acquisition.
- Overexpression of *hflKC* increases the rate of adaptation.
- Overexpression of *ftsH* causes papillae to arise earlier.
- Overexpression of *ftsZ* decreases the rate of spacer acquisition.

Chapter 7

Deletion of LapB/FtsH Inhibitors Decreases the Rate of Spacer Acquisition

7.1 Introduction

The bacterial envelope acts as the interface between the extracellular and intracellular environment. In Gram-negative bacteria, it consists of a cytoplasmic and outer membrane with peptidoglycan present in the periplasmic space [314]. The outer membrane is an asymmetric bilayer consisting of phospholipids and lipopolysaccharide (LPS). Covalent and non-covalent interactions between outer membrane proteins and peptidoglycan link the two together. Consequently, cell membrane synthesis and peptidoglycan biogenesis need to be carefully coordinated to maintain the integrity of the cell envelope.

To discover host factors required for naïve CRISPR adaptation in *E. coli*, Dr. Jack Braithwaite performed a random Tn5 transposon mutagenesis screen in the JB028 papillation reporter strain to select for hypopapilating host mutants [237]. The screen recovered transposon insertions into the *lapC*, *rfaH*, *waaG* and *waaQ* genes (Figure 7.1). LapC functions as part of a pathway that maintains LPS homeostasis [315, 316]. RfaH is a transcription anti-terminator that upregulates the expression of the *waaQ* and *waaG* genes, which play a role in the modification of LPS [317–319]. Since multiple mutations in pathways that modulate LPS have extreme hypopapillation phenotypes, I decided to investigate the role that these genes play in spacer acquisition.

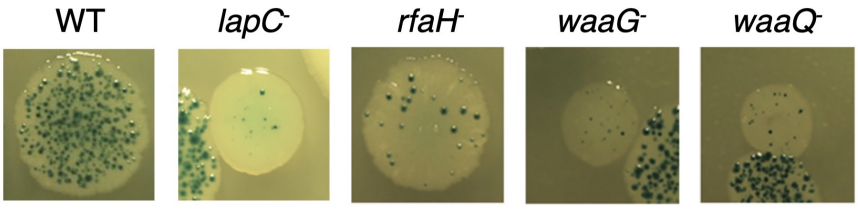


Figure 7.1. Tn5 insertion into *lapC*, *rfaH*, *waaG* and *waaQ* reduces the rate of papillation

Papillation assays were performed with the indicated Tn5 transposon insertion mutants. Compared to the *E. coli* JB028 wild type host, the mutants produced fewer papillae. Images of day 5 colonies are shown. Images taken with permission from (Braithwaite, 2021).

7.2 Truncation of *lapC* reduces the rate of spacer acquisition

LapC is an essential inner membrane signalling-protein that indirectly controls lipid A biosynthesis by protecting LpxC from degradation by the FtsH-LapB protease complex [315, 316]. Although *lapC* is essential, a nonsense mutation has been recovered that removes the 396-residue periplasmic domain while leaving the 190 residue transmembrane domain intact [320]. It came to our attention because a Tn5 insertion was recovered in a screen for adaptation mutants (Figure 7.1). This insertion removes the final 139 codons of the gene. This truncation reduces the rate of spacer acquisition compared to the wild type in the PCR-based SPIN assay (Figure 7.2a).

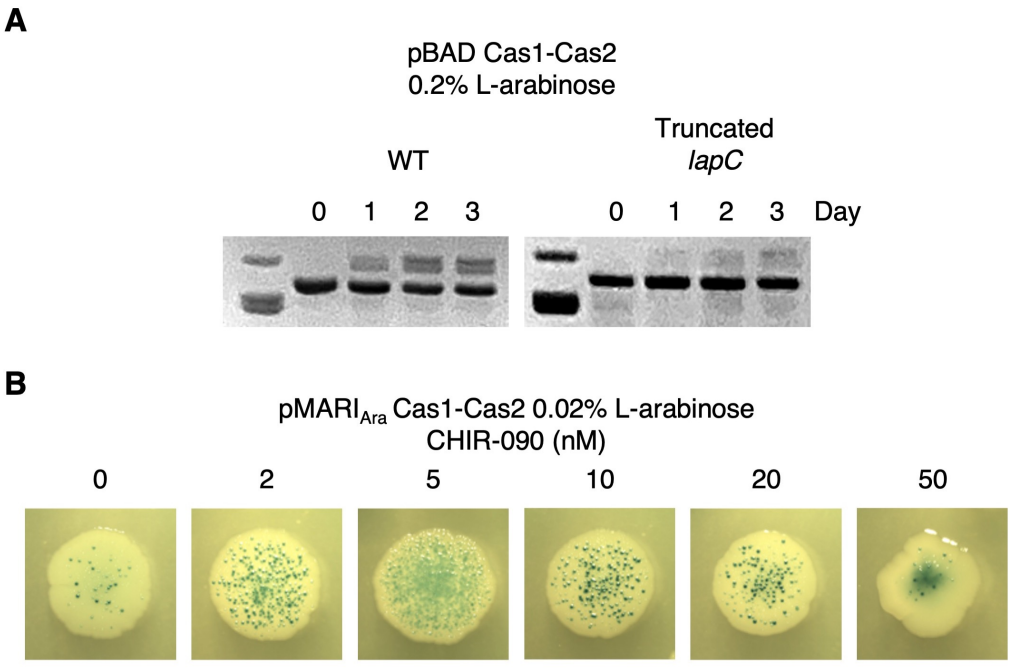


Figure 7.2. Truncation of *lapC* reduces the rate of adaptation

(A) PCR-based SPIN assays were performed in *E. coli* JB028 and the Tn5 truncation *lapC* mutant. pBAD Cas1-Cas2 expression was induced by 0.2 % L-arabinose. Sub-cultures (1:1000 dilution) were initiated daily for three days.
(B) Papillation assays were performed in *E. coli* JB028 across a range of 0 - 50 nM CHIR-090. pMARI$_{Ara}$ Cas1-Cas2 expression was induced by 0.02% L-arabinose. Representative day 5 colonies are shown.

The target of LapC signalling, LpxC, is also essential [321]. However, the antibiotic candidate CHIR-090 is a potent and specific chemical inhibitor [322]. *In vitro*, the inhibitory constant (Ki) is 4 nM, which is the amount needed to reduce the activity of purified LapC protein by 50%. In contrast, the minimal inhibitory concentration (MIC) for *E. coli* is 500 nM. When papillation assays were performed, spacer acquisition was significantly stimulated by 5 nM CHIR-090 (Figure 7.2b). At higher concentrations, the number of papillae reduced progressively, presumably due to the effects of inhibiting LpxC. It remains to be seen whether this reflects an increase in the rate of spacer acquisition in the SPIN assay.

7.3 Deletion of *waaG* and *waaQ* decreases the rate of spacer acquisition

Insertion into the *waaG* and *waaQ* genes in a random Tn5 mutagenesis screen produced colonies with a hypopapillating phenotype (Figure 7.1). These genes are located in the same operon and modify the core structure of LPS [319]. As the truncation of *lapC* decreases the rate of spacer acquisition, I wanted to study the roles of *waaG* and *waaQ* on CRISPR adaptation.

The *waaG* and *waaQ* genes were deleted from the reporter strain by P1 transduction from the Keio collection (Figure 7.3a). Papillation assays were performed and the deletion strains showed a reduced rate of adaptation compared to the wild type (Figure 7.3b). PCR-based SPIN assays were also performed. The $\triangle$*waaG* and $\triangle$*waaQ* mutants had a decreased rate of spacer acquisition relative to the wild type (Figure 7.3c). However, the difference is smaller than that seen in the papillation assay. Therefore, the deletion of *waaG* and *waaQ* decreases the rate of CRISPR adaptation.

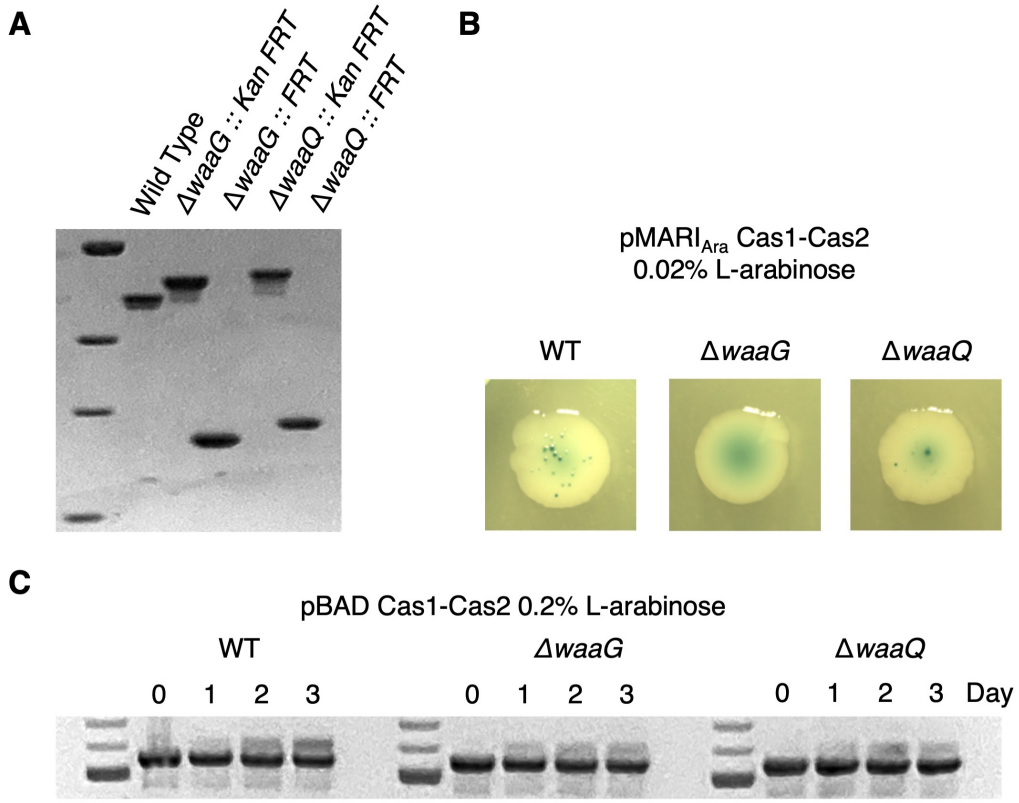


Figure 7.3. Deletion of *waaG* and *waaQ* decreases the rate of spacer acquisition

(A) PCR Verification of the deletion of *waaG* and *waaQ* from JB028.
(B) Papillation assays were performed in *E. coli* JB028, Δ*waaG* and Δ*waaQ*. pMARI$_{Ara}$ Cas1-Cas2 expression was induced by 0.02% L-arabinose. Representative day 5 colonies are shown.
(C) SPIN assays were performed in JB028, Δ*waaG* and Δ*waaQ*. pBAD Cas1-Cas2 expression was induced by 0.2% L-arabinose. Sub-cultures (1:1000 dilution) were initiated daily for three days.

7.4 Deletion of *rfaH* decreases the rate of spacer acquisition

In a mutagenesis screen, Tn5 insertion into the *rfaH* gene produced a hypopapillating colony (Figure 7.1). RfaH is a transcriptional anti-terminator of multiple operons involved in the synthesis, assembly, and export of the LPS core [323, 324]. These include the *waaG* and *waaQ* genes, which I showed the deletion of decreases the rate of spacer acquisition (Figure 7.3). Consequently, I decided to investigate the effect of *rfaH*.

To study the role of *rfaH* in CRISPR adaptation, the gene was removed from the reporter strain by P1 transduction from the Keio collection (Figure 7.4a). I tested the rate of spacer acquisition in the papillation reporter and its Δ*rfaH* derivative. The number of papillae per colony was significantly lower in the *rfaH* background (Figure 7.4b). PCR-based SPIN assays for adaptation also showed that the Δ*rfaH* mutant had a decreased rate of spacer acquisition compared to the wild type (Figure 7.4c). Therefore, the deletion of *rfaH* decreases the rate of CRISPR adaptation.

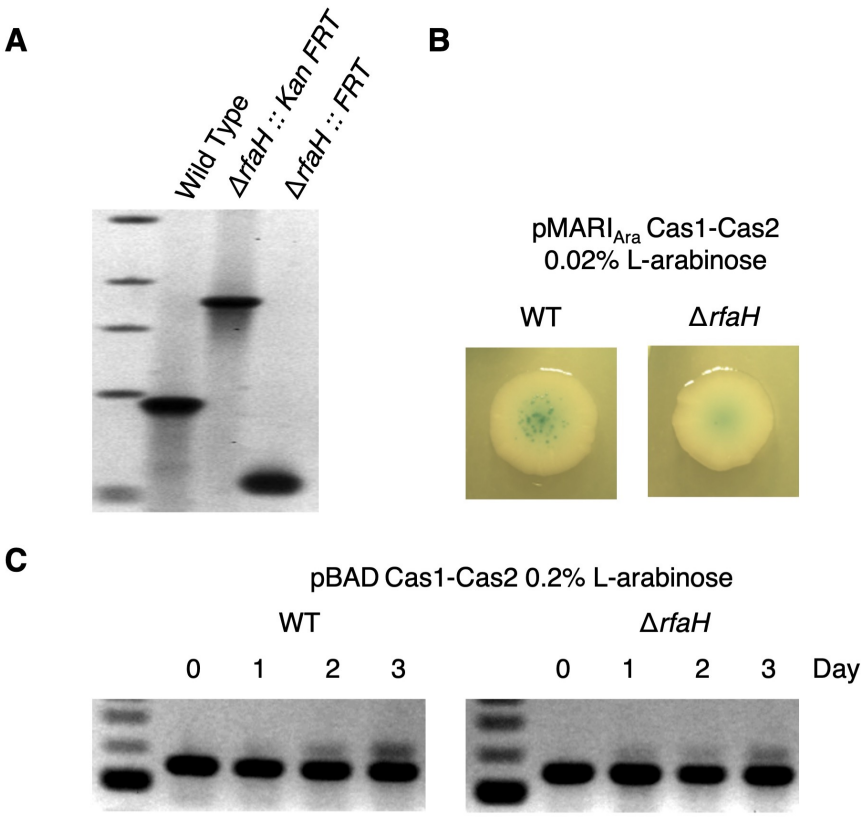


Figure 7.4. Deletion of *rfaH* reduces the rate of spacer acquisition

(A) PCR Verification of the deletion of *rfaH* from JB028.
(B) Papillation assays were performed in *E. coli* JB028 and Δ*rfaH*. pMARI$_{Ara}$ Cas1-Cas2 expression was induced by 0.02% L-arabinose. Representative day 5 colonies are shown.
(C) SPIN assays were performed in JB028 and Δ*rfaH*. pBAD Cas1-Cas2 expression was induced by 0.2% L-arabinose. Sub-cultures (1:1000 dilution) were initiated daily for three days.

7.5 Overexpression of *lapB* decreases the rate of papillation

LapC, WaaG and WaaQ are all negative regulators of LapB [315, 316, 318]. As the disruption of these genes decreases the rate of papillation, I wanted to determine the role that *lapB* plays in spacer acquisition. The *lapB* gene has been reported to be both essential and non-essential [240, 325]. I was unable to delete it from the reporter strain by P1 transduction from the Keio collection. Therefore, to determine the effect of *lapB* overexpression on the rate of adaptation, I decided to clone the gene into the vanillic acid expression vector. This was transformed into the reporter strain along with pBAD Cas1-Cas2. Papillation assays were performed across a range of 0 - 10 μM vanillic acid to induce *lapB* expression. The overexpression of *lapB* at 10 μM significantly reduced the rate of papillation (Figure 7.5). Therefore, *lapB* is a negative regulator of spacer acquisition in *E. coli*.

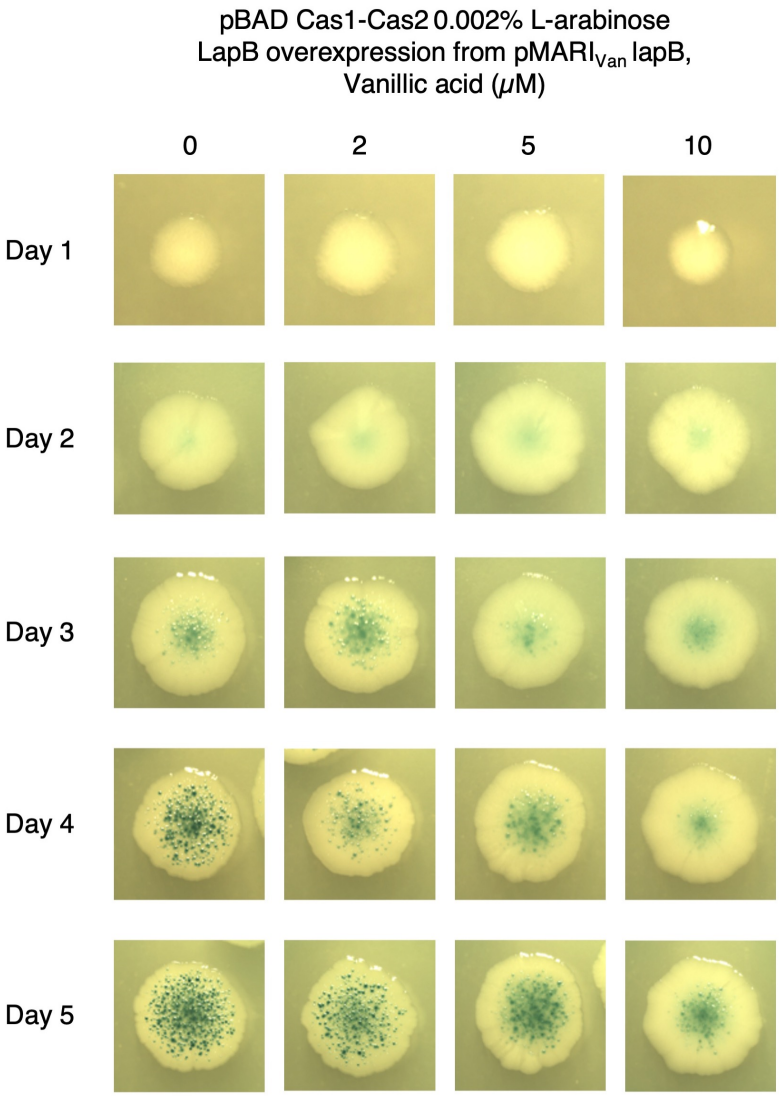


Figure 7.5. Overexpression of *lapB* reduces the rate of papillation

Papillation assays were performed in JB028 while overexpressing *lapB*. pBAD Cas1-Cas2 expression was induced by 0.002% L-arabinose. pMARI$_{Van}$ lapB expression was induced by 0 - 10 μM vanillic acid. Daily representative colonies are shown for all conditions.

7.6 Chapter Summary

- Truncation of *lapC* decreases the rate of spacer acquisition.
- CHIR-090 treatment increases the rate of papillation.
- Deletion of *rfaH*, *waaG* and *waaQ* decreases the rate of spacer acquisition.
- Overexpression of *lapB* decreases the rate of papillation.

Chapter 8

Discussion and Future Work

The work described in this thesis was undertaken to characterise novel host factors required for CRISPR Cas adaptation in *E. coli*. The function of the *Cas* genes was quickly determined due to their proximity to the CRISPR array. Other host factors have also been characterised, such as IHF and DnaQ, but their roles need to be better understood [120, 297, 298]. I hypothesized that more genes might be involved. Consequently, I used a papillation spacer acquisition reporter strain to determine the role of unknown host factors in CRISPR adaptation.

8.1 Coupling the SOS Response and CRISPR Adaptation

I showed that the Cas1-Cas2 complex induces filamentation because the catalytic activity of Cas1 activates the SOS response and the consequent expression of the cell cycle inhibitor *sulA* (Figures 4.1 and 4.3). The induction of filamentation by Cas1-Cas2 overexpression has previously been reported to be due to the activity of Cas2, as the L88A point mutation prevents both filamentation and spacer acquisition [254]. Cas2 functions as a molecular ruler which controls the length of spacers and mutations that disrupt the formation of the Cas1-Cas2 complex alter spacer acquisition [127, 129]. The L88 residue of Cas2 forms hydrogen bonds with V81, is located in a beta-sheet that stabilises prespacer binding and is at the interface between Cas1 and Cas2 proteins [127, 129]. As a result, I hypothesise that the L88A mutation would disrupt the structure of the Cas1-Cas2 complex, which indirectly perturbs the catalytic activity. As the Cas1-Cas2 complex cannot integrate spacers, the SOS response is not induced and *sulA* is not expressed. Consequently, filamentation does not arise. Therefore, the nuclease activity of Cas1 is what induces filamentation.

Disintegration reactions are the most frequently catalysed by the Cas1-Cas2 complex [326]. I showed that the expression of Cas1-Cas2 induces filamentation in an $\triangle$*IHF* strain (Figure 4.3), and it has been reported that spacers can be integrated at locations away from the CRISPR array [327–330]. The induction of the SOS response, therefore, may be a consequence of aborted integration events.

Activating the SOS response would allow for the repair of DNA damage caused by these off-target events, protecting the host from deleterious mutations. It would also allow time for the newly integrated spacer-repeat unit in the CRISPR array to be efficiently repaired [136], providing adaptive immunity against future infections (Figure 8.1).

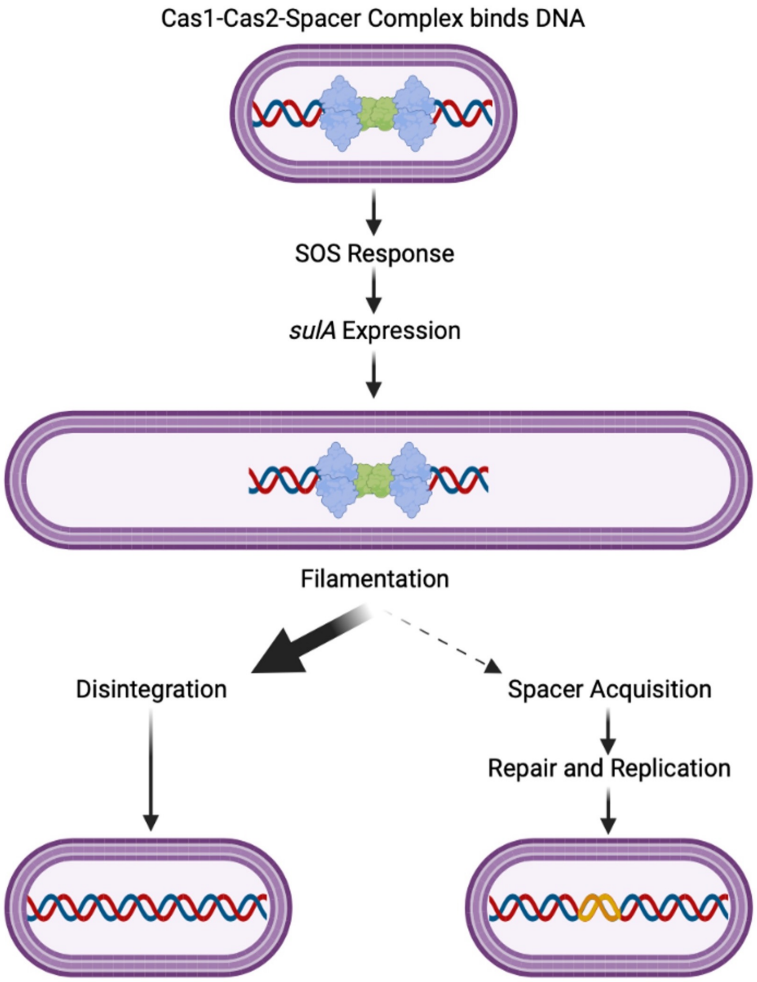


Figure 8.1. Model linking induction of the SOS response to spacer acquisition

The Cas1-Cas2-Spacer complex (shown in purple and green) binds to DNA (shown in red and blue). The catalytic activity of Cas1 induces the SOS response, which induces *sulA* expression to inhibit FtsZ polymerisation so the cell undergoes filamentation. In most cells, the Cas1-Cas2-Spacer complex disintegrates from the DNA without adaptation. In a subpopulation, the spacer is integrated into the CRISPR array (the DNA shown in yellow). The DNA is repaired and replicated to provide immunity against future infections.

The SOS response has been linked to CRISPR interference in *Serratia*, *P. aeruginosa* and *S. aureus* [331–333]. The data I have presented show that induction of the SOS response aids in naive spacer acquisition in *E. coli*. This would provide maximum immunity when the risk of infection is highest. Infection from foreign genetic elements, such as plasmids and bacteriophages, has been shown to induce the SOS response [334, 335]. These pose a potential fitness risk to the host bacterium. The linking of the SOS response and CRISPR Cas adaptation increases the likelihood that spacers will be acquired against these invading genetic elements when innate defence mechanisms have been overcome.

The deletion of *recA* has previously been shown not to alter the rate of spacer acquisition [336]. This work was performed using the PCR-based SPIN assay. The data generated by the papillation assay and flow cytometry demonstrates that the deletion of *recA* significantly increases the rate of adaptation (Figures 5.6 and 5.7). Since these assays are more sensitive than the PCR-based SPIN assay, this is why the effect of *recA* deletion was not previously determined.

RecA plays a role in DNA repair beyond LexA cleavage. The binding of RecA to ssDNA in regions where replication has stalled has been suggested to serve a role in protection from degradation by exonucleases whilst awaiting repair [337]. The digestion products of restriction nucleases are a source of spacers for adaptation [145, 148]. Therefore, I hypothesise that the deletion of *recA* increases the rate of adaptation due to an increase in the prespacer substrate.

The overexpression of *sulA* in the *lexA3* background restores the rate of papillation to that of the wild type (Figure 5.9). Constitutive high expression of *sulA* prevents cell division due to the inability to form FtsZ protofilaments and results in cell lysis [338]. As Cas1-Cas2 induces native *sulA* expression (Figure 5.3c), it can only be moderately expressed from the vanillic acid expression vector in the wild type. This is why papillae arise earlier, but the total number remains the same. The *lexA3* allele prevents induction of the SOS response and chromosomal *sulA* expression

(Figure 5.2b). A moderate level of *sulA* expression is, therefore, possible in this background, which will increase the time taken for cell division to arise but not inhibit it altogether. This allows extra time for the Cas1-Cas2 complex to integrate spacers. I hypothesise that this is why *sulA* expression increases the rate of papillation in the *lexA3* background. This implies that sulA is a key protein of the SOS response to support adaptation.

There could be an overlap in the function of genes that inhibit FtsZ polymerisation. Antibiotic exposure has been shown to upregulate cell division inhibitor genes from three prophages in *E. coli* K12 [196]. In addition, the MINCDE and Nucleoid occlusion systems, downregulation of cell division genes and induction of the SOS response also modulate the assembly of the Z-ring [249–253]. These genes are under the control of different regulatory mechanisms. For example, the induction of the SOS response leads to *sulA* and *ymfM* expression. However, this is due to the derepression of distinct inhibitors [252, 253, 271]. Bacteriophages have been shown to encode proteins that inhibit LexA cleavage and enhance its DNA binding [339, 340]. Expressing a gene that enhances filamentation independent of LexA will overcome this phage defence mechanism and facilitate spacer acquisition. This could explain why the *lexA3* mutation has a decreased rate of adaptation. Exposure to nalidixic acid does not induce *sulA* expression in this background (Figure 5.2). However, *ymfM* will be expressed as it is repressed by YmfK instead of LexA [284–286]. Therefore, the activity of YmfM will inhibit FtsZ polymerization and delay cell division. This may not induce filamentation as strongly as *sulA* expression, so the rate of spacer acquisition is reduced but not abolished.

Induction of *kilR*, encoded by the rac prophage, induces filamentation in *E. coli* [341]. Tn5 insertion into this gene produced a hypopapillating phenotype during a random transposon mutagenesis screen (Figure S20). Its expression is upregulated following exposure to nalidixic acid and the beta-lactam antibiotic azlocillin [237, 342]. However, the deletion of the *kilR* gene from the reporter by P1 transduc-

tion from the Keio collection did not alter the rate of papillation (Figure S20). This is the same as when *sulA* and *ymfM* are deleted (Figure 5.11). It would be interesting to overexpress *kilR* to determine if this also increases the rate of adaptation.

8.2 Effect of Sub-inhibitory concentrations of Antibiotics

Sub-inhibitory concentrations of bacteriostatic but not bactericidal antibiotics have been reported to increase the rate of spacer acquisition due to a decrease in phage growth rate in *P. aeruginosa* [343]. This includes exposure to mitomycin c, which did not increase CRISPR immunity. The data presented here argue the opposite of this (Figure 5.15). These phage challenge assays were performed in liquid culture, which I found less permissive than growth on an agar plate. I want to determine the effects of sub-inhibitory concentrations of antibiotics on adaptation when *P. aeruginosa* is challenged with phage in a biofilm environment.

The fact that all four antibiotics tested increased the rate of papillation, but only nalidixic acid and mitomycin c induced the SOS response, implies a different mechanism. The data presented in Chapter 5 suggests that activation of the SOS response supports spacer acquisition. Therefore, the induction of the SOS response by exposure to nalidixic acid and mitomycin c is likely the mechanism that increases the rate of papillation. Ampicillin and cefalexin must increase the rate of adaptation by an alternative mechanism.

Exposure to sub-inhibitory concentrations of ampicillin promotes cell-to-cell plasmid transformation in *E. coli* [344]. This study was performed using an *E. coli* biofilm model, which mimics the papillation assay more closely than liquid-culture assays [345]. Cell-to-cell plasmid transformation could be the DNA source from which the spacers are derived to increase the rate of papillation when cells are exposed to sub-inhibitory concentrations of beta-lactam antibiotics.

Exposure of *E.coli* DH5α to ampicillin alters the expression of multiple transcription factors, including IHF, which was upregulated over ten-fold [346]. The expression

of IHF is tightly regulated, with small reductions in abundance having a significant effect on several IHF-dependent functions [347]. IHF is an essential host factor for spacer acquisition in the type I-E CRISPR system of *E. coli* [123]. Consequently, exposure to sub-inhibitory concentrations of beta-lactam antibiotics may increase the rate of adaptation due to the upregulation of IHF expression.

Sub-inhibitory concentrations of ampicillin have been reported to induce and not induce the SOS response [247, 348–351]. The data in Figure 5.14 supports the hypothesis that sub-inhibitory concentrations of ampicillin do not induce the SOS response. This contrasts with the majority of the literature, which suggests that beta-lactam antibiotics induce the SOS response. Again, this data was generated from experiments performed in LB broth. I found that liquid culture growth was much less permissive than on an agar plate. I hypothesise that the different reported effects of sub-inhibitory concentrations of ampicillin are due to the growth method.

8.3 HflKC and LapB: Equilibrium of FtsH Specificity Factors

The deletion of the *hflK* and *hflC* genes by P1 transduction from the Keio collection produced a hypopapillating phenotype (Figure 6.4). HflC and HflK form a complex to regulate the activity of the metalloprotease FtsH [304]. Overexpression of either subunit individually does not alter the rate of papillation, but overexpression of both causes papillae to arise earlier and increases the rate of papillation (Figure 6.6). Overexpression of FtsH also causes papillae to arise earlier and increases the rate of papillation (Figure 6.7).

Tn5 transposon insertion into *lapC* and the deletion of either the *waaG* or *waaQ* genes produced colonies with a hypopappilating phenotype (Figures 7.2 and 7.3). These all interact with LapB to regulate the activity of the FtsH/LapB complex. The overexpression of *lapB* also decreases the rate of papillation (Figure 7.5).

I hypothesise that the concentration of FtsH specificity factors changes the equilibrium position to determine the substrate for degradation (Figure 8.2). Increased abundance of LapB promotes FtsH/LapB catalysed proteolysis of LpxC to decrease LPS concentration in the inner membrane [315, 316]. The increased LapB concentration decreases free FtsH available for HflKC to guide to substrates. Deleting *hflK* or *hflC* will also shift the equilibrium to favour FtsH/LapB complex formation. Conversely, overexpression of *hflKC* will alter the equilibrium to promote FtsH/HflKC complex formation and favour FtsZ degradation. This shift will enhance the Cas1-Cas2 induced filamentation phenotype to prolong the time taken for cell division and support adaptation.

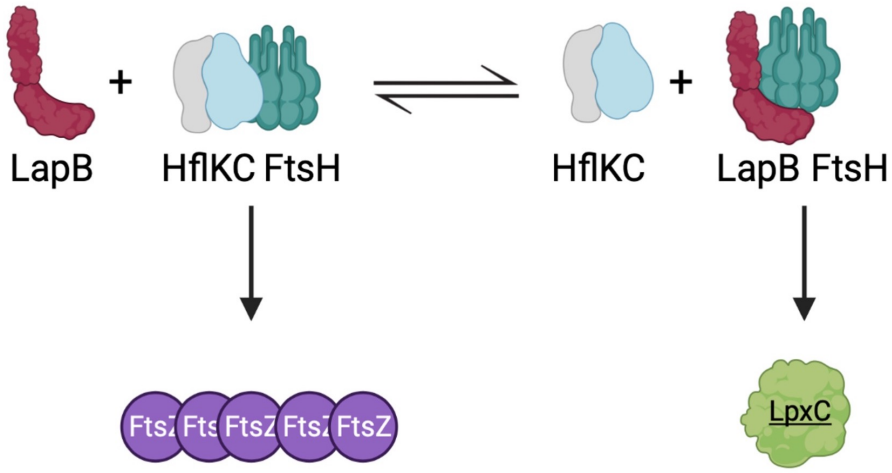


Figure 8.2. The equilibrium of FtsH specificity factors determines the choice of substrate

When FtsH/HflKC is favoured in the equilibrium, FtsH degrades FtsZ at an enhanced rate. LpxC concentration consequently increases, which leads to LPS build-up in the inner membrane. This relieves LapC repression of LapB and shifts the equilibrium to favour the formation of FtsH/LapB and degradation of LpxC. Cellular levels of FtsZ consequently increase. Deletion of LapB repressors results in hyperactive FtsH/LapB due to a shift in the equilibrium away from ftsH/HflKC.

This hypothesis is dependent upon FtsH-mediated degradation of FtsZ. However, FtsH has only been shown to degrade FtsZ *in vitro* [352]. FtsH localises to the mid-cell site during septation, where the FtsZ ring structure forms during cell division [353, 354]. This links the proteins spatially within the cell. FtsH overexpression also prolongs the D phase of the cell cycle [355]. This is the same as when the SOS response is induced, which results in filamentation to prevent DNA damage from being passed onto daughter cells. The data presented in this thesis supports the hypothesis that FtsZ is a substrate of FtsH *in vivo*.

The ClpXP protease degrades FtsZ *in vivo* [356]. The deletion of either subunit increases cellular FtsZ levels. However, as it is possible to delete either *clpX* or *clpP* [240, 356], this can not be the only protease involved in FtsZ degradation. Both genes were deleted by P1 transduction from the reporter strain, and the rate of papillation was not altered (Figure S21). Consequently, another protease must be involved in FtsZ degradation to aid in spacer acquisition, which needs to be determined.

FtsH may not degrade FtsZ under the conditions previously tested, or a factor may be protecting FtsZ from proteolysis. For example, GTP/GDP can stabilise FtsZ against FtsH degradation *in vitro* [357]. The *ftsH* gene is essential, so it cannot be removed by P1 transduction [240]. As FtsZ is not a regular substrate of FtsH *in vivo* [358], there may be a stimulus to activate FtsH-mediated degradation. In *D. radiodurans*, FtsZ can undergo phosphorylation following DNA damage which inhibits growth [359, 360]. FtsZ has been shown to undergo phosphotyrosine modifications in *E. coli* and the overexpression of the *Mycobacterium* Ser/Thr Kinase PknA in *E. coli* results in phosphorylation and cell filamentation [361, 362]. Post-translational modifications, such as phosphorylation, may modify FtsZ to bring about FtsH-mediated degradation in *E. coli*.

8.4 FtsZ: the keystone of spacer acquisition

The data presented in Chapters 4, 5, 6 and 7 are linked through FtsZ. Either through the inhibition of polymerisation by induction of the SOS response or by the degradation by HflKC-FtsH (Figure 8.3). Controlled inhibition of cell division appears to be the critical link to support CRISPR adaptation. This will allow time for immunity to be generated against invading genetic elements.

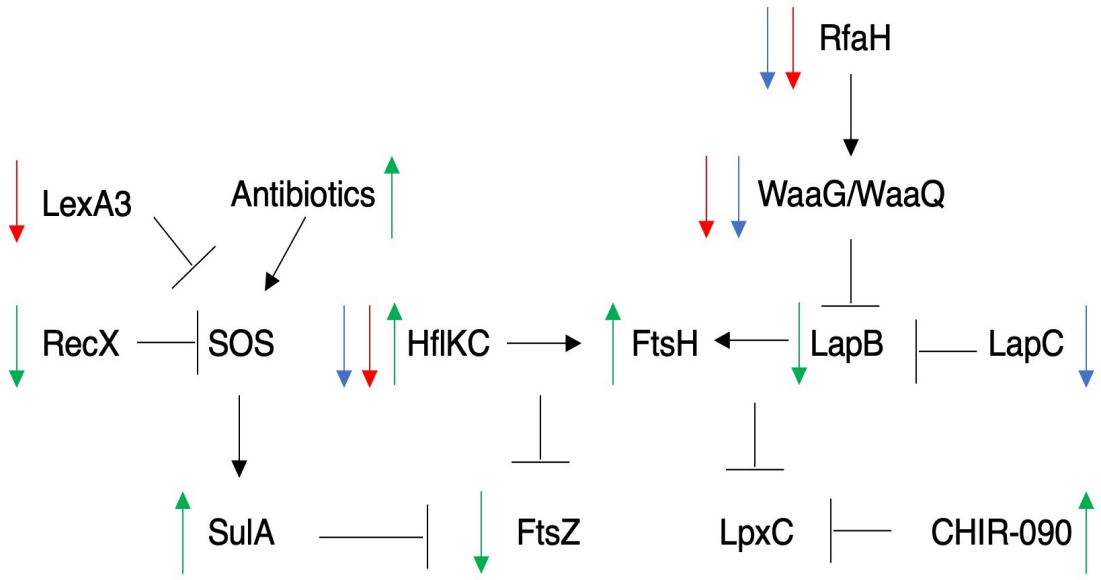


Figure 8.3. Linking the SOS Response, HflKC-FtsH and LapB-FtsH

Summary of the data presented in Chapters 4 - 7. Black arrows represent the induction of gene expression. Lines with bars indicate repression of gene expression. Coloured arrows indicate the effect on the rate of adaptation. Blue arrows refer to insertion into the gene during Tn5 random mutagenesis. Red arrows refer to a gene deletion. Green arrows refer to gene overexpression. Downward arrows show a decrease in the rate of spacer acquisition. Upward arrows represent an increase in the rate of adaptation.

It is difficult to predict what benefit filamentation provides to a cell during adaptation. The pause of cell division may give the host more time to destroy the invading genetic element by CRISPR interference. However, the time taken for adaptation, crRNA transcription and maturation, and interference is likely too long to prevent the bacterium from becoming overcome by the infection. Indeed, infection with defective phage, that is either unmethylated or mutated, significantly increases the rate of spacer acquisition [148, 150]. The CRISPR system may, therefore, provide immunity against future reinfection and the host may rely on alternative defence systems to deal with the invading genetic element, such as restriction-modification or argonaute.

During filamentation, DNA replication continues in the absence of cell division. The extra copies of the chromosome mean multiple CRISPR arrays can acquire spacers. Multiple arrays in the filament may acquire spacers with different DNA sequences to increase diversity. When the cells divide after the resolution of filamentation, the colony will have spacers complementary to multiple sequences in the invading genetic element. The increased diversity of spacers will mean that escape mutants are less likely to kill the whole colony during future infections. Since the crRNA of the first spacer in the array is twice as abundant as the fifth [102], having multiple cells in a filament acquire a spacer instead of one cell acquiring multiple will help to maximise the immunity provided by the colony's CRISPR systems.

8.5 Future Work of SOS and Adaptive Immunity

I hypothesise that more genes of SOS response will play a role in adaptation. As overexpression of *sulA* and *ymfM* increases the rate of papillation, this implies that these aid in spacer acquisition. However, as adaptation arises when they are deleted, they are not essential. I want to determine which genes are responsible for the decreased rate of papillation in the *lexA3* mutant.

RecA isoforms from different organisms have been shown to possess alternate activities [363]. The *P. aeruginosa* and *D. radiodurans* recA proteins bind to ssDNA with the same affinity as that in *E. coli*. However, *D. radiodurans* recA does not induce the SOS response, whereas *P. aeruginosa* recA induces it to a greater degree than the *E. coli* recA protein. The mutant *E. coli recA430* has DNA recombination activities but does not cleave LexA to induce the SOS response, due to the G204S mutation in the region that triggers LexA autoproteolysis [267]. To precisely determine the role that *recA* plays in spacer acquisition, I would complement the $\triangle$*recA* reporter strain with these isoforms. They would be placed under the control of the *recA* promoter, RBS, -10 & -35 sites and LexA box to provide native expression [259, 364]. I would insert these genes onto the chromosome using the clonetegration kit [275]. I hypothesise that the SOS-deficient isoforms would have a decreased rate of papillation relative to the wild type reporter, and the SOS+ isoform would be higher. These would be lower than the $\triangle$*recA* mutant, as this strain has an increased rate of adaptation over and above the decrease caused by the loss of the SOS response.

To determine how the catalytic activity of the Cas1-Cas2 complex induces the SOS response, I would use a gene conversion assay to study if the Cas1-Cas2 complex acts as a DNA roadblock. A modified reporter system based on the recombination assay described by Klaric et al., 2021 [365] is shown in Figure 8.4. Upstream of the minimal CRISPR reporter locus is a *lacZ* gene with a loss of function active site mutation. A recovery fragment that contains the wild-type active site but also a

non-functional truncated *lacZ* would be located elsewhere in the genome. These colonies will not metabolise lactose, so they will be white when grown on agar supplemented with X-gal. If the Cas1-Cas2 complex acts as a DNA roadblock, there will be a crossing over event between the mutated and recovery *lacZ* fragments to restore the wild-type active site. If there is also a spacer acquisition event, the *lacZ* will become in-frame, and papillae will form.

To determine why exposure to sub-inhibitory concentrations of ampicillin increases the rate of papillation, I would perform a cell-to-cell plasmid transformation experiment. I would mix the papillation reporter strain, transformed with pBADCas1-Cas2, with a lactose non-metabolizing strain of *E. coli* transformed with an alternative plasmid, such as p15a with a chloramphenicol resistance gene (Figure 8.5). Selection of colonies on minimal media agar supplemented with lactose as the carbon source and the two antibiotics encoded by the plasmids would show colonies that have undergone cell-to-cell plasmid transformation and spacer acquisition. Sequencing of the spacers would determine if they were derived from the transferred plasmid. Repeating this assay in the presence of sub-inhibitory concentrations of ampicillin should increase the number of colonies if the transformed plasmid is the source of acquired spacers.

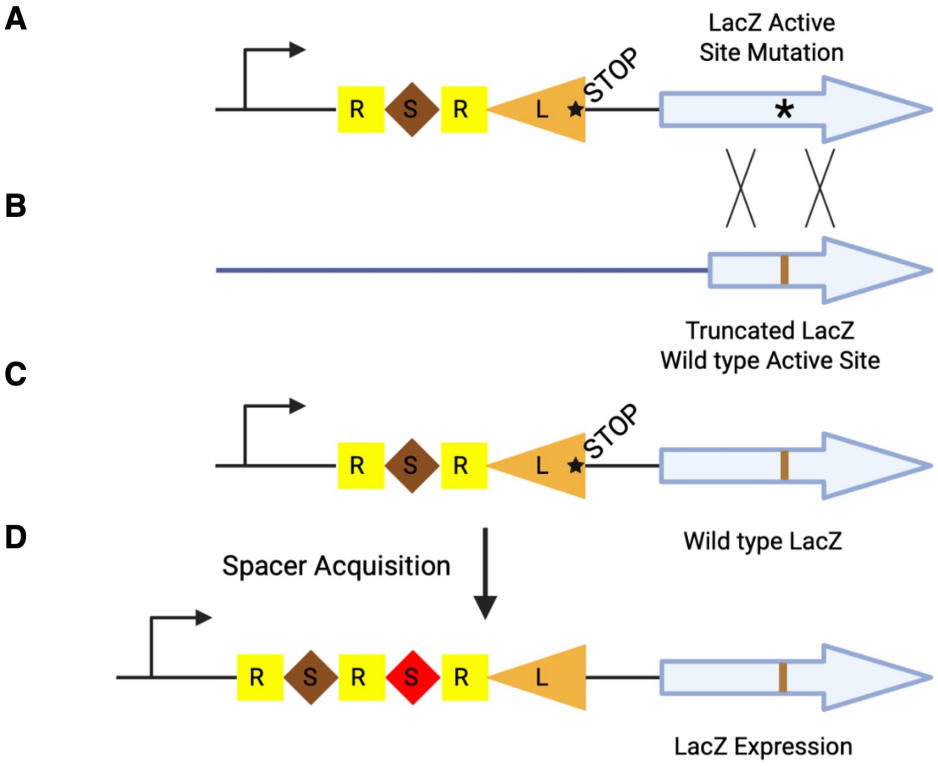


Figure 8.4. Gene Crossover Assay for Cas1-Cas2 as a DNA roadblock

(A) A minimal CRISPR array consists of a Leader sequence (orange arrow), two type A repeats (yellow square) and a single spacer (brown diamond). The Leader contains a STOP codon. The *lacZ* is out-of-frame and contains an active site mutation (asterisk) which abolishes function.
(B) A recovery *lacZ* fragment is inserted at a distant location in the genome (blue line). This contains the wild type active site (light brown box). This is a truncated form of *lacZ*, which is functionally inactive.
(C) A crossover event restores the wild type *lacZ* active site to restore function.
(D) Spacer acquisition (red diamond) will provide a frameshift, so *lacZ* is expressed.

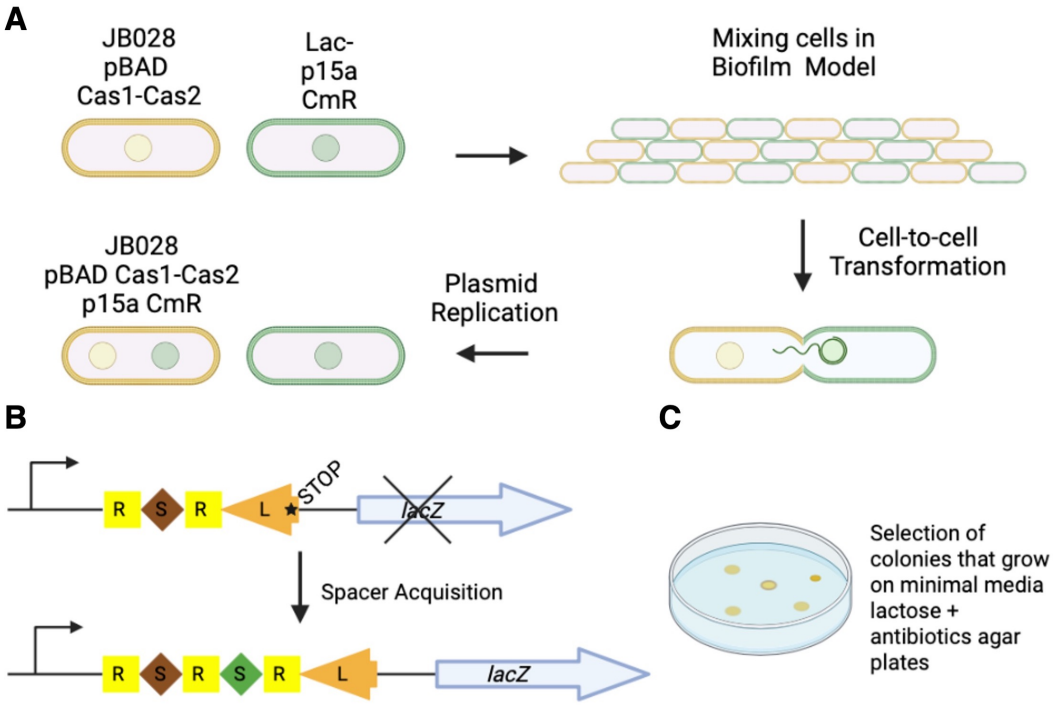


Figure 8.5. Cell-to-cell transformation as a substrate for spacers

(A) A model where cell-to-cell transformation arises. The JB028 papillation reporter strain (orange cell) is transformed with pBAD Cas1-Cas2 (orange circle). It is mixed with a lactose non-metabolizing strain of *E. coli* (green cell) transformed with a p15a chloramphenicol plasmid (green circle). The cells are mixed in a biofilm model in the presence of arabinose to induce Cas1-Cas2 expression. Cell-to-cell transformation occurs to move the p15a chloramphenicol plasmid into the reporter strain.
(B) A minimal CRISPR array consists of a Leader sequence (orange arrow), two type A repeats (yellow square) and a single spacer (brown diamond). The Leader sequence contains a STOP codon (asterisk) which prevents *lacZ* expression. Spacer acquisition (green diamond) will provide a frameshift and result in *lacZ* expression.
(C) Growth on minimal lactose media selects for cells that have acquired a spacer and express *lacZ*. The presence of two antibiotics selects for cells that have received the p15a chloramphenicol plasmid. PCR amplification across the reporter CRISPR array and Sanger sequencing will show where the spacer DNA is derived from.

8.6 Future Work of Membrane Stress and Adaptive Immunity

A BacterioMatch two-hybrid system could determine the equilibrium between the HflKC and LapB. The construction of a reporter system where HflKC and FtsH need to come together to induce the expression of a GFP reporter gene would allow this (Figure 8.6) [366]. HflKC would be linked to the N-terminal of GFP and FtsH to the C-terminal. When these fragments are nearby, the GFP protein will form and the cells will fluoresce. When the FtsH and HflKC proteins are distant from each other, GFP will not form, so the cells will not fluoresce. Alteration of the equilibrium would determine if this hypothesis is correct. When the equilibrium is shifted to favour FtsH/LapB complex formation, either by deletion of hflK or hflC, truncation of *lapC* or overexpression of *lapB*, GFP fluorescence should decrease. When the equilibrium is shifted to favour FtsH/HflKC complex formation by overexpression of hflKC or negative regulators of LapB, induction of GFP fluorescence should increase.

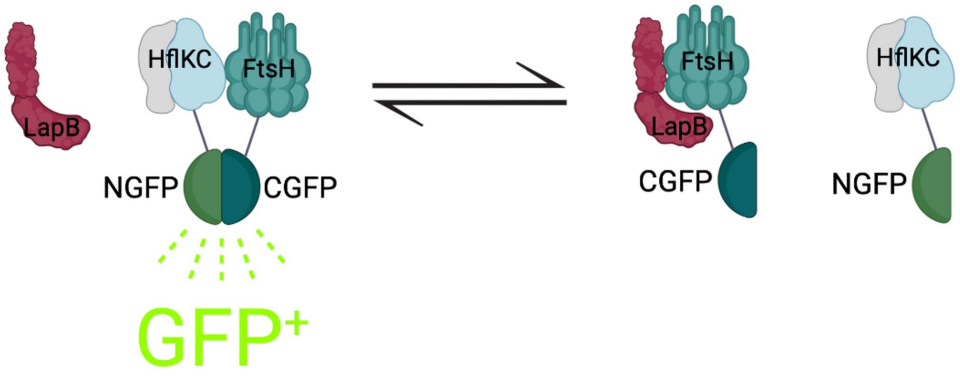


Figure 8.6. Principle of an *E. coli* two-hybrid system based on functional complementation of GFP fragments to study FtsH/HflKC and FtsH/LapB Interactions

The N- and C-terminal halves of the GFP protein are split. The two fragments, fused to two interacting proteins, FtsH and HflKC, are brought into proximity, resulting in GFP fluorescence.

The mutation of the three tyrosine residues of FtsZ would show whether post-translational modifications support FtsH-mediated degradation. The wild-type chromosomal *ftsZ* gene would be replaced with the point mutants. If these mutations prevent FtsH-mediated degradation, overexpression of FtsH will not increase the rate of papillation.

A microarray should be performed to discover any host factors that modify FtsZ to facilitate FtsH-mediated degradation. Analysis should be performed in the absence and presence of Cas1-Cas2 induction. Any genes that are upregulated following overexpression, especially those with known or predicted post-translational modification capability, will be of interest. These proteins could then be purified and *in vitro* assays performed to determine if they modify FtsZ.

Appendix

Figure	Source	Licence Number
Figure 1.1	Isaev et al., 2021	Creative Commons licence
Figure 1.4	Gao et al., 2022	Creative Commons licence
Figure 1.6	Hille et al., 2018	5319241302768
Figure 1.7	Xue and Sashital, 2019	Creative Commons licence
Figure 1.8	Wang et al., 2015	5319240363088
Figure 1.9	Ma et al., 2021	Creative Commons licence
Figure 1.10	Rice et al., 1996	5319240497977
Figure 1.11	Xue and Sashital, 2019	Creative Commons licence
Figure 1.12	Makarova et al., 2020	5319240091213
Figure S8	Amlinger et al., 2017	Creative Commons licence

Table S1. Licence numbers for the reproduction of published figures in this work.

Figure	Condition	Values (a.u.)			P Value
3.8a	Cuminic Acid 0 μM	6522	6548	6571	-
	Cuminic Acid 25 μM	27025	26380	35328	0.0013
	Cuminic Acid 50 μM	30975	38238	37914	0.18
	Cuminic Acid 100 μM	37810	35946	37735	0.58
3.8b	Cuminic Acid 0 μM	7020	6404	6196	-
	Cuminic Acid 25 μM	21163	22063	22891	<0.0001
	Cuminic Acid 50 μM	24537	24119	24192	0.012
	Cuminic Acid 100 μM	24064	24778	23033	0.57
3.8c	Salicylic Acid 0 μM	5860	5900	5859	-
	Salicylic Acid 25 μM	41571	40460	40945	<0.0001
	Salicylic Acid 50 μM	46257	44410	49066	0.016
	Salicylic Acid 100 μM	51300	47844	48304	ns
3.8d	Salicylic Acid 0 μM	6651	6871	6567	-
	Salicylic Acid 25 μM	47317	55585	48192	<0.0001
	Salicylic Acid 50 μM	45375	42711	49169	0.23
	Salicylic Acid 100 μM	33380	24399	21799	0.0084
3.8e	Vanillic Acid 0 μM	5694	5540	4764	-

Figure	Condition	Values (a.u.)			P Value
	Vanillic Acid 25 μM	8153	7846	7695	0.0013
	Vanillic Acid 50 μM	14398	14890	13212	0.0003
	Vanillic Acid 100 μM	24304	22655	22132	0.0004
3.8f	Vanillic Acid 0 μM	3756	4427	3589	-
	Vanillic Acid 25 μM	10152	10447	10117	<0.0001
	Vanillic Acid 50 μM	16358	18042	16981	0.0002
	Vanillic Acid 100 μM	29149	27096	29301	0.0002
3.8g	Vanillic Acid 0 μM	8246	10949	9214	-
	Vanillic Acid 25 μM	9733	10870	9593	0.53
	Vanillic Acid 50 μM	9266	9408	10525	0.78
	Vanillic Acid 100 μM	9689	8440	9094	0.67
3.8h	Vanillic Acid 0 μM	5206	4143	3806	-
	Vanillic Acid 25 μM	7000	6560	7331	0.0057
	Vanillic Acid 50 μM	14551	14796	14933	<0.0001
	Vanillic Acid 100 μM	23502	25527	25791	0.0002
4.3b	Nalidixic Acid 0 μg/mL	10430	9314	8364	-
	Nalidixic Acid 0.1 μg/mL	12415	12550	12360	0.0069
	Nalidixic Acid 0.2 μg/mL	21555	19485	17365	0.0017
	Nalidixic Acid 0.4 μg/mL	25728	19958	19563	0.004
4.3c	0% Ara	6582	6301	5907	-
	0.05% Ara	6449	6743	6177	0.49
	0.1% Ara	6318	6634	6130	0.71
	0.2% Ara	7253	6737	6699	0.075
4.3d	Cas1-Cas2 0% Ara	9602	8698	10199	-
	Cas1-Cas2 0.05% Ara	18075	18840	21666	0.0010
	Cas1-Cas2 0.1% Ara	21541	21474	21268	<0.0001
	Cas1-Cas2 0.2% Ara	20928	26225	25300	0.0010
4.3e	dCas1-Cas2 0% Ara	8162	8650	7932	0.0612
	dCas1-Cas2 0.05% Ara	13622	14326	14248	0.0080
	dCas1-Cas2 0.1% Ara	13226	15415	15457	0.0062
	dCas1-Cas2 0.2% Ara	14251	14634	14865	0.0043
4.3f	ΔIHFα 0% Ara	9685	9422	9824	0.7670
	ΔIHFα 0.05% Ara	19705	18150	20135	0.8817
	ΔIHFα 0.1% Ara	20217	20216	21036	0.0301

Figure	Condition	Values (a.u.)			P Value
	ΔIHFα 0.2% Ara	20450	23053	21455	0.2376
5.2b JB028	Nalidixic Acid 0 μg/mL	8726	9314	10123	-
5.8a	Nalidixic Acid 0.2 μg/mL	12831	13849	13578	0.0014
	Nalidixic Acid 0.4 μg/mL	15296	15581	15918	0.0002
	Nalidixic Acid 0.8 μg/mL	22654	25262	23813	<0.0001
5.2b *lexA3*	Nalidixic Acid 0 μg/mL	19834	20988	19212	-
	Nalidixic Acid 0.2 μg/mL	19983	21182	23779	0.2557
	Nalidixic Acid 0.4 μg/mL	18912	21508	19535	0.9792
	Nalidixic Acid 0.8 μg/mL	24781	19390	20425	0.4295
5.3c JB028	0% Ara	8506	9236	10704	-
	0.05% Ara	18776	18950	20499	0.0003
	0.1% Ara	20283	19598	22358	0.0004
	0.2% Ara	22757	22547	25448	0.0002
5.3c *lexA3*	0% Ara	4134	4448	5148	-
	0.05% Ara	1899	4706	4247	0.36
	0.1% Ara	4526	3613	4028	0.26
	0.2% Ara	2521	3688	5360	0.46
5.8a Δ*recA*	Nalidixic Acid 0 μg/mL	12644	10022	11982	-
	Nalidixic Acid 0.2 μg/mL	128867	12068	12648	0.2980
	Nalidixic Acid 0.4 μg/mL	11439	11298	9740	0.4916
	Nalidixic Acid 0.8 μg/mL	8955	12712	8507	0.3899
5.8b Δ*recA*	0% Ara	4134	4448	5148	-
	0.05% Ara	1899	4706	4247	0.36
	0.1% Ara	4526	3613	4028	0.26
	0.2% Ara	2521	3688	5360	0.46
5.14a	Ampicillin 0 μg/mL	13350	12412	13593	-
	Ampicillin 1 μg/mL	12100	11877	12785	0.13
	Ampicillin 2 μg/mL	13208	11988	10731	0.23
	Ampicillin 4 μg/mL	12644	12906	13112	0.58
	Ampicillin 8 μg/mL	13841	15070	17493	0.11
5.14b	Cefalexin 0 μg/mL	13184	9925	13672	-
	Cefalexin 1 μg/mL	12798	12098	13067	0.76
	Cefalexin 2 μg/mL	12836	12253	13512	0.65
	Cefalexin 4 μg/mL	12935	12605	14059	0.50

Figure	Condition	Values (a.u.)			P Value
	Cefalexin 8 μg/mL	16224	22866	18299	0.04
5.14c	Nalidixic Acid 0 μg/mL	7910	4516	5102	-
	Nalidixic Acid 1 μg/mL	8927	8597	6499	0.17
	Nalidixic Acid 2 μg/mL	13844	12381	12215	0.004
	Nalidixic Acid 4 μg/mL	28631	23242	25425	0.0005
	Nalidixic Acid 8 μg/mL	31952	23651	30239	0.0011
5.14d	Mitomycin C 0 μg/mL	3644	3631	3955	-
	Mitomycin C 0.1 μg/mL	25785	21389	36752	0.0061
	Mitomycin C 0.2 μg/mL	28061	26090	38458	0.0021
	Mitomycin C 0.5 μg/mL	31042	30405	38186	0.0003
	Mitomycin C 1.0 μg/mL	39453	38719	39044	<0.0001
S10c	Nalidixic Acid 0 μg/mL	8123	7933	8429	-
	Nalidixic Acid 0.1 μg/mL	8781	8992	9069	0.0095
	Nalidixic Acid 0.2 μg/mL	9576	10932	10434	0.0070
	Nalidixic Acid 0.4 μg/mL	13644	14337	14912	<0.0001
S10d	0% Ara	12176	12939	11455	-
	0.05% Ara	23377	23521	23324	<0.0001
	0.1% Ara	24056	25088	26428	<0.0001
	0.2% Ara	23954	24934	24232	<0.0001

Table S2. Raw Fluorescence Intensity and P Values

Figure	Condition	Total Cells	YFP- Cells	%	YFP+ Cells	%	P Value
4.2c	Mixed 6 hours	25445	25331	99.55	114	0.45	0.3959
		20000	19910	99.55	90	0.45	
		20000	19912	99.56	88	0.44	
	Filamentous 6 hours	21090	20986	99.51	104	0.49	
		20000	19900	99.5	100	0.10	
		20000	19886	99.43	114	0.57	
	Rod 6 hours	17268	17170	99.43	98	0.57	
		20000	19917	99.59	83	0.42	
		20000	19932	99.66	68	0.34	
	Mixed 24 hours	20000	19556	97.78	444	2.22	0.7492
		20000	19502	97.51	498	2.49	
		20000	19573	97.87	427	2.14	
	Filamentous 24 hours	20000	19559	97.80	441	2.21	
		20000	19534	97.67	466	2.33	
		20000	19384	96.92	616	3.08	
	Rod 24 hours	20000	19556	97.78	444	2.22	
		20000	19525	97.63	475	2.38	
		20000	19362	96.81	638	3.19	
5.7b	MLS989	20000	19992	99.96	8	0.04	0.0226
		20000	19991	99.96	9	0.05	
		20000	19990	99.95	10	0.05	
	MLS989 Δ*recA*	20000	19965	99.83	35	0.18	
		20000	19939	99.70	61	0.31	
		20000	19969	99.85	31	0.16	
5.7c	MLS989	20000	19876	99.38	124	0.62	0.0498
		20000	19802	99.01	198	0.99	
		20000	19811	99.06	189	0.95	
	MLS989 Δ*recA*	20000	19781	98.91	219	1.10	
		20000	19673	98.37	327	1.64	
		84750	83287	98.27	1463	1.73	

Table S3. Raw Cell Sorting Data

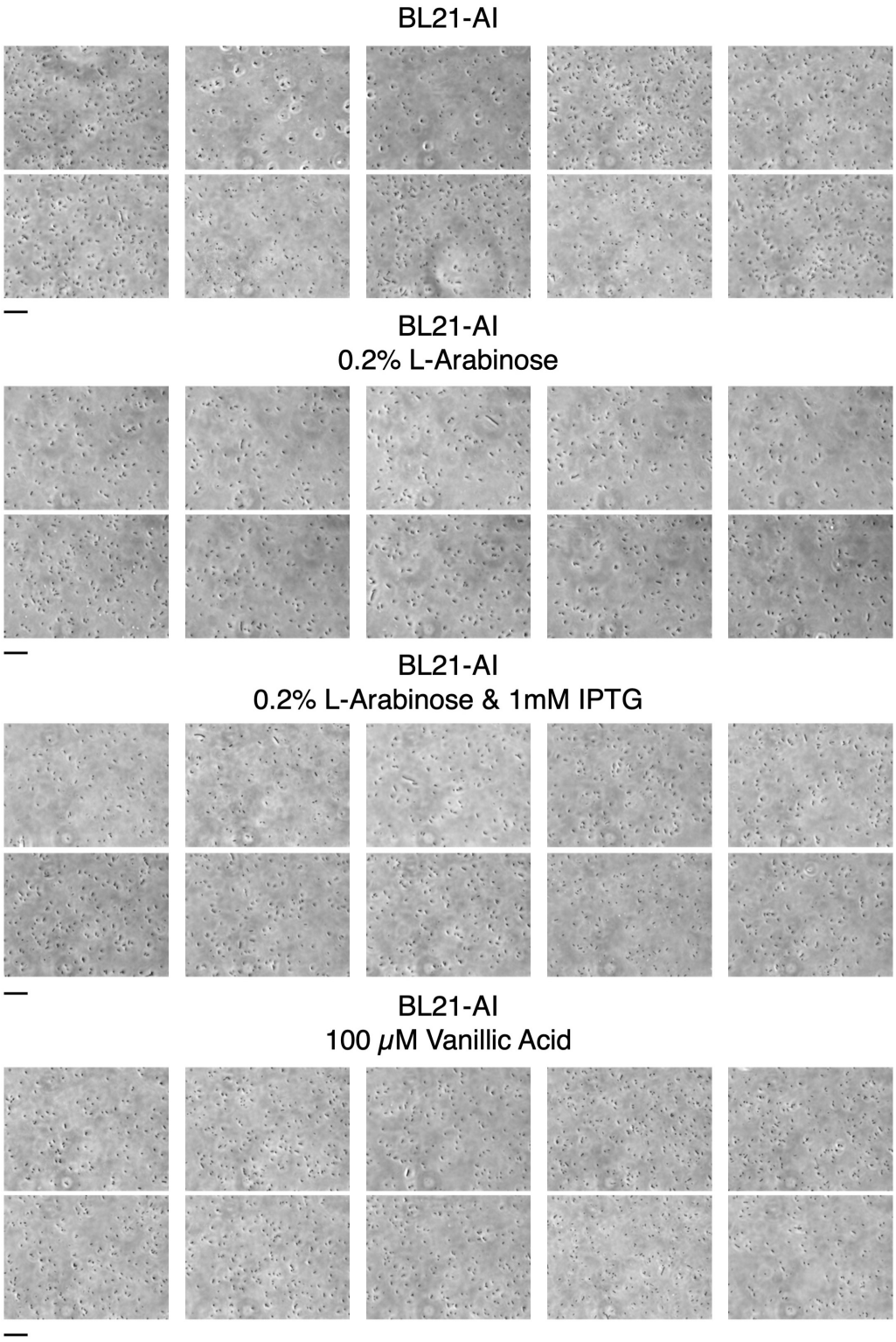


Figure S1. Control Images of BL21-AI
BL21-AI grown in the absence of inducer, in 0.2% L-arabinose, in 0.2% L-arabinose & 1 mM IPTG and in 100 μ M Vanillic Acid. 10 images included for each condition. The scale bar is 2 μm.

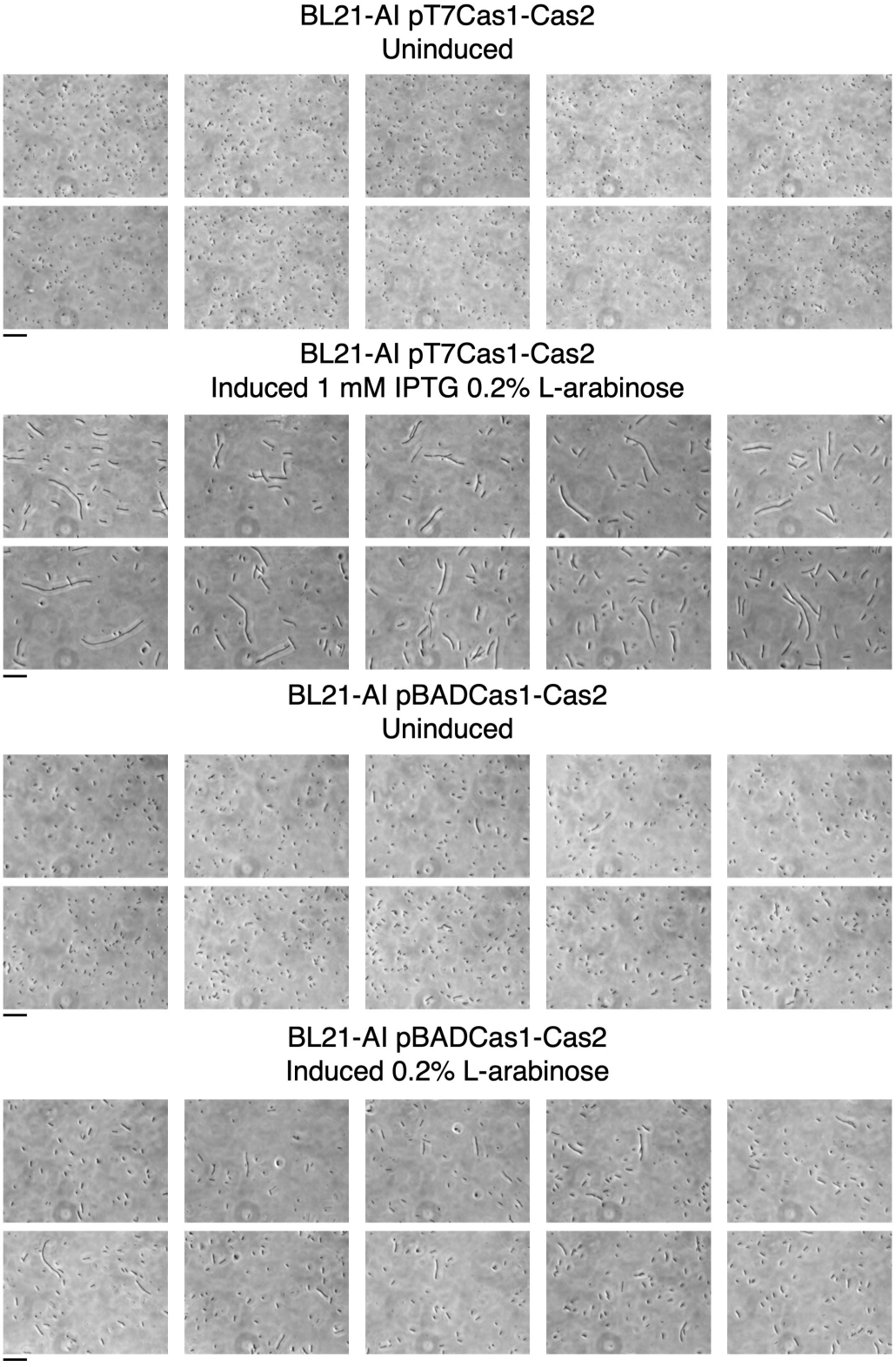


Figure S2. Overexpression of Cas1-Cas2 from either a T7 or pBAD plasmid induces filamentation

BL21-AI pT7Cas1-Cas2 grown in the absence of inducer and induced at 0.2% L-arabinose & 1 mM IPTG. BL21-AI pBADCas1-Cas2 grown in the absence of inducer and induced at 0.2% L-arabinose. 10 images included for each condition. The scale bar is 2 μm.

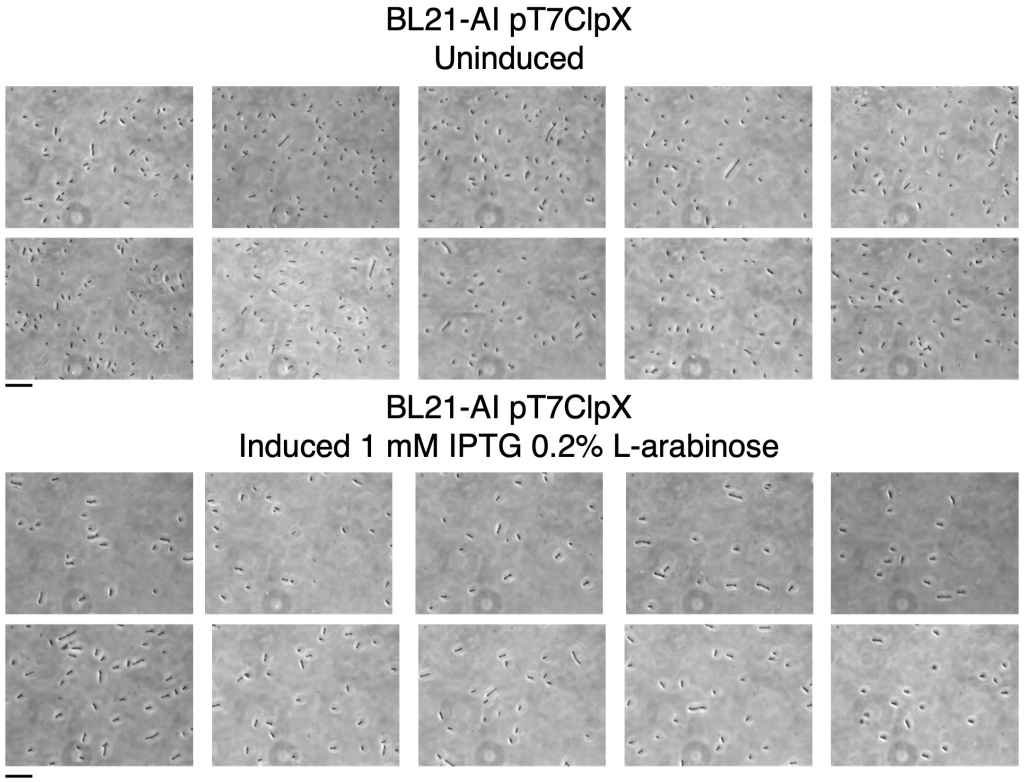


Figure S3. ClpX overexpression from a T7 promoter does not induce filamentation BL21-AI pT7ClpX grown in the absence and presence of 0.2% L-arabinose & 1 mM IPTG. 10 images included for each condition. The scale bar is 2 μm.

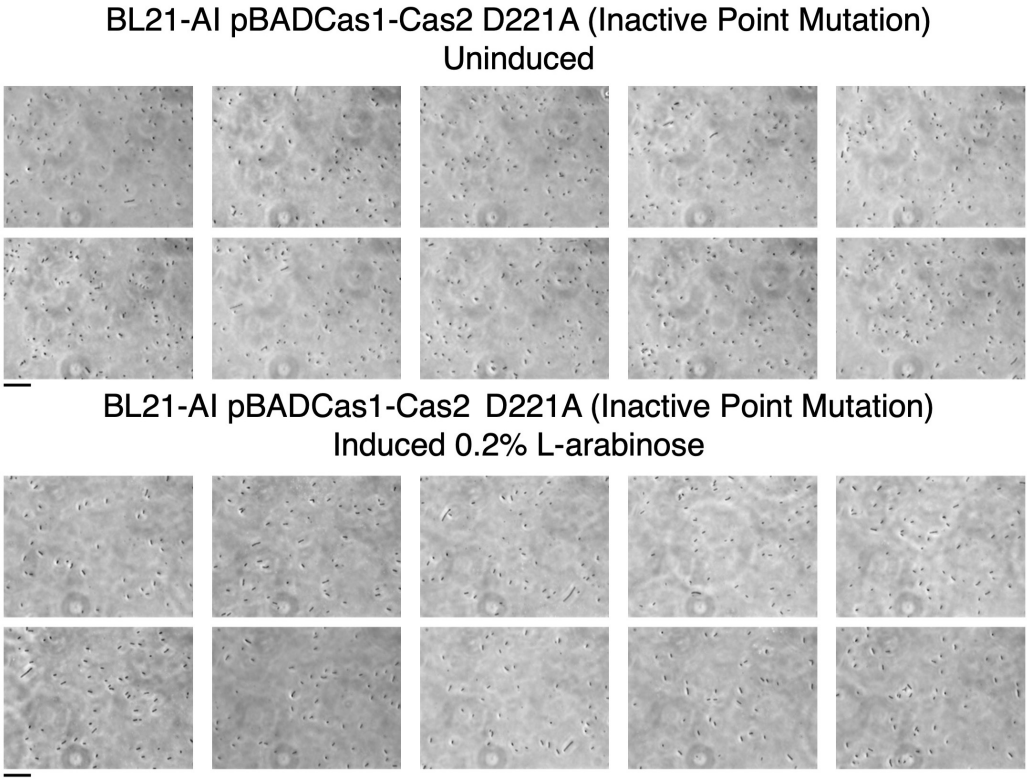


Figure S4. Overexpression of dCas1-Cas2 does not induce filamentation BL21-AI pBADdCas1-Cas2 (D221A) grown in the absence and presence of 0.2% L-arabinose. 10 images included for each condition. The scale bar is 2 μm.

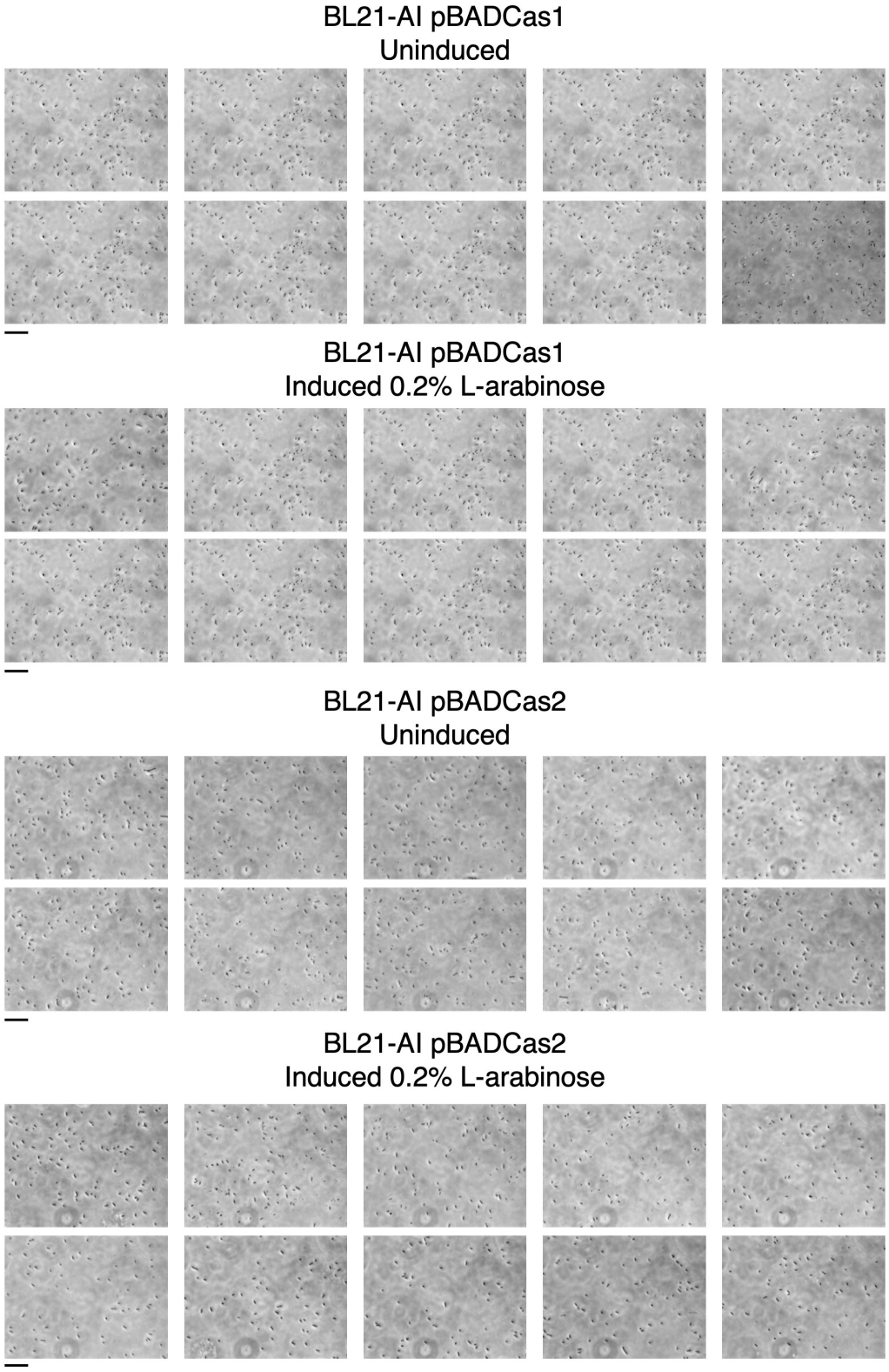


Figure S5. Overexpression of Cas1 or Cas1 does not induce filamentation BL21-AI pBADCas1 and BL21-AI pBADCas2 grown in the absence of inducer and induced at 0.2% L-arabinose. 10 images included for each condition. The scale bar is 2 μm.

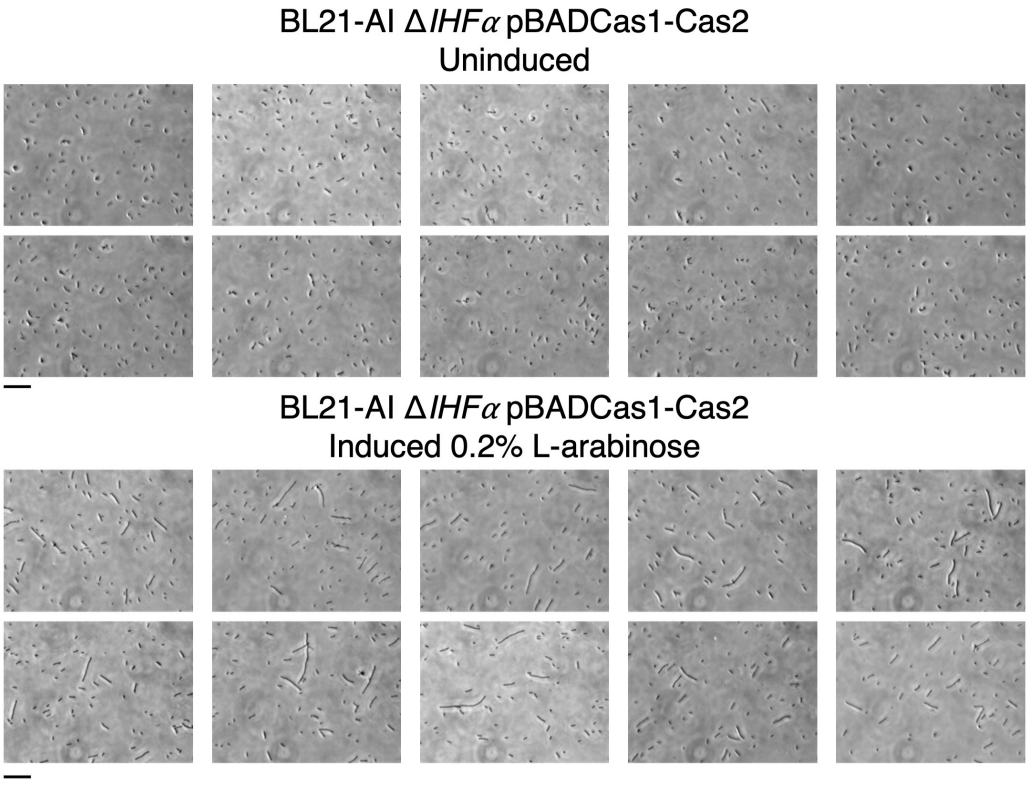


Figure S6. Cas1-Cas2 overexpression induces filamentation in BL21-AI *IHF*α BL21-AI Δ*IHF*α pBADCas1-Cas2 grown in the absence of inducer and induced at 0.2% L-arabinose. 10 images included for each condition. The scale bar is 2 μm.

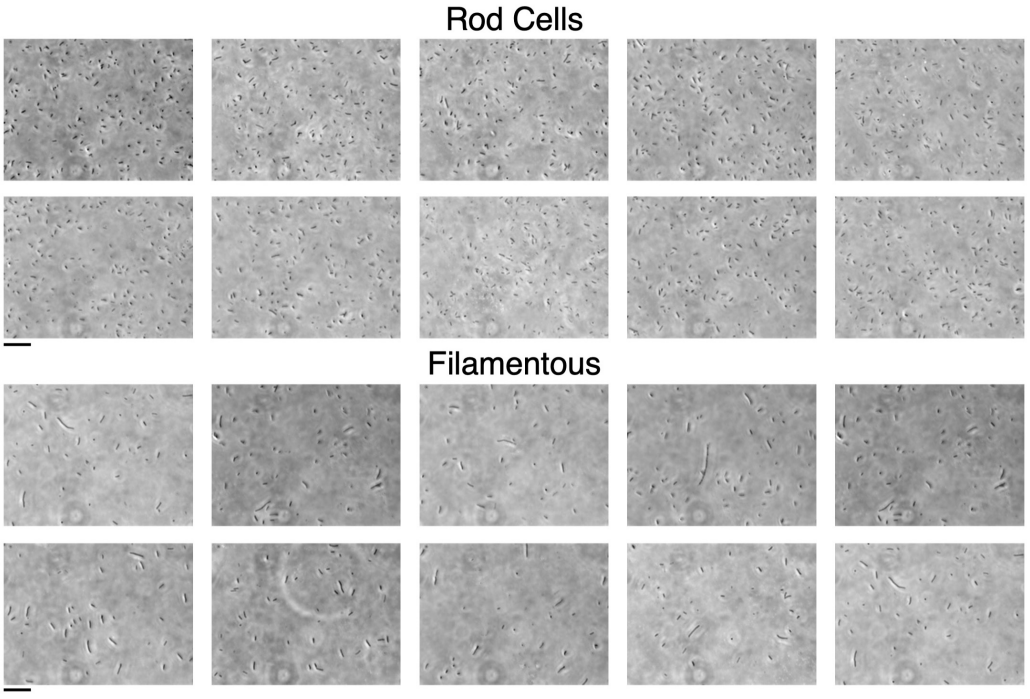


Figure S7. Passing cells through a 1.2 μm filter separates filamentous from rod-shaped cells
BL21-AI pT7Cas1-Cas2 grown in 0.2% L-arabinose & 1 mM IPTG. Passed through a 1.2 μm filter to separate filamentous and rod-shaped cells. The scale bar is 2 μm.

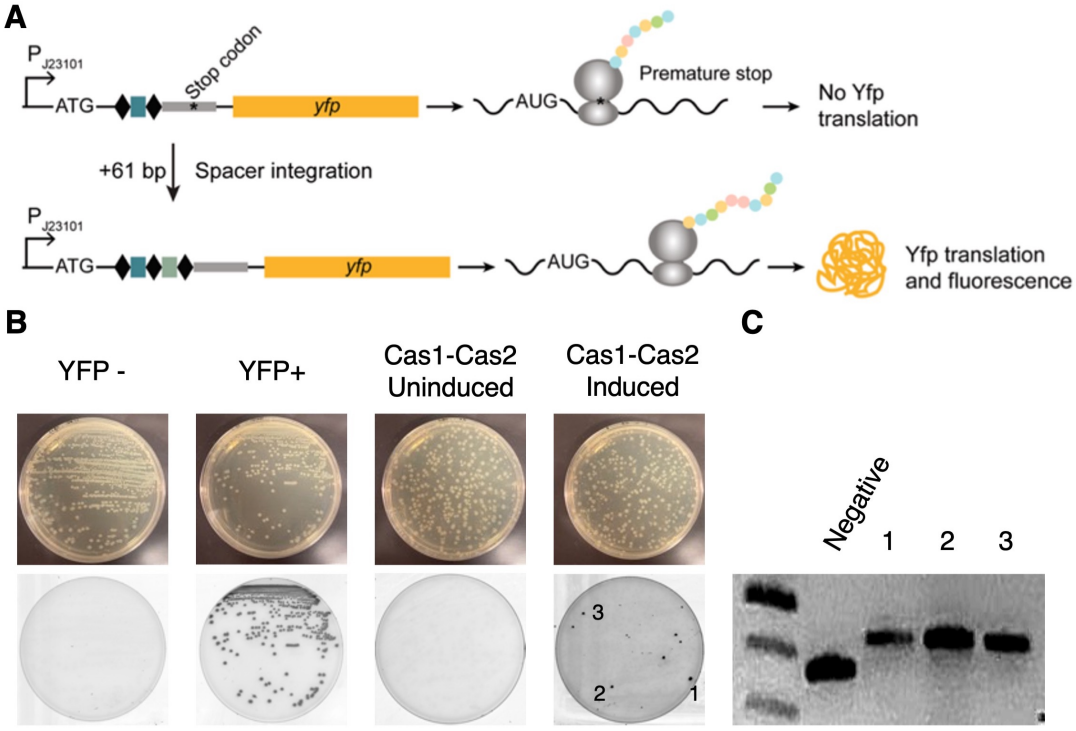


Figure S8. Verification of YFP Spacer Acquisition Reporter Strain

(A) Schematic of fluorescent CRISPR adaptation reporter. An unexpanded CRISPR array, consisting of two repeats (diamonds), one spacer (rectangle) and partial leader (grey) with in-frame stop codon, is inserted downstream of a constitutive promoter and RBS (top). The reporter *yfp* gene is in the +2 frame of the ATG and not translated with unexpanded array (top). Spacer acquisition adds 61 bp to the array (bottom), moving *yfp* into frame and stop codons out of frame, resulting in expression and fluorescence. Taken with permission from Amlinger et al., 2017, Figure 1 [236].
(B) Detection of fluorescent colonies after spacer acquisition. MLS989 used as negative control and MLS990 used as positive control. A liquid culture of MLS989 pBAD Cas1-Cas2 grown for 24 hours in the absence and presence of 0.2% L-arabinose to induce Cas1-Cas2 expression. Culture diluted to give ~200 colonies per plate. Grown overnight and imaged with Cy3 setting of Amersham Typhoon. Plate photos and YFP+ images shown.
(C) PCR Verification of YFP -/+ colonies. MLS989 used as negative control. Fluorescent colonies 1-3 from (B) used.

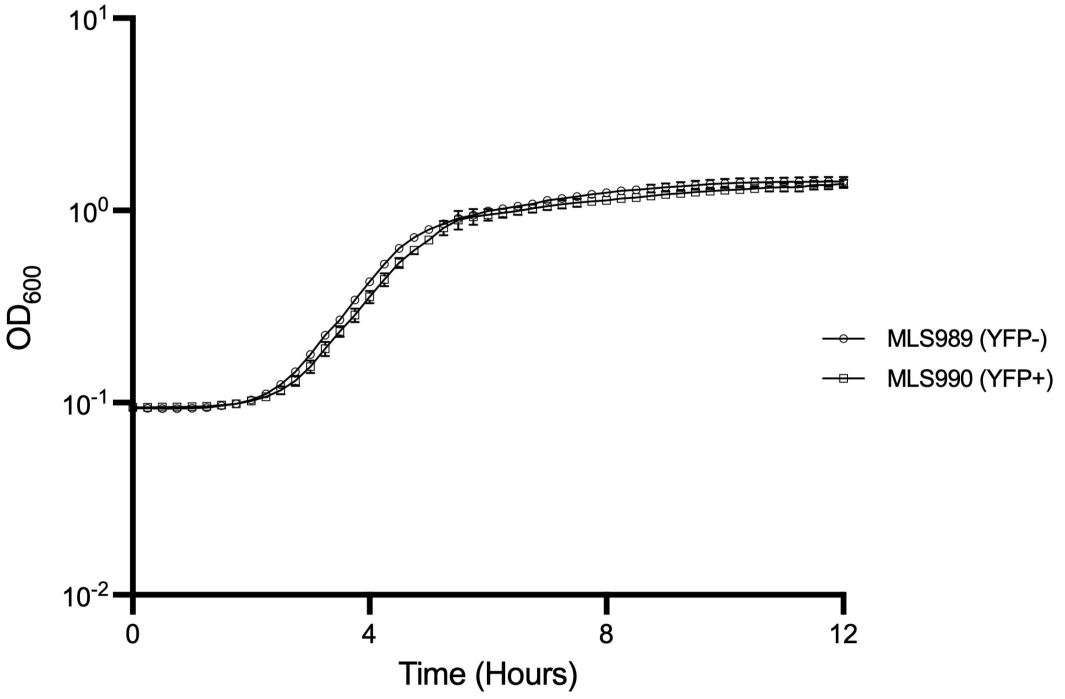


Figure S9. YFP- cells grow faster than YFP+ cells

Overnight cultures of YFP- (MLS989) and YFP+ (MLS990) cells washed in PBS three times. The OD_{600} was measured and normalised to 1.0. Cultures were diluted 1:1000 in LB broth and incubated overnight in a 96-well plate shaking at 37 °C. The OD_{600} was measured every 15 minutes using the Biotek Epoch 2 microplate spectrophotometer. This was repeated in triplicate. The mean is plotted and the error bars are SEM. MLS989 (YFP-) is represented by open circles. MLS990 (YFP+) is represented by open squares.

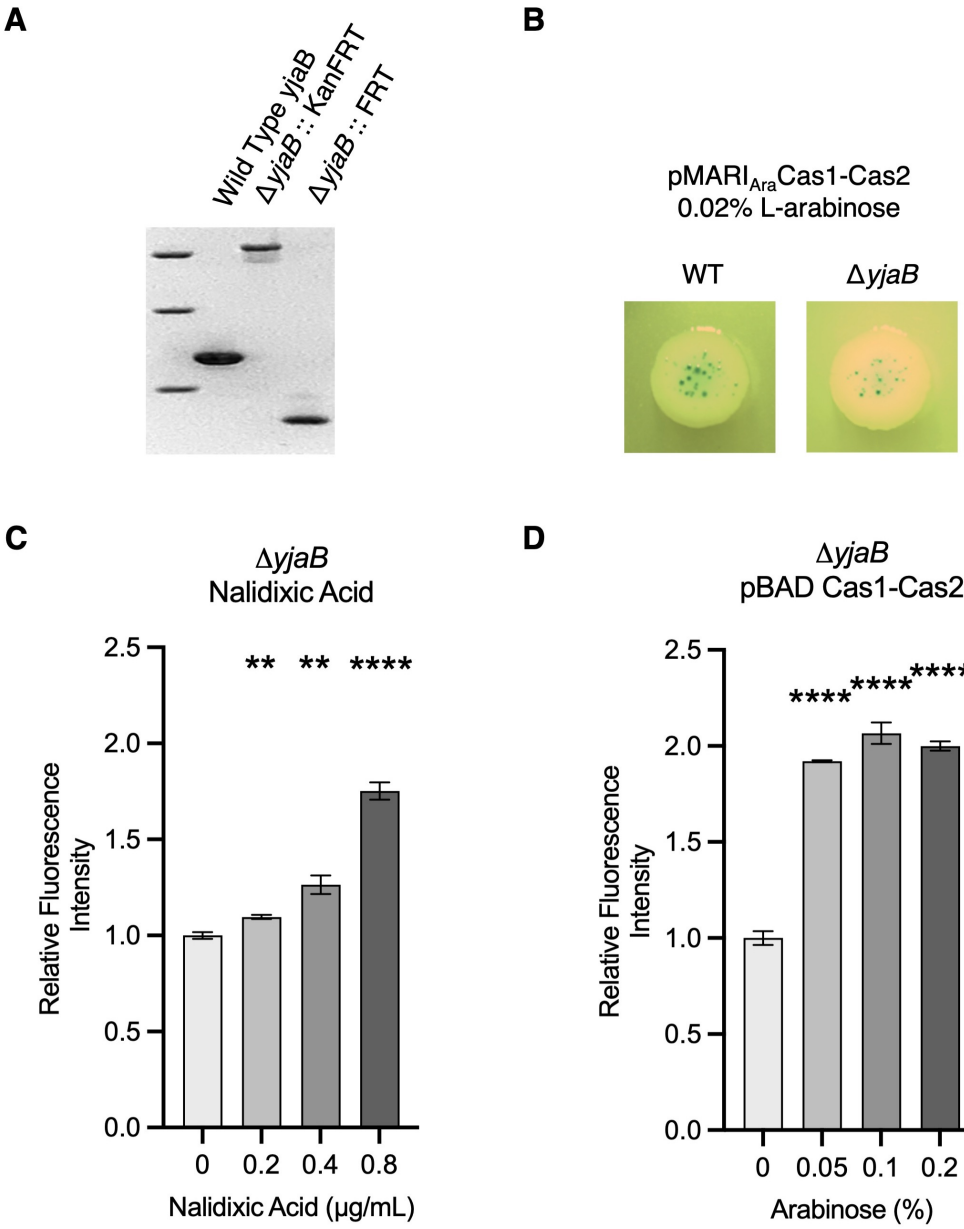


Figure S10. Deletion of *yjaB* does not alter the rate of papillation or induction of the SOS Response

(A) PCR Verification of deletion of *yjaB* from JB028
(B) Papillation assays were performed in *E. coli* JB028 and Δ*yjaB*. $pMARI_{Ara}$ Cas1-Cas2 expression was induced by 0.02% L-arabinose. Representative day 5 colonies are shown.
(C) *E. coli* JB028 Δ*yjaB* grown in the presence of a gradient of 0 - 0.8 μg/mL Nalidixic Acid.
(D) Cas1-Cas2 overexpressed in *E. coli* JB028 Δ*yjaB* from pBAD Cas1-Cas2 across a gradient of 0 - 0.2 % L-arabinose.
SOS reporter plasmid with GFP downstream of SulA promoter used to measure induction of the SOS response. Repeated in triplicate. The mean is plotted and the error bars are SEM. Intensity compared to no treatment control. P value: ns = non-significant, * < 0.05, ** < 0.01, *** < 0.001, **** < 0.0001. Raw intensity values and P values listed in S2.

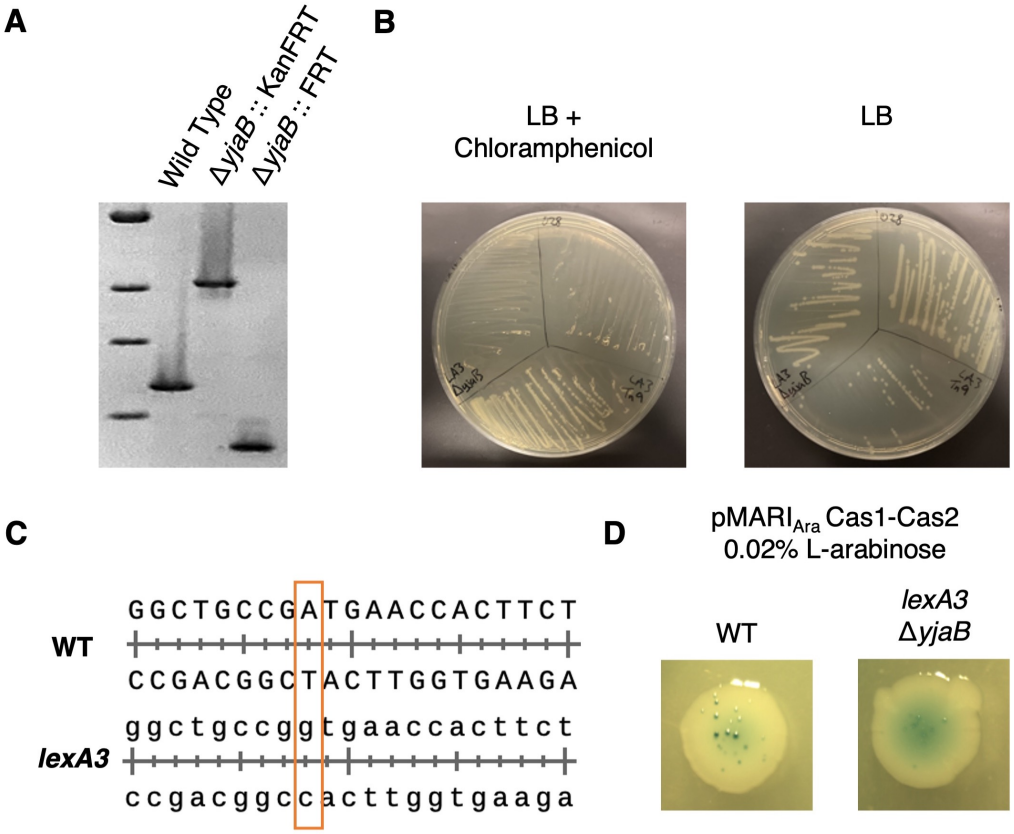


Figure S11. Verification of *yjaB* deletion from *lexA3* to remove the *Tn9* marker

(A) PCR Verification of deletion of *yjaB* from JB028 *lexA3*.
(B) Streaks to show chloramphenicol sensitivity. JB028 used as negative control. JB028 *lexA3 malB::Tn9* used as positive control.
(C) Sequence data to confirm the *lexA3* mutation.
(D) Papillation assays were performed in JB028 and *lexA3* Δ*yjaB*. pMARI$_{Ara}$ Cas1-Cas2 expression was induced by 0.02% L-arabinose. Representative day 5 colonies are shown. JB028 *lexA3* Δ*yjaB* has a decreased rate of papillation compared to wild type JB028.

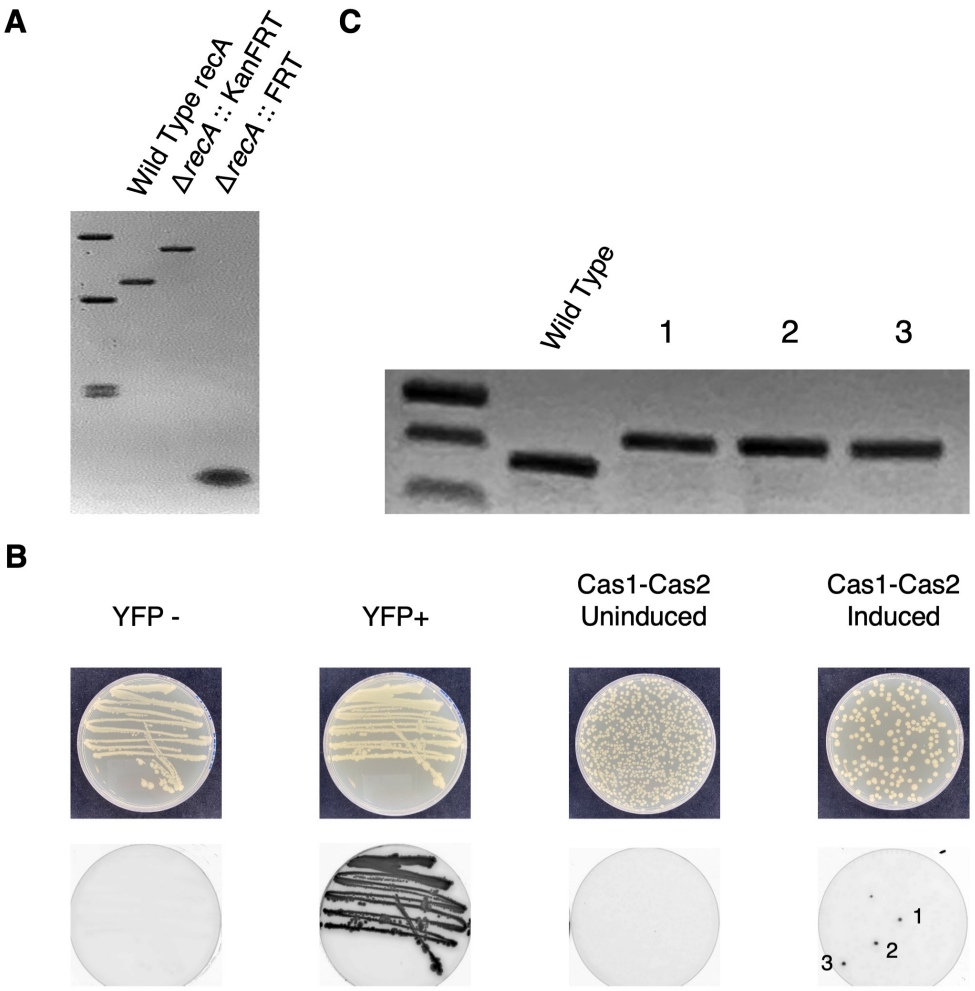


Figure S12. Verification of spacer acquisition in MLS989 Δ*recA*

(A) PCR verification of Δ*recA* deletion from MLS989
(B) Detection of fluorescent colonies after spacer acquisition. MLS989 used as negative control and MLS990 used as positive control. A liquid culture of MLS989 Δ*recA* pBAD Cas1-Cas2 grown for 24 hours in the absence and presence of 0.2% L-arabinose to induce Cas1-Cas2 expression. Culture diluted to give ~200 colonies per plate. Grown overnight and imaged with Cy3 setting of Amersham Typhoon. Plate photos and YFP+ images shown.
(C) PCR Verification of YFP -/+ colonies. MLS989 used as negative control. Fluorescent colonies 1-3 from (B) used.

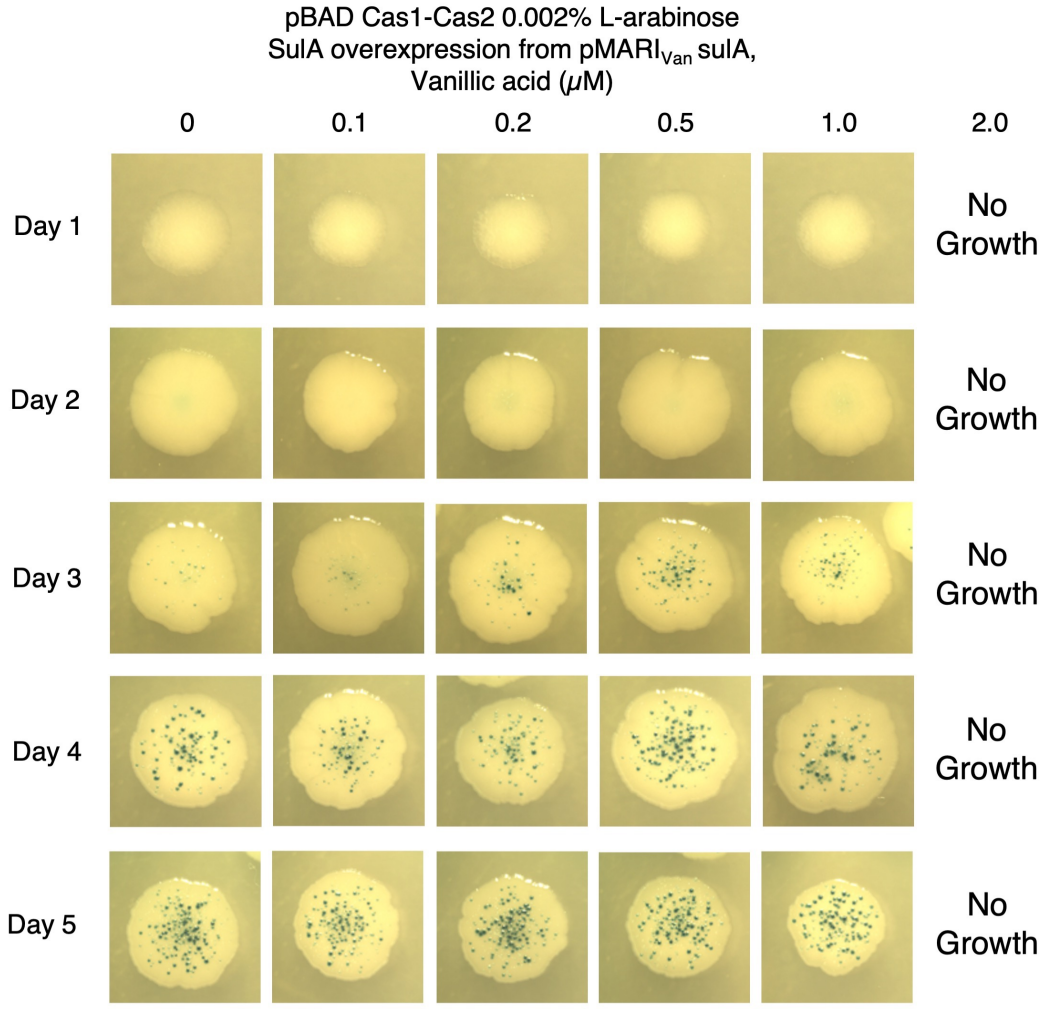


Figure S13. Overexpression of *sulA* increases the rate of papillation in JB028

Papillation assays were performed while overexpressing *sulA* in *E. coli* JB028. pBAD Cas1-Cas2 expression was induced by 0.002% L-arabinose. pMARI$_{Van}$ sulA expression was induced across 0 - 2.0 μM vanillic acid. Daily representative colonies are shown for all conditions.

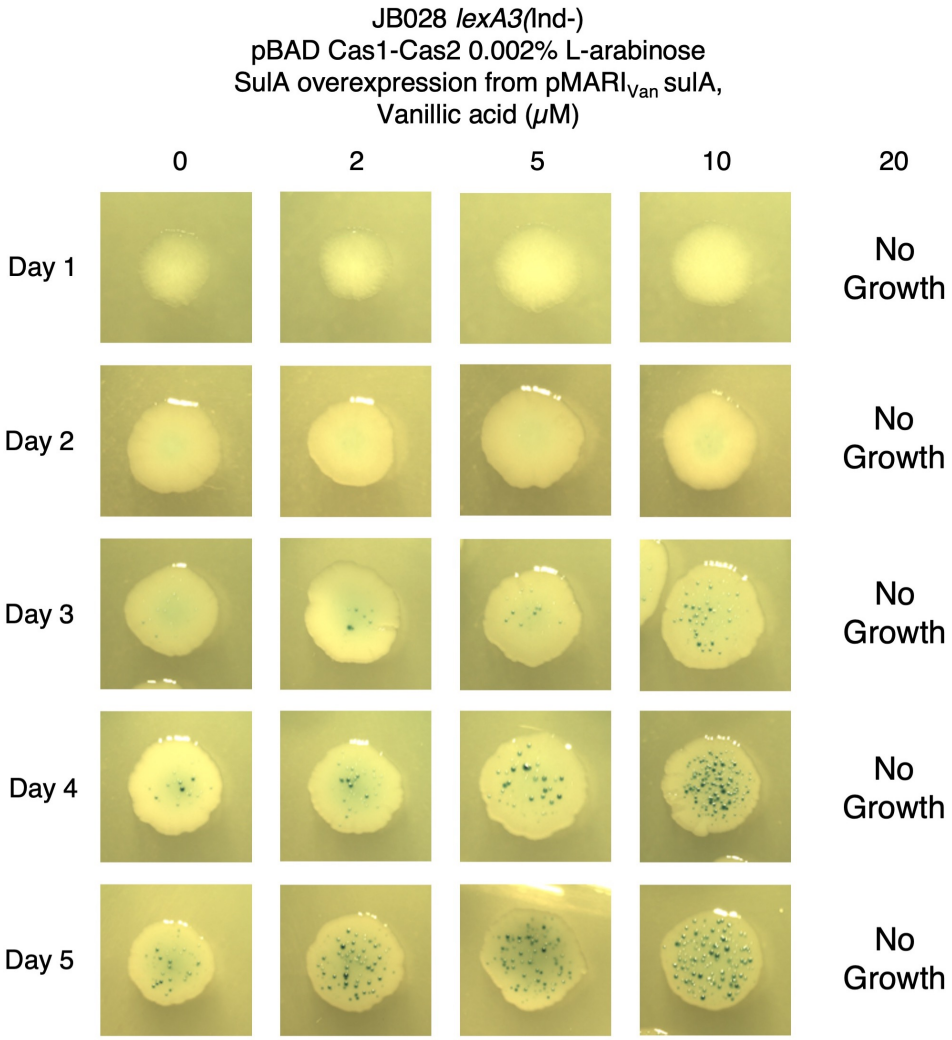


Figure S14. Overexpression of *sulA* increases the rate of papillation in JB028 *lexA3*

Papillation assays were performed in *E. coli* JB028 *lexA3* while overexpressing *sulA*. pBAD Cas1-Cas2 expression was induced by 0.002% L-arabinose. pMARI$_{Van}$ sulA expression was induced across 0 - 20 μM vanillic acid. Daily representative colonies are shown for all conditions.

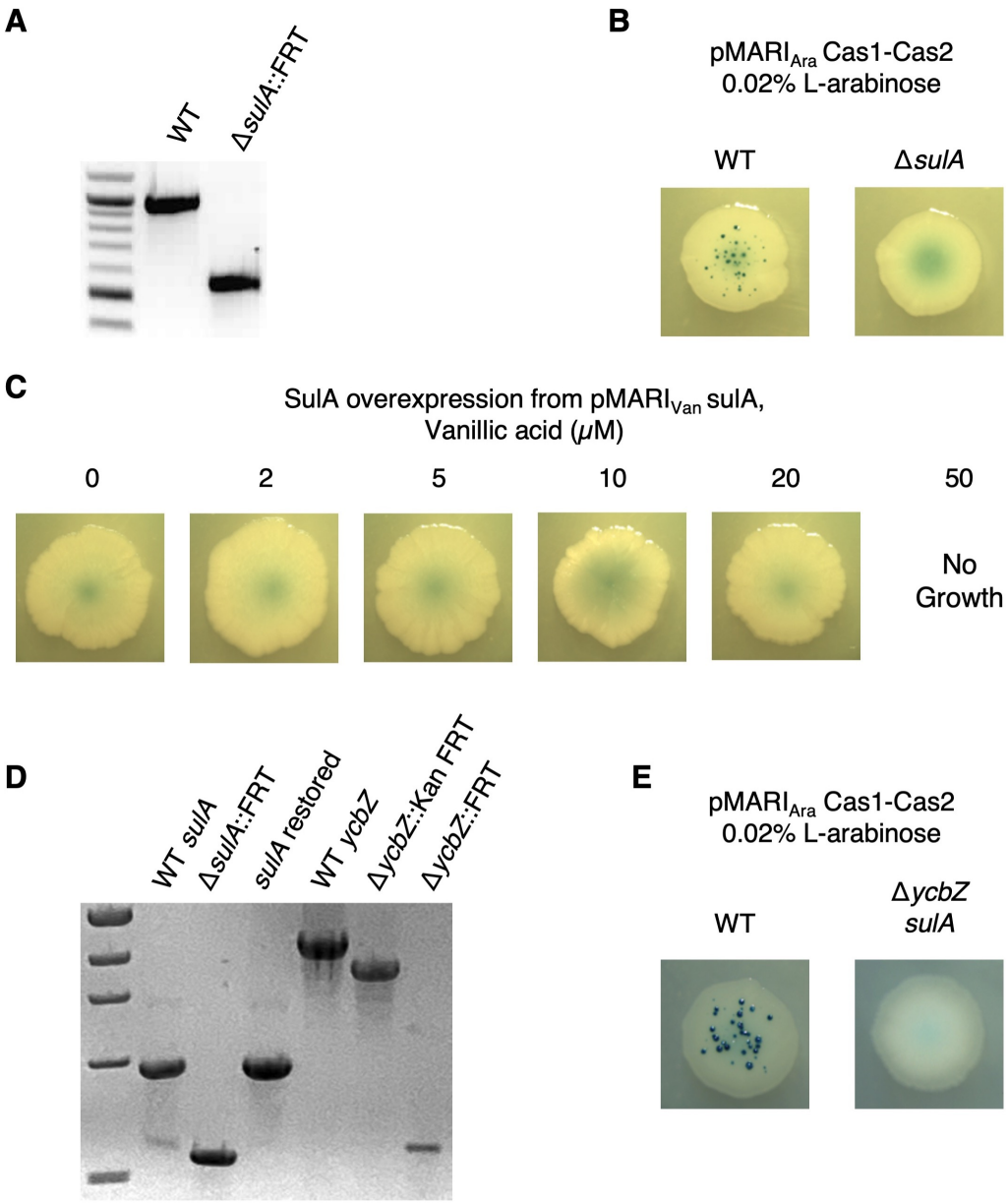


Figure S15. Deletion of *sulA* by P1 transduction from the Keio collection abolishes papillation but complementation does not restore adaptation

(A) PCR verification of the *sulA* deletion from JB028.
(B) Papillation assays were performed in JB028 and Δ*sulA*. pMARI$_{Ara}$ Cas1-Cas2 expression was induced by 0.02% L-arabinose. Representative day 5 colonies are shown.
(C) Papillation assays performed while overexpressing *sulA* in JB028 Δ*sulA*. pBAD Cas1-Cas2 expression was induced by 0.002% L-arabinose. pMARI$_{Van}$sulA expression was induced by 0 - 50 μM vanillic acid. Representative colony images from day 5 are shown. (D) PCR verification of *ycbZ* deletion and restoration of *sulA* by P1 transduction.
(E) Papillation assays were performed in JB028 and ΔycbZ. pMARI$_{ARA}$ Cas1-Cas2 expression was induced by 0.02% L-arabinose. Representative day 5 colonies are shown.

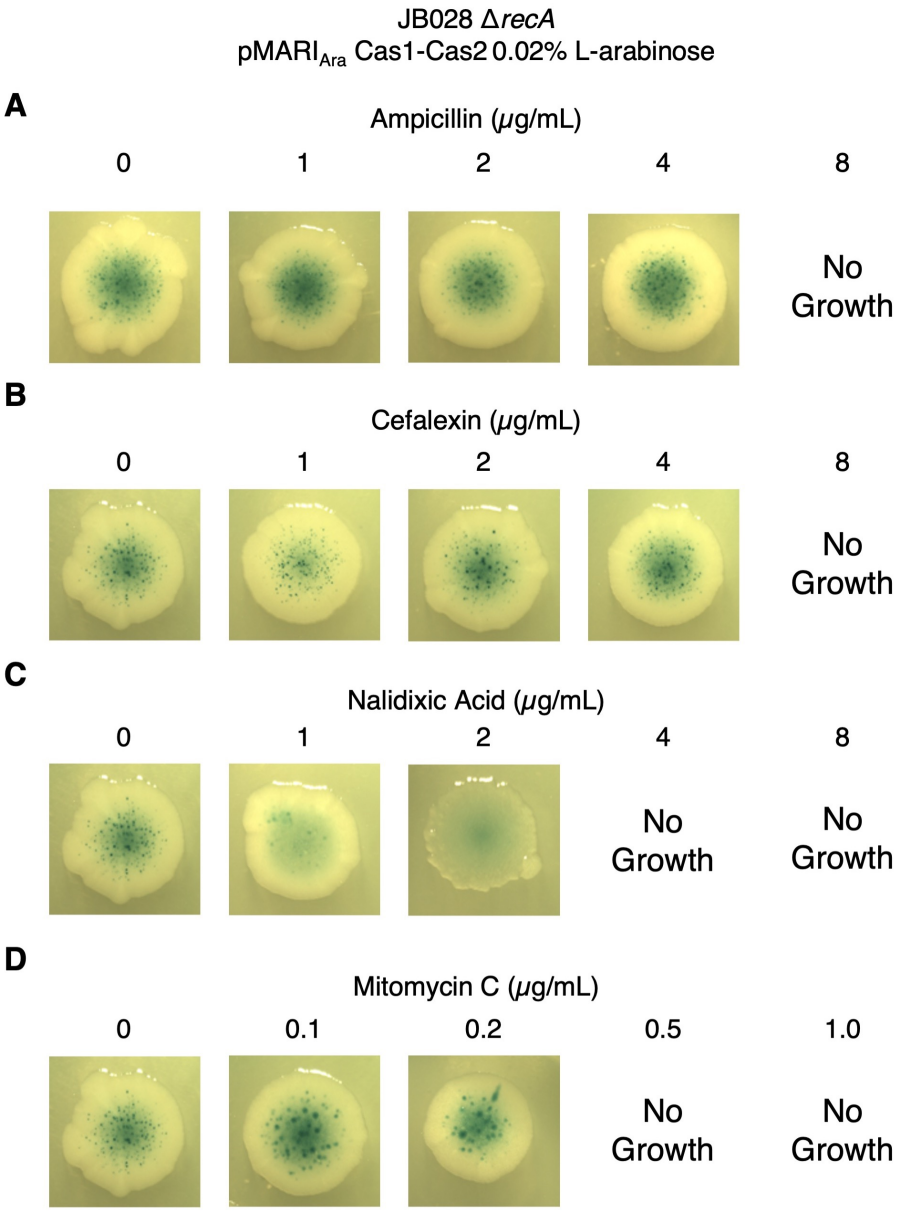


Figure S16. Papillation assays performed in the presence of sub-inhibitory concentrations of antibiotics in the Δ*recA* background decreases the rate of papillation

Papillation assays were performed in JB028 Δ*recA* in sub-inhibitory concentrations of antibiotics. Ampicillin (A), Cefalexin (B) and Nalidixic Acid (C) were used across a gradient of 0 – 8 µg/mL. Mitomycin C (D) was used across a gradient of 0 – 1.0 µg/mL. pMARI$_{ARA}$ Cas1-Cas2 expression was induced by 0.02% L-arabinose. Representative day 5 colonies are shown.

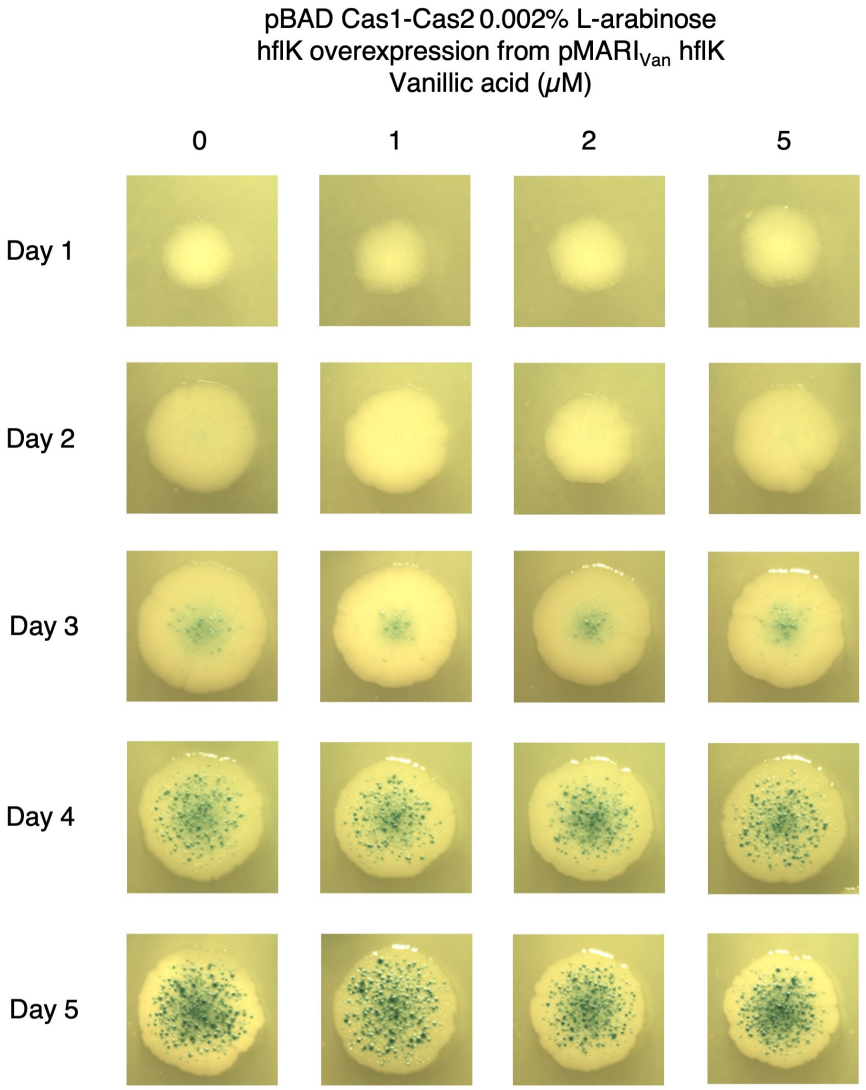


Figure S17. Overexpression of *hflK* does not increase the rate of papillation

Papillation Assays performed while overexpressing *hflK* in JB028. pBAD Cas1-Cas2 expression was induced by 0.002% L-arabinose. pMARI$_{Van}$hflK expression was induced by 0 – 5 µM vanillic acid. Representative daily colonies are shown for each condition tested.

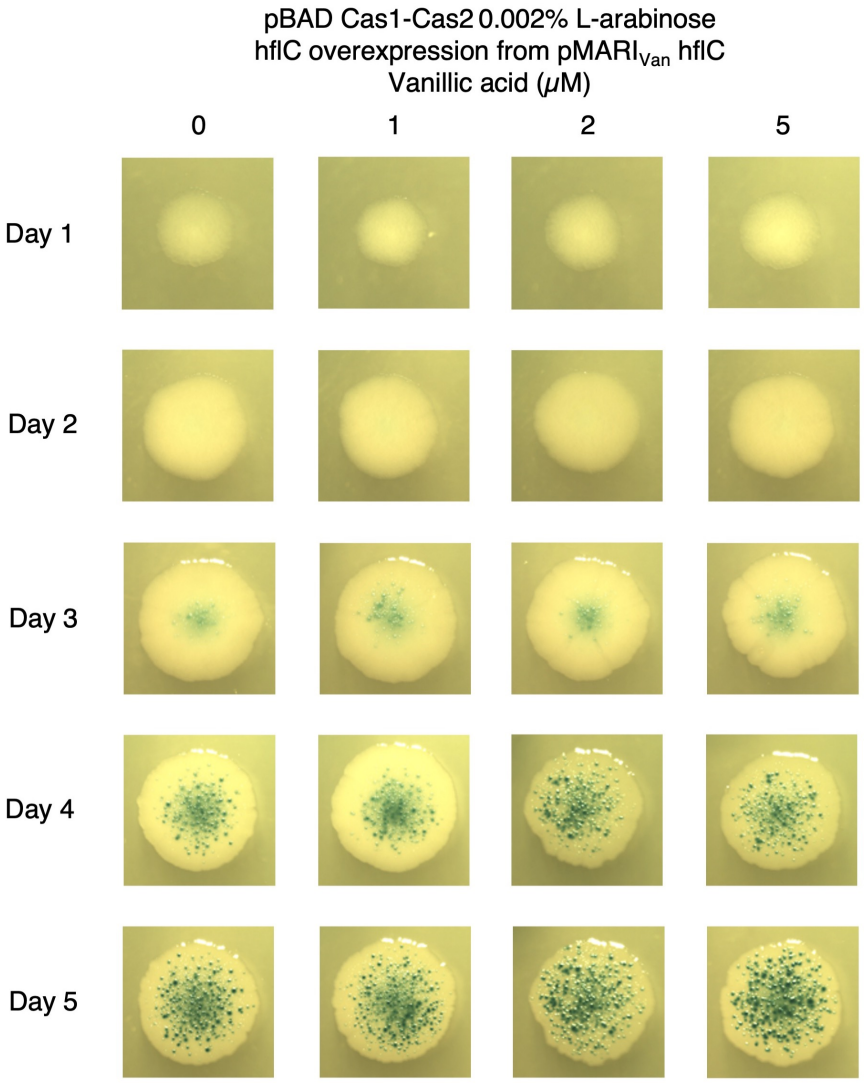


Figure S18. Overexpression of *hflC* does not increase the rate of papillation

Papillation Assays performed while overexpressing *hflC* in JB028. pBAD Cas1-Cas2 expression was induced by 0.002% L-arabinose. pMARI$_{Van}$hflC expression was induced by 0 – 5 µM vanillic acid. Representative daily colonies are shown for each condition tested.

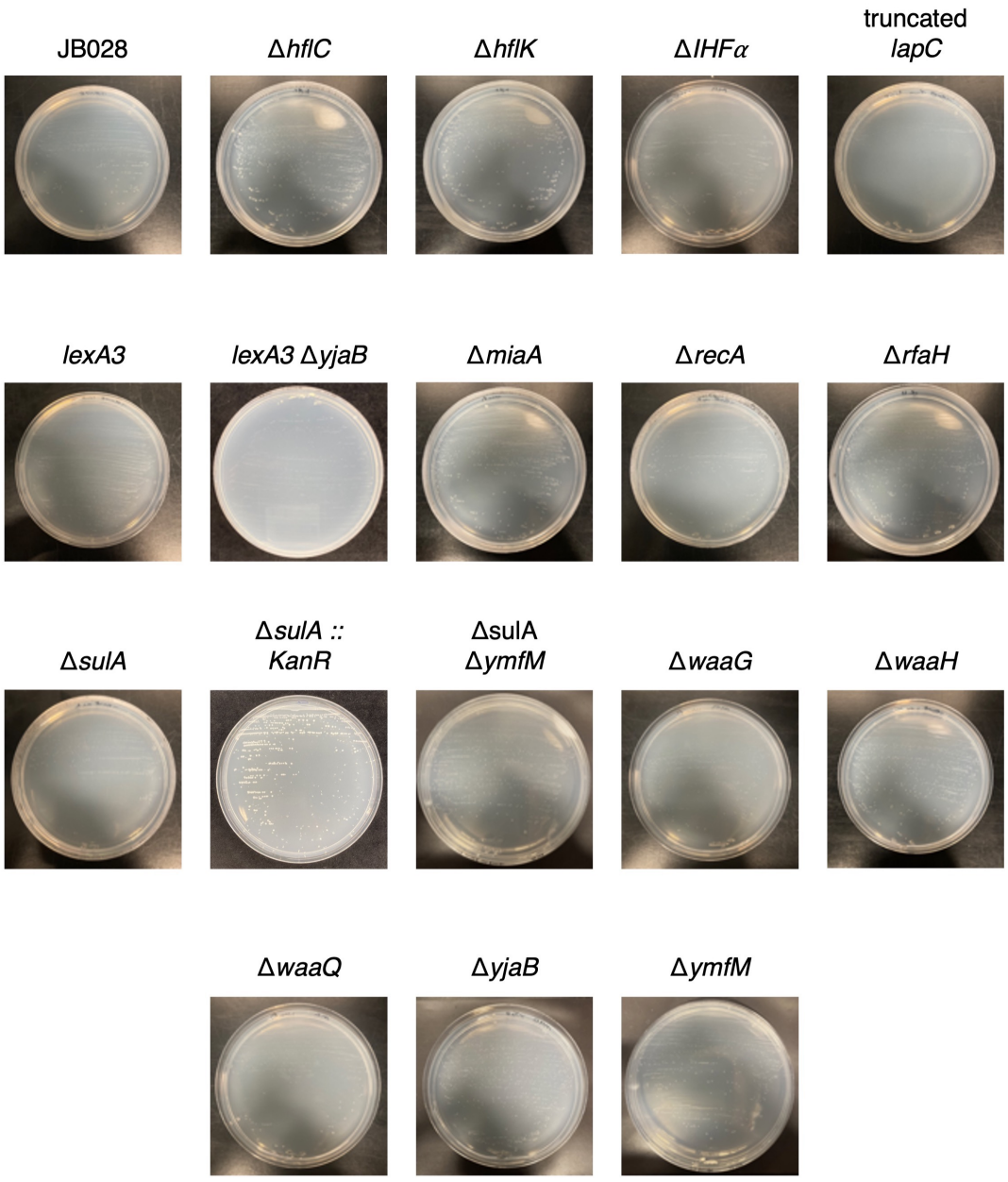


Figure S19. All genetic deletion strains grown on M9 minimal media agar

JB028 and deletion mutants grown on M9 minimal media agar supplemented with 0.2 % glucose. An overnight culture was grown in LB broth. This was washed in sterile PBS three times and looped onto the agar plate. Incubated at 37 °C for 3 days. Whole plate images taken. All mutant strains grew.

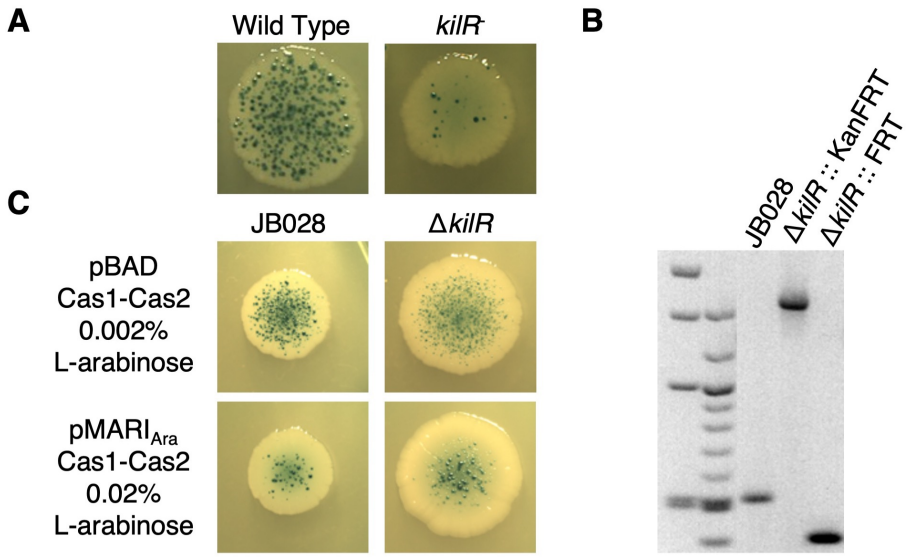


Figure S20. Deletion of *kilR* does not alter the rate of papillation
(A) Tn5 insertion into *kilR* in a random mutagenesis screen produces a colony with few papillae. (B) PCR Verification of deletion of *kilR* from JB028. (C) Papillation assays performed in JB028 and Δ*kilR*. pBAD Cas1-Cas2 expression was induced by 0.002% L-arabinose and $pMARI_{Ara}$ Cas1-Cas2 expression was induced by 0.02% L-arabinose. Representative colonies from day 5 shown.

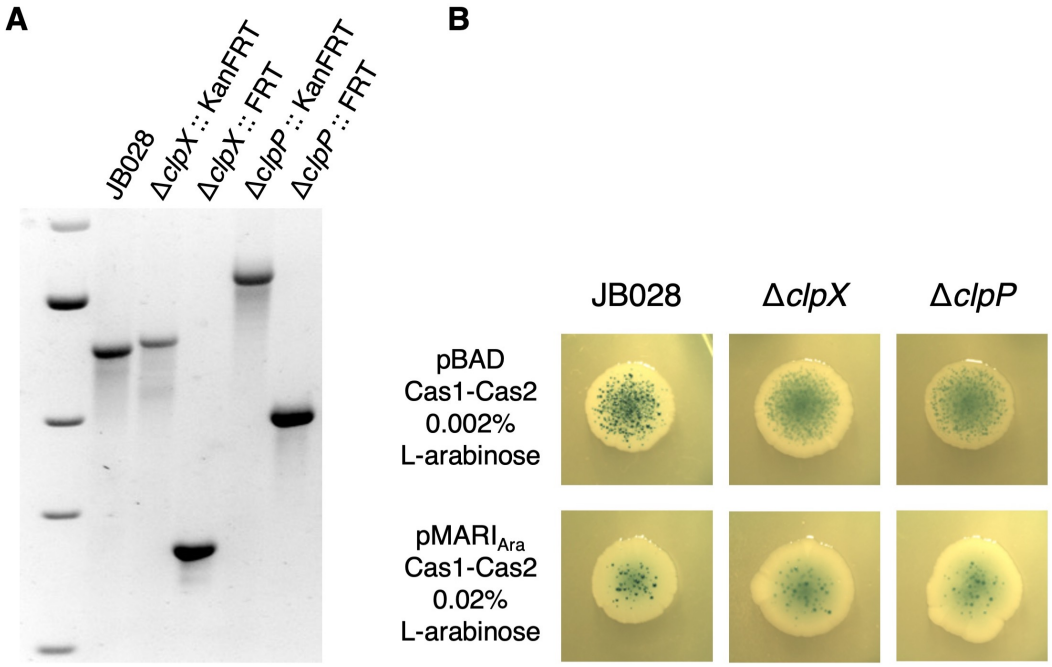


Figure S21. Deletion of *clpX* or *clpP* does not alter the rate of papillation
(A) PCR Verification of deletion of *clpX* and *clpP* from JB028. (B) Papillation assays performed in JB028, Δ*clpX* and Δ*clpP*. pBAD Cas1-Cas2 expression was induced by 0.002% L-arabinose and $pMARI_{Ara}$ Cas1-Cas2 expression was induced by 0.02% L-arabinose. Representative colonies from day 5 shown.

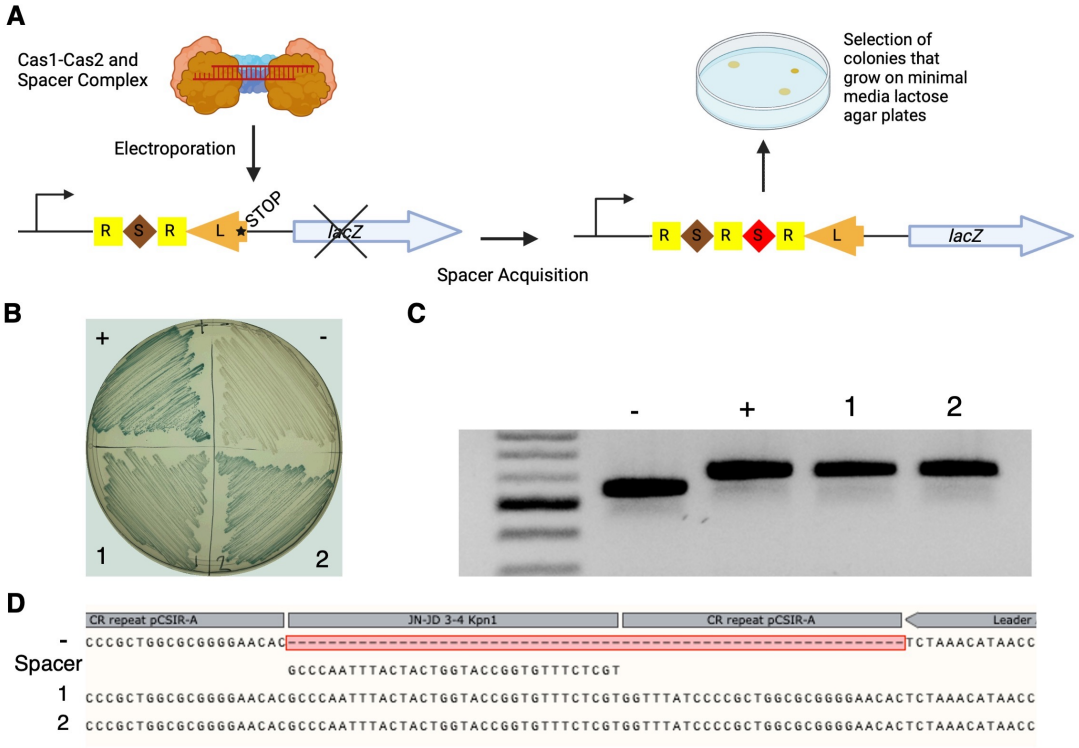


Figure S22. Electroporation of spacer DNA and Cas1-Cas2 complex results in spacer acquisition in the CRISPR array

(A) Selection of spacer acquisition events. An unexpanded CRISPR array, consists of two repeats (yellow), one spacer (brown) and leader (orange) with an in-frame stop codon. Cas1-Cas2 and spacer DNA was electroporated into cells. Spacer acquisition adds 61 bp to the array (bottom), moving *lacZ* into frame and the stop codon out of frame resulting in *lacZ* expression. Plating onto minimal media agar plates supplemented with lactose selects for cells that have acquired the ability to metabolise lactose as a carbon source.
(B) Growth on LB agar supplemented with X-Gal for a negative and positive control and replicates 1 & 2. White colonies do not express *lacZ*, whereas blue colonies do.
(C) PCR amplification of the CRISPR array. JB028 used as the negative control & pRC1644 used as a positive control template. Replicates 1 & 2 are blue colonies from (B).
(D) Sanger sequencing of the two replicates across the CRISPR array. Aligned against the unexpanded locus and the electroporated spacer.

Acknowledgements

I would like to thank my supervisor Professor Ronald Chalmers for all the help and support throughout my PhD. I would like to thank Dr. Jack Braithwaite BTEC NVQ for teaching me the ropes when I first started and all the help along the way, and (future Dr.) Chris Cannon BA for all our discussions about our research.

I would like to thank my parents for all their support along the way. Not just during the PhD, but throughout the 26 years up to this point. None of this work would have been possible without this. Also, thanks to George for keeping them in check when I am not home.

A special thanks has to go to Grandma for everything. Especially for buying me the coffee machines that helped me through work and writing. I hope that I have made you and would have made Grandad proud. I also need to thank Grandpa and Di for providing a different perspective when it was needed.

I need to thank all my friends for their help and support along the way. For listening with sympathy when experiments failed and giving me a boost when required.

I also gratefully acknowledge the financial support of the University of Nottingham as part of the Wellcome Trust Doctoral Training Program in Antimicrobials and Antimicrobial Resistance.

(And to Noel and Liam for forming the best band in history and providing me the songs that got me through my experiments and the writing of this thesis).

Bibliography

1. Barrangou, R. *et al.* CRISPR provides acquired resistance against viruses in prokaryotes. *Science (New York, N.Y.)* **315,** 1709–1712 (Mar. 23, 2007).
2. Makarova, K. S., Grishin, N. V., Shabalina, S. A., Wolf, Y. I. & Koonin, E. V. A putative RNA-interference-based immune system in prokaryotes: computational analysis of the predicted enzymatic machinery, functional analogies with eukaryotic RNAi, and hypothetical mechanisms of action. *Biology Direct* **1,** 7 (Mar. 16, 2006).
3. Makarova, K. S., Wolf, Y. I., Snir, S. & Koonin, E. V. Defense Islands in Bacterial and Archaeal Genomes and Prediction of Novel Defense Systems. *Journal of Bacteriology* **193,** 6039–6056 (Nov. 2011).
4. Makarova, K. S., Wolf, Y. I. & Koonin, E. V. Comparative genomics of defense systems in archaea and bacteria. *Nucleic Acids Research* **41,** 4360–4377 (Apr. 2013).
5. Labrie, S. J., Samson, J. E. & Moineau, S. Bacteriophage resistance mechanisms. *Nature Reviews. Microbiology* **8,** 317–327 (May 2010).
6. Riede, I. & Eschbach, M. L. Evidence that TraT interacts with OmpA of Escherichia coli. *FEBS letters* **205,** 241–245 (Sept. 15, 1986).
7. Pedruzzi, I., Rosenbusch, J. P. & Locher, K. P. Inactivation in vitro of the Escherichia coli outer membrane protein FhuA by a phage T5-encoded lipoprotein. *FEMS microbiology letters* **168,** 119–125 (Nov. 1, 1998).
8. Clément, J. M., Lepouce, E., Marchal, C. & Hofnung, M. Genetic study of a membrane protein: DNA sequence alterations due to 17 lamB point mutations affecting adsorption of phage lambda. *The EMBO journal* **2,** 77–80 (1983).
9. Seed, K. D. *et al.* Evolutionary consequences of intra-patient phage predation on microbial populations. *eLife* **3,** e03497 (Aug. 26, 2014).
10. Deng, L. *et al.* Unveiling cell surface and type IV secretion proteins responsible for archaeal rudivirus entry. *Journal of Virology* **88,** 10264–10268 (Sept. 1, 2014).
11. Harvey, H. *et al.* Pseudomonas aeruginosa defends against phages through type IV pilus glycosylation. *Nature Microbiology* **3,** 47–52 (Jan. 2018).
12. Kim, M. & Ryu, S. Spontaneous and transient defence against bacteriophage by phase-variable glucosylation of O-antigen in Salmonella enterica serovar Typhimurium. *Molecular Microbiology* **86,** 411–425 (Oct. 2012).
13. Van der Woude, M. W. Re-examining the role and random nature of phase variation. *FEMS microbiology letters* **254,** 190–197 (Jan. 2006).
14. Høyland-Kroghsbo, N. M., Mærkedahl, R. B. & Svenningsen, S. L. A Quorum-Sensing-Induced Bacteriophage Defense Mechanism. *mBio* **4** (Feb. 19, 2013).
15. Tan, D., Svenningsen, S. L. & Middelboe, M. Quorum Sensing Determines the Choice of Antiphage Defense Strategy in Vibrio anguillarum. *mBio* **6.** Number: 3 (July 1, 2015).
16. Isaev, A. B., Musharova, O. S. & Severinov, K. V. Microbial Arsenal of Antiviral Defenses – Part I. *Biochemistry* **86,** 319–337 (Mar. 1, 2021).
17. Hosseinidoust, Z., Tufenkji, N. & van de Ven, T. G. M. Formation of biofilms under phage predation: considerations concerning a biofilm increase. *Biofouling* **29,** 457–468 (2013).
18. Vidakovic, L., Singh, P. K., Hartmann, R., Nadell, C. D. & Drescher, K. Dynamic biofilm architecture confers individual and collective mechanisms of viral protection. *Nature Microbiology* **3,** 26–31 (Jan. 2018).

19. Wilkinson, B. J., Peterson, P. K. & Quie, P. G. Cryptic peptidoglycan and the antiphagocytic effect of the Staphylococcus aureus capsule: model for the antiphagocytic effect of bacterial cell surface polymers. *Infection and Immunity* **23,** 502–508 (Feb. 1979).
20. Mutalik, V. K. *et al.* High-throughput mapping of the phage resistance landscape in E. coli. *PLOS Biology* **18,** e3000877 (Oct. 13, 2020).
21. Scanlan, P. D. & Buckling, A. Co-evolution with lytic phage selects for the mucoid phenotype of Pseudomonas fluorescens SBW25. *The ISME journal* **6,** 1148–1158 (June 2012).
22. Tan, D., Dahl, A. & Middelboe, M. Vibriophages Differentially Influence Biofilm Formation by Vibrio anguillarum Strains. *Applied and Environmental Microbiology* **81.** Publisher: American Society for Microbiology, 4489–4497 (July 2015).
23. Bull, J. J. *et al.* Phage-Bacterial Dynamics with Spatial Structure: Self Organization around Phage Sinks Can Promote Increased Cell Densities. *Antibiotics (Basel, Switzerland)* **7,** E8 (Jan. 29, 2018).
24. Manning, A. J. & Kuehn, M. J. Contribution of bacterial outer membrane vesicles to innate bacterial defense. *BMC microbiology* **11,** 258 (Dec. 1, 2011).
25. Reyes-Robles, T. *et al.* Vibrio cholerae Outer Membrane Vesicles Inhibit Bacteriophage Infection. *Journal of Bacteriology* **200,** e00792–17 (Aug. 1, 2018).
26. Oliveira, P. H., Touchon, M. & Rocha, E. P. C. The interplay of restriction-modification systems with mobile genetic elements and their prokaryotic hosts. *Nucleic Acids Research* **42,** 10618–10631 (2014).
27. Bertani, G. & Weigle, J. J. HOST CONTROLLED VARIATION IN BACTERIAL VIRUSES. *Journal of Bacteriology* **65,** 113–121. (2022) (Feb. 1953).
28. Pingoud, A. & Jeltsch, A. Structure and function of type II restriction endonucleases. *Nucleic Acids Research* **29,** 3705–3727 (Sept. 15, 2001).
29. Bickle, T. A. Restricting restriction. *Molecular Microbiology* **51,** 3–5 (Jan. 2004).
30. Loenen, W. A. M. Tracking EcoKI and DNA fifty years on: a golden story full of surprises. *Nucleic Acids Research* **31,** 7059–7069 (Dec. 15, 2003).
31. Tock, M. R. & Dryden, D. T. F. The biology of restriction and anti-restriction. *Current Opinion in Microbiology* **8,** 466–472 (Aug. 2005).
32. Bickle, T. A. & Krüger, D. H. Biology of DNA restriction. *Microbiological Reviews* **57,** 434–450 (June 1993).
33. Duckworth, D. H., Dunn, G. B., Pinkerton, T., Rose, K. & Walia, S. K. Colicin activity and abortive infection of T5 bacteriophage in Escherichia coli (ColIb). *Journal of Virology* **37,** 916–921 (Mar. 1981).
34. Dy, R. L., Przybilski, R., Semeijn, K., Salmond, G. P. C. & Fineran, P. C. A widespread bacteriophage abortive infection system functions through a Type IV toxin-antitoxin mechanism. *Nucleic Acids Research* **42,** 4590–4605 (Apr. 2014).
35. Sekiguchi, M. Studies on the physiological defect in rII mutants of bacteriophage T4. *Journal of Molecular Biology* **16,** 503–522 (Apr. 1, 1966).
36. Snyder, L. Phage-exclusion enzymes: a bonanza of biochemical and cell biology reagents? *Molecular Microbiology* **15,** 415–420 (Feb. 1995).
37. Parma, D. H. *et al.* The Rex system of bacteriophage lambda: tolerance and altruistic cell death. *Genes & Development* **6,** 497–510 (Mar. 1992).
38. Yamaguchi, Y., Park, J.-H. & Inouye, M. Toxin-antitoxin systems in bacteria and archaea. *Annual Review of Genetics* **45,** 61–79 (2011).
39. Mruk, I. & Kobayashi, I. To be or not to be: regulation of restriction–modification systems and other toxin–antitoxin systems. *Nucleic Acids Research* **42,** 70–86 (Jan. 1, 2014).
40. Gerdes, K., Rasmussen, P. B. & Molin, S. Unique type of plasmid maintenance function: postsegregational killing of plasmid-free cells. *Proceedings of the National Academy of Sciences of the United States of America* **83,** 3116–3120 (May 1986).
41. Aizenman, E., Engelberg-Kulka, H. & Glaser, G. An Escherichia coli chromosomal "addiction module" regulated by guanosine [corrected] 3',5'-bispyrophosphate: a model for programmed bacterial cell death. *Proceedings of the National Academy of Sciences of the United States of America* **93,** 6059–6063 (June 11, 1996).
42. Zhang, Y. *et al.* MazF Cleaves Cellular mRNAs Specifically at ACA to Block Protein Synthesis in Escherichia coli. *Molecular Cell* **12,** 913–923 (Oct. 1, 2003).

43. Cohen, D. *et al.* Cyclic GMP–AMP signalling protects bacteria against viral infection. *Nature* **574.** Number: 7780 Publisher: Nature Publishing Group, 691–695 (Oct. 2019).
44. Severin, G., Ramliden, M. & Ng, W.-L. Direct activation of a phospholipase by cyclic GMP-AMP in El Tor Vibrio cholerae. *PNAS* **115,** E6048–E6055 (June 11, 2018).
45. Koonin, E. V. & Aravind, L. The NACHT family – a new group of predicted NTPases implicated in apoptosis and MHC transcription activation. *Trends in Biochemical Sciences* **25.** Publisher: Elsevier, 223–224 (May 1, 2000).
46. Caruso, R., Warner, N., Inohara, N. & Núñez, G. NOD1 and NOD2: Signaling, Host Defense, and Inflammatory Disease. *Immunity* **41.** Publisher: Elsevier, 898–908 (Dec. 18, 2014).
47. Koonin, E. V. & Aravind, L. Origin and evolution of eukaryotic apoptosis: the bacterial connection. *Cell Death & Differentiation* **9.** Number: 4 Publisher: Nature Publishing Group, 394–404 (Apr. 2002).
48. Leipe, D. D., Koonin, E. V. & Aravind, L. STAND, a Class of P-Loop NTPases Including Animal and Plant Regulators of Programmed Cell Death: Multiple, Complex Domain Architectures, Unusual Phyletic Patterns, and Evolution by Horizontal Gene Transfer. *Journal of Molecular Biology* **343,** 1–28 (Oct. 8, 2004).
49. Gao, L. A. *et al.* Prokaryotic innate immunity through pattern recognition of conserved viral proteins. *Science.* Publisher: American Association for the Advancement of Science (Aug. 12, 2022).
50. Koonin, E. V. *et al.* Global Organization and Proposed Megataxonomy of the Virus World. *Microbiology and Molecular Biology Reviews* **84.** Publisher: American Society for Microbiology, e00061–19 (Mar. 4, 2020).
51. Casjens, S. R. The DNA-packaging nanomotor of tailed bacteriophages. *Nature Reviews Microbiology* **9.** Number: 9 Publisher: Nature Publishing Group, 647–657 (Sept. 2011).
52. Dedeo, C. L., Cingolani, G. & Teschke, C. M. Portal Protein: The Orchestrator of Capsid Assembly for the dsDNA Tailed Bacteriophages and Herpesviruses. *Annual Review of Virology* **6,** 141–160 (2019).
53. Gao, L. *et al.* Diverse enzymatic activities mediate antiviral immunity in prokaryotes. *Science* **369.** Publisher: American Association for the Advancement of Science, 1077–1084 (Aug. 28, 2020).
54. Makarova, K. S., Wolf, Y. I., van der Oost, J. & Koonin, E. V. Prokaryotic homologs of Argonaute proteins are predicted to function as key components of a novel system of defense against mobile genetic elements. *Biology Direct* **4,** 29 (Aug. 25, 2009).
55. Bohmert, K. *et al.* AGO1 defines a novel locus of Arabidopsis controlling leaf development. *The EMBO journal* **17,** 170–180 (Jan. 2, 1998).
56. Meister, G. Argonaute proteins: functional insights and emerging roles. *Nature Reviews. Genetics* **14,** 447–459 (July 2013).
57. Hammond, S. M., Bernstein, E., Beach, D. & Hannon, G. J. An RNA-directed nuclease mediates post-transcriptional gene silencing in Drosophila cells. *Nature* **404,** 293–296 (Mar. 16, 2000).
58. Haley, B. & Zamore, P. D. Kinetic analysis of the RNAi enzyme complex. *Nature Structural & Molecular Biology* **11,** 599–606 (July 2004).
59. Grewal, S. I. S. RNAi-dependent formation of heterochromatin and its diverse functions. *Current opinion in genetics & development* **20.** Publisher: NIH Public Access, 134 (Apr. 2010).
60. Bernstein, E., Caudy, A. A., Hammond, S. M. & Hannon, G. J. Role for a bidentate ribonuclease in the initiation step of RNA interference. *Nature* **409.** Number: 6818 Publisher: Nature Publishing Group, 363–366 (Jan. 2001).
61. Lisitskaya, L. *et al.* Programmable RNA targeting by bacterial Argonaute nucleases with unconventional guide binding and cleavage specificity. *Nature Communications* **13.** Number: 1 Publisher: Nature Publishing Group, 4624 (Aug. 8, 2022).
62. Swarts, D. C. *et al.* DNA-guided DNA interference by a prokaryotic Argonaute. *Nature* **507,** 258–261 (Mar. 13, 2014).
63. Swarts, D. C. *et al.* Argonaute of the archaeon Pyrococcus furiosus is a DNA-guided nuclease that targets cognate DNA. *Nucleic Acids Research* **43,** 5120–5129 (May 26, 2015).

64. Swarts, D. C., Koehorst, J. J., Westra, E. R., Schaap, P. J. & van der Oost, J. Effects of Argonaute on Gene Expression in Thermus thermophilus. *PloS One* **10,** e0124880 (2015).
65. Kuzmenko, A. *et al.* DNA targeting and interference by a bacterial Argonaute nuclease. *Nature* **587.** Number: 7835 Publisher: Nature Publishing Group, 632–637 (Nov. 2020).
66. Xing, J. *et al.* Expression and Functional Analysis of the Argonaute Protein of Thermus thermophilus (TtAgo) in E. coli BL21(DE3). *Biomolecules* **11,** 524 (Mar. 31, 2021).
67. Swarts, D. C. *et al.* Autonomous Generation and Loading of DNA Guides by Bacterial Argonaute. *Molecular Cell* **65,** 985–998.e6 (Mar. 16, 2017).
68. Zeng, Z. *et al.* A short prokaryotic Argonaute activates membrane effector to confer antiviral defense. *Cell Host & Microbe* **30,** 930–943.e6 (July 13, 2022).
69. Makarova, K. S. *et al.* An updated evolutionary classification of CRISPR-Cas systems. *Nature Reviews. Microbiology* **13,** 722–736 (2015).
70. Bolotin, A., Quinquis, B., Sorokin, A. & Ehrlich, S. D. Clustered regularly interspaced short palindrome repeats (CRISPRs) have spacers of extrachromosomal origin. *Microbiology (Reading, England)* **151,** 2551–2561 (Pt 8 Aug. 2005).
71. Mojica, F. J. M., Díez-Villaseñor, C., García-Martínez, J. & Soria, E. Intervening sequences of regularly spaced prokaryotic repeats derive from foreign genetic elements. *Journal of Molecular Evolution* **60,** 174–182 (Feb. 2005).
72. Pourcel, C., Salvignol, G. & Vergnaud, G. CRISPR elements in Yersinia pestis acquire new repeats by preferential uptake of bacteriophage DNA, and provide additional tools for evolutionary studies. *Microbiology (Reading, England)* **151.** Number: Pt 3, 653–663 (Pt 3 Mar. 2005).
73. Jansen, R., Embden, J. D. A. v., Gaastra, W. & Schouls, L. M. Identification of genes that are associated with DNA repeats in prokaryotes. *Molecular Microbiology* **43,** 1565–1575 (2002).
74. Makarova, K. S. *et al.* Evolutionary classification of CRISPR–Cas systems: a burst of class 2 and derived variants. *Nature Reviews Microbiology* **18.** Number: 2 Publisher: Nature Publishing Group, 67–83 (Feb. 2020).
75. Mojica, F. J. M., Díez-Villaseñor, C., García-Martínez, J. & Almendros, C. Short motif sequences determine the targets of the prokaryotic CRISPR defence system. *Microbiology (Reading, England)* **155,** 733–740 (Pt 3 Mar. 2009).
76. Marraffini, L. A. & Sontheimer, E. J. Self vs. non-self discrimination during CRISPR RNA-directed immunity. *Nature* **463,** 568–571 (Jan. 28, 2010).
77. Deveau, H. *et al.* Phage Response to CRISPR-Encoded Resistance in Streptococcus thermophilus. *Journal of Bacteriology* **190,** 1390–1400 (Feb. 15, 2008).
78. Brouns, S. J. J. *et al.* Small CRISPR RNAs guide antiviral defense in prokaryotes. *Science (New York, N.Y.)* **321,** 960–964 (Aug. 15, 2008).
79. Charpentier, E., Richter, H., van der Oost, J. & White, M. F. Biogenesis pathways of RNA guides in archaeal and bacterial CRISPR-Cas adaptive immunity. *FEMS Microbiology Reviews* **39,** 428–441. (2022) (May 1, 2015).
80. Behler, J. & Hess, W. R. Approaches to study CRISPR RNA biogenesis and the key players involved. *Methods. Methods for characterizing, applying, and teaching CRISPR-Cas systems* **172,** 12–26 (Feb. 1, 2020).
81. Wiedenheft, B. *et al.* RNA-guided complex from a bacterial immune system enhances target recognition through seed sequence interactions. *Proceedings of the National Academy of Sciences of the United States of America* **108,** 10092–10097 (June 21, 2011).
82. Jinek, M. *et al.* A programmable dual RNA-guided DNA endonuclease in adaptive bacterial immunity. *Science (New York, N.Y.)* **337,** 816–821 (Aug. 17, 2012).
83. Jinek, M. *et al.* Structures of Cas9 endonucleases reveal RNA-mediated conformational activation. *Science* **343,** 1247997 (Mar. 14, 2014).
84. Jore, M. M. *et al.* Structural basis for CRISPR RNA-guided DNA recognition by Cascade. *Nature Structural & Molecular Biology* **18,** 529–536 (May 2011).
85. Mulepati, S., Héroux, A. & Bailey, S. Crystal structure of a CRISPR RNA–guided surveillance complex bound to a ssDNA target. *Science* **345.** Publisher: American Association for the Advancement of Science, 1479–1484 (Sept. 19, 2014).

86. Sternberg, S. H., Haurwitz, R. E. & Doudna, J. A. Mechanism of substrate selection by a highly specific CRISPR endoribonuclease. *RNA (New York, N.Y.)* **18,** 661–672 (Apr. 2012).
87. Sashital, D. G., Wiedenheft, B. & Doudna, J. A. Mechanism of foreign DNA selection in a bacterial adaptive immune system. *Molecular Cell* **46,** 606–615 (June 8, 2012).
88. Guo, T. W. *et al.* Cryo-EM Structures Reveal Mechanism and Inhibition of DNA Targeting by a CRISPR-Cas Surveillance Complex. *Cell* **171,** 414–426.e12. ISSN: 1097-4172 (Oct. 5, 2017).
89. Xue, C. & Sashital, D. G. Mechanisms of Type I-E and I-F CRISPR-Cas Systems in Enterobacteriaceae. *EcoSal Plus* **8** (Feb. 2019).
90. Hayes, R. P. *et al.* Structural basis for promiscuous PAM recognition in type I-E Cascade from E. coli. *Nature* **530,** 499–503 (Feb. 25, 2016).
91. Redding, S. *et al.* Surveillance and Processing of Foreign DNA by the Escherichia coli CRISPR-Cas System. *Cell* **163,** 854–865 (Nov. 5, 2015).
92. Xue, C., Whitis, N. R. & Sashital, D. G. Conformational control of Cascade interference and priming activities in CRISPR immunity. *Molecular cell* **64,** 826–834 (Nov. 17, 2016).
93. Van Erp, P. B. G. *et al.* Mechanism of CRISPR-RNA guided recognition of DNA targets in Escherichia coli. *Nucleic Acids Research* **43,** 8381–8391 (Sept. 30, 2015).
94. Xiao, Y. *et al.* Structure Basis for Directional R-loop Formation and Substrate Handover Mechanisms in Type I CRISPR-Cas System. *Cell* **170,** 48–60.e11 (June 29, 2017).
95. Loeff, L., Brouns, S. J. J. & Joo, C. Repetitive DNA Reeling by the Cascade-Cas3 Complex in Nucleotide Unwinding Steps. *Molecular Cell* **70,** 385–394.e3 (2018).
96. Rollins, M. F. *et al.* Cas1 and the Csy complex are opposing regulators of Cas2/3 nuclease activity. *Proceedings of the National Academy of Sciences of the United States of America* **114.** Number: 26, E5113–E5121 (2017).
97. Künne, T. *et al.* Cas3-Derived Target DNA Degradation Fragments Fuel Primed CRISPR Adaptation. *Molecular Cell* **63,** 852–864 (2016).
98. Vale, P. F. & Little, T. J. CRISPR-mediated phage resistance and the ghost of coevolution past. *Proceedings. Biological Sciences* **277,** 2097–2103 (July 22, 2010).
99. Shmakov, S. A. *et al.* The CRISPR Spacer Space Is Dominated by Sequences from Species-Specific Mobilomes. *mBio* **8,** e01397–17 (Sept. 19, 2017).
100. Yosef, I., Goren, M. G. & Qimron, U. Proteins and DNA elements essential for the CRISPR adaptation process in Escherichia coli. *Nucleic Acids Research* **40,** 5569–5576 (July 2012).
101. Wei, Y., Chesne, M. T., Terns, R. M. & Terns, M. P. Sequences spanning the leader-repeat junction mediate CRISPR adaptation to phage in Streptococcus thermophilus. *Nucleic Acids Research* **43,** 1749–1758 (Feb. 18, 2015).
102. McGinn, J. & Marraffini, L. A. CRISPR-Cas Systems Optimize Their Immune Response by Specifying the Site of Spacer Integration. *Molecular Cell* **64.** Number: 3, 616–623 (2016).
103. Wei, Y., Terns, R. M. & Terns, M. P. Cas9 function and host genome sampling in Type II-A CRISPR–Cas adaptation. *Genes & Development* **29.** Number: 4, 356–361 (Feb. 15, 2015).
104. Heler, R. *et al.* Cas9 specifies functional viral targets during CRISPR-Cas adaptation. *Nature* **519,** 199–202 (Mar. 12, 2015).
105. Datsenko, K. A. *et al.* Molecular memory of prior infections activates the CRISPR/Cas adaptive bacterial immunity system. *Nature Communications* **3.** Number: 1 Publisher: Nature Publishing Group, 945 (July 10, 2012).
106. Semenova, E. *et al.* Interference by clustered regularly interspaced short palindromic repeat (CRISPR) RNA is governed by a seed sequence. *Proceedings of the National Academy of Sciences* **108.** Publisher: National Academy of Sciences Section: Biological Sciences, 10098–10103 (June 21, 2011).
107. Fineran, P. C. *et al.* Degenerate target sites mediate rapid primed CRISPR adaptation. *Proceedings of the National Academy of Sciences* **111,** E1629–E1638 (Apr. 22, 2014).
108. Swarts, D. C., Mosterd, C., Passel, M. W. J. v. & Brouns, S. J. J. CRISPR Interference Directs Strand Specific Spacer Acquisition. *PLOS ONE* **7,** e35888 (Apr. 27, 2012).
109. Staals, R. H. J. *et al.* Interference-driven spacer acquisition is dominant over naive and primed adaptation in a native CRISPR-Cas system. *Nature Communications* **7,** 12853 (2016).

110. Stringer, A. M., Cooper, L. A., Kadaba, S., Shrestha, S. & Wade, J. T. Characterization of Primed Adaptation in the Escherichia coli type I-E CRISPR-Cas System. *bioRxiv,* 2020.02.10.942821 (Feb. 12, 2020).
111. Richter, C. *et al.* Priming in the Type I-F CRISPR-Cas system triggers strand-independent spacer acquisition, bi-directionally from the primed protospacer. *Nucleic Acids Research* **42,** 8516–8526 (July 2014).
112. Krivoy, A. *et al.* Primed CRISPR adaptation in Escherichia coli cells does not depend on conformational changes in the Cascade effector complex detected in Vitro. *Nucleic Acids Research* **46.** Number: 8, 4087–4098 (2018).
113. Semenova, E. *et al.* Highly efficient primed spacer acquisition from targets destroyed by the Escherichia coli type I-E CRISPR-Cas interfering complex. *Proceedings of the National Academy of Sciences* **113.** Publisher: National Academy of Sciences Section: Biological Sciences, 7626–7631 (July 5, 2016).
114. Severinov, K., Ispolatov, I. & Semenova, E. The Influence of Copy-Number of Targeted Extrachromosomal Genetic Elements on the Outcome of CRISPR-Cas Defense. *Frontiers in Molecular Biosciences* **3** (Aug. 31, 2016).
115. Savitskaya, E., Semenova, E., Dedkov, V., Metlitskaya, A. & Severinov, K. High-throughput analysis of type I-E CRISPR/Cas spacer acquisition in E. coli. *RNA biology* **10,** 716–725 (May 2013).
116. Musharova, O. *et al.* Avoidance of Trinucleotide Corresponding to Consensus Protospacer Adjacent Motif Controls the Efficiency of Prespacer Selection during Primed Adaptation. *mBio* **9** (Dec. 21, 2018).
117. Krupovic, M., Makarova, K. S., Forterre, P., Prangishvili, D. & Koonin, E. V. Casposons: a new superfamily of self-synthesizing DNA transposons at the origin of prokaryotic CRISPR-Cas immunity. *BMC Biology* **12,** 36 (May 19, 2014).
118. Krupovic, M., Béguin, P. & Koonin, E. V. Casposons: mobile genetic elements that gave rise to the CRISPR-Cas adaptation machinery. *Current opinion in microbiology* **38,** 36–43 (Aug. 2017).
119. Hudaiberdiev, S. *et al.* Phylogenomics of Cas4 family nucleases. *BMC evolutionary biology* **17.** Number: 1, 232 (2017).
120. Nuñez, J. K., Lee, A. S. Y., Engelman, A. & Doudna, J. A. Integrase-mediated spacer acquisition during CRISPR-Cas adaptive immunity. *Nature* **519,** 193–198 (Mar. 12, 2015).
121. Carte, J. *et al.* The three major types of CRISPR-Cas systems function independently in CRISPR RNA biogenesis in Streptococcus thermophilus. *Molecular microbiology* **93,** 98–112. (2020) (July 2014).
122. Kieper, S. N., Almendros, C. & Brouns, S. J. J. Conserved motifs in the CRISPR leader sequence control spacer acquisition levels in Type I-D CRISPR-Cas systems. *FEMS Microbiology Letters* **366** (June 28, 2019).
123. Nuñez, J. K., Bai, L., Harrington, L. B., Hinder, T. L. & Doudna, J. A. CRISPR Immunological Memory Requires a Host Factor for Specificity. *Molecular Cell* **62,** 824–833 (2016).
124. Yosef, I. *et al.* DNA motifs determining the efficiency of adaptation into the Escherichia coli CRISPR array. *Proceedings of the National Academy of Sciences* **110,** 14396–14401 (Aug. 27, 2013).
125. Vorontsova, D. *et al.* Foreign DNA acquisition by the I-F CRISPR-Cas system requires all components of the interference machinery. *Nucleic Acids Research* **43,** 10848–10860 (Dec. 15, 2015).
126. Liu, T. *et al.* Coupling transcriptional activation of CRISPR–Cas system and DNA repair genes by Csa3a in Sulfolobus islandicus. *Nucleic Acids Research* **45.** Number: 15, 8978–8992 (Sept. 6, 2017).
127. Wang, J. *et al.* Structural and Mechanistic Basis of PAM-Dependent Spacer Acquisition in CRISPR-Cas Systems. *Cell* **163.** Number: 4, 840–853 (Nov. 5, 2015).
128. Fagerlund, R. D. *et al.* Spacer capture and integration by a type I-F Cas1-Cas2-3 CRISPR adaptation complex. *Proceedings of the National Academy of Sciences of the United States of America* **114,** E5122–E5128 (2017).

129. Nuñez, J. K. *et al.* Cas1-Cas2 complex formation mediates spacer acquisition during CRISPR-Cas adaptive immunity. *Nature Structural & Molecular Biology* **21.** Number: 6, 528–534 (June 2014).
130. Babu, M. *et al.* A dual function of the CRISPR–Cas system in bacterial antivirus immunity and DNA repair. *Molecular Microbiology* **79,** 484–502. (2020) (2011).
131. Kim, S. *et al.* Selective loading and processing of prespacers for precise CRISPR adaptation. *Nature* **579,** 141–145 (2020).
132. Moch, C., Fromant, M., Blanquet, S. & Plateau, P. DNA binding specificities of Escherichia coli Cas1–Cas2 integrase drive its recruitment at the CRISPR locus. *Nucleic Acids Research* **45,** 2714–2723 (Mar. 17, 2017).
133. Kim, J. G., Garrett, S., Wei, Y., Graveley, B. R. & Terns, M. P. CRISPR DNA elements controlling site-specific spacer integration and proper repeat length by a Type II CRISPR–Cas system. *Nucleic Acids Research* **47,** 8632–8648 (Sept. 19, 2019).
134. Xiao, Y., Ng, S., Nam, K. H. & Ke, A. How Type II CRISPR-Cas establish immunity through Cas1-Cas2 mediated spacer integration. *Nature* **550,** 137–141 (Oct. 5, 2017).
135. Budhathoki, J. B. *et al.* Real-time Observation of CRISPR spacer acquisition by Cas1–Cas2 integrase. *Nature structural & molecular biology* **27,** 489–499. (2022) (May 2020).
136. Ivančić-Baće, I., Cass, S. D., Wearne, S. J. & Bolt, E. L. Different genome stability proteins underpin primed and naïve adaptation in E. coli CRISPR-Cas immunity. *Nucleic Acids Research* **43.** Number: 22, 10821–10830 (Dec. 15, 2015).
137. Wright, A. V. *et al.* Structures of the CRISPR genome integration complex. *Science (New York, N.Y.)* **357,** 1113–1118 (2017).
138. Yoganand, K., Sivathanu, R., Nimkar, S. & Anand, B. Asymmetric positioning of Cas1–2 complex and Integration Host Factor induced DNA bending guide the unidirectional homing of protospacer in CRISPR-Cas type I-E system. *Nucleic Acids Research* **45,** 367–381 (Jan. 9, 2017).
139. Zulianello, L., de la Gorgue de Rosny, E., van Ulsen, P., van de Putte, P. & Goosen, N. The HimA and HimD subunits of integration host factor can specifically bind to DNA as homodimers. *The EMBO Journal* **13,** 1534–1540 (Apr. 1, 1994).
140. Yang, C.-C. & Nash, H. A. The interaction of E. coli IHF protein with its specific binding sites. *Cell* **57,** 869–880 (June 2, 1989).
141. Goodrich, J. A., Schwartz, M. L. & McClure, W. R. Searching for and predicting the activity of sites for DNA binding proteins: compilation and analysis of the binding sites for Escherichia coli integration host factor (IHF). *Nucleic Acids Research* **18,** 4993–5000 (Sept. 11, 1990).
142. Rice, P. A., Yang, S.-w., Mizuuchi, K. & Nash, H. A. Crystal Structure of an IHF-DNA Complex: A Protein-Induced DNA U-Turn. *Cell* **87,** 1295–1306 (Dec. 27, 1996).
143. Dillon, S. C. & Dorman, C. J. Bacterial nucleoid-associated proteins, nucleoid structure and gene expression. *Nature Reviews. Microbiology* **8,** 185–195 (Mar. 2010).
144. Wright, A. V. & Doudna, J. A. Protecting genome integrity during CRISPR immune adaptation. *Nature Structural & Molecular Biology* **23,** 876–883 (Oct. 2016).
145. Levy, A. *et al.* CRISPR adaptation biases explain preference for acquisition of foreign DNA. *Nature* **520,** 505–510 (Apr. 23, 2015).
146. Stern, A., Keren, L., Wurtzel, O., Amitai, G. & Sorek, R. Self-targeting by CRISPR: gene regulation or autoimmunity? *Trends in genetics : TIG* **26,** 335–340 (Aug. 2010).
147. Dillingham, M. S. & Kowalczykowski, S. C. RecBCD enzyme and the repair of double-stranded DNA breaks. *Microbiology and molecular biology reviews: MMBR* **72,** 642–671, Table of Contents (Dec. 2008).
148. Maguin, P., Varble, A., Modell, J. W. & Marraffini, L. A. Cleavage of viral DNA by restriction endonucleases stimulates the type II CRISPR-Cas immune response. *Molecular Cell* **82,** 907–919.e7 (Mar. 3, 2022).
149. Modell, J. W., Jiang, W. & Marraffini, L. A. CRISPR-Cas systems exploit viral DNA injection to establish and maintain adaptive immunity. *Nature* **544,** 101–104 (2017).
150. Hynes, A. P., Villion, M. & Moineau, S. Adaptation in bacterial CRISPR-Cas immunity can be driven by defective phages. *Nature Communications* **5,** 4399 (July 24, 2014).
151. Koonin, E. V., Makarova, K. S. & Zhang, F. Diversity, classification and evolution of CRISPR-Cas systems. *Current Opinion in Microbiology* **37,** 67–78 (June 2017).

152. Beloglazova, N. *et al.* Structure and activity of the Cas3 HD nuclease MJ0384, an effector enzyme of the CRISPR interference. *The EMBO Journal* **30,** 4616–4627 (Nov. 16, 2011).
153. Peters, J. E., Makarova, K. S., Shmakov, S. & Koonin, E. V. Recruitment of CRISPR-Cas systems by Tn7-like transposons. *Proceedings of the National Academy of Sciences of the United States of America* **114,** E7358–E7366 (Aug. 29, 2017).
154. Klompe, S. E., Vo, P. L. H., Halpin-Healy, T. S. & Sternberg, S. H. Transposon-encoded CRISPR-Cas systems direct RNA-guided DNA integration. *Nature* **571,** 219–225 (July 2019).
155. Strecker, J. *et al.* RNA-guided DNA insertion with CRISPR-associated transposases. *Science (New York, N.Y.)* **365,** 48–53 (July 5, 2019).
156. Goldberg, G. W., Jiang, W., Bikard, D. & Marraffini, L. A. Conditional tolerance of temperate phages via transcription-dependent CRISPR-Cas targeting. *Nature* **514.** Number: 7524 Publisher: Nature Publishing Group, 633–637 (Oct. 2014).
157. Deng, L., Garrett, R. A., Shah, S. A., Peng, X. & She, Q. A novel interference mechanism by a type IIIB CRISPR-Cmr module in Sulfolobus. *Molecular Microbiology* **87,** 1088–1099 (Mar. 2013).
158. Elmore, J. R. *et al.* Bipartite recognition of target RNAs activates DNA cleavage by the Type III-B CRISPR–Cas system. *Genes & Development* **30.** Company: Cold Spring Harbor Laboratory Press Distributor: Cold Spring Harbor Laboratory Press Institution: Cold Spring Harbor Laboratory Press Label: Cold Spring Harbor Laboratory Press Publisher: Cold Spring Harbor Lab, 447–459 (Feb. 15, 2016).
159. Samai, P. *et al.* Co-transcriptional DNA and RNA Cleavage during Type III CRISPR-Cas Immunity. *Cell* **161,** 1164–1174 (May 21, 2015).
160. Van der Oost, J., Westra, E. R., Jackson, R. N. & Wiedenheft, B. Unravelling the structural and mechanistic basis of CRISPR–Cas systems. *Nature Reviews Microbiology* **12.** Number: 7 Publisher: Nature Publishing Group, 479–492 (July 2014).
161. Rouillon, C. *et al.* Structure of the CRISPR interference complex CSM reveals key similarities with cascade. *Molecular Cell* **52,** 124–134 (Oct. 10, 2013).
162. Benda, C. *et al.* Structural Model of a CRISPR RNA-Silencing Complex Reveals the RNA-Target Cleavage Activity in Cmr4. *Molecular Cell* **56,** 43–54 (Oct. 2, 2014).
163. Ramia, N. F., Tang, L., Cocozaki, A. I. & Li, H. Staphylococcus epidermidis Csm1 is a 3'–5' exonuclease. *Nucleic Acids Research* **42,** 1129–1138 (Jan. 2014).
164. Zhu, X. & Ye, K. Cmr4 is the slicer in the RNA-targeting Cmr CRISPR complex. *Nucleic Acids Research* **43,** 1257–1267 (Jan. 30, 2015).
165. Kazlauskiene, M., Kostiuk, G., Venclovas, Č., Tamulaitis, G. & Siksnys, V. A cyclic oligonucleotide signaling pathway in type III CRISPR-Cas systems. *Science (New York, N.Y.)* **357,** 605–609 (Aug. 11, 2017).
166. Niewoehner, O. *et al.* Type III CRISPR-Cas systems produce cyclic oligoadenylate second messengers. *Nature* **548,** 543–548 (Aug. 31, 2017).
167. Pinilla-Redondo, R. *et al.* Type IV CRISPR–Cas systems are highly diverse and involved in competition between plasmids. *Nucleic Acids Research* **48,** 2000–2012 (Feb. 28, 2020).
168. Pinilla-Redondo, R. *et al.* CRISPR-Cas systems are widespread accessory elements across bacterial and archaeal plasmids. *Nucleic Acids Research* **50,** 4315–4328 (May 6, 2022).
169. Faure, G. *et al.* CRISPR-Cas in mobile genetic elements: counter-defence and beyond. *Nature Reviews. Microbiology* **17,** 513–525 (Aug. 2019).
170. Moya-Beltrán, A. *et al.* Evolution of Type IV CRISPR-Cas Systems: Insights from CRISPR Loci in Integrative Conjugative Elements of Acidithiobacillia. *The CRISPR journal* **4,** 656–672 (Oct. 2021).
171. Deltcheva, E. *et al.* CRISPR RNA maturation by trans-encoded small RNA and host factor RNase III. *Nature* **471,** 602–607 (Mar. 31, 2011).
172. Chylinski, K., Le Rhun, A. & Charpentier, E. The tracrRNA and Cas9 families of type II CRISPR-Cas immunity systems. *RNA Biology* **10,** 726–737 (May 1, 2013).
173. Shao, Y. & Li, H. Recognition and Cleavage of a non-structured CRISPR RNA by its Processing Endoribonuclease Cas6. *Structure (London, England : 1993)* **21,** 385–393 (Mar. 5, 2013).

174. Ka, D. *et al.* Crystal Structure of Streptococcus pyogenes Cas1 and Its Interaction with Csn2 in the Type II CRISPR-Cas System. *Structure (London, England: 1993)* **24,** 70–79 (Jan. 5, 2016).
175. Ka, D., Jang, D. M., Han, B. W. & Bae, E. Molecular organization of the type II-A CRISPR adaptation module and its interaction with Cas9 via Csn2. *Nucleic Acids Research* **46,** 9805–9815 (Oct. 12, 2018).
176. Zetsche, B. *et al.* Cpf1 is a single RNA-guided endonuclease of a Class 2 CRISPR-Cas system. *Cell* **163,** 759–771 (Oct. 22, 2015).
177. Fonfara, I., Richter, H., Bratovič, M., Le Rhun, A. & Charpentier, E. The CRISPR-associated DNA-cleaving enzyme Cpf1 also processes precursor CRISPR RNA. *Nature* **532,** 517–521 (Apr. 28, 2016).
178. Chen, J. S. *et al.* CRISPR-Cas12a target binding unleashes indiscriminate single-stranded DNase activity. *Science (New York, N.Y.)* **360,** 436–439 (Apr. 27, 2018).
179. Swarts, D. C., van der Oost, J. & Jinek, M. Structural basis for guide RNA processing and seed-dependent DNA targeting and cleavage by CRISPR-Cas12a. *Molecular cell* **66,** 221–233.e4 (Apr. 20, 2017).
180. Shmakov, S. *et al.* Discovery and Functional Characterization of Diverse Class 2 CRISPR-Cas Systems. *Molecular Cell* **60,** 385–397 (Nov. 5, 2015).
181. Abudayyeh, O. O. *et al.* C2c2 is a single-component programmable RNA-guided RNA-targeting CRISPR effector. *Science* **353.** Publisher: American Association for the Advancement of Science, aaf5573 (Aug. 5, 2016).
182. Zhang, B. *et al.* Two HEPN domains dictate CRISPR RNA maturation and target cleavage in Cas13d. *Nature Communications* **10.** Number: 1 Publisher: Nature Publishing Group, 2544 (June 11, 2019).
183. Özcan, A. *et al.* Type IV CRISPR RNA processing and effector complex formation in Aromatoleum aromaticum. *Nature Microbiology* **4,** 89–96 (Jan. 2019).
184. East-Seletsky, A. *et al.* Two distinct RNase activities of CRISPR-C2c2 enable guide-RNA processing and RNA detection. *Nature* **538.** Number: 7624 Publisher: Nature Publishing Group, 270–273 (Oct. 2016).
185. Wimmer, F. & Beisel, C. L. CRISPR-Cas Systems and the Paradox of Self-Targeting Spacers. *Frontiers in Microbiology* **10** (Jan. 22, 2020).
186. Westra, E. R. *et al.* Parasite Exposure Drives Selective Evolution of Constitutive versus Inducible Defense. *Current biology: CB* **25,** 1043–1049 (Apr. 20, 2015).
187. Dupuis, M.-È., Villion, M., Magadán, A. H. & Moineau, S. CRISPR-Cas and restriction–modification systems are compatible and increase phage resistance. *Nature Communications* **4.** Number: 1 Publisher: Nature Publishing Group, 2087 (July 2, 2013).
188. Vale, P. F. *et al.* Costs of CRISPR-Cas-mediated resistance in Streptococcus thermophilus. *Proceedings of the Royal Society B: Biological Sciences* **282** (Aug. 7, 2015).
189. Young, J. C. *et al.* Phage-Induced Expression of CRISPR-Associated Proteins Is Revealed by Shotgun Proteomics in Streptococcus thermophilus. *PLoS ONE* **7.** Number: 5 (May 30, 2012).
190. Liu, T. *et al.* Transcriptional regulator-mediated activation of adaptation genes triggers CRISPR de novo spacer acquisition. *Nucleic Acids Research* **43.** Number: 2, 1044–1055 (Jan. 2015).
191. Wei, J. *et al.* The Mycobacterium tuberculosis CRISPR-Associated Cas1 Involves Persistence and Tolerance to Anti-Tubercular Drugs. *BioMed Research International* **2019,** 7861695 (Apr. 2, 2019).
192. Wheatley, R. M. & MacLean, R. C. CRISPR-Cas systems restrict horizontal gene transfer in Pseudomonas aeruginosa. *The ISME journal* **15,** 1420–1433 (May 2021).
193. Palmer, K. L. & Gilmore, M. S. Multidrug-Resistant Enterococci Lack CRISPR-cas. *mBio* **1,** e00227–10 (Oct. 12, 2010).
194. Dorman, C. J. H-NS: a universal regulator for a dynamic genome. *Nature Reviews Microbiology* **2,** 391–400 (May 2004).
195. Fang, F. C. & Rimsky, S. New Insights into Transcriptional Regulation by H-NS. *Current opinion in microbiology* **11,** 113–120 (Apr. 2008).

196. Wang, W., Li, G.-W., Chen, C., Xie, X. S. & Zhuang, X. Chromosome organization by a nucleoid-associated protein in live bacteria. *Science (New York, N.Y.)* **333,** 1445–1449 (Sept. 9, 2011).
197. Hommais, F. *et al.* Large-scale monitoring of pleiotropic regulation of gene expression by the prokaryotic nucleoid-associated protein, H-NS. *Molecular Microbiology* **40.** Number: 1, 20–36 (Apr. 2001).
198. Navarre, W. W. *et al.* Selective silencing of foreign DNA with low GC content by the H-NS protein in Salmonella. *Science (New York, N.Y.)* **313,** 236–238 (July 14, 2006).
199. Tupper, A. E. *et al.* The chromatin-associated protein H-NS alters DNA topology in vitro. *The EMBO Journal* **13,** 258–268 (Jan. 1, 1994).
200. Dame, R. T. *et al.* DNA Bridging: a Property Shared among H-NS-Like Proteins. *Journal of Bacteriology* **187,** 1845–1848 (Mar. 2005).
201. Schröder, O. & Wagner, R. The Bacterial Regulatory Protein H-NS A Versatile Modulator of Nucleic Acid Structures. **383.** Publisher: De Gruyter Section: Biological Chemistry, 945–960 (June 26, 2002).
202. Pul, U. *et al.* Identification and characterization of E. coli CRISPR-cas promoters and their silencing by H-NS. *Molecular Microbiology* **75,** 1495–1512 (Mar. 2010).
203. Medina-Aparicio, L. *et al.* The CRISPR/Cas immune system is an operon regulated by LeuO, H-NS, and leucine-responsive regulatory protein in Salmonella enterica serovar Typhi. *Journal of Bacteriology* **193,** 2396–2407 (May 2011).
204. Westra, E. R. *et al.* H-NS-mediated repression of CRISPR-based immunity in Escherichia coli K12 can be relieved by the transcription activator LeuO. *Molecular Microbiology* **77,** 1380–1393 (Sept. 2010).
205. Stoebel, D. M., Free, A. & Dorman, C. J. Anti-silencing: overcoming H-NS-mediated repression of transcription in Gram-negative enteric bacteria. *Microbiology (Reading, England)* **154.** Number: Pt 9, 2533–2545 (Pt 9 Sept. 2008).
206. Shimada, T., Bridier, A., Briandet, R. & Ishihama, A. Novel roles of LeuO in transcription regulation of E. coli genome: antagonistic interplay with the universal silencer H-NS. *Molecular Microbiology* **82,** 378–397 (2011).
207. Busby, S. & Ebright, R. H. Transcription activation by catabolite activator protein (CAP). *Journal of Molecular Biology* **293,** 199–213 (Oct. 22, 1999).
208. Yang, C.-D., Chen, Y.-H., Huang, H.-Y., Huang, H.-D. & Tseng, C.-P. CRP represses the CRISPR/Cas system in Escherichia coli: evidence that endogenous CRISPR spacers impede phage P1 replication. *Molecular Microbiology* **92,** 1072–1091 (June 2014).
209. Shinkai, A. *et al.* Transcription Activation Mediated by a Cyclic AMP Receptor Protein from Thermus thermophilus HB8. *Journal of Bacteriology* **189.** Number: 10, 3891–3901 (May 15, 2007).
210. Agari, Y. *et al.* Transcription profile of Thermus thermophilus CRISPR systems after phage infection. *Journal of Molecular Biology* **395.** Number: 2, 270–281 (Jan. 15, 2010).
211. Patterson, A. G., Chang, J. T., Taylor, C. & Fineran, P. C. Regulation of the Type I-F CRISPR-Cas system by CRP-cAMP and GalM controls spacer acquisition and interference. *Nucleic Acids Research* **43,** 6038–6048 (July 13, 2015).
212. Nagasawa, S., Ishige, K. & Mizuno, T. Novel members of the two-component signal transduction genes in Escherichia coli. *Journal of Biochemistry* **114,** 350–357 (Sept. 1993).
213. Nakano, S., Zheng, G., Nakano, M. M. & Zuber, P. Multiple Pathways of Spx (YjbD) Proteolysis in Bacillus subtilis. *Journal of Bacteriology* **184.** Number: 13, 3664–3670 (July 2002).
214. Perez-Rodriguez, R. *et al.* Envelope stress is a trigger of CRISPR RNA-mediated DNA silencing in Escherichia coli. *Molecular Microbiology* **79.** Number: 3, 584–599 (2011).
215. Baranova, N. & Nikaido, H. The BaeSR Two-Component Regulatory System Activates Transcription of the yegMNOB (mdtABCD) Transporter Gene Cluster in Escherichia coli and Increases Its Resistance to Novobiocin and Deoxycholate. *Journal of Bacteriology* **184,** 4168–4176 (Aug. 2002).
216. Fallico, V., Ross, R. P., Fitzgerald, G. F. & McAuliffe, O. Genetic Response to Bacteriophage Infection in Lactococcus lactis Reveals a Four-Strand Approach Involving Induction of Membrane Stress Proteins, d-Alanylation of the Cell Wall, Maintenance of Proton Motive

Force, and Energy Conservation. *Journal of Virology* **85.** Number: 22, 12032–12042 (Nov. 2011).
217. Ahator, S. D., Jianhe, W. & Zhang, L.-H. The ECF sigma factor PvdS regulates the type I-F CRISPR-Cas system in Pseudomonas aeruginosa. *bioRxiv,* 2020.01.31.929752. (2020) (Feb. 2, 2020).
218. Leoni, L., Orsi, N., Lorenzo, V. d. & Visca, P. Functional Analysis of PvdS, an Iron Starvation Sigma Factor of Pseudomonas aeruginosa. *Journal of Bacteriology* **182.** Number: 6, 1481–1491 (Mar. 15, 2000).
219. Leoni, L., Ciervo, A., Orsi, N. & Visca, P. Iron-regulated transcription of the pvdA gene in Pseudomonas aeruginosa: effect of Fur and PvdS on promoter activity. *Journal of Bacteriology* **178.** Number: 8, 2299–2313 (Apr. 1, 1996).
220. Hantke, K. Regulation of ferric iron transport in Escherichia coli K12: Isolation of a constitutive mutant. *Molecular and General Genetics MGG* **182,** 288–292 (July 1, 1981).
221. Fuqua, W. C., Winans, S. C. & Greenberg, E. P. Quorum sensing in bacteria: the LuxR-LuxI family of cell density-responsive transcriptional regulators. *Journal of Bacteriology* **176,** 269–275 (Jan. 1994).
222. Patterson, A. G. *et al.* Quorum Sensing Controls Adaptive Immunity through the Regulation of Multiple CRISPR-Cas Systems. *Molecular Cell* **64,** 1102–1108 (2016).
223. Thomson, N. R., Crow, M. A., McGowan, S. J., Cox, A. & Salmond, G. P. C. Biosynthesis of carbapenem antibiotic and prodigiosin pigment in Serratia is under quorum sensing control. *Molecular Microbiology* **36,** 539–556 (2000).
224. Eberl, L. *et al.* Involvement of N-acyl-L-hormoserine lactone autoinducers in controlling the multicellular behaviour of Serratia liquefaciens. *Molecular Microbiology* **20,** 127–136 (Apr. 1996).
225. Høyland-Kroghsbo, N. M. *et al.* Quorum sensing controls the Pseudomonas aeruginosa CRISPR-Cas adaptive immune system. *Proceedings of the National Academy of Sciences of the United States of America* **114,** 131–135 (2017).
226. Campa, A. R. *et al.* The Rsm (Csr) post-transcriptional regulatory pathway coordinately controls multiple CRISPR–Cas immune systems. *Nucleic Acids Research* **49,** 9508–9525 (Sept. 20, 2021).
227. Zhou, C.-m. *et al.* Calcium-responsive kinase LadS modulates type I–F CRISPR-Cas adaptive immunity. *Biochemical and Biophysical Research Communications* **546,** 155–161 (Mar. 26, 2021).
228. Vakulskas, C. A., Potts, A. H., Babitzke, P., Ahmer, B. M. M. & Romeo, T. Regulation of Bacterial Virulence by Csr (Rsm) Systems. *Microbiology and Molecular Biology Reviews : MMBR* **79,** 193–224 (Apr. 1, 2015).
229. Lee, J. H., Ancona, V., Chatnaparat, T., Yang, H.-w. & Zhao, Y. The RNA-Binding Protein CsrA Controls Virulence in Erwinia amylovora by Regulating RelA, RcsB, and FlhD at the Posttranscriptional Level. *Molecular Plant-Microbe Interactions®* **32.** Publisher: Scientific Societies, 1448–1459 (Oct. 2019).
230. Broder, U. N., Jaeger, T. & Jenal, U. LadS is a calcium-responsive kinase that induces acute-to-chronic virulence switch in Pseudomonas aeruginosa. *Nature Microbiology* **2,** 16184 (Oct. 24, 2016).
231. Ventre, I. *et al.* Multiple sensors control reciprocal expression of Pseudomonas aeruginosa regulatory RNA and virulence genes. *Proceedings of the National Academy of Sciences of the United States of America* **103,** 171–176 (Jan. 3, 2006).
232. Ennis, D. G., Fisher, B., Edmiston, S. & Mount, D. W. Dual role for Escherichia coli RecA protein in SOS mutagenesis. *Proceedings of the National Academy of Sciences of the United States of America* **82,** 3325–3329 (May 1985).
233. Meyer, A. J., Segall-Shapiro, T. H., Glassey, E., Zhang, J. & Voigt, C. A. Escherichia coli "Marionette" strains with 12 highly optimized small-molecule sensors. *Nature Chemical Biology* **15,** 196–204 (Feb. 2019).
234. St-Pierre, F. *et al.* One-step cloning and chromosomal integration of DNA. *ACS synthetic biology* **2,** 537–541 (Sept. 20, 2013).
235. Robinson, A. *et al.* Regulation of Mutagenic DNA Polymerase V Activation in Space and Time. *PLoS Genetics* **11,** e1005482 (Aug. 28, 2015).

236. Amlinger, L., Hoekzema, M., Wagner, E. G. H., Koskiniemi, S. & Lundgren, M. Fluorescent CRISPR Adaptation Reporter for rapid quantification of spacer acquisition. *Scientific Reports* **7,** 10392. (2021) (Sept. 4, 2017).
237. Braithwaite, J. *Development of a High-Throughput Screen for the study of CRISPR Spacer Acquisition* Thesis (The University of Nottingham, 2021).
238. Cherepanov, P. P. & Wackernagel, W. Gene disruption in Escherichia coli: TcR and KmR cassettes with the option of Flp-catalyzed excision of the antibiotic-resistance determinant. *Gene* **158,** 9–14 (May 26, 1995).
239. Cui, L. & Bikard, D. Consequences of Cas9 cleavage in the chromosome of Escherichia coli. *Nucleic Acids Research* **44,** 4243–4251 (May 19, 2016).
240. Baba, T. *et al.* Construction of Escherichia coli K-12 in-frame, single-gene knockout mutants: the Keio collection. *Molecular Systems Biology* **2,** 2006.0008 (Feb. 21, 2006).
241. Schindelin, J. *et al.* Fiji: an open-source platform for biological-image analysis. *Nature Methods* **9.** Number: 7 Publisher: Nature Publishing Group, 676–682 (July 2012).
242. Shiriaeva, A., Fedorov, I., Vyhovskyi, D. & Severinov, K. Detection of CRISPR adaptation. *Biochemical Society Transactions* **48,** 257–269 (Feb. 28, 2020).
243. Díez-Villaseñor, C., Guzmán, N. M., Almendros, C., García-Martínez, J. & Mojica, F. J. CRISPR-spacer integration reporter plasmids reveal distinct genuine acquisition specificities among CRISPR-Cas I-E variants of Escherichia coli. *RNA Biology* **10,** 792–802 (May 1, 2013).
244. Dewachter, L., Verstraeten, N., Fauvart, M. & Michiels, J. An integrative view of cell cycle control in Escherichia coli. *FEMS Microbiology Reviews* **42,** 116–136 (Mar. 1, 2018).
245. Justice, S. S., Hunstad, D. A., Cegelski, L. & Hultgren, S. J. Morphological plasticity as a bacterial survival strategy. *Nature Reviews Microbiology* **6,** 162–168 (Feb. 2008).
246. Justice, S. S., Hunstad, D. A., Seed, P. C. & Hultgren, S. J. Filamentation by Escherichia coli subverts innate defenses during urinary tract infection. *Proceedings of the National Academy of Sciences* **103.** Publisher: National Academy of Sciences Section: Biological Sciences, 19884–19889 (Dec. 26, 2006).
247. Miller, C. *et al.* SOS response induction by beta-lactams and bacterial defense against antibiotic lethality. *Science (New York, N.Y.)* **305,** 1629–1631 (Sept. 10, 2004).
248. Wainwright, M., Canham, L. T., Al-Wajeeh, K. & Reeves, C. L. Morphological changes (including filamentation) in Escherichia coli grown under starvation conditions on silicon wafers and other surfaces. *Letters in Applied Microbiology* **29,** 224–227 (1999).
249. Dajkovic, A., Lan, G., Sun, S. X., Wirtz, D. & Lutkenhaus, J. MinC spatially controls bacterial cytokinesis by antagonizing the scaffolding function of FtsZ. *Current biology: CB* **18,** 235–244 (Feb. 26, 2008).
250. Bernhardt, T. G. & de Boer, P. A. J. SlmA, a nucleoid-associated, FtsZ binding protein required for blocking septal ring assembly over Chromosomes in E. coli. *Molecular Cell* **18,** 555–564 (May 27, 2005).
251. Heinrich, K., Sobetzko, P. & Jonas, K. A Kinase-Phosphatase Switch Transduces Environmental Information into a Bacterial Cell Cycle Circuit. *PLOS Genetics* **12.** Publisher: Public Library of Science, e1006522 (Dec. 12, 2016).
252. Huisman, O., D'Ari, R. & Gottesman, S. Cell-division control in Escherichia coli: specific induction of the SOS function SfiA protein is sufficient to block septation. *Proceedings of the National Academy of Sciences* **81,** 4490–4494 (July 1984).
253. Schoemaker, J. M., Gayda, R. C. & Markovitz, A. Regulation of cell division in Escherichia coli: SOS induction and cellular location of the sulA protein, a key to lon-associated filamentation and death. *Journal of Bacteriology* **158,** 551–561 (May 1984).
254. Wang, L. *et al.* Filamentation initiated by Cas2 and its association with the acquisition process in cells. *International Journal of Oral Science* **11.** Number: 3 Publisher: Nature Publishing Group, 1–7 (Oct. 3, 2019).
255. Sugino, A., Peebles, C. L., Kreuzer, K. N. & Cozzarelli, N. R. Mechanism of action of nalidixic acid: purification of Escherichia coli nalA gene product and its relationship to DNA gyrase and a novel nicking-closing enzyme. *Proceedings of the National Academy of Sciences of the United States of America* **74,** 4767–4771 (Nov. 1977).

256. Khodursky, A. B., Zechiedrich, E. L. & Cozzarelli, N. R. Topoisomerase IV is a target of quinolones in Escherichia coli. *Proceedings of the National Academy of Sciences of the United States of America* **92,** 11801–11805 (Dec. 5, 1995).
257. Kreuzer, K. N. DNA damage responses in prokaryotes: regulating gene expression, modulating growth patterns, and manipulating replication forks. *Cold Spring Harbor Perspectives in Biology* **5,** a012674 (Nov. 1, 2013).
258. Napolitano, R., Janel-Bintz, R., Wagner, J. & Fuchs, R. P. All three SOS-inducible DNA polymerases (Pol II, Pol IV and Pol V) are involved in induced mutagenesis. *The EMBO journal* **19,** 6259–6265 (Nov. 15, 2000).
259. Little, J. W., Mount, D. W. & Yanisch-Perron, C. R. Purified lexA protein is a repressor of the recA and lexA genes. *Proceedings of the National Academy of Sciences of the United States of America* **78,** 4199–4203 (July 1981).
260. Brent, R. & Ptashne, M. Mechanism of action of the lexA gene product. *Proceedings of the National Academy of Sciences of the United States of America* **78,** 4204–4208 (July 1981).
261. Mohana-Borges, R. *et al.* LexA repressor forms stable dimers in solution. The role of specific dna in tightening protein-protein interactions. *The Journal of Biological Chemistry* **275,** 4708–4712 (Feb. 18, 2000).
262. Zhang, A. P., Pigli, Y. Z. & Rice, P. A. Structure of the LexA-DNA complex and implications for SOS box measurement. *Nature* **466,** 883–886 (Aug. 12, 2010).
263. Gillor, O., Vriezen, J. A. C. & Riley, M. A. The role of SOS boxes in enteric bacteriocin regulation. *Microbiology (Reading, England)* **154,** 1783–1792 (Pt 6 June 2008).
264. Little, J. W. Autodigestion of lexA and phage lambda repressors. *Proceedings of the National Academy of Sciences of the United States of America* **81,** 1375–1379 (Mar. 1984).
265. Butala, M. *et al.* Interconversion between bound and free conformations of LexA orchestrates the bacterial SOS response. *Nucleic Acids Research* **39,** 6546–6557 (Aug. 2011).
266. Radding, C. M. Helical interactions in homologous pairing and strand exchange driven by RecA protein. *The Journal of Biological Chemistry* **266,** 5355–5358 (Mar. 25, 1991).
267. Adikesavan, A. K. *et al.* Separation of Recombination and SOS Response in Escherichia coli RecA Suggests LexA Interaction Sites. *PLOS Genetics* **7.** Publisher: Public Library of Science, e1002244 (Sept. 1, 2011).
268. Trusca, D., Scott, S., Thompson, C. & Bramhill, D. Bacterial SOS checkpoint protein SulA inhibits polymerization of purified FtsZ cell division protein. *Journal of Bacteriology* **180,** 3946–3953 (Aug. 1998).
269. Mukherjee, A., Cao, C. & Lutkenhaus, J. Inhibition of FtsZ polymerization by SulA, an inhibitor of septation in Escherichia coli. *Proceedings of the National Academy of Sciences of the United States of America* **95,** 2885–2890 (Mar. 17, 1998).
270. Chen, Y., Milam, S. L. & Erickson, H. P. SulA inhibits assembly of FtsZ by a simple sequestration mechanism. *Biochemistry* **51,** 3100–3109 (Apr. 10, 2012).
271. Maguin, E., Lutkenhaus, J. & D'Ari, R. Reversibility of SOS-associated division inhibition in Escherichia coli. *Journal of Bacteriology* **166,** 733–738 (June 1986).
272. Lewis, L. K., Harlow, G. R., Gregg-Jolly, L. A. & Mount, D. W. Identification of high affinity binding sites for LexA which define new DNA damage-inducible genes in Escherichia coli. *Journal of Molecular Biology* **241,** 507–523 (Aug. 26, 1994).
273. Lin, L. L. & Little, J. W. Isolation and characterization of noncleavable (Ind-) mutants of the LexA repressor of Escherichia coli K-12. *Journal of Bacteriology* **170.** Publisher: American Society for Microbiology, 2163–2173. (2022) (May 1988).
274. Christensen, D. G. *et al.* Identification of Novel Protein Lysine Acetyltransferases in Escherichia coli. *mBio* **9,** e01905–18 (Oct. 23, 2018).
275. Cui, L. & Shearwin, K. E. in *Synthetic DNA: Methods and Protocols* (ed Hughes, R. A.) 139–155 (Springer, New York, NY, 2017).
276. Stohl, E. A. *et al.* Escherichia coli RecX inhibits RecA recombinase and coprotease activities in vitro and in vivo. *The Journal of Biological Chemistry* **278,** 2278–2285 (Jan. 24, 2003).
277. VanLoock, M. S. *et al.* Complexes of RecA with LexA and RecX differentiate between active and inactive RecA nucleoprotein filaments. *Journal of Molecular Biology* **333,** 345–354 (Oct. 17, 2003).

278. Ragone, S., Maman, J. D., Furnham, N. & Pellegrini, L. Structural basis for inhibition of homologous recombination by the RecX protein. *The EMBO journal* **27,** 2259–2269 (Aug. 20, 2008).
279. Yakimov, A. *et al.* Blocking the RecA activity and SOS-response in bacteria with a short alpha-helical peptide. *Nucleic Acids Research* **45,** 9788–9796 (Sept. 19, 2017).
280. Crane, J. K., Broome, J. E., Reddinger, R. M. & Werth, B. B. Zinc protects against shigatoxigenic Escherichia coli by acting on host tissues as well as on bacteria. *BMC Microbiology* **14,** 145. (2022) (June 5, 2014).
281. Bunnell, B. E., Escobar, J. F., Bair, K. L., Sutton, M. D. & Crane, J. K. Zinc blocks SOS-induced antibiotic resistance via inhibition of RecA in Escherichia coli. *PLOS ONE* **12.** Publisher: Public Library of Science, e0178303 (May 22, 2017).
282. Mellies, J. L. *et al.* Zinc-induced envelope stress diminishes type III secretion in enteropathogenic Escherichia coli. *BMC microbiology* **12,** 123 (June 24, 2012).
283. Li, J. *et al.* Zinc Toxicity and Iron-Sulfur Cluster Biogenesis in Escherichia coli. *Applied and Environmental Microbiology* **85,** e01967–18 (Apr. 18, 2019).
284. Ansari, S. *et al.* A Newly Identified Prophage Gene, ymfM, Causes SOS-Inducible Filamentation in Escherichia coli. *Journal of Bacteriology* **203,** e00646–20 (May 7, 2021).
285. D'Ari, R. & Huisman, O. Novel mechanism of cell division inhibition associated with the SOS response in Escherichia coli. *Journal of Bacteriology* **156,** 243–250. ISSN: 0021-9193 (Oct. 1983).
286. Burke, C. *et al.* Harnessing Single Cell Sorting to Identify Cell Division Genes and Regulators in Bacteria. *PLoS ONE* **8,** e60964 (Apr. 2, 2013).
287. Chung, H. S. *et al.* Rapid beta-lactam-induced lysis requires successful assembly of the cell division machinery. *Proceedings of the National Academy of Sciences of the United States of America* **106,** 21872–21877 (Dec. 22, 2009).
288. Sulaiman, J. E. & Lam, H. Proteomic Study of the Survival and Resuscitation Mechanisms of Filamentous Persisters in an Evolved Escherichia coli Population from Cyclic Ampicillin Treatment. *mSystems* **5,** e00462–20 (July 28, 2020).
289. Suzuki, H., Pangborn, J. & Kilgore, W. W. Filamentous Cells of Escherichia coli Formed in the Presence of Mitomycin. *Journal of Bacteriology* **93,** 683–688 (Feb. 1967).
290. Amaral, L., Schwarz, U. & Lorian, V. Penicillin-binding proteins of filaments of Escherichia coli induced by low concentrations of nalidixic acid, oxolinic acid, novobiocin or nitrofurantoin. *Drugs Under Experimental and Clinical Research* **12,** 653–656 (1986).
291. Bonner, C. A. *et al.* Purification and characterization of an inducible Escherichia coli DNA polymerase capable of insertion and bypass at abasic lesions in DNA. *The Journal of Biological Chemistry* **263,** 18946–18952. ISSN: 0021-9258 (Dec. 15, 1988).
292. Wagner, J. *et al.* The dinB Gene Encodes a Novel E. coli DNA Polymerase, DNA Pol IV, Involved in Mutagenesis. *Molecular Cell* **4,** 281–286 (Aug. 1, 1999).
293. Tang, M. *et al.* UmuD'(2)C is an error-prone DNA polymerase, Escherichia coli pol V. *Proceedings of the National Academy of Sciences of the United States of America* **96,** 8919–8924 (Aug. 3, 1999).
294. Gutierrez, A. *et al.* Beta-Lactam antibiotics promote bacterial mutagenesis via an RpoS-mediated reduction in replication fidelity. *Nature Communications* **4,** 1610 (2013).
295. Pérez-Capilla, T. *et al.* SOS-Independent Induction of dinB Transcription by Beta-Lactam-Mediated Inhibition of Cell Wall Synthesis in Escherichia coli. *Journal of Bacteriology* **187.** Publisher: American Society for Microbiology, 1515–1518 (Feb. 15, 2005).
296. Cairns, J. & Foster, P. L. Adaptive reversion of a frameshift mutation in Escherichia coli. *Genetics* **128,** 695–701 (Aug. 1991).
297. Ramachandran, A., Summerville, L., Learn, B. A., DeBell, L. & Bailey, S. Processing and integration of functionally oriented prespacers in the Escherichia coli CRISPR system depends on bacterial host exonucleases. *The Journal of Biological Chemistry* **295,** 3403–3414 (Mar. 13, 2020).
298. Drabavicius, G. *et al.* DnaQ exonuclease-like domain of Cas2 promotes spacer integration in a type I-E CRISPR-Cas system. *EMBO reports* **19.** Number: 7 (2018).

299. Zhang, A., Schu, D. J., Tjaden, B. C., Storz, G. & Gottesman, S. Mutations in interaction surfaces differentially impact E. coli Hfq association with small RNAs and their mRNA targets. *Journal of molecular biology* **425,** 3678–3697 (Oct. 9, 2013).
300. Bilusic, I., Popitsch, N., Rescheneder, P., Schroeder, R. & Lybecker, M. Revisiting the coding potential of the E. coli genome through Hfq co-immunoprecipitation. *RNA Biology* **11,** 641–654. (2022) (May 1, 2014).
301. Vold, B. S., Lazar, J. M. & Gray, A. M. Characterization of a deficiency of N6-(delta 2-isopentenyl)-2-methylthioadenosine in the Escherichia coli mutant trpX by use of antibodies to N6-(delta 2-isopentenyl)adenosine. *The Journal of Biological Chemistry* **254,** 7362–7367. ISSN: 0021-9258 (Aug. 10, 1979).
302. Moore, J. A. & Poulter, C. D. Escherichia coli dimethylallyl diphosphate:tRNA dimethylallyltransferase: a binding mechanism for recombinant enzyme. *Biochemistry* **36,** 604–614. ISSN: 0006-2960 (Jan. 21, 1997).
303. Leung, H. C., Chen, Y. & Winkler, M. E. Regulation of substrate recognition by the MiaA tRNA prenyltransferase modification enzyme of Escherichia coli K-12. *The Journal of Biological Chemistry* **272,** 13073–13083. ISSN: 0021-9258 (May 16, 1997).
304. Kihara, A., Akiyama, Y. & Ito, K. A protease complex in the Escherichia coli plasma membrane: HflKC (HflA) forms a complex with FtsH (HflB), regulating its proteolytic activity against SecY. *The EMBO Journal* **15,** 6122–6131 (Nov. 15, 1996).
305. Kihara, A., Akiyama, Y. & Ito, K. Host regulation of lysogenic decision in bacteriophage lambda: transmembrane modulation of FtsH (HflB), the cII degrading protease, by HflKC (HflA). *Proceedings of the National Academy of Sciences of the United States of America* **94,** 5544–5549 (May 27, 1997).
306. Bandyopadhyay, K., Parua, P. K., Datta, A. B. & Parrack, P. Escherichia coli HflK and HflC can individually inhibit the HflB (FtsH)-mediated proteolysis of lambdaCII in vitro. *Archives of Biochemistry and Biophysics* **501,** 239–243 (Sept. 15, 2010).
307. Banuett, F. & Herskowitz, I. Identification of polypeptides encoded by an Escherichia coli locus (hflA) that governs the lysis-lysogeny decision of bacteriophage lambda. *Journal of Bacteriology* **169,** 4076–4085 (Sept. 1987).
308. Kihara, A. & Ito, K. Translocation, folding, and stability of the HflKC complex with signal anchor topogenic sequences. *The Journal of Biological Chemistry* **273,** 29770–29775 (Nov. 6, 1998).
309. Tomoyasu, T. *et al.* The Escherichia coli FtsH protein is a prokaryotic member of a protein family of putative ATPases involved in membrane functions, cell cycle control, and gene expression. *Journal of Bacteriology* **175,** 1344–1351 (Mar. 1993).
310. Deuerling, E., Paeslack, B. & Schumann, W. The ftsH gene of Bacillus subtilis is transiently induced after osmotic and temperature upshift. *Journal of Bacteriology* **177,** 4105–4112 (July 1995).
311. Deuerling, E., Mogk, A., Richter, C., Purucker, M. & Schumann, W. The ftsH gene of Bacillus subtilis is involved in major cellular processes such as sporulation, stress adaptation and secretion. *Molecular Microbiology* **23,** 921–933 (Mar. 1997).
312. Herman, C., Thévenet, D., D'Ari, R. & Bouloc, P. Degradation of sigma 32, the heat shock regulator in Escherichia coli, is governed by HflB. *Proceedings of the National Academy of Sciences of the United States of America* **92,** 3516–3520 (Apr. 11, 1995).
313. Srinivasan, R., Rajeswari, H. & Ajitkumar, P. Analysis of degradation of bacterial cell division protein FtsZ by the ATP-dependent zinc-metalloprotease FtsH in vitro. *Microbiological Research* **163,** 21–30 (2008).
314. Silhavy, T. J., Kahne, D. & Walker, S. The Bacterial Cell Envelope. *Cold Spring Harbor Perspectives in Biology* **2,** a000414 (May 2010).
315. Guest, R. L., Samé Guerra, D., Wissler, M., Grimm, J. & Silhavy, T. J. YejM Modulates Activity of the YciM/FtsH Protease Complex To Prevent Lethal Accumulation of Lipopolysaccharide. *mBio* **11,** e00598–20 (Apr. 14, 2020).
316. Fivenson, E. M. & Bernhardt, T. G. An Essential Membrane Protein Modulates the Proteolysis of LpxC to Control Lipopolysaccharide Synthesis in Escherichia coli. *mBio* **11,** e00939–20 (May 19, 2020).

317. Klein, G. *et al.* Multiple Transcriptional Factors Regulate Transcription of the rpoE Gene in Escherichia coli under Different Growth Conditions and When the Lipopolysaccharide Biosynthesis Is Defective *. *Journal of Biological Chemistry* **291.** Publisher: Elsevier, 22999–23019 (Oct. 28, 2016).
318. Nagy, G. *et al.* Down-Regulation of Key Virulence Factors Makes the Salmonella enterica Serovar Typhimurium rfaH Mutant a Promising Live-Attenuated Vaccine Candidate. *Infection and Immunity* **74,** 5914–5925 (Oct. 2006).
319. Parker, C. T. *et al.* Role of the rfaG and rfaP genes in determining the lipopolysaccharide core structure and cell surface properties of Escherichia coli K-12. *Journal of Bacteriology* **174,** 2525–2538 (Apr. 1992).
320. De Lay, N. R. & Cronan, J. E. Genetic interaction between the Escherichia coli AcpT phosphopantetheinyl transferase and the YejM inner membrane protein. *Genetics* **178,** 1327–1337 (Mar. 2008).
321. Beall, B. & Lutkenhaus, J. Sequence analysis, transcriptional organization, and insertional mutagenesis of the envA gene of Escherichia coli. *Journal of Bacteriology* **169,** 5408–5415 (Dec. 1987).
322. Barb, A. W. *et al.* Inhibition of lipid A biosynthesis as the primary mechanism of CHIR-090 antibiotic activity in Escherichia coli. *Biochemistry* **46,** 3793–3802 (Mar. 27, 2007).
323. Creeger, E. S., Schulte, T. & Rothfield, L. I. Regulation of membrane glycosyltransferases by the sfrB and rfaH genes of Escherichia coli and Salmonella typhimurium. *The Journal of Biological Chemistry* **259,** 3064–3069 (Mar. 10, 1984).
324. Pradel, E. & Schnaitman, C. A. Effect of rfaH (sfrB) and temperature on expression of rfa genes of Escherichia coli K-12. *Journal of Bacteriology* **173,** 6428–6431 (Oct. 1991).
325. Mahalakshmi, S., Sunayana, M. R., SaiSree, L. & Reddy, M. yciM is an essential gene required for regulation of lipopolysaccharide synthesis in Escherichia coli. *Molecular Microbiology* **91,** 145–157 (Jan. 2014).
326. Ma, C.-H., Javanmardi, K., Finkelstein, I. J. & Jayaram, M. Disintegration promotes protospacer integration by the Cas1-Cas2 complex. *eLife* **10** (eds Berger, J. M. & Storz, G.) Publisher: eLife Sciences Publications, Ltd, e65763 (Aug. 26, 2021).
327. Nivala, J., Shipman, S. L. & Church, G. M. Spontaneous CRISPR loci generation in vivo by non-canonical spacer integration. *Nature Microbiology* **3,** 310–318 (Mar. 2018).
328. Grainy, J., Garrett, S., Graveley, B. R. & P. Terns, M. CRISPR repeat sequences and relative spacing specify DNA integration by Pyrococcus furiosus Cas1 and Cas2. *Nucleic Acids Research* **47,** 7518–7531 (Aug. 22, 2019).
329. Achigar, R., Magadán, A. H., Tremblay, D. M., Julia Pianzzola, M. & Moineau, S. Phage-host interactions in Streptococcus thermophilus: Genome analysis of phages isolated in Uruguay and ectopic spacer acquisition in CRISPR array. *Scientific Reports* **7.** Number: 1 Publisher: Nature Publishing Group, 43438 (Mar. 6, 2017).
330. Achigar, R. *et al.* Ectopic Spacer Acquisition in Streptococcus thermophilus CRISPR3 Array. *Microorganisms* **9.** Number: 3 Publisher: Multidisciplinary Digital Publishing Institute, 512 (Mar. 2021).
331. Malone, L. M., Hampton, H. G., Morgan, X. C. & Fineran, P. C. Type I CRISPR-Cas provides robust immunity but incomplete attenuation of phage-induced cellular stress. *Nucleic Acids Research* **50,** 160–174 (Jan. 11, 2022).
332. Heussler, G. E. *et al.* Clustered Regularly Interspaced Short Palindromic Repeat-Dependent, Biofilm-Specific Death of Pseudomonas aeruginosa Mediated by Increased Expression of Phage-Related Genes. *mBio* **6,** e00129–00115 (May 12, 2015).
333. Mo, C. Y. *et al.* Type III-A CRISPR immunity promotes mutagenesis of staphylococci. *Nature* **592.** Number: 7855 Publisher: Nature Publishing Group, 611–615 (Apr. 2021).
334. Baharoglu, Z., Bikard, D. & Mazel, D. Conjugative DNA Transfer Induces the Bacterial SOS Response and Promotes Antibiotic Resistance Development through Integron Activation. *PLOS Genetics* **6.** Publisher: Public Library of Science, e1001165. (2021) (Oct. 21, 2010).
335. Higashitani, N., Higashitani, A., Roth, A. & Horiuchi, K. SOS induction in Escherichia coli by infection with mutant filamentous phage that are defective in initiation of complementary-strand DNA synthesis. *Journal of Bacteriology* **174,** 1612–1618 (Mar. 1992).

336. Radovčić, M. *et al.* CRISPR–Cas adaptation in Escherichia coli requires RecBCD helicase but not nuclease activity, is independent of homologous recombination, and is antagonized by 5' ssDNA exonucleases. *Nucleic Acids Research* **46,** 10173–10183 (Nov. 2, 2018).
337. Courcelle, J., Donaldson, J. R., Chow, K.-H. & Courcelle, C. T. DNA Damage-Induced Replication Fork Regression and Processing in Escherichia coli. *Science* **299.** Publisher: American Association for the Advancement of Science, 1064–1067. (2022) (Feb. 14, 2003).
338. Murata, M. *et al.* Cell Lysis Directed by SulA in Response to DNA Damage in Escherichia coli. *International Journal of Molecular Sciences* **22,** 4535 (Apr. 26, 2021).
339. Fornelos, N. *et al.* Bacteriophage GIL01 gp7 interacts with host LexA repressor to enhance DNA binding and inhibit RecA-mediated auto-cleavage. *Nucleic Acids Research* **43,** 7315–7329. (2022) (Sept. 3, 2015).
340. Azulay, G. *et al.* A dual-function phage regulator controls the response of cohabiting phage elements via regulation of the bacterial SOS response. *Cell Reports* **39,** 110723 (Apr. 19, 2022).
341. Conter, A., Bouché, J. P. & Dassain, M. Identification of a new inhibitor of essential division gene ftsZ as the kil gene of defective prophage Rac. *Journal of Bacteriology* **178,** 5100–5104 (Sept. 1996).
342. Wang, X. *et al.* Cryptic prophages help bacteria cope with adverse environments. *Nature Communications* **1.** Number: 1 Publisher: Nature Publishing Group, 147 (Dec. 21, 2010).
343. Dimitriu, T. *et al.* Bacteriostatic antibiotics promote CRISPR-Cas adaptive immunity by enabling increased spacer acquisition. *Cell Host & Microbe* **30,** 31–40.e5 (Jan. 12, 2022).
344. Kasagaki, S., Hashimoto, M. & Maeda, S. Subminimal inhibitory concentrations of ampicillin and mechanical stimuli cooperatively promote cell-to-cell plasmid transformation in Escherichia coli. *Current Research in Microbial Sciences* **3,** 100130 (Jan. 1, 2022).
345. Twiss, E., Coros, A. M., Tavakoli, N. P. & Derbyshire, K. M. Transposition is modulated by a diverse set of host factors in Escherichia coli and is stimulated by nutritional stress. *Molecular Microbiology* **57,** 1593–1607 (Sept. 2005).
346. Deter, H. S., Hossain, T. & Butzin, N. C. Antibiotic tolerance is associated with a broad and complex transcriptional response in E. coli. *Scientific Reports* **11,** 6112. (2022) (Mar. 17, 2021).
347. Ditto, M. D., Roberts, D. & Weisberg, R. A. Growth phase variation of integration host factor level in Escherichia coli. *Journal of Bacteriology* **176,** 3738–3748 (June 1994).
348. Maiques, E. *et al.* Beta-Lactam Antibiotics Induce the SOS Response and Horizontal Transfer of Virulence Factors in Staphylococcus aureus. *Journal of Bacteriology* **188,** 2726–2729 (Apr. 2006).
349. Chittò, M., Berger, M., Klotz, L. & Dobrindt, U. Sub-Inhibitory concentrations of SOS-Response inducing antibiotics stimulate integrase expression and excision of pathogenicity islands in uropathogenic Escherichia coli strain 536. *International journal of medical microbiology: IJMM* **310,** 151361 (Jan. 2020).
350. Mathieu, A. *et al.* Discovery and Function of a General Core Hormetic Stress Response in E. coli Induced by Sublethal Concentrations of Antibiotics. *Cell Reports* **17,** 46–57 (Sept. 27, 2016).
351. Blázquez, J. *et al.* PBP3 inhibition elicits adaptive responses in Pseudomonas aeruginosa. *Molecular Microbiology* **62.** _eprint: https://onlinelibrary.wiley.com/doi/pdf/10.1111/j.1365-2958.2006.05366.x, 84–99 (2006).
352. Anilkumar, G., Srinivasan, R., Anand, S. P. & Ajitkumar, P. Y. Bacterial cell division protein FtsZ is a specific substrate for the AAA family protease FtsH. *Microbiology* **147.** Publisher: Microbiology Society, 516–517 (Mar. 2001).
353. Wehrl, W., Niederweis, M. & Schumann, W. The FtsH protein accumulates at the septum of Bacillus subtilis during cell division and sporulation. *Journal of Bacteriology* **182,** 3870–3873 (July 2000).
354. Bi, E. F. & Lutkenhaus, J. FtsZ ring structure associated with division in Escherichia coli. *Nature* **354,** 161–164 (Nov. 14, 1991).
355. Ding, Q. *et al.* Light-powered Escherichia coli cell division for chemical production. *Nature Communications* **11.** Number: 1 Publisher: Nature Publishing Group, 2262 (May 8, 2020).

356. Camberg, J. L., Hoskins, J. R. & Wickner, S. ClpXP protease degrades the cytoskeletal protein, FtsZ, and modulates FtsZ polymer dynamics. *Proceedings of the National Academy of Sciences* **106.** Publisher: National Academy of Sciences Section: Biological Sciences, 10614–10619 (June 30, 2009).
357. Srinivasan, R., Rajeswari, H., Bhatt, B. N., Indi, S. & Ajitkumar, P. GTP/GDP binding stabilizes bacterial cell division protein FtsZ against degradation by FtsH protease in vitro. *Biochemical and Biophysical Research Communications* **357,** 38–43 (May 25, 2007).
358. Srinivasan, R. & Ajitkumar, P. Bacterial cell division protein FtsZ is stable against degradation by AAA family protease FtsH in Escherichia coli cells. *Journal of Basic Microbiology* **47,** 251–259 (2007).
359. Maurya, G. K. *et al.* Phosphorylation of FtsZ and FtsA by a DNA Damage-Responsive Ser/Thr Protein Kinase Affects Their Functional Interactions in Deinococcus radiodurans. *mSphere* **3,** e00325–18 (July 18, 2018).
360. Chaudhary, R., Mishra, S., Maurya, G. K. & Misra, H. S. *FtsZ phosphorylation brings about growth arrest upon DNA damage in Deinococcus radiodurans* Pages: 2022.06.16.496254 Section: New Results. June 16, 2022.
361. Hansen, A.-M. *et al.* The Escherichia coli Phosphotyrosine Proteome Relates to Core Pathways and Virulence. *PLOS Pathogens* **9.** Publisher: Public Library of Science, e1003403 (June 13, 2013).
362. Thakur, M. & Chakraborti, P. K. GTPase Activity of Mycobacterial FtsZ Is Impaired Due to Its Transphosphorylation by the Eukaryotic-type Ser/Thr Kinase, PknA*. *Journal of Biological Chemistry* **281,** 40107–40113 (Dec. 29, 2006).
363. Del Val, E., Nasser, W., Abaibou, H. & Reverchon, S. Design and comparative characterization of RecA variants. *Scientific Reports* **11.** Number: 1 Publisher: Nature Publishing Group, 21106 (Oct. 26, 2021).
364. Weisemann, J. M. & Weinstock, G. M. The promoter of the recA gene of Escherichia coli. *Biochimie* **73,** 457–470 (Apr. 1991).
365. Klaric, J. A. *et al.* DNA damage-signaling, homologous recombination and genetic mutation induced by 5-azacytidine and DNA-protein crosslinks in Escherichia coli. *Mutation research* **822,** 111742 (2021).
366. Ding, Z. *et al.* A Novel Cytology-Based, Two-Hybrid Screen for Bacteria Applied to Protein-Protein Interaction Studies of a Type IV Secretion System. *Journal of Bacteriology* **184,** 5572–5582 (Oct. 2002).